A consistent turbulence formulation for the dynamic wake meandering model in the atmospheric boundary layer

Keck, Rolf-Erik; Veldkamp, Dick ; Wedel-Heinen, Jens Jakob ; Forsberg, Jan

Publication date:
2013

Document Version
Publisher's PDF, also known as Version of record

A consistent turbulence formulation for the dynamic wake meandering model in the atmospheric boundary layer

DTU Vindenergi
PhD Rapport 2013

Rolf-Erik Keck

DTU Wind Energy PhD-0012 (EN)

July 2013

DTU Vindenergi
Institut for Vindenergi

Author: Rolf-Erik Keck
Title: A consistent turbulence formulation for the dynamic wake meandering model in the atmospheric boundary layer
Institute: Risø-DTU

Resume:
This thesis describes the further development and validation of the dynamic meandering wake model for simulating the flow field and power production of wind farms operating in the atmospheric boundary layer. The overall objective of the conducted research is to improve the modelling capability of the dynamics wake meandering model to a level where it is sufficiently mature to be applied in industrial applications and for an augmentation of the IEC standard for wind turbine wake modelling.

Based on a comparison of capabilities of the dynamic wake meandering model to the requirement of the wind industry, four areas were identified as high prioritizations for further research:

1. the turbulence distribution in a single wake
2. multiple wake deficits and build-up of turbulence over a row of turbines
3. the effect of the atmospheric boundary layer on wake turbulence and wake deficit evolution
4. atmospheric stability effects on wake deficit evolution and meandering

The conducted research is to a large extent based on detailed wake investigations and reference data generated through computational fluid dynamics simulations, where the wind turbine rotor has been represented by an actuator line model. As a consequence, part of the research also targets the performance of the actuator line model when generating wind turbine wakes in the atmospheric boundary layer.

DTU Wind Energy PhD-0012 (EN)
July 2013

ISBN: 978-87-92896-30-8

Projektnr.:
DTU Wind Energy PhD-0012 (EN)

Sponsorship:
Vestas Wind Systems A/S &
The Danish agency for Science Technology and Innovation

Contact information:
rolf.keck@gmail.com

Pages: 216

Danmarks Tekniske Universitet
DTU Vindenergi
Nils Koppels Allé
Bygning 403
2800 Kgs. Lyngby
Telefon

www.vindenergi.dtu.dk

Abstract

This thesis describes the further development and validation of the dynamic meandering wake model for simulating the flow field and power production of wind farms operating in the atmospheric boundary layer (ABL). The overall objective of the conducted research is to improve the modelling capability of the dynamics wake meandering model to a level where it is sufficiently mature to be applied in industrial applications and for an augmentation of the IEC-standard for wind turbine wake modelling.

Based on a comparison of capabilities of the dynamic wake meandering model to the requirement of the wind industry, four areas were identified as high prioritizations for further research:

1. the turbulence distribution in a single wake
2. multiple wake deficits and build-up of turbulence over a row of turbines
3. the effect of the atmospheric boundary layer on wake turbulence and wake deficit evolution
4. atmospheric stability effects on wake deficit evolution and meandering

The conducted research is to a large extent based on detailed wake investigations and reference data generated through computational fluid dynamics simulations, where the wind turbine rotor has been represented by an actuator line model. As a consequence, part of the research also targets the performance of the actuator line model when generating wind turbine wakes in the atmospheric boundary layer.

Highlights of the conducted research:

1. A description is given for using the dynamic wake meandering model as a standalone flow-solver for the velocity and turbulence distribution, and power production in a wind farm. The performance of the standalone implementation is validated against field data, higher-order computational fluid dynamics models, as well as the most common engineering wake models in the wind industry.
2. The EllipSys3D actuator line model, including the synthetic methods used to model atmospheric boundary layer shear and turbulence, is verified for modelling the evolution of wind turbine wake turbulence by comparison to field data and wind tunnel experiments.
3. A two-dimensional eddy viscosity model is implemented to govern the distribution of turbulent stresses in the wake deficit. The modified eddy viscosity model improves the least-square fit of the velocity field in the wake by ~13% when compared to higher-order models.
4. A method is proposed to couple the increased turbulence level experienced by a turbine operating in waked conditions, to the downstream wake evolution of the wake-affected turbine. The intra-turbine turbulence coupling improved the fit of the turbulence distribution by ~40% and the wind speed distribution by ~30% over a row of eight turbines.
5. The effect of the atmospheric shear on the turbulent stresses in the wake is captured by including a local strain-rate contribution for the ambient shear gradient. This results in more realistic turbulent stress levels in regions of small wake deficit gradients; this is particularly important in the far-wake region where atmospheric shear gradients are an important contribution to the local strain-rate.
6. A method to include the effect of atmospheric stability on the wake deficit evolution and wake meandering is described. Including the atmospheric stability effects improved the model prediction of the mean velocity field by ~19% and of turbulence distribution by ~28% in unstable atmospheric conditions compared to actuator line results. The power production by a row of wind turbines aligned with the wind direction is reduced by ~10% in very stable conditions compared to very unstable conditions at the same turbulence intensity. This power drop is comparable to measurements from the North Hoyle and OWEZ wind farms.

Acknowledgements

This PhD thesis is the result of a research collaboration between Vestas Wind Systems, Risø-DTU and the University of Karlstad. First and foremost, I would like to express my gratitude to the Danish agency for Science Technology and Innovation (Styrelsen for Forskning og Innovation) and to Vestas Wind Systems A/S for financing this research project, giving me the opportunity to pursue this interesting long term research project.

I would also like to thank my supervisors; Helge A. Madsen, Gunner Larsen, Dick Veldkamp, Jens Jakob Wedel-Heinen and Jan Forsberg for their support and encouragement throughout this research project. Their enthusiasm for discussing any idea of varying quality I might have at the moment, together with the ability to provide invaluable suggestions and know-how has greatly contributed to making this a successful research project.

My appreciation also goes out to all my colleagues at Vestas, Risø-DTU and the University of Karlstad for the helpfulness and kindness I have encountered when bothering people for information in their day-to-day work. The input given from all of you has been a tremendous help and inspiration for me. I would especially like to thank the rest of the DWM development team at Vestas, Martin de Maré and Dick Veldkamp, for a great cooperation and for all the time and effort poured into this project. I would also like to thank Jens-Jakob Wedel-Heinen, Brad Johnson, Shreyas Ananthan and Greg Oxley for all the help and feedback during the project.

I also want to thank Risø-DTU and DTU for allowing me to use their computational code EllipSys3D and cluster to conduct the computational fluid dynamics experiment which is the basis for the DWM development, and for all the guidance in conducting the numerical calculations given to by Robert Mikkelsen and Niels Troldborg.

A special thanks also goes out to the National Renewable Energy Laboratory for allowing me to spend a period of time working with the talented people at the National Wind Technology Centre, which lead to the very fruitful collaboration with Matt Churchfield and Sang Lee.

Finally, I would like to thank my wonderful fiancé AnnLouise for her constant love and support, but most of all for her unbelievable patience in accepting my bi-weekly commute routine back and forth between Karlstad and Roskilde for the entire PhD period. For this I am severely indebted for a long time to come.

Technical university of Denmark

July 2013

Rolf-Erik Keck

Preface

This dissertation is submitted to the Technical university of Denmark (DTU) in partial fulfilment of the requirements for the degree of Doctor of Philosophy in Mechanical Engineering. This thesis is divided into eight chapters. The first chapter gives an introduction to the research question and the conducted research projects. Chapters two and three are included to give the reader a background to the research and a fundamental understanding of the most important aspects of wind turbine wake modelling. The fourth chapter describes the concept of model driven development, which refers to the use of higher-order computational models to develop and calibrate engineering type models. This chapter also describes the higher-order model used in this research project and contain a summary of the first publication which is aimed at validating the wake turbulence of the actuator line model. The fifth chapter describes the research aimed at improving the wake modelling capabilities of the dynamic wake meandering model. This part of the thesis gives summaries of publications II to IV. The last three chapter of the thesis describes the final version of the dynamic meandering wake model including all the proposed correction together with calibration, validation of the model and conclusions.

This thesis is based on the research results described in the following publications:

I. Keck, R.-E., Mikkelsen, R., Troldborg, N., de Maré, M. and Hansen, K. S. (2013), Synthetic atmospheric turbulence and wind shear in large eddy simulations of wind turbine wakes. Wind Energy. doi: 10.1002/we.1631

II. Keck RE., Veldkamp D., Madsen H.Aa. and Larsen G.C., Implementation of a Mixing Length Turbulence Formulation Into the Dynamic Wake Meandering Model, Journal of Solar Energy Engineering, Volume 134, Issue 2, 021012 (13 pages).

III. Keck RE., de Maré M., Churchfield, M.J. Lee, S. Larsen, G. and Madsen H.Aa, Two Improvements to the Dynamic Wake Meandering Model: Including the Effects of Atmospheric Shear on Wake Turbulence and Incorporating Turbulence Build Up in a Row of Wind Turbines, submitted to Wind Energy July 2012, accepted with revision December 2012.

IV. Keck RE., de Maré M., Churchfield M.J., Lee S., Larsen G. and Madsen H.Aa, On Atmospheric Stability in the Dynamic Wake Meandering Model, submitted to Wind Energy January 2013, accepted with minor revision June 2013.

The author's contributions to these publications apart from leading the documentation process are:

I. Defining the test matrix, conducting the large eddy simulations in EllipSys3D and writing post-processing algorithms in Matlab to extract the results. In the evaluation stage, defining and executing the relevant comparisons for model validation of the synthetic turbulence methods both in an empty domain and in wake cases with a wind turbine present.

   R. Mikkelsen and N. Troldborg contributed with expertise on the actuator line model, supported the construction of the computational grid and helped interpreting the results. M. de Maré and K. S. Hansen contributed with field data for model validation. M. de Maré also developed the algorithm for investigating the wake transport time and conducted the validation of the turbulence spectra to field data.

II. Identifying the need for a radially varying eddy viscosity formulation by studying the eddy viscosity distribution resulting from actuator line calculations. Derived the modified eddy viscosity equation

and conducted the least-square optimization to quantitatively prove that the new eddy viscosity model yields a better description of the turbulence distribution in the wake.

D. Veldkamp contributed to creating and implementing the solution scheme for the dynamic wake meandering model in Matlab and interpretation the results. H. Aa. Madsen and G. Larsen contributed with support and direction for implementing the dynamic wake meandering model.

III. Identifying, deriving and implement a method to incorporate the effect of a linear atmospheric boundary layer shear in the axisymmetric wake deficit in the dynamic wake meandering model, as well as deriving and implement a consistent method for coupling the wake-added turbulence to the wake deficit evolution of the downstream turbine(s). In the evaluation stage, conducting all dynamics wake meandering calculations and quantifying the improvements achieved by the modifications to the model by comparison to actuator line and field data.

M. de Maré contributed by improvements to the mathematic formulation of the algorithm to include the atmospheric boundary layer shear resulting in more accurate results and short computational times, and proposing the application of a wiener filter to solve the issues of numerical instability. The actuator line calculations in OpenFOAM used for model validation have been conducted by M. Churchfield and S. Lee. H. Aa. Madsen and G. Larsen contributed with support expertise about the dynamic wake meandering model and general wake physics.

IV. The method to use the turbulence spectra of the Mann turbulence model to estimate the effect of non-neutral atmospheric conditions on the wake dynamics in the dynamic wake meandering model by estimating the length and velocity scale of turbulence in the wake meandering and wake deficit scales. As well as conducting all dynamics wake meandering calculations and model validation to actuator line and field data.

The calculations of the non-neutrals atmospheric coefficients are conducted by M. de Maré, and the actuator line calculations used as reference and validation data have been conducted by M. Churchfield and S. Lee. H. Aa. Madsen and G. Larsen contributed with support expertise about the dynamic wake meandering model and general wake physics.

Apart from the publications presented in the dissertation other related publications by the author are:

- Veldkamp D., Keck RE., and Mikkelsen R., Verification of CFD-AL and Dynamic Wake Meandering model, Proceedings Torque 2010, Greece.

- Keck RE., Mikkelsen R. and Troldborg N., Investigation of Prescribed Wind Shear and Synthetic Atmospheric Turbulence for Rotor Wake Simulations, Proceedings Gotland Wake Conference, 2011.

- Alblas L., Keck RE., Mikkelsen R., Troldborg N. and Veldkamp D., Comparing CFD-AL and BEM for closely-spaced wind turbines, Proceedings Gotland Wake Conference, 2011.

- Keck RE., A numerical investigation of the nacelle anemometry of a HAWT using actuator disc and line models in CFX, Journal of Renewable Energy, Volume 48, December 2012, Pages 72-84

- Lee S., Moriarty P. J., Keck RE., Jonkman J., Wind Turbine Wakes and Fatigue Loadings, to be submitted to Journal of wind energy June 2013.

Table of contents

1 Introduction

Nowadays, the majority of wind turbines are erected in wind farms for practical and economic reasons of land ownership, maintenance and infrastructure. However, an important drawback of this configuration is the turbine-to-turbine wake effects. The wake refers to the downstream flow regime of a wind turbine which is affected by the presence of the turbine. The two most important characteristics of a wind turbine wake are lower wind speeds and higher turbulence intensity. The wind turbine wake persists for long distances (on the order of 20 rotor diameters). As a consequence, a wind turbine inside a wind farm experiences significantly different operational conditions compared to a solitary turbine. For modern wind farms the wake effects typically result in 5-20% lower annual energy production. At the same time, the fatigue loads of a wake-affected turbine increase by 20-80% depending on the wind turbine component considered.

The ability to predict wake effects on component loads and power production is an important aspect in both wind turbine and wind farm design. Unfortunately, simulating the effects of the wakes is a complex problem. In particular, the combination of a large range of turbulence length scales affecting the wake dynamics and the requirement of high computational speed of the wind power industry is challenging. To maintain acceptable computational time the wake models used for industrial application have to be based on reduced order physics. Current wake models used by the wind industry have two main drawbacks: 1) they are based on parametric description of the wake and are not capable of physically modelling the wake evolution and 2) they are designed to handle one aspect of wake operation (i.e. the evolution of wind speed deficit or the increased turbulence).

The aim of the research described in this thesis is to improve the modelling capability of the dynamic wake meandering (DWM) model (described in detail later). The DWM model is designed to capture the most important effects of wind turbine wake operation in a physically consistent manner, while at the same time maintaining computational requirements at a sufficiently low level to enable wind turbine and wind farm design simulations. By modelling both the downstream evolution of the wind speed and turbulence of multiple length scales, the DWM model has the capability of capturing the wake effects on both power production and component loads of wake-affected turbines simultaneously. This avoids the use of multiple models for wind turbine and park design and thus allows for a consistent design tool.

1.1 Wind energy in the world

Wind power is an increasingly important contributor to the world's energy production and it is forecast to maintain rapid expansion in the years to come. This may be concluded from the information in the 2011 report from the World Wind Energy Association (WWEA) [1] and from the executive summary of the "Wind Energy – The Facts" reports given out by the European Wind Energy Association (EWEA) in 2009 [2]:

- According to WWEA, the total installed capacity at the end of 2011 was 237GW. This yields an annual energy production (AEP) on the order of 500TWh, which is equivalent to 3% of the world's electricity production
- The forecast given by WWEA is 500GW of global installed capacity by 2015 and 1000GW by 2020

- The Global Wind Energy Council (GWEC) predicts that the wind power will cover 11.5 to 12.7% of the global electricity demand in 2020, and 20.2 to 24.9% by 2030
- EWEA predicts that the EU-27 will reach 180GW of installed capacity by 2020, and 300GW by 2030. This would require annual installation of 9.5GW (approximately 3000 turbines) and investments on the order of €11 billion per year. Wind energy in expected to deliver 12-14% of the total energy demand in EU by 2020, which in line with the binding goals made by the EU that 20% of the total energy production should come from renewable sources by 2020

The main reason for the predicted growth is the improved price competitiveness of modern wind turbines compared to conventional electricity sources. According to a report by EWEA [3] the cost of producing electricity from wind turbines erected at high wind sites onshore is 4 to 5 €cent/kWh. The production cost at low to medium wind sites is 6 to 8 €cent/kWh. The same report also refers to results presented by the European Commission, which states that the cost for generating electricity from natural gas is on the order of 3.5 to 4.5 €cent/kWh and 4 to 5 €cent/kWh using coal. A study on the same topic by Massachusetts Institute of Technology (MIT) [4] claims that newly established nuclear power costs 8.4 $cent /kWh (~6.4 €cent/kWh). The MIT study reached the price for coal and gas of 6.2 and 4.2 to 8.7 $cent /kWh (~4.95 and 3.2 to 6.67 €cent/kWh), respectively. This shows that, at the current maturity level, wind power is a competitive electricity source in the current market without any subsidies at sites with favourable wind conditions.

Wind power would be significantly more competitive if a comprehensive cost model was used to establish the price of energy. A research project aimed at estimating the external cost to society by various forms of electricity production has been carried out by the European commission [5]. The external costs are defined as the addition cost that should be added to the production cost to cover all aspects of the electricity production. The conclusion of the study is that the average external costs for the conventional power sources are: 0.4 €cent/kWh for nuclear power, 1.7 €cent/kWh for gas power, 5.7 €cent/kWh for oil power and 7.0 €cent/kWh for coal power. The same number for wind power is 0.15 €cent/kWh. Including the external cost in the calculation for the production price would make wind power highly competitive, also in low to medium wind sites.

1.2 Research and the competitiveness of wind energy

Wind turbine technology is still relatively immature, so the cost of energy (CoE) declines with additional investments on research and development activities. Historically the technological improvements have resulted in a cost reduction of 9-17% per produced kWh every time the total installed capacity has doubled according to EWEA [3].

To date, the most important technological advances for cost reductions have been made on the individual wind turbine level. Early research targeted fundamental design questions such as: number of blades, blade material selections and blade design. In the 1990s developments of pitch control, variable speed, and direct drive configurations, as well as composite material research enabled the turbines to grow in size by reductions in component weights and loads. Aerodynamic rotor design and improved turbine controls have over the last 20 years enabled the overall efficiency of the wind turbines to go from 0.4 to 0.5 (the theoretical maximum for a wind turbine is 0.592 known as the Betz limit) according to Vermeer et al. [6]. Another factor enabling larger and more reliable wind turbines is the availability of better design tools including aero-elastic models which allow better estimations of component loads and thereby smarter design strategies. As larger wind turbines produce more power relative to infrastructure and maintenance costs, and suffer less from ground level turbulence due to the high

towers, the CoE generally decreases with increasing turbine size ([3]). This caused turbine size to become a competitive advantage and much research over the last 20 years has been targeted towards larger wind turbines. Furthermore, the CoE has also been reduced by the improved quality of the wind turbines. The technical availability of a modern wind turbine is around 97-98%, according to [7] and Lemming et al. [8].

The current trend in wind power research is that an increasing attention is directed towards wind turbines in clusters, operating as a wind power plant, as opposed to optimization of individual turbines. A report on the subject by EWEA [9] mentions the ability to predict local wind conditions in complex terrain, intra-turbine and wind farm interactions through wakes, meteorological effects and short term forecasting as major research areas. These topics are increasingly important as almost all new wind turbines are placed in wind farms. Improved knowledge and simulation capability of wake dynamics is expected to facilitate improved wind turbine design, more cost effective wind farm layouts, improved wind farm control algorithms and higher predictability of wind farm output.

1.3 State of the art of wake modelling in the industry

At present the individual wind turbines are designed for solitary operation even though a large majority of the turbines are erected in wind farms. It is known that the wake effects cause different operational conditions in wind farms compared to solitary operation (Larsen et al. [10]). The current design procedure is based on verifying the strength of the various components in the wind turbines by numerical simulations according to a list of design load cases as specified by the IEC 61400-1 standard [11]. The manufacturers use extended envelopes of loads cases based on company specific experience, but to the author's knowledge there are no cases specified which take wake loads into account. For wind farm applications the site specific loads of the wind turbines are calculated based on the Frandsen model (Frandsen [12]), and compared to the design loads to ensure that the loads are maintained at an acceptable level.

The main reason why wake loads are not included in the wind turbine design process is the lack of a physics-based wake model with sufficient computational speed. The currently available wake models are either too computationally expensive for design calculations, or overly simplified to the extent where they cannot model basic design driving events such as partial wake operation. The Frandsen model (Frandsen [12]), suggested in the IEC 61400-1 standard, the falls into the second category. It is designed to give conservative estimates of the lifetime fatigue load of a wind turbine by parametric scaling of the oncoming turbulence intensity. This approach is reasonable as fatigue loads scale approximately linearly with fluctuations in wind speeds (wake operation is experienced as increased wind speed fluctuations by the affected turbine). The results of the Frandsen model (Frandsen [12]) have been verified against wind farm data at distances between three and eight rotor diameters (D). However, the model does not contain the physics required to simulate specific wake load cases. As described by Thomsen and Madsen [13], the inability to capture the physics of the wake also means that the model cannot be used to simulate extreme loads on wind turbines in wake situations. Thomsen et al. [14] concluded that the Frandsen model underestimates extreme loads in wake operation. The largest discrepancy was seen for the yaw moments, which were under-predicted by a factor 2-3 depending on distance between the wind turbines.

A consequence of the limited physics of the current engineering wake models is that knowledge of loads on wake-affected turbines is limited. As concluded by Crespo et al. [15], the method proposed by the IEC

standards to account for wake loads is insufficient. The engineering methods used to simulate wake effects are overly simplified and cannot accurately account for the complex structure of the wake and its interactions with the surrounding environment and the ABL. Vermeer et al. [6] state that the engineering rules applied in wind turbine aerodynamics, while being useful in design processes, have a limited range of applicability and should be replaced with a better physical understanding and improved models. The uncertainty of the fatigue loads of a turbine operating in solitary operation is estimated to be ~10-15% based on the work by Veldkamp [16], Schreck [17] and Schepers and Snel [18]. Due to the complexity of the problem, and the shortcomings of the current wake models, the uncertainty of the fatigue loads in wake operation is thought to be significantly higher than in solitary operations. This contention is supported by the findings of Duckworth and Barthelmie [19] where estimates of wind speed and turbulence in the wake vary significantly between various wake models. The investigations by Thomsen et al. [14] and Larsen et al. [20] showed similar differences in load estimations for a wake-affected turbine for different models. Politis et al. [21] draw the same conclusions when modelling wind farm aerodynamic using Navier-Stokes (N-S) based wake models. A similar argument can be made for the uncertainty of power production estimates of wind farms (Barthelmie et al. [22]). Increasing the accuracy of wind turbine wake simulations, and thereby reducing the uncertainty in wind farm load and power estimations, may drive down the overall CoE by wind turbines in two different ways:

1) The uncertainty in power production of a wind farm reduces the business case certainty for potential investors. The business case certainty is directly tied to the interest rate required to finance the development of the wind farm and thereby also influences the total CoE of the project.

2) The safety factor applied in component design can be reduced. The total cost of a wind turbine over its lifetime is a balance between initial investment cost and the operation and maintenance (O&M) costs over the turbine's lifetime. A conceptual representation of this balance is shown in figure 1.1. If the true loads on the wind turbines are known, a component designer can select the operating point on this curve. Due to the shape of the curve (and aspects that are not covered by this representation such as safety and public relations) it is desirable to be conservative in the load estimation. Therefore a safety factor is applied in the calculations. By reducing the uncertainty of the component loads experienced in the field, the designer can reduce the safety factor and move closer to the optimum operational point with the same level of confidence with respect to component failure.

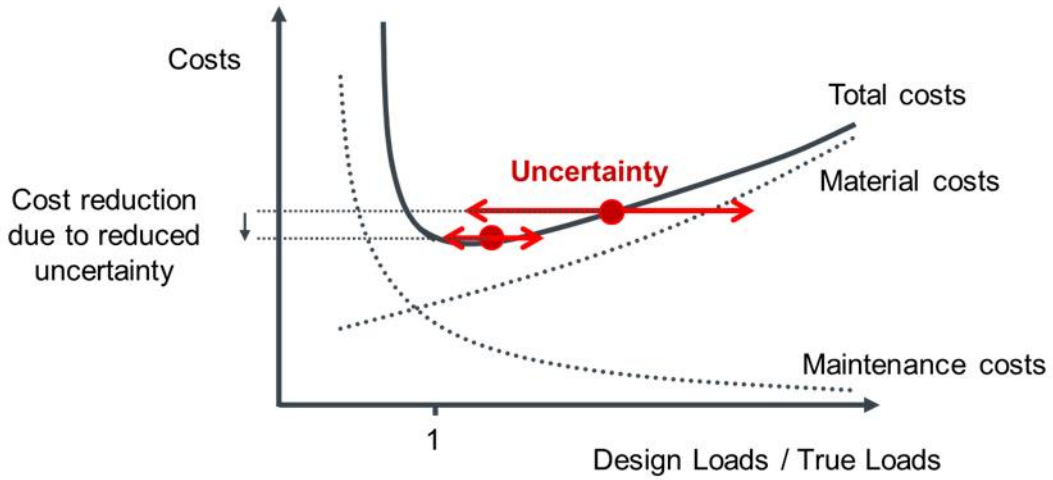

Figure 1.1: Conceptual representation of the total cost of wind turbines over its lifetime based on uncertainty in the load estimations. Overestimating the component loads in the field leads to an over dimensioned turbine and underestimation leads to higher degree of component failures.

Wake effects are currently considered by the wind industry in wind farm design. The standard process is to first design the wind farm for optimal power output (or possibly land usage or other practical aspects). The second step is to calculate the loads of the individual wind turbines to ensure that the loads at the turbine location do not exceed the design load of the turbine model. Typically this is performed with two separate models designed for either power or loads. The need for two models to simulate the wake effects originates from the fact that the wakes are not treated physically. Introducing a single model which can simulate the effect of wake operation on both power and loads would enable the development of a comprehensive wind farm design philosophy as pointed out by Larsen et al. [23, 24]. This was the high level objective of the EU funded TOPFARM project (Larsen et al. [24]). The idea is to create a cost model for the wind farm over the entire lifespan. The central part of the analysis is the DWM model which simulates both the increased loads and power output of the wind farm for various configurations. The model also includes a cost function for infrastructure, the cost of turbines and foundations at various location as well as power production and operation and maintenance cost. CoE-gains on the order of 6.5% were reported in the TOPFARM project for optimized layout compared to the baseline suggestion.

1.4 The dynamic wake meandering model

This thesis describes further development, validation and application of the DWM model for wind farm simulations. The DWM model is an engineering wake model developed at Risø DTU since 2003, Madsen et al. [25], Thomsen et al. [26, 27]. It is developed specifically to solve the problems associated with the limitations of the current engineering wake models. The main idea behind the model is to capture the most important features of the wake dynamics with regard to wind turbine loads and power production in a physical manner. Based on field observations (Larsen et al. [10], Madsen et al. [28], Vølund [29], Bingöl et al. [30] and Trujillo et al. [31]), the wake deficit evolution, the increased small-scale wake turbulence and the wake meandering (these concepts are described in chapter 2) can be identified as the most important factors for the wind turbine loads, see figure 1.2.

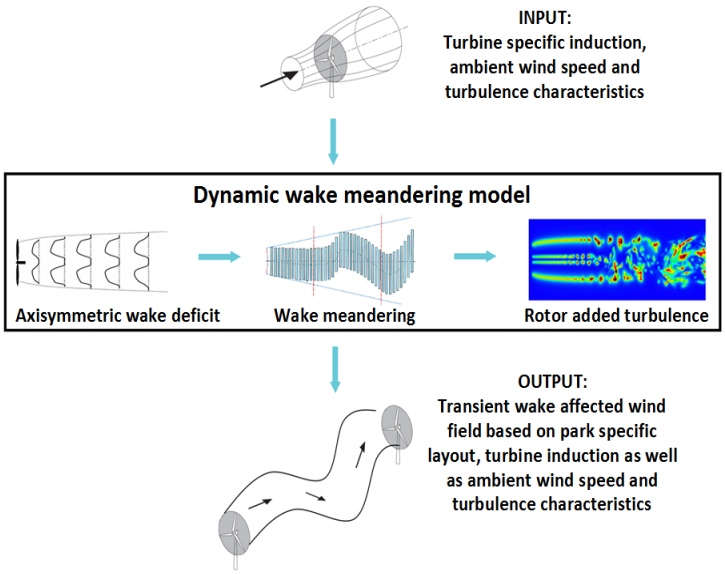

Figure 1.2: Schematic representation of the DWM model and its sub-modules.

Since the first formulation of the DWM model, the model has been subject to much research at Risø-DTU. Over the last decade many aspects of the model have been gradually improved and the main model assumptions have been validated by field and wind tunnel experiments and by higher-order computational fluid dynamics (CFD) models. The long term goal is to develop the DWM model to a stage where it is sufficiently mature to be used by the wind turbine industry and to be included in the IEC standard for wake modelling. Based on this ambition it was decided to prioritise the research activities in this project by evaluating the performance of the current DWM model (Madsen et al. [32]) and compare the model capabilities to the requirements of the wind industry. This was achieved by first conducting a technical investigation, where the DWM model was compared to a higher-order CFD model under a range of ambient conditions. Secondly, a gap-analysis was conducted together with researchers from Risø-DTU and industrial loads and wind farm design specialist from Vestas Wind Systems A/S to identify crucial model aspects for broad industrial acceptance. Based on this analysis four main areas of research were identified:

1. the turbulence distribution in a single wake
2. multiple wake deficits and build-up of turbulence over a row of turbines
3. the effect of the atmospheric boundary layer on wake turbulence and wake deficit evolution
4. atmospheric stability effects on wake deficit evolution and meandering

In all model development, especially targeted lower-order models, access to reliable high resolution reference data is crucial for calibration and to evaluate the model performance. However, full scale field measurements of the wind turbine wake with sufficient spatial and temporal resolution to study the turbulence properties are seldom available. Instead, higher-order computational models or wind tunnel experiments are commonly used. Vermeer et al. [6] concluded that CFD models have reached a maturity where it is suitable for predicting and understanding the detailed wake physics. Sørensen et al. [33] demonstrated that full rotor CFD can be used to study the detailed aerodynamics of wind turbine rotors such as three-dimensional effects of the rotating blade, even though separation and dynamic stall continues to be problematic. Sørensen's model also demonstrated the best agreement of all models in the blind test against the NASA Ames experiment facilitated by NREL Schreck [17], where it was compared against blade element momentum (BEM) models, prescribed wake models, free wake models and other N-S based models. Sørensen [34] stated that the main motivation in developing higher-order CFD tools is to enable lower-order model development. The research presented in this thesis is to a large extent driven by detailed wake investigations and reference data generated using CFD actuator line (AL) models. As a consequence, part of the conducted research also targets the performance of the AL model when generating wind turbine wakes in the ABL. Both the concept of model driven development and the AL model is described in detail in chapter 4.

1.5 Summary of the research projects

The research described in this thesis has been organized in five projects. This summary introduces the projects with a short description of the purpose and an explanation of the significance in terms of reaching the overall research target to improve the wake modelling capability of the DWM model.

1.5.1 Project 1: Evaluate the turbulence description of the EllipSys3D AL model

In order to further develop fast wake models suitable for industrial applications, the ability to conduct experiments and access to reliable data is crucial for success. In wind turbine wake modelling in general,

and particularly in turbulence research, the use of full scale experiments is important for model validation. However, it is of limited use in the development and calibration stages due the problems in achieving sufficient spatial and temporal resolution as well as issues with having the right inflow conditions. Therefore a large portion of the DWM research is based on model driven development (described in detail in chapter 4). This puts high requirements on the ability of the selected higher-order tool to accurately capture all relevant physics. Hence a study was conducted to evaluate the performance of the EllipSys3D AL model, including the synthetic turbulence description, for wind turbine wake simulations. The turbulence spectra and turbulence intensity evolution with downstream distance were evaluated both in an empty domain and with a single turbine operating in the ABL. The results were validated against the theoretical results and field data. This research is described in Keck et al. [35, 36].

1.5.2 Project 2: The turbulence distribution of a single wind turbine wake

The previous turbulence model in the DWM model assumed the eddy viscosity to be invariant in cross flow direction of the wake. However, from numerical investigations carried out with an EllipSys3D AL model, it was concluded that the wake evolution required long transport distances (6-15D depending of the ambient turbulence) to reach a stage where the eddy viscosity distributions are radially invariant. To capture these effects, and achieve a wake turbulence distribution consistent with the CFD predictions, a two-dimensional eddy viscosity formulation is developed. This research is described in Keck et al. [37].

1.5.3 Project 3: The effect of ABL shear on the Reynolds stresses in the far-wake

In the previous formulations of the DWM model the wake deficit evolution is calculated without influence of the ABL shear. The turbulent stresses in the wake deficit are based solely on the velocity gradient in the axisymmetric wake deficit. Only after the wake deficit evolution has been calculated, is the effect of ABL shear superimposed on the mean flow field. This method neglects the effect of the ABL shear on the local strain-rate in the wake deficit evolution stage. As the DWM model is based on the Boussinesq assumption (Panton [38]), where the turbulent stress is directly proportional to the local mean strain-rate, the consequence is that the turbulence level in the wake will be underestimated and the wake deficit will not diffuse accurately. To incorporate the effect of the ABL shear on the Reynolds stresses in the DWM model, a method was derived to combine the ABL gradient (du/dz_{ABL}) and the wake velocity gradient (du/dr_{DEF}) to calculate a representative axisymmetric strain-rate to apply in the wake evolution equations. This research is described in Keck et al. [39].

1.5.4 Project 4: Coupling of turbulence over a row of wind turbines

To accurately model the turbulence field inside a wind farm, and by extension the evolution of the velocity field, it is crucial to allow the turbulence in the wake of upstream turbines to influence the wake evolution of the wake-affected turbines. In previous methods for simulating wind farms using the DWM model this effect was neglected and the wakes were assumed independent of each other (Larsen et al. [40]). In the method proposed by Keck et al. [39] the turbulence stresses of the oncoming wake of the wind turbine are directly coupled to the downstream wake evolution. The significance of such a coupling is illustrated by figure 1.3.

The method is based on using a convolution of the turbulence and velocity distribution in the meandering frame of reference (MFoR, i.e. aligning the coordinate system with the instantaneous wake

centre position) and the wake meandering to calculate the mean value of the oncoming turbulence intensity at the downstream rotor. This enables the turbulence in the simulations to build-up over a row of turbines in a wind farm. This is a more physically consistent manner of determining the wake-added turbulence affecting fatigue loads at the downstream rotors, compared to the previous method based to the local depth and gradient of the wake deficit proposed by Madsen et al. [41].

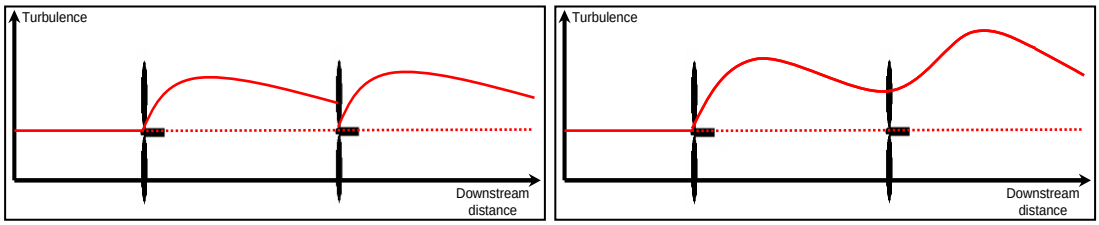

Figure 1.3: Illustration of the effect of enabling the turbulent energy to build-up over a row of turbines (right), as opposed to using the ambient turbulence level as inflow condition for all rotors in the row (left). The solid line indicates the average turbulence intensity level in the wake and the dashed line indicates the ambient turbulence level.

1.5.5 Project 5: The effect of atmospheric stability effect on wake and wind farm dynamics

The fifth project is aimed at capturing the effect of non-neutral atmospheric stability on wake and wind farm dynamics. Atmospheric stability affects three aspects of wake physics; the turbulence intensity, the turbulent length scale and the ABL shear. At the start of the fifth project the effect of ambient turbulence intensity and ABL shear (based on results from the third project) were included as input parameters to the DWM model. These effects are therefore captured by the DWM model simply by giving appropriate initial conditions. The effect of the shift in turbulent length scale, however, requires additional functionality to be developed.

The approach taken to capture the change in turbulence length scale is based on the ability to model the turbulence spectra in the ABL under various atmospheric stabilities. This is achieved using the Mann model (Mann [42, 43]), combined with a correction for non-neutral atmospheric stability using the results presented by Peña et al. [44]. The turbulence spectra are used to estimate the turbulent length and velocity scales for the eddy viscosity formulation in the wake deficit model and the ABL shear. The atmospheric stability also influences the turbulence field used to simulate the wake meandering. This research is described in Keck et al. [45].

2 Review of wind turbine wake dynamics

A wind turbine converts part of the kinetic energy of the oncoming wind to mechanical and electrical energy. As a consequence, the wind speed decreases as the air passes the rotor. The region of air which is affected by rotor is called the wake of the wind turbine. The wind turbine wake is characterized by two main features; a higher degree of fluctuations in the wind speed (turbulence) and lower average wind speed (the wake deficit), see figure 2.1.

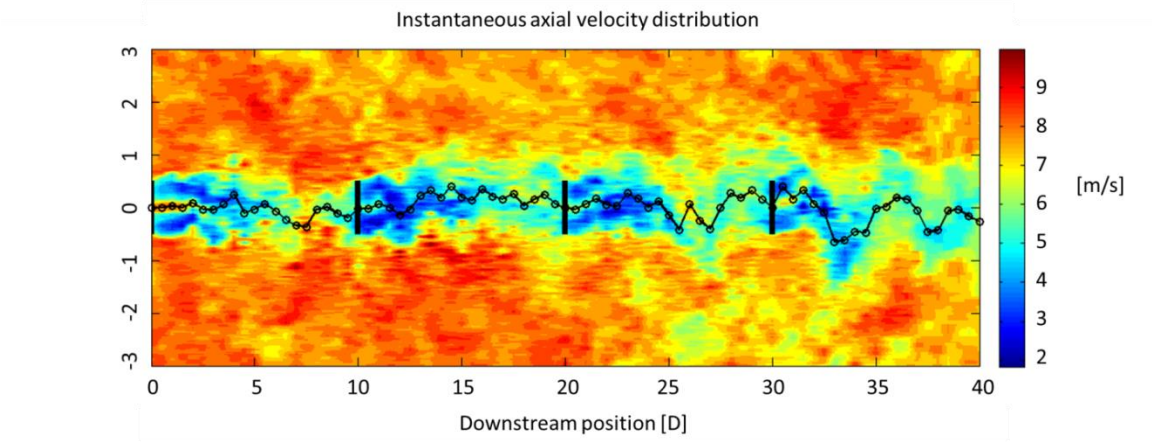

Figure 2.1: Top view of contour plot of the instantaneous axial velocity field (from left to right) over a row of four wind turbines (solid black lines) from a CFD simulation. Behind each turbine the wake can be seen as a region of low and fluctuating wind speed. The thin black line indicates the centre position of the wake and thus represents the meandering of the wake.

The reduced wind speed and the increased turbulence in the wake affect the power production and increase the fatigue loads of wake-affected wind turbines. From field observations the reduction in annual power production is on the order of 5-20% (Larsen et al. [40], Schepers [46], Barthelmie et al. [22, 47, 48], Hansen et al. [49], Larsen et al. [50]) for typical wind farm configurations, see figure 2.2a.

The increased turbulence experienced by a wake-affected wind turbine consists of two main contributions. The first contribution is an increased level of small-scale turbulence due the breakdown of tip vortices and turbulence generated by the shear layer in the edges of the wake (both terms are explained later in this section). The other contribution comes from the meandering of the wake deficit relative to the position of the wake-affected rotor. This term is referred to as “apparent turbulence”, to emphasize that it is generated by a different mechanism compared to conventional turbulence. The apparent turbulence has a larger length scale compared to the shear layer continuation. The size in terms of turbulent kinetic energy of the two contributions is often comparable, and is a function of the atmospheric state, the topography and the layout of the wind farm (see figure 7.17). This is important as the various components of the wind turbine are sensitive to different length scale of the oncoming turbulence. Some loads are driven by small-scale turbulent fluctuations (i.e the shear layer generated wake-added turbulence), while other loads are driven by rotor integrated momentum variations (i.e. the apparent turbulence due to wake meandering). Both categories of loads are affected by wake operation. The rotor integrated loads, however, increase more as they are sensitive to situations generated

specifically by the meandering wake deficit, which creates partial wake situations at the wake-affected rotor (see fourth turbine in figure 2.1). The fact that the increase in fatigue loads due to wake operation varies between components are shown by Larsen et al. [20], Vølund [29] and Schmidt et al. [51]. Results from an unpublished investigation of load of turbine operating in waked conditions from Horn Rev wind farm are presented in figure 2.2b. The blade edge fatigue (which is sensitive to small-scale turbulence) is relatively insensitive to wake operation and only increase about 15%, whereas the tower top yaw moment (sensitive to turbulent scales of the same size as the rotor) is more sensitive and increases by about 60%.

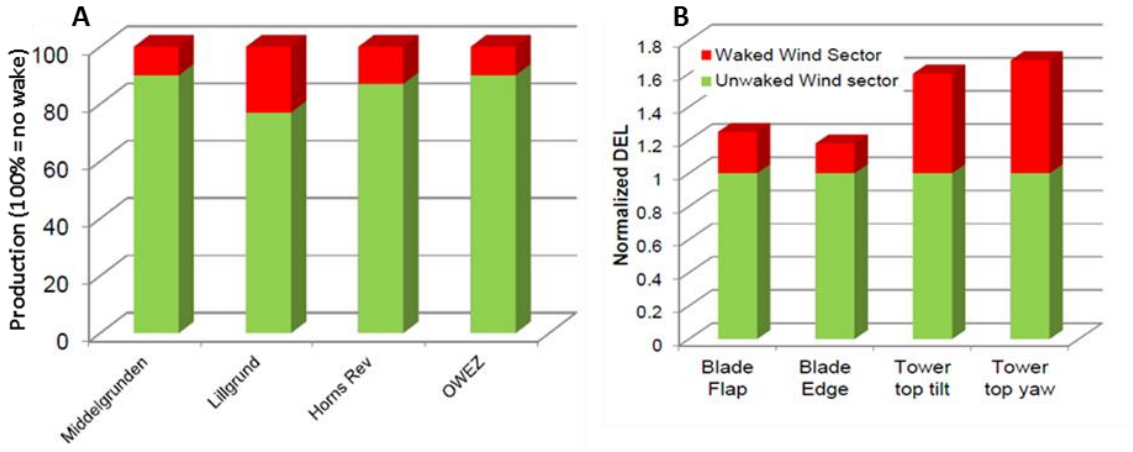

Figure 2.2: Effect of wind turbine wakes on power and fatigue loads. Figure from an internal study conducted at Vestas wind systems based on publically available data.

As a consequence of the fact that some of the wind turbine loads are driven by large scale wake dynamics, it is not sufficient to describe the wake as long term averages of wind speed and turbulence intensity, as this does not accurately capture the effect of wake on wind turbine loads. Instead, the random large scale movements of the wake need to be taken into consideration to capture the dynamic effects (Larsen et al. [10], Thomsen and Madsen [13] and Larsen et al. [40]). This can be achieved by separating the wake into two fundamentally different processes; wake deficit evolution and wake meandering caused by large scale atmospheric turbulence. This is commonly referred to as *the split of scales,* since it is assumed that turbulent eddies below a certain size mainly affect the wake deficit and large eddies affect the wake meandering. Typically this cut-off is taken to be in the order two rotor diameters (D) (Larsen et al. [52] and Müller et al. [53]). Furthermore, experimental results by Bingöl et al. [30], Trujillo et al. [31] and España et al. [54, 55], suggest that the evolution of the wake deficit is independent of the large scale wake meandering, allowing the two processes to be treated separately.

2.1 Wake deficit

The wake deficit of a wind turbine evolves in several fundamentally different stages. As the air approaches the wind turbine the velocity decrease and the pressure is increased by the presence of the rotor. When the air passes the rotor the pressure and velocity is abruptly reduced due to rotor induction. A region of large velocity gradients is created in the outer part of wake deficit, where the unaffected air meets the wake deficit, commonly called *the wake shear layer*. Due to the large velocity gradients, the ambient turbulence is amplified and the shear layer becomes highly turbulent. The wake shear layer is the key driver for the increased turbulence level in the wake, and the recovery of mean

velocity by turbulent momentum transfer into the wake. In the tip and root regions of the three rotor blades a stable coherent vortex system is formed. Also some weaker bound vortices are created along the blades due to the radial gradient of lift force. The bound vortices normally diffuse close to the rotor and create some extra small-scale turbulence.

The pressure field gradually recovers over the first 1-2D of flow after the turbine (Crespo et al. [15], Schepers and Snel [18] and Eecen et al. [56]). As a result the flow experiences a braking force due to a positive pressure gradient in flow direction. This causes the air in the wake to decelerate and the wake deficit to expand. The location where the pressure field has recovered coincides with the location in the wake with the lowest mean velocity. This is commonly referred to as the end of the *near-wake region*, see figure 2.3. The turbulent stresses in the flow cause the tip and root vortex systems to become unstable and break down. This usually occur within the first 2D of flow (Troldborg [57], Ivanell [58]), but the vortex system can exist longer downstream in flows with low ambient turbulence (Troldborg [57], Ivanell [58], Sanderse [59], Odemark et al. [60]). The wake shear layer (the green region in figure 2.3) expands with downstream distance, both outwards into the surrounding flow by turbulent diffusion and entrainment of air outside the wake, and towards the centre of the wake by turbulent diffusion.

After the initial phase of wake recovery, dominated by inviscid pressure effects, the wake recovery due to turbulent transfer of momentum into the wake from the surrounding air is the main effect. The wake shear layer continues to expand and reach the centre of the wake after 2-5D (Vermeer et al. [6] and Crespo et al. [15]). Initially the turbulence in the shear layer intensifies as the production of turbulence is greater than the dissipation. Maximum turbulence intensity is reached 2-6 D after the rotor (Keck et al. [36]). From CFD simulations it can be seen that this distance is dependent on both rotor induction and ambient turbulence intensity level. Once maximum turbulence intensity in the wake is reached, the turbulence in the wake can be considered to have reached quasi-equilibrium with the mean flow field. This equilibrium is important in wake modelling as it implies that the Boussinesq assumption (see Panton [38]) can be used to model the wake turbulence without including a transport equation for the turbulence. This enables the use of simple eddy viscosity closures. It should be noted however, as pointed out by Réthoré [61], that inclusion of the ABL turbulence still violates the Boussinesq assumption due to the difference in length scales.

At sufficiently large downstream distances (depending on the ambient conditions), both the velocity and the turbulence of the wake deficit profile assume a near Gaussian shape due to the turbulent mixing. At this stage the wake does not reflect any details of the wake-emitting turbine, instead the wake distribution is close to self-similar and can be assumed to be independent of rotor characteristics except the aggregated thrust.

The three phases of the wake described above is commonly referred to as:

- *The near-wake,* where the pressure field behind the rotor recovers, the vortex structures breakdown and the shear layer expands towards to centre line of the wake. There are two different definitions for the location where the near-wake ends. The most common definition is that the near-wake end when the axial pressure gradient has recovered. This is the definition used in this thesis. The other definition refers to the region where the pressure behind the rotor is recovering as the *expansion region*, and the end of the near-wake is taken to be when the shear layer has met the wake axis.
- *The intermediate region,* where the shear layer erases the traces of the turbine which generated the wake (e.g. the distributions of rotor induction) by turbulent diffusion and the wake approaches Gaussian shape.

- *The far-wake,* where the wake is approximately of Gaussian shape and both the turbulence and velocity profiles are close to self-similar (due to ABL shear the wake never becomes completely Gaussian and self-similar). In this region the specific turbine which generated the wake does not influence the wake dynamics. Instead, it is possible to describe the wake distribution by a few parameters such as radius, thrust, wind speed and turbulence intensity.

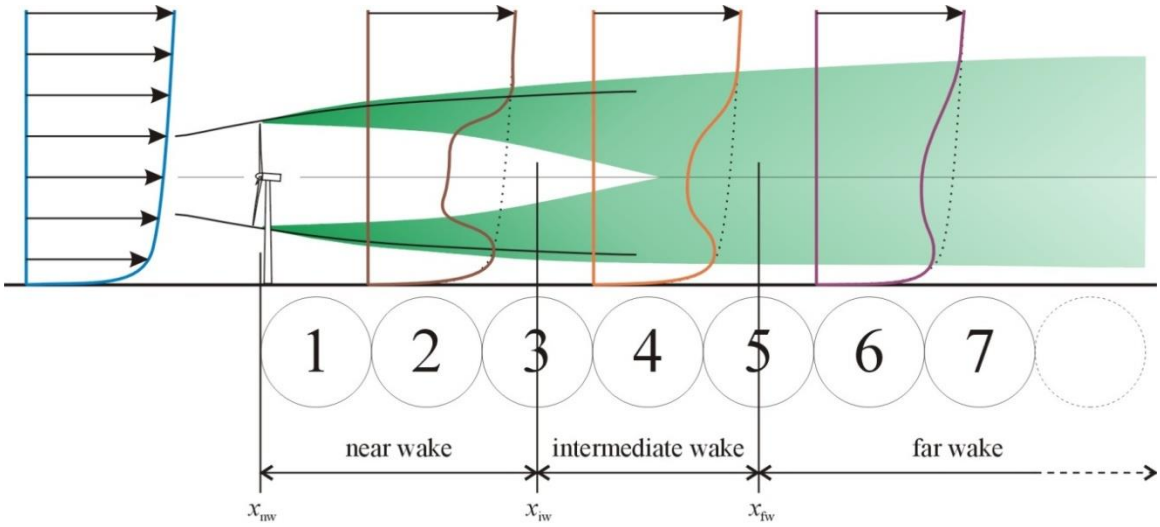

Figure 2.3: The various regions of the wind turbine wake deficit (courtesy of ECN, Eecen at al. [56]).

2.2 Wake meandering

Wake meandering refers to the large scale movement of the entire wake deficit. The phenomenon of random motion of the whole wake deficit was observed in field observations already in the 1980s by Ainslie [62, 63] and Taylor et al. [64]. However, due to the complexity of isolating the wake meandering, it was only recently that field studies using LIDAR, wind tunnel experiments and CFD modelling enabled detailed studies of the meandering process.

Based on field observations from inflow measurement conducted on the Tellus research turbine at Risø and inflow measurements with a pitot tube on the NM80 turbine in the Tjæreborg wind farm, Madsen et al. [28] and Larsen et al. [52] proposed to model the wake meandering by modelling the wake deficit movement as a passive tracer in the turbulent wind field, i.e. that the wake movements follows the large scale eddies without influencing the oncoming turbulence field. This is consistent with the method used to model dispersion of smoke from a chimney. A difference between the wind turbine wakes and chimney smoke is that the wake has a lower momentum than the surrounding air. This difference is challenging to the passive tracer assumption.

Medici and Alfredsson [65] proposed another source of underlying physics which could govern the wake meandering. In a wind tunnel study targeted at studying wind turbine wakes in yawed inflow, Medici and Alfredsson [65] found a low frequency component in the time series of the velocity measurements. These low frequency oscillations were created by periodic vortex shedding of the highly loaded rotor (effectively the same as seen on a bluff body), and therefore a conclusion of the paper was that these oscillations might be a probable cause of wake meandering.

Further studies were conducted by Bingöl et al. [30] and Trujillo et al. [31], where a backwards facing LIDAR mounted on the nacelle of a full scale wind turbine was used to measure the wake in a reference frame following the incoming wind direction. In post-processing of the recorded data it was possible to find the wake centre and correlate the movements of the wake centre to the incoming large scale turbulence. España et al. [55, 66] and Aubrun et al. [67] used wind tunnel experiments to study wake movements. Both studies concluded that wake deficit meandering is governed by the oncoming turbulence and is correlated to the large eddies. Keck et al. [36] showed numerically that although wakes follow the wind as a passive tracer, the transport velocity of the wake deficit is lower than the ambient wind speed. By studying the correlation of the wakes centre position in several different cross sections in the wake, the transport velocity of the wake deficit was found to be a function of the average velocity in the wake and the ambient wind speed.

Currently the passive tracer analogy has reached academic acceptance as an appropriate model for wake meandering. However, further research is needed to determine which scales of the incoming turbulence affect the wake meandering. Under the assumption that only turbulence eddies which are sufficiently large to affect the whole cross section of the wake in a similar manner contribute to wake meandering, and the notion that smaller eddies only affect the wake deficit evolution, the wind turbine rotor may be thought of as a Bessel filter (Goodman and Gustafson [68]) acting on the incoming turbulence. In the frequency space the Bessel filter of a circular disc of 1D almost completely removes the influence of eddies smaller than 2D, includes an increasing fraction of the scales from 2 to 5D, and scales over 5D remain unaffected by the filter. Müller et al. [53] used a combination of Particle image velocimetry (PIV) and hotwire anemometry to yield sufficient temporal resolution of the wind tunnel data to enable a study of the spectral characteristics of the wake meandering. Preliminary results suggest that turbulent eddies larger than 2-3D governs the wake meandering process and that scales larger than 2D have similar influence as predicted by the Bessel filter function. These values correspond well to the cut-off frequency as proposed by Larsen et al. [52].

2.3 Key parameters for wind turbine wake evolution

The wind turbine wake dynamics and its interactions with the ABL, the surrounding turbines and topography is a multifaceted and complex problem. The fact that many parameters are important to accurately describe the wake physics is a challenge in the field of wind turbine wake modelling. Furthermore, many of the parameters are correlated and vary together in nature which makes it difficult to isolate one parameter from field measurements. Therefore wind tunnel data or higher-order CFD modelling are often used to study the effects. A further complication is that the wake dynamics to a large extent are governed by the evolution of turbulence in the wind turbine wake, which by nature is highly non-linear. Consequently, the influence of the single parameters cannot be considered independently. This section gives a brief overview of the wake physics with regards to the most important parameters affecting the wind turbine wake evolution.

As described in the next section, the turbulence intensity is a key quantity when describing wake evolution. However, turbulence intensity alone is not sufficient to describe the properties of atmospheric turbulence. The ABL contain turbulent eddies with a large variation in length scales ranging from 10^{-6} to 10^{4} meters. Large anisotropic turbulence structures (eddies) are created from the mean flow gradients. These large eddies are in turn stretched, deformed and tilted resulting in turbulence amplification and transfer of turbulence energy to smaller scales and an increasing isotropy. The pattern is repeated from the largest scales down to the smallest scales where the turbulence is dissipated to

heat by viscous effects; this process is commonly referred to as the turbulent energy cascade (Tennekes and Lumley [69]). This is important to wake dynamics due to the split in scales, as discussed above. The large eddies influence wake meandering and the small-scale affect wake deficit evolution. Many of the factors which influence wake evolution are related both to the amount of turbulence (turbulence intensity) and distribution of turbulence in various length scales present in the flow. This is often represented by the turbulent energy spectrum, see figure 2.4. The total area of the turbulent energy spectra represents the variance of turbulence. In general; complex terrain, obstacles and wind turbine wakes generate small-scale turbulence (Madsen et al. [70]), whereas buoyancy effects on the turbulence due to atmospheric stability or mesoscale phenomena influence large scale turbulence.

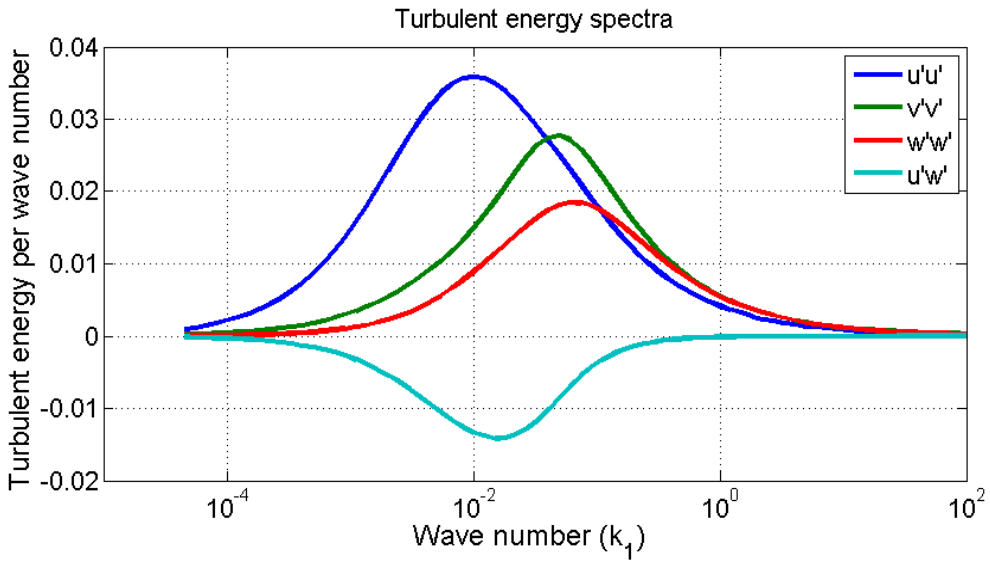

Figure 2.4: The spectral distribution of turbulent energy in a neutral atmosphere in flat terrain.

2.3.1 Ambient turbulence intensity level

The ambient turbulence intensity is the most important parameter for wake evolution. The interaction between the wake shear layer and the ambient turbulence dominates the process of the wake deficit diffusion, see figure 2.5 and 2.6. Furthermore the large scale wake meandering is proportional to the turbulence intensity under neutral atmospheric conditions. The definition of turbulence intensity in wind power applications is,

$$TI = \frac{std(u)}{U} \tag{2.1}$$

The effect of turbulence intensity on wind turbine wake effect is well documented. Larsen et al. [40], Schepers [46], Barthelmie and Jensen [48], Hansen et al. [49] and Troldborg [57], amongst others, showed that increased turbulence intensity led to faster wake deficit recovery. Barthelmie [47] gives a quantitative approximation of 1-2.5% increased power production due to reduced wake loss from a 1% increase in turbulence intensity based on the Horns reef and the Nysted wind farms. Experimental work by España et al. [55] and Aubrun et al. [67] showed that the wake meandering increases with higher turbulence intensity. This was also confirmed in numerical work by Keck et al. [36], see figure 2.7.

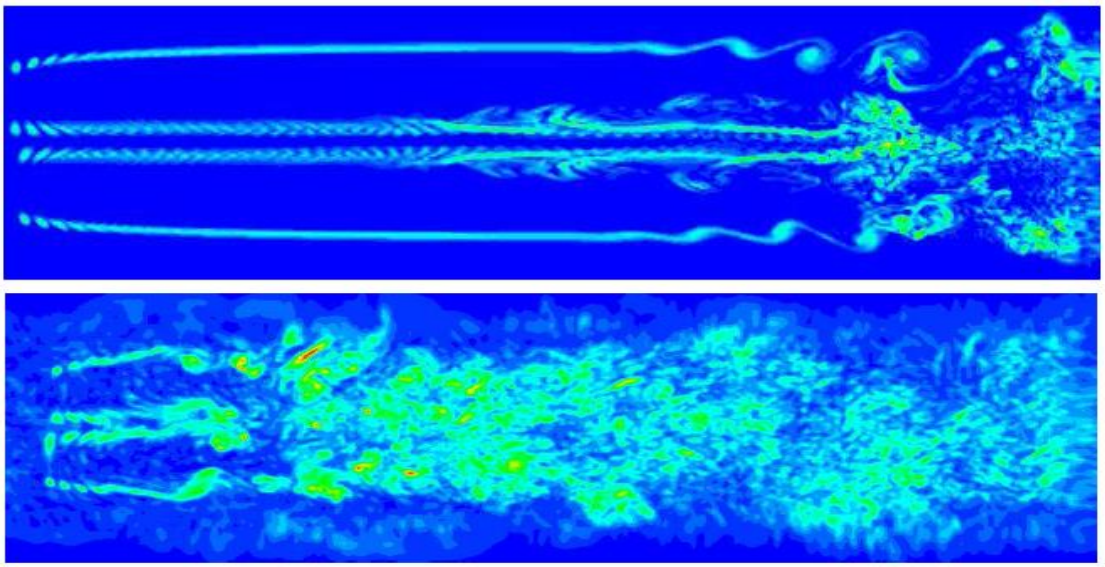

Figure 2.5: Wake evolution as iso-contours of vorticity from CFD simulations of the wake behind an NM80 wind turbine operating in wind speeds of 10m/s. In the top figure the ambient flow is laminar and in the bottom figure the ambient turbulence is 9%. Courtesy of Troldborg [57].

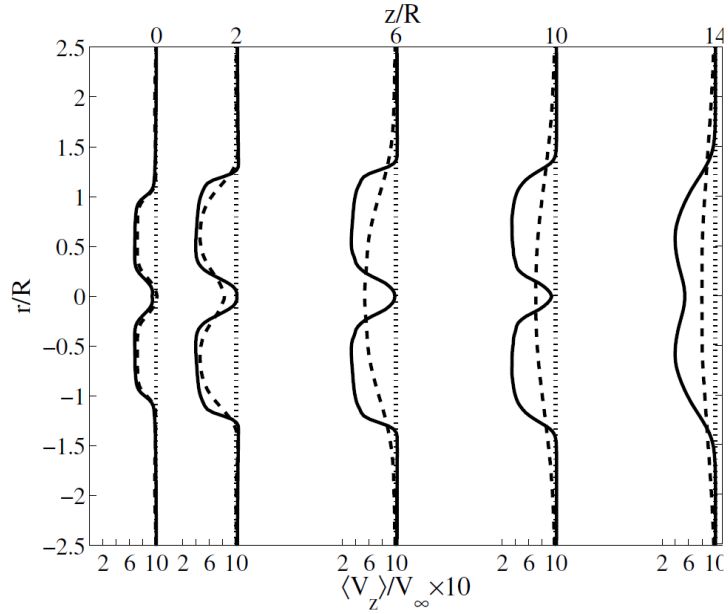

Figure 2.6: Comparison of downstream evolution of the azimuthally and time averaged velocity field in the wake of an NM80 wind turbine operating in laminar conditions (solid lines) and in a flow with 9% turbulence intensity (dashed lines). Courtesy of Troldborg [57].

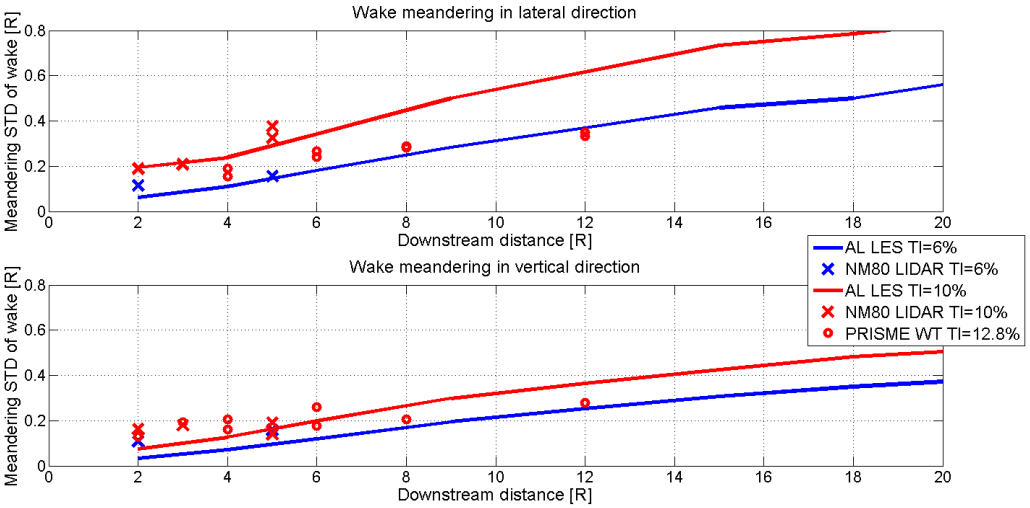

Figure 2.7: Wake meandering, given as standard deviation of the wake centre displacement, as function of ambient turbulence intensity in neutral atmospheric conditions.

2.3.2 Atmospheric stability

Atmospheric stability is related to the temperature distribution with height, which has an important effect for the turbulence in the atmosphere due to buoyancy effects. In a stable atmosphere the buoyancy effects suppress vertical fluctuations of the air, and in an unstable atmosphere the vertical fluctuations are enhanced. The neutral condition, in which buoyancy effects are negligible, are only experienced a fraction of the time in the atmosphere (Sathe et al. [71]). The stability of the atmosphere is dictated by the direction of the vertical heat flux. The transfer of heat from the surface upwards to the air leads to an unstable ABL, and when the heat flux is directed downwards the air becomes stratified and the ABL stable. In simple terms, this can be expressed as when the surface is warmer than the air an unstable atmosphere will develop and when the surface is cooler the ABL will be stable (Stull [72]).

The vertical temperature gradient alone is not sufficient to determine the atmospheric stability. The reason is that pressure effects on the air temperature need to be corrected for, in order to compare the relative density of air from two different layer of the atmosphere. This is done by calculating the potential temperature, θ, of an air parcel, which should be seen as the temperature the air parcel would have if it were moved adiabatically to a reference pressure, p_0.

$$\theta = T\left(\frac{p_0}{p}\right)^{R/C_p} \tag{2.2}$$

Here T and p refer to the temperature and pressure of the air parcel at its current location, R is the specific gas constant and C_p is the heat capacity. The potential temperature of an air parcel does not change under adiabatic transport. As a consequence, if a parcel is moved upwards in the atmosphere where the potential temperature gradient is positive ($d\theta/dz > 0$), it will be cooler and heavier than the surrounding air, and buoyancy will return the parcel to its original air layer. The opposite will happen if the air parcel is moved downwards, the surrounding air would have a lower potential temperature, and the air parcel will be lighter an rise to its original air layer. This illustrates a stable atmosphere. By the

same argument a negative potential temperature gradient ($d\theta/dz < 0$) leads to an unstable atmosphere, and cases with small potential temperature gradients ($d\theta/dz \sim 0$) can be considered neutral. The change in temperature which yields a potential temperature gradient close to zero is ~6.5K/km and is referred to as the lapse rate of a standard atmosphere (Stull [72]). A similar quantity called virtual potential temperature, θ_v, exists for incorporating the effect due to humidity and condensation. θ_v is calculated and used in the same way as θ, with the exception that T is replaced by the temperature of dry air which has the same density, T_v, as the investigated air parcel.

The Monin-Obukhov (M-O) length is the most commonly used quantity to characterise the atmospheric stability,

$$L = \frac{\overline{\theta_v} u_*^3}{\kappa g \left(\overline{w' \theta_v'}\right)_s} \tag{2.3}$$

where θ_v is the virtual potential temperature, κ is the von Karman coefficient, g is the specific gravity and u_* is the friction velocity. The M-O length can be described as the height of a sub-layer where the mechanically driven turbulence due to ABL shear is more important than the buoyancy driven turbulence. This means that a large M-O number corresponds to near neutral conditions. The sign of the M-O length indicates whether the atmosphere is stable (positive) or unstable (negative). For more details see Obukhov [73] and Monin and Obukhov [74]. The physical effect due to non-neutral atmosphere is to enhance (unstable atmosphere) or dampen (stable atmosphere) the vertical turbulent fluctuations due to buoyancy effects. This in turn influences the turbulence intensity, the vertical shear of the ABL (Kirchhoff and Kaminsky [75], Irvin et al. [76], Zoumakis [77]) and the length scale of the ABL turbulence (Peña et al. [44], Sathe et al. [71] and Stull [72]).

The effect of atmospheric stability on wake evolution, turbine loads and power production has become an increasingly researched field in academia. A number of studies has documented that there is an influence by the atmospheric stability on turbine loads and power production; this is observed both in measurements (Barthelmie et al. [22], Barthelmie et al. [78], Wharton et al. [79], Schepers et al. [46] and Hansen et al. [49]) and by simulations (Larsen et al. [50], Sathe et al. [71], Churchfield et al. [80], Lee et al. [81] and Lavely et al. [82]). So far, however, few experiments conducted have been designed in such a way that it is possible to separate the effect of atmospheric stability from turbulence intensity. Keck et al. [45] isolated the effect of atmospheric stability by conducting a series of numerical simulations where the atmospheric stratification was varied, but the turbulence intensity level was maintained constant. The results showed that the effect of atmospheric stability requires a more thorough treatment than the standard approach of altering the ambient turbulence intensity levels, and that atmospheric stability influences the wake dynamics even when the turbulence intensity level is kept constant, see figure 2.8 (and figure 5.10). This effect on the wake dynamics stems from the effect of atmospheric stability on the characteristic turbulence length scale of the ABL. According to the fundamental idea of a split in scales, a change in turbulent length scale should modify the distribution of turbulent energy between the wake meandering and the wake deficit evolution for a given turbulence intensity level.

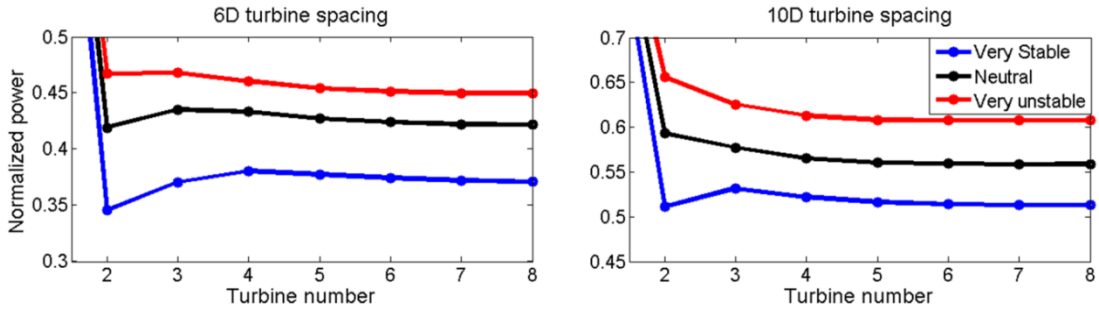

Figure 2.8: Power loss due to wind turbines wake effects as a function of atmospheric stability in a row of eight turbines predicted by the DWM model. The ambient conditions for all simulations are 8m/s wind speed and 6% turbulence intensity.

2.3.3 Wind speed, tip speed ratio and turbine induction

The ambient wind speed is important for the power production of the wind turbines, but less important for the wake evolution. It is common practice when presenting wake data to normalize the average wind speed profile in the wake by the ambient wind speed. As long as the turbine operates in such a manner that the induction and the tip-speed ratio (eqs. 2.4 and 2.5) are maintained at similar levels and the ambient turbulence intensity level is comparable, the wind speed distribution in the wake normalized by the ambient wind speed will be similar.

$$a = \frac{U_{amb} - U_{rotor}}{U_{amb}} \tag{2.4}$$

$$\lambda = \frac{\omega R}{U_{amb}} \tag{2.5}$$

The reasons for including wind speed among the important parameters to characterize wake effects are:

1) For a given site the turbulence intensity is usually negatively correlated to the wind speed, i.e. the lower the wind speed the higher the turbulence. The importance of turbulence intensity for wake evolution has been discussed above, see figures 2.5 - 2.7.

2) Atmospheric stability is less important in higher wind speeds. The ratio of mechanical turbulence to buoyancy driven turbulence increase with higher wind speeds. Resulting in larger M-O length scales and near neutral conditions, see figure 2.9 (Barthelmie et al. [47]).

3) The turbine tip-speed ratio and rotor induction are affected by the wind speed. A wind turbine operates in two characteristically different regions. At wind speeds below a certain threshold value (corresponding to the rated power of the wind turbine, typically ~10-12m/s) the turbine attempts to run optimally to generate as much power as possible from the wind. For modern wind turbines, with the possibility to operate at variable rotor speeds, this typically involves maintaining the tip-speed ratio and the induction nearly constant at optimal levels (typically at ~8 and 0.3 respectively). At wind speeds above the threshold value the turbine controller aims at maintaining rated power. This means reducing the turbine induction, which is achieved by stalling the blades or by pitching towards smaller angle of attack in combination with allowing the tip-speed ratio to fall. The distribution of induction over the rotor governs the local depth of the wake deficit, the magnitude of the shear layer gradients and the turbulence evolution of the wake deficit. Figure 2.10 shows the effect of different turbine induction on the wake deficit evolution.

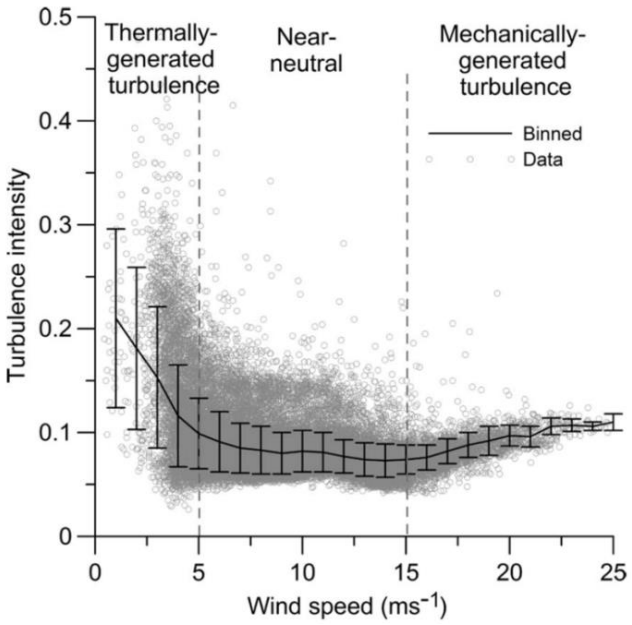

Figure 2.9: Turbulence intensity and atmospheric stability as a function of ambient wind speed. Courtesy of Barthelmie et al. [47] .

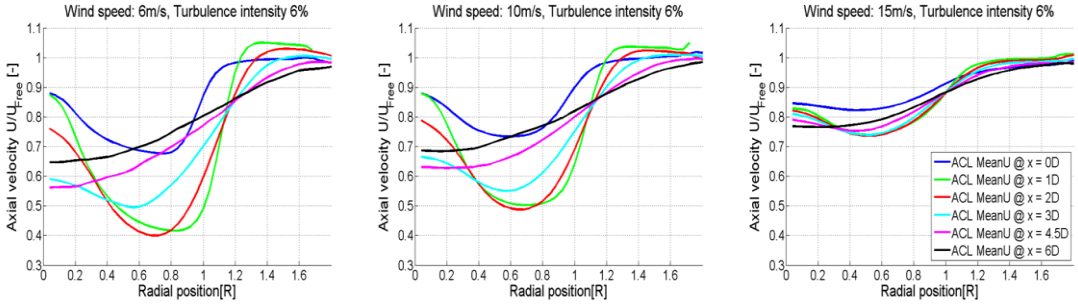

Figure 2.10: Comparison of downstream evolution of the azimuthally and time averaged velocity field in the wake of an NM80 wind turbine operating in ambient conditions of 6% turbulence intensity and wind speeds of 6, 10 and 15m/s from left to right.

The rotor induction is also linked to the strength of shed vortex structures through the distribution of lift force over the blades. The vortex structures behind the rotor are related to the radial gradient of circulation, *dΓ/dr,* where the circulation is defined as,

$$\Gamma = \frac{c_L V_{REL} c}{2} \tag{2.6}$$

The effect of the tip-speed ratio on the wake evolution in laminar flow can be seen in figure 2.11. Close to the wind turbine rotor the tip vortices are stable structures, but with higher tip-speed ratios the vortex structures are released from the rotor closer together. This leads to early interaction between the vortices, causing them to break down into a distributed vorticity sheet close to the wake-emitting turbine. As the vortex structures brakes down, small-scale turbulence is created in the wake shear layer which adds to the turbulent mixing and recovery of the wake deficit.

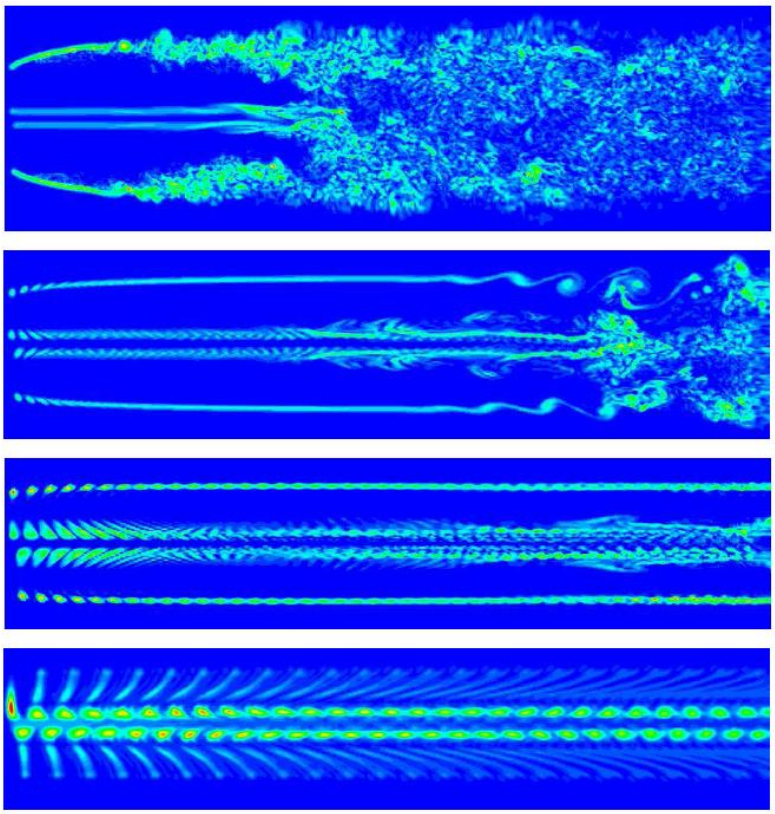

Figure 2.11: Wake evolution as a function of wind turbine tip-speed ratio illustrated as iso-contours of vorticity in a set of CFD simulations of the wake behind an NM80 wind turbine in laminar flow. The turbine is operated as tip-speed ratios of 11.78, 7.07, 5.05 and 3.21 (constant tip speed of 70.7m/s and ambient wind speeds are 6, 10, 14 and 22m/s) from the top down. Courtesy of Troldborg [57].

2.3.4 Wind farm effects and wake merging

The interaction of wakes with downstream turbines or other wakes influences the wake evolution process. The term used as two wakes starts to interact with each other is *wake merging*. A distinction is made between *lateral* wake merging, where the wakes of two turbines interact in open air, and *downstream* wake merging where an upstream wake hits a downstream turbine resulting in a combined wake being emitted downstream. Both cases are characterised by non-linear effects due to turbulence interactions between the wakes and non-symmetric combined wake deficits. Barthelmie et al. [47] mentions that there is a direct effect that wake merging limits the wake recovery due to a lower availability of momentum in the air surrounding the wake in lateral direction. The increased level of small-scale turbulence effectively diffuses the wake, creating a wide wake deficit with less severe velocity gradients. These effects have been studied experimentally by Mechali et al. [83] and Barthelmie et al. [47], and numerically by Troldborg [84], Mikkelsen [85].

When considering a wind farm, downstream wake merging can be further separated into *full* wake merging, referring to flow along the lines of the wind farm, and *partia*l wake merging where the inflow angle results in partial wake operation of the turbines in the wind farm. In full wake merging, Schepers [46] found that the 2nd turbine in the array experienced the deepest wind speed deficit, and that the subsequent turbines experienced a slightly higher wind speed. Vermeulen and Builtjes [86] and Builtjes [87] found that the turbulence intensity over a row of wind turbines reaches a saturation level after 3-4

rows through wind tunnel experiments. Both the findings regarding the wind speed deficit and the turbulence intensity where confirmed numerically by Keck et al. [39, 45], although the relative depth of the velocity deficit at the downstream turbines was found to be a function of turbine spacing and ambient conditions.

The process of partial wake merging is more difficult to describe in general terms due to the extra degree of freedom associated with the fraction of wake coverage of the downstream turbine. Troldborg et al. [88] studied the loads and wake evolution of a wind turbine operating in half wake conditions numerically. The investigation showed that partial wake operation caused non-symmetrical wakes and also influenced the direction of the wake emitted from the downstream turbine. Barthelmie et al. [47] showed that wind speed deficit at the 2nd turbine was not the deepest in partial wake operation (as seen in full wake operation), instead the power production of downstream turbines continued to decrease inside the wind farm. In terms of loads, Vølund [29] showed that the periodic loads due to the wind turbine blade passing in and out of the wake deficit of the upstream turbines resulted in higher loads than full wake situations.

Another important effect is the interaction between the turbulence in the multiple wakes. An interesting effect occurs in large wind farms. A number of rows into the wind farm, the upstream wakes have merged laterally due to wake expansion and meandering, see figure 2.12. As a consequence, the regions of free stream air between the turbines in the park have been “absorbed” by the wakes. In this situation the horizontal recovery of the wake deficit is reduced and most of the momentum transferred into the wake enters vertically. This effect is referred to as the *deep array effect* and it has been described by Frandsen [12], Barthelmie et al. [48], Meyer and Meneveau [89], Smith et al. [90], Schlez et al. [91], Andersen et al. [92], Calaf et al. [93]. After a sufficient number of turbines the flow field may be considered to be in equilibrium with the ambient conditions and the wind farm layout. This means that the oncoming flow field to all subsequent downstream wind turbines are statistically the same, which in turn means that the power production and loads of all turbines down the row after will be similar. At this state the wakes gains the same amount of momentum by the vertical flux as was extracted by the closest upstream wake-emitting turbine. As a consequence, turbine efficiency under these circumstances is governed by the vertical momentum flux which is closely linked to atmospheric stability.

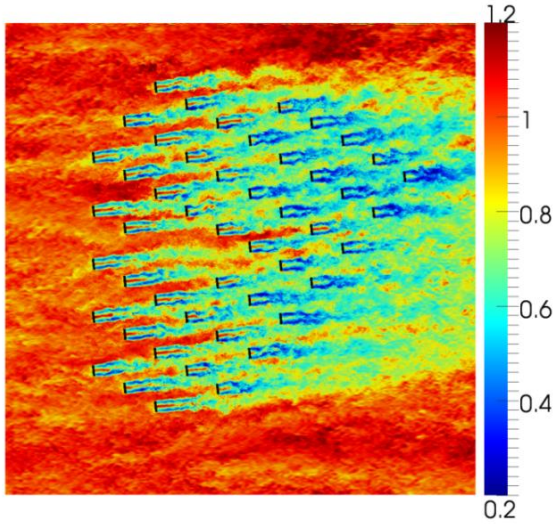

Figure 2.12: Normalized Instantaneous velocity field from a CFD simulation at Lillgrund wind farm. Courtesy of NREL.

2.3.5 Turbine hub height

The height of the rotor from the ground level influences the wake dynamics in several ways. First of all there is a direct effect by the proximity to the ground on the wake recovery. The wake recovery occurs primarily due to turbulent transfer of momentum into the wake from surrounding air. If the wake is created close to the ground the amount of kinetic energy available below the wake is limited. As observed by Barthelmie et al. [47] this reduces wake recovery. The most important indirect effect is that the turbulence intensity decreases and the turbulent length scale increases with height (Peña et al. [44]). This will in turn mean that a higher turbine experience more wake meandering, but a lower degree of wake deficit evolution at a given site. Another effect is that the wind shear is less severe with a taller tower, which leads to less effect due to non-axial inflow.

For large wind turbines there is a separate issue that the ABL scaling techniques are not valid as the rotor (or at least part of the rotor) operates outside the region referred to as the *surface boundary layer*. In the surface boundary layer the total shear stress (the sum of laminar and turbulent shear stress) is approximately constant with height (Schlicting [94]). This approximation is used to estimate the turbulent length and velocity scales, and by extension for estimations of distribution of average velocity and wind shear. The knowledge about the wind characteristics and thereby the turbine loadings and wake evolution are limited outside the surface boundary layer. This matter is further complicated by the fact that the height of the surface boundary layer varies with atmospheric stability. Peña et al. [44] state that the surface layer can vary from as low as 50m in stable conditions to several hundred meters or even kilometres under unstable conditions.

2.3.6 Non-axial inflow due to wind shear, wind veer, slopes and yaw error

Non-axial inflow conditions lead to periodic variation in turbine induction due to the differences in oncoming wind speed and angle of attack over the rotor disc. This reduces overall efficiency of the rotor and creates less severe wake deficits. Typically this will also cause one part of the rotor to have a higher induction, which causes the wake deficit to be less symmetric. Non-axial inflow directions also influence the direction of the shed wakes. From wind tunnel measurements on turbines operating with a yaw error it has been seen that the wake direction deviates more than the inflow angle to the turbine, Medici et al. [65]. This phenomenon is also described by Snel [95]. The effect on rotor aerodynamics by yawed turbine operation has been studied by Schepers and Snel [18], Mikkelsen [96], Sørensen et al. [97] and Shen et al. [98].

Wake rotation combined with the effect of wind shear will cause the wake deficit on the right hand side of the turbine (viewed from the front) to become deeper in the near-wake (Schepers and Snel [18] and Madsen et al. [99]). The wind shear also interacts with the wake shear layer. In the top part of the wake the ABL shear and the wake shear layer is aligned, which will cause an amplified turbulence production. The lower part of the wake ABL shear leads to a reduction in the mean local strain-rate, which in turn leads to a lower turbulence production. This will also influence the velocity and turbulence distribution in the far-wake. As a consequence the assumption of a Gaussian self-similar wake deficit is less correct in flow field with severe shear (Vermeer et al. [6]).

2.3.7 Terrain and Obstacles

Complex terrain and obstacles mainly affect the wake evolution by increasing the turbulence intensity level at a site, see figure 2.13 (Hattori and Nagano [100], Summer et al. [101], Jimenez et al. [102] and Helmis et al. [103]). The current IEC standard, [11], via the Frandsen model of equivalent turbulence [12] includes a first order correction to incorporate the effect by scaling the ambient turbulence by 15% when the complex terrain criteria are fulfilled.

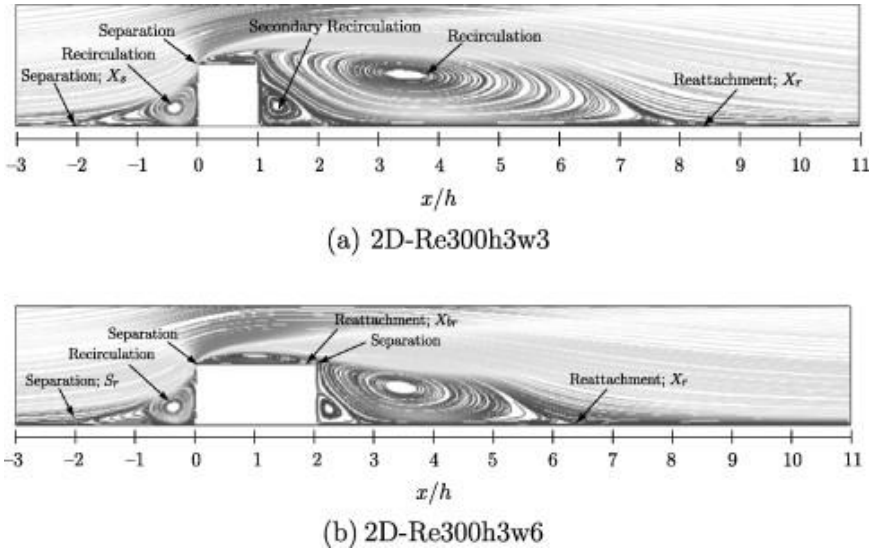

Figure 2.13: turbulence generated around an obstacle. Courtesy of Hattori and Nagano [100].

2.3.8 Mesoscale effects

Mesoscale effects refer to the meteorological conditions or systems which are on a smaller scale than the large scale synoptic weather systems. The mesoscale phenomena are commonly of length scales of 10-100km and time scales of a few hours to a day. They are created by air flow interacting with large terrain formations such as ridges, gaps or channels in mountains or large terrain slopes, or by local heating or cooling of the surface relative to the flowing air. Many of the effects are complex combinations of topography, wind speed, turbulence, and atmospheric stability.

As discussed by Hunt [104] mesoscale effects can have a strong influence on wind farm dynamics. It is difficult to generally characterize the effect of mesoscale phenomena on wind turbines and wind turbine wakes as there are such a large variety of possible situations and effects. Helmis et al. [103] and Politis et al. [21] showed that large terrain formations do not only affect the mean wind speed and turbulence; it may also cause negative shear, wind veer and non-linear effects to the wake evolution.

The mesoscale effects can be divided into being predominantly driven by terrain or by thermal effects, but often they are a combination of both. Two examples of terrain effects which influence mesoscale wind conditions are flow facing a steep mountains ridge (figure 2.14) and flow entering a large downslope from a higher altitude (figure 2.15). Both situations lead to regions of high wind speeds, severe wind shear and a significant increase in turbulence.

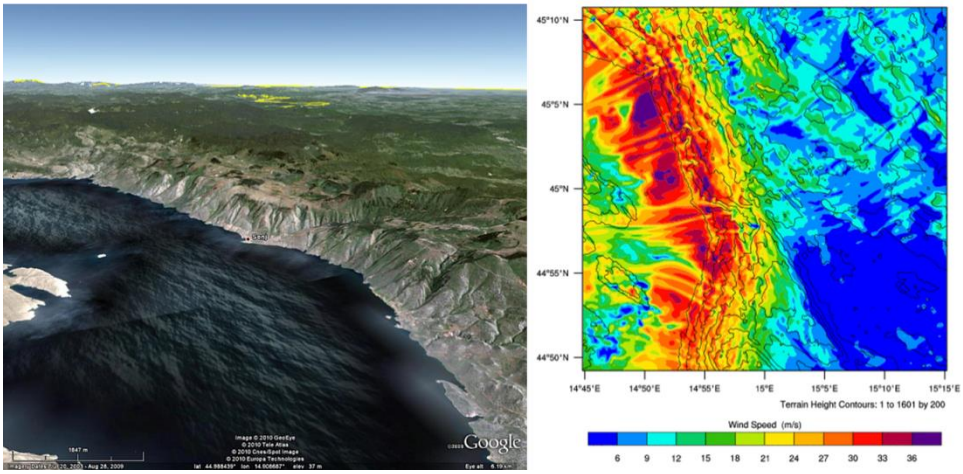

Figure 2.14: Flow facing a coastal mountain ridge. Left shows the topography (courtesy of Google earth) and the right figure shows a top view of the velocity distribution from a WRF-LES [105] simulation (courtesy of Vestas wind systems) where the wind direction is from the ocean. Clear streaks of high and low wind occur close together in the flow pattern over the ridge. This will generate a large amount of turbulence over the high plateau behind the ridge.

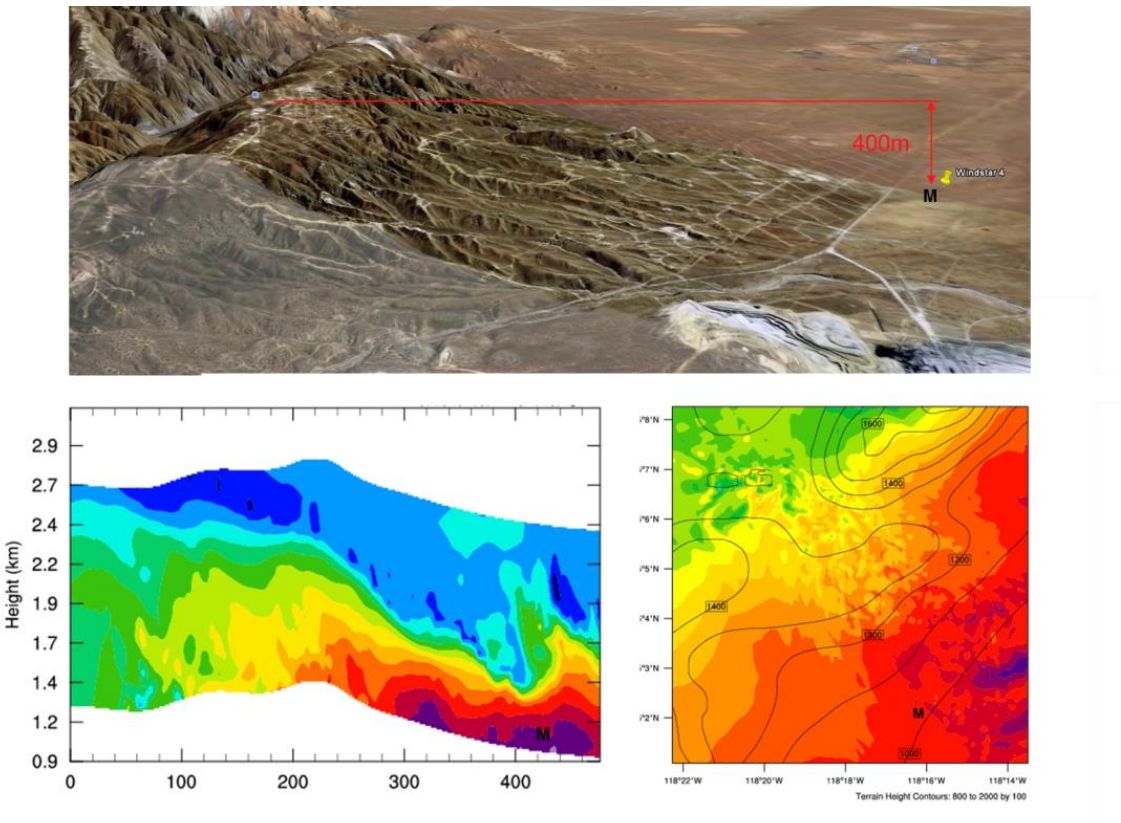

Figure 2.15: An example of downslope acceleration simulated using WRF-LES [105] (courtesy of Vestas wind systems). Top figure shows the topography (courtesy of Google earth), the bottom figures show the wind speed distribution as the air accelerates down the slope. Warm colours indicate higher wind speeds. The left figure shows the flow field in a vertical cross section and the right bottom figure shows the wind speed distribution from a top view. In the top view the increased turbulence in the flow after the acceleration in the bottom right corner.

A typical combinatory effect of terrain and atmospheric stability is up and downslope flow at low wind speeds (figure 2.16). These conditions can create situations of negative and sometimes severe wind shear. In extreme cases, downslope wind under stable conditions can lead to regions of concentrated high wind speeds situated close to ground level (a few tenths to a few hundred meters up), this phenomena is called *low level jets* and can cause large damages to wind farms.

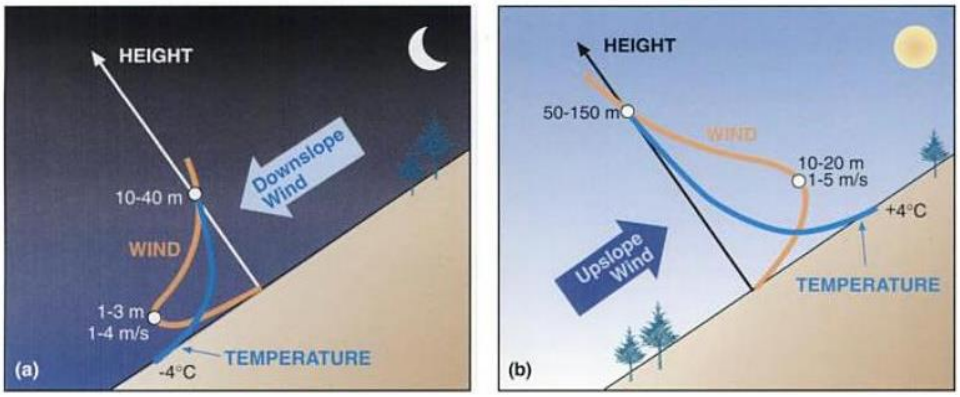

Figure 2.16: Schematics description of down (left) and up (right) slope winds which is a combinatorial effect of terrain slopes and atmospheric stability. These types of flow often generate situations of severe wind shear.

Another example of combinatory effects of terrain and atmospheric stability is the flow of a hill which is narrow in the direction perpendicular to the flow. If the hill is sufficiently low, a stable atmosphere will create a large speed-up over the hill (figure 2.17a), and create a wave pattern know as Martin de Vivies wave patter downwind of the obstacle (figure 2.18a). A neutral (or unstable) atmosphere would create a smaller speed-up on the top (figure 2.17b). However, if the hill is too high (the critical height is a function of the wind speed, atmospheric stability and the height to width ratio) the flow will go around the hill (figure 2.17d), creating von Karman vortex streets without generating a speed-up on top of the hill (figure 2.18b).

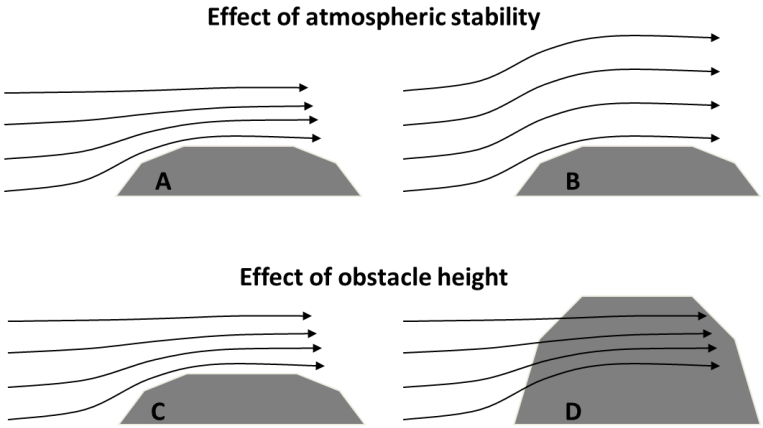

Figure 2.17: Schematics description of flow over/around an obstacle.

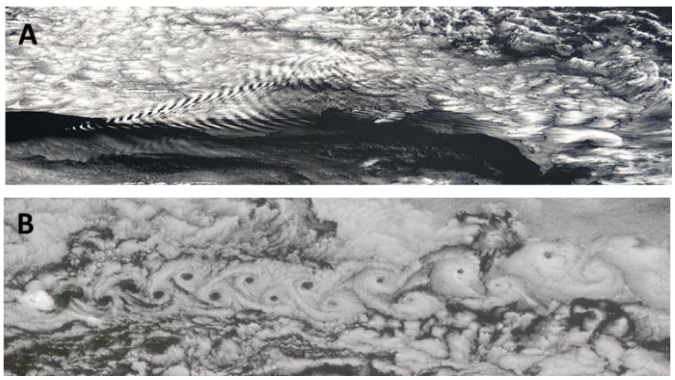

Figure 2.18: Top view of a Martin de Vivies wave pattern (A) and a von Karman street (B) occurring downwind of an obstacle in a stable atmosphere (courtesy of NASA).

There are also a number of thermal systems influencing the local climate. The most common which occur in coastal regions is the sea/land breeze cycle illustrated in figure 2.19. This cycle is driven by the difference in temperature close to the surfaces occurring when the sun radiation differentially heats the land and water due to their heat capacities. During the day the land heats up faster than the water causing the warm air over land to rise. The rinsing air creates a low-pressure which generates a wind from the ocean close to surface level. Higher up the atmosphere air is transported out towards the sea, closing the circulation cell. At night the reverse circulation occur as the sea water cools down slower. This may lead to a narrow windrose, and is therefore important to consider in wind farm design.

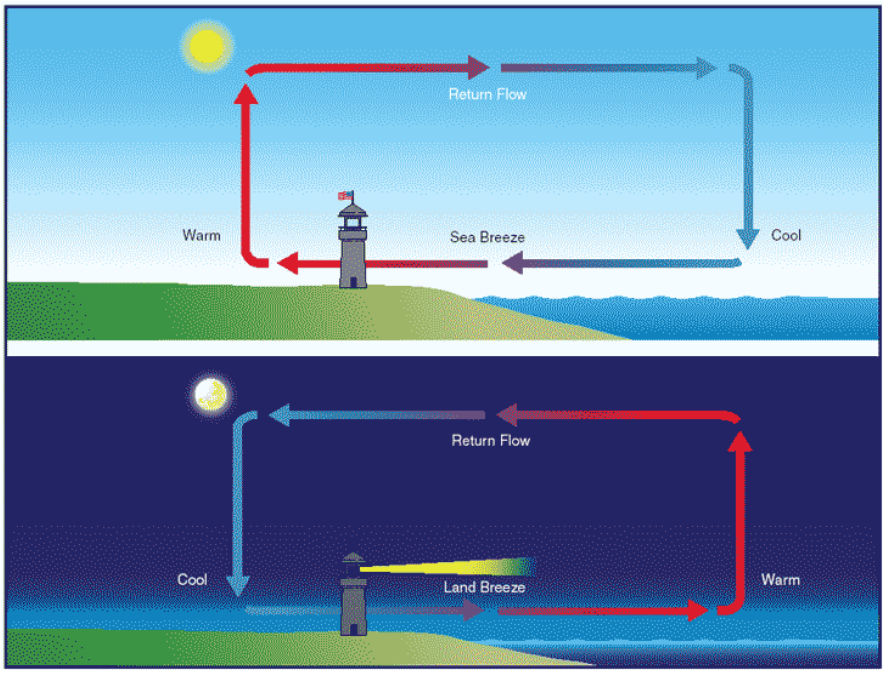

Figure 2.19: The sea and land breeze cycle driven by the temperature difference at surface level between the ocean and the land mass over 24 hours.

3 Review of wind turbine wake modelling

The ability to accurately model wind turbine wakes and the wake interactions with the surrounding topography and the ABL is an important aspect of individual wind turbine design and micro siting. The field of wake modelling can be divided into near-wake and far-wake applications. Near-wake modelling targets individual turbine design without including wake effects of surrounding turbines. Examples of near-wake design and research topics are: aerodynamic performance of the rotor (i.e. modelling the rotor induction), nacelle and spinner design and nacelle anemometry. The objective in far-wake modelling is to capture loss of production and increase in loads of wind turbines operating in a wind farm, see figure 2.2. Improved far-wake modelling capability enables improvements in wind farm design and the development of wind farm control strategies to reduce the loss of power and the wake induced loads. Furthermore, it will also enable the components of the individual turbines to be design based on loads which correspond better to the loads experienced by turbines situated inside a wind farm.

In numerical modelling it is necessary to compromise between model fidelity and computational time. This is particularly true for wind turbine wake modelling due to the large differences in turbulent length scales influencing the wake dynamics. Reduction of wake model complexity is commonly achieved by reducing computational domain and/or temporal and spatial resolution and, depending on the application, simplifying the underlying physics. These model simplifications have to be made with careful consideration to the physical effects and detail level required for the particular model application.

As a consequence of the complexity of wake modelling and the wide range of wake modelling applications, there are a variety of specialized wake models designed to tackle specific wake problems. The available wake models can be categorized based on fidelity classification.

3.1 High fidelity models

Many applications require a high level of detail in order for the results to be reliable. In general this is the case for applications in the near-wake as vortex shedding from the blades or the initial interaction between atmospheric turbulence and the wake are of interest. Models of this type include few model assumptions, however, as a consequence they are generally too computationally expensive to use in industrial applications for large scale problems. Instead, the usage is research oriented, where relatively few interactions are conducted and high computational times are acceptable to ensure that the relevant physics is well represented. The results are typically used to gain insight to flow phenomena close to the rotor and in the near-wake, or to calibrate and validate lower order wake models for far-wake modelling.

The flow field of current high fidelity models is based on the N-S equations. For accurate representation of the turbulence structure and length scales in the wake, the turbulence is often resolved by the large eddy simulation (LES) method (Pope [106]) or by a hybrid of Reynolds Averaged Navier Stokes (RANS) and LES method. However, also, eddy viscosity closures of turbulence in RANS calculations are frequently applied. Direct numerical simulations (DNS) are still not feasible to use for wind turbine wakes due to the high computational demand (see chapter 4).

In terms of rotor representation, the most straight forward approach is to model the rotor geometry as solid boundaries in the CFD domain. The benefit of doing so is that very few assumptions need to be made. The geometry of the blades is used to find the pressure distribution lift and drag distributions around the airfoils, and the complex three dimensional effects are accounted for directly in the simulation. The drawback is the high mesh requirement to resolve the boundary layer and to predict the stall characteristics and rotational effects of the blades. Resolving the boundary layer on the blade using an LES approach is computationally expensive, and commonly full rotor simulations require the researcher to use unsteady RANS (URANS) or hybrid RANS-LES, where an eddy viscosity model is used close to the surface. For research aimed at near-wake, or even single wake evolution, this is an expensive but feasible approach with modern computational resources. Examples of wake investigations conducted with full rotor simulations are the work of Sørensen et al. [33], Zahle and Sørensen [107, 108], Réthoré et al. [109], Wussow et al. [110] and Hahm et al. [111].

However, for high fidelity representation of the wake interactions with the ABL or multiple turbines in wind farms, the use of physically represented rotors is still too computationally expensive to be practical. Furthermore, it is usually necessary to resolve turbulence by LES representation to accurately capture the effect of the wide range of turbulent length scales present when the wake interacts with the ABL and downstream turbines. This led to the development of the actuator line (AL) model (Sørensen and Shen [112]). The AL model is based on representing the wind turbine rotor as three rotating lines, each containing body forces to capture the influence of the individual blades on the oncoming flow. The body forces are based on local inflow conditions and tabulated blade profile data, allowing for accurate calculations of the rotor forces without resolving the boundary layer on the blades. As a consequence, the AL method is (at least) an order of magnitude less computationally expensive compared to full rotor representation. Due to the relatively low computational demand and high fidelity wake dynamics, this method has grown in popularity the last few years and a large number of wake research projects has been conducted by Shen et al. [98], Porté Agel et al. [113], Mikkelsen et al. [85, 96], Troldborg et al. [57, 88], Ivanell et al. [114], Jimenez et al. [115], Réthoré et al. [109], Keck et al. [36, 45], Andersen et al. [92] Churchfield et al. [80], and Lee et al. [81]. As this model has been used to conduct numerical experiments for low-fidelity model development in this work, a description is given in chapter 4.

3.2 Medium fidelity models

The medium fidelity models include most of the underlying wake physics, but the complexity is reduced by simplification of features less important for the application. An example is the use of time averaged physics to represent the wind turbine by the actuator disc method (well described by Mikkelsen [96]) when studying far-wake dynamics. This formulation does not represent the details of the near-wake or the vortex structure, but the physics in the far-wake and the average rotor induction is captured with acceptable accuracy. In academic research models of this kind are typically used for large clusters of wind turbines (Ivanell et al. [116], Steinfeld et al. [117], Calaf et al. [93], Migoya et al. [118]) or for investigations with a large design space (Madsen et al. [119], Smaili and Masson [120], Keck [121]). Sarlak et al. [122] and Steinfeld et al. [117] applied an AD model to study intra wind farm effects. In industrial applications these models serve as a higher fidelity option where higher detail level is required than available through the engineering models. Examples of applications could be turbine siting in complex situations (terrain, obstacles), forensic study of a wind turbine, or the effect on rotor induction as a consequence of turbine design modifications.

Like the high fidelity models most applications of medium fidelity models are based on the N-S equations, but typically less expensive methods for modelling the turbulence are used such as coarse LES, URANS and time averaged simulations using RANS. However, free wake models based on vortex segments of panel methods is also commonly used. This method is based on modelling the vortex structures of the wake and finding the inviscid flow field by using the Biot-Savart integral. The benefit of this kind of method is computational speed and ability to computationally effectively find rotor induction and near-wake flow field. The main drawback is that the wake recovery is not included in the model, making it difficult to apply for far-wake simulations. In order to be useful in far-wake calculations panel methods needs to be coupled to a viscous model to include turbulent mixing effects. Examples of such applications are Xu and Sankar [123] and Voutsinas et al. [124]. A more thorough review of vortex wake modelling is given by Vermeer et al. [6] and Sorensen [34].

3.3 Low fidelity models

Fast tools are needed for standard industrial applications related to turbine, wind farm and controller design. An average loads or siting engineer conducts on the order of 10,000 ten-minute simulations per day. This means that the engineering models need to have a computational time on the order of one second per case to be applicable. As a consequence, the engineering models are based on some form of reduced order physics to maintain manageable computational time. Due to the simplified physical description most engineering models are not applicable for use in the near-wake region.

The low fidelity wake models are either based on reduced formulations of the N-S equations, analytical approximations or empirical observations. Since the models in this model segment are based on simplified physics, the range of applicability of each model is relatively small. This in combination with the fact that the wind industry to a large extent use engineering models in the design processes, has led to the need for a large number of models. This brief overview will only mention the most common models and the ones most relevant for the research conducted.

3.3.1 Blade Element Momentum model

The most common engineering model is the Blade Element Momentum (BEM) model developed by Glauert [125], which is still the industry standard for calculating rotor induction, aerodynamic performance and turbine loads. The basis of the model is a steady-state control volume conservation of mass, momentum and angular momentum. The major assumptions made are 1) half the far-wake induction is realised at the rotor plane, 2) the wake is axisymmetric, and 3) there is no radial flow, which effectively means that the induction can be modelled by annulus. Phenomena which the original BEM theory cannot account for are handled by engineering models, such as:

- Finite number of blades and flow around the tip (Shen et al. [126])
- Break down of BEM theory at high induction (Glauert [127] and Buhl [128])
- Dynamic stall (Oye [129] and Hansen et al. [130])
- Dynamic and oblique inflow and wake inertia (Snel and Schepers [95])
- Tower influence (Bak et al. [131])

The BEM theory is well described by Hansen in “Aerodynamics of Wind Turbines” [132] and the Wind Energy Handbook by Burton et al. [133].

3.3.2 The Jensen model

The most popular model for estimating the power production of turbines placed in wind farms is the Jensen model (Jensen [134]). This model was later extended by Katic et al. [135], and is therefore sometimes also referred to as the Katic model. The Jensen model is based on conservation of the momentum deficit in the wake caused by the wind turbine. There are two main assumptions which drastically simplify the calculations; 1) the wake is assumed to have a uniform wind speed in cross flow direction and 2) the wake expands radially with downstream distance according to a fixed model coefficient "*k*". For the model to give accurate results the *k*-coefficient should be a function of oncoming turbulence intensity and atmospheric stability according to Duckworth and Barthelmie [19] and Albas [136]. The wake deficit is formulated as,

$$U_{wake} = 1 - 2a\left(1 + 2k\frac{X}{D}\right)^2 \tag{3.1}$$

$$D_{wake} = \sqrt{\frac{D_{WTG}^2 U_{wake} + (D_{wake}^2 - D_{WTG}^2) U_{amb}}{U_{wake}}} \tag{3.2}$$

where *U* and *D* refer to the velocity and the diameter. The subscripts *wake, WTG* and *amb* refer to values of *U* and *D* taken at a downstream wake location, the turbine position and in the ambient flow. Multiple wake deficits are modelled by conservation of the total momentum deficits at each downstream position,

$$\left(1 - \frac{U_{wake}}{U_{Amb}}\right)^2 = \left(1 - \frac{U_{wake\,1}}{U_{Amb}}\right)^2 + \left(1 - \frac{U_{wake\,2}}{U_{Amb}}\right)^2 \tag{3.3}$$

3.3.3 The Frandsen model

The Frandsen model of effective turbulence (Frandsen [12]) is the current IEC 61400-1 industry standard for increased turbine loads due to wake operation ([11]). This is a semi-empirical model, where the effects on a wind turbine operating in wake conditions is described as an increase of the oncoming *effective turbulence intensity* based on parametric scaling. The parameters taken into account are the ambient turbulence, the distance to the closest wake-emitting turbine and first order corrections for complex terrain and park effects. The effective turbulence is found by averaging the wake effects and incoming ambient turbulence over all inflow direction based on the site specific wind rose. The effective turbulence should not be thought of as a physical description of the turbulence (i.e. fluctuating wind speeds), but rather as the magnitude of free stream turbulence which induce the same loads on a specific component. This means that the effective turbulence for the same turbine is different for different components. This effect is taken into consideration by including the Wöhler exponent in the calculation of the effective turbulence. The purpose is to capture the fact that the different materials of the components are more or less sensitive to fatigue loading resulting from wake operation.

3.3.4 WAsP

WAsP (the Wind Atlas Analysis and Application Program) is a software package developed by Risø-DTU to model wind resource for micro siting of wind turbines (WAsP [137], Mortensen et al. [138]). The flow model is based on the linearized N-S equations (Corbett et al. [139]). This allows for fast numerical simulations in large computational domains. An issue raised is the performance in complex terrain and turbine wakes, where the non-linear terms are important for accurate flow representations (Berge et al.

[140]). Wind farm production are estimated based on the Jensen model (Jensen [134], Katic et al. [135]), or from the Frandsen model for wind farm boundary layer build-up (Frandsen et al. [141, 142]) corrected for atmospheric stability by Larsen et al. [143]. A recent addition to the WAsP software is the FUGA park model, developed by Ott et al. [144], also based on the linearized N-S solution designed for modelling offshore wind farms. This model is claimed to be five orders of magnitude faster the conventional CFD and is shown to give good approximations of power predictions in wind farms. A drawback of using linearized steady-state equations is that dynamic effects such as wake meandering are not captured by the models and the wake deficit in multiple wake situations tend to become too deep as linear superposition of wake effects are used.

3.3.5 The Dynamic Wake Meandering model

The DWM model is developed with the ambition of achieving a fast low fidelity wake model where the key features affecting power production and loads of a turbine in wake operation are modelled in a physically consistent manner. Based on field observations together with physical and numerical experiments; the wake deficit evolution, the increased turbulence level in the wake and the large scale meandering have been identified as the most important effects. A fundamental assumption of the DWM model is the split in scales (described in chapter 2) which results in the decoupling of the wake deficit evolution in the MFoR from the wake meandering. Furthermore, the split in scales also govern how the wind turbine wake is coupled to the ambient turbulence. Turbulent eddies smaller than 2D is assumed to influence the wake deficit evolution and larger scales to affect the wake meandering. The first version of the DWM model was developed by Thomsen and Madsen [13] at Risø-DTU in the year 2003. Thereafter continues research efforts have been conducted at Risø-DTU to further develop and improve the model to reach a maturity level where it is applicable to use in industrial applications. An overview of the early research activities is given by Larsen et al. [10, 145]. In 2008 the DWM model was implemented into the in-house aero-elastic tool HAWC2 at Risø-DTU. The next year a comprehensive research article describing the DWM model version included in HAWC2, including numerical calibration against actuator disc and line calculations, was published by Madsen et al. [32]. This implementation of the DWM model serves as the baseline for the research presented in this thesis. The workflow of the DWM model can be seen in figure 1.2. The inlet condition is based on the ambient wind speed and turbulence together with the turbine specific induction profile. The wake deficit is based on a steady-state solution to the thin-shear layer approximation of the Navies-Stokes (N-S) equations as proposed by Ainslie [62, 63]. Wake meandering is included by a method derived from the passive tracer analogy by Larsen et al. [52]. Finally, Wake-added turbulence, affecting the loads of the downstream rotor, is implemented by an empirical formulation based on the local depth and the radial gradient of the wake deficit derived by Madsen et al. [41]. The governing equations and the numerical solution method are described in details in chapter 6.

4 Research topic 1: CFD driven engineering model development

Access to reliable high resolution reference data is vital in the process of developing lower order models. The first step of model development is to study the physics of the problem to gain an understanding of the fundamental processes to be described, and their dependence on ambient conditions. This commonly includes studying the processes by data mining, theoretical descriptions and higher-order models. Once the underlying processes are sufficiently documented and understood, a lower-order model can be formulated to mimic the most important features of the problem. After the ansatz of the lower-order model is formulated, reference data is also commonly used to calibrate some model parameters or constants in the model, and finally for model validation.

In this research the objective is to further develop an engineering model capable of modelling the evolution of wind speed and turbulence distribution in a wind turbine wake. The use of full scale measurements as reference data in the development of such a model is important but often of limited use. In the initial phase of investigating the wake physics there is a requirement of high temporal and spatial resolution of the flow field in the wake. Furthermore, it is difficult to isolate the effect of a single parameter in full scale measurement. To do so requires long and costly measurement campaigns with heavily instrumented turbines and metrological masts, where all relevant aspects to the wake dynamics is measured, to enable binning of the data to separate various effects. A further complication is that a specific site only offers limited variation of wake distances and surface roughness, which also leads to a few combinations of wind speed, turbulence intensity, wind shear and atmospheric stability as these ambient conditions are closely correlated. The same argument can be made for using field data for model calibration; it is difficult, time consuming and costly to achieve the detail required in terms of spatial and temporal resolution as well as the effect of the various ambient variables influencing the wake dynamics.

The main use of full scale field data in wake model development lies in the validation stage. In the model validation stage it is possible to perform high quality measurements of aspects captured by the wake model over a relatively short time period. The main difference in the use of field data in model development and in model validation, is that in the latter the inlet condition for the computational model can be selected based on the field data. This significantly reduces the measurement periods required.

The discussion above motivates the use of model driven development for wind turbine wake models. The use of CFD modelling to study the wind turbine wake dynamics and its evolution over a row of wind turbines has many benefits compared to field measurements. It is possible to define the specific numerical experiments required for the investigation, as numerical modelling offers full control of the topography, wind farm layout and inlet boundary conditions. This makes it possible to isolate the effect of a physical parameter and to conduct structured reference data acquisition campaigns according to design of experiment (DOE) schedule to capture variable interaction. This gives the researcher the ability to plan the time required to achieve a desired database. Furthermore, CFD model offers unparalleled spatial and temporal resolution which allows for very detailed investigations of turbulence

characteristics such as energy spectra or length scales in all directions. Similar arguments for model driven development when studying wind turbine wakes have been expressed by Sørensen [34], Troldborg [57] and Sanderse [59].

However, there are possible pitfalls associated with using CFD models as reference data sources in the development of low-order models. In all CFD models for industrial applications there are a number of model assumptions made. Common areas of simplifications are to reduce the physical effects included in the governing equations (as an example the buoyancy or Coriolis effects are often neglected), simplify the representation of geometries, the use of wall functions to represent the flow close to physical boundaries, or the use of symmetry or cyclic boundary assumptions to reduce the computational domain. An important model aspect that is subject to model simplifications in wind turbine wake dynamics is the representation of turbulence. To use the N-S equations directly by resolving all length scales of the flow (commonly referred to as direct numerical simulations, or DNS) is not a feasible as this would require a cell resolution fine enough to resolve the Kolmogorov micro scale of the flow ~10^{-6} m. Therefore all applied CFD modelling use some form of averaging of the turbulence to avoid the resolving the small-scale fluctuations. As a consequence of the model assumptions, the results of the CFD models must always be critically evaluated based on the model limitations induced by the assumptions.

In the conducted research project most of the reference data has been generated using the EllipSys3D AL model. The EllipSys3D AL model and the model simplifications made are described in the next sections. The first section motivates the need for the model simplification based on a turbulent length scale perspective. The following sections contain the technical description of the methods applied and a summary of the "*Synthetic Atmospheric Turbulence and Wind Shear in Large Eddy Simulations of Wind Turbine Wake*" article (Keck et al. [36]) describing a validation campaign of the turbulence evolution in the EllipSys3D AL model to field- and wind tunnel data.

4.1 Model simplification due to length scale considerations

The main difficulty in using CFD models for wind turbine wake modelling is to reduce the complexity to achieve manageable computational requirement while maintaining acceptable accuracy of the results. As previously mentioned, the use of DNS techniques would require a computational grid fine enough to capture turbulence scales on the order of ~10^{-6} m. If a full wind farm in the ABL were to be simulated using such a fine grid it would result in a computational grid on the order of ~10^{30} grid points. As a reference it can be mentioned that a modern super computer requires on the order of one month's time to perform a CFD simulation of ~10^{10} grid points. The use of DNS simulations are thereby clearly unfeasible for wind farm simulations for long time to come. Therefore, all applied CFD modelling use some form of averaging of the turbulence to avoid resolving the small-scale fluctuations.

4.1.1 Turbulence modelling

There are two fundamentally different methods to averaging the N-S equations, Reynolds averaging and spatial averaging. If the N-S equations are Reynolds averaged (as in RANS modelling), all turbulent scales are modelled via some turbulence closure. As a consequence, the fluctuations in wind speed due to turbulence are not resolved and only the effect of turbulence on the mean flow field is considered by keeping track of a transport equation for the amount of turbulent kinetic energy. If the turbulence is spatially filtered, on the other hand, the instantaneous wind speed is calculated as an average over

some computational volume. As a consequence, turbulence of length scaled larger than the averaging volume is physically resolved directly via the N-S equations. The scales smaller than the averaging volume, called the sub-grid scales (SGS), are modelled by a turbulence closure as in RANS modelling. The method is the basis of the large eddy simulation (LES) technique. In practice the averaging volume is the size of the computational cell.

The main difference between the two methods lies in how the turbulence is treated. The RANS modelling approach does not resolve the turbulent fluctuations. Consequently, RANS simulations suffer from limited ability to model the influence of turbulence of different length scales. As this is a very important effect when modelling wind turbine wake dynamics in the ABL, the computationally more expensive LES technique has been applied in the conducted research.

In relations to DNS modelling, the main idea of employing the LES method is that instead of resolving all scales of the turbulence, it is sufficient to resolve the scales which are relevant to the studied flow. The strength of the LES approach lies in the fact that small-scale turbulence is easier to model, as all the smaller scales of turbulence behave in a similar manner for most problems. The LES method is particularly appropriate for problems of high Reynolds number where an internal sub-range exist, Davidsson [146]. In these cases the computational grid should be made fine enough to resolve the turbulent energy into the inertial sub-range, where turbulence is highly isotropic and the energy spectrum assumes the -5/3 slope (Schicting [94]), to ensure high accuracy with a simple eddy viscosity closures for the SGS stresses.

Let us consider the problem of simulating the flow through a typical wind farm using LES. The largest length scale of the problem is the atmospheric turbulence ~10^4 m and the smallest scale of the problem is defined by the boundary layer on wind turbine blade ~10^{-3} m. This means that the resulting computational mesh would contain ~ 10^{21} cells to represent all relevant scales in the wind farm. This is still several orders of magnitude too high to handle with the current computational capacity.

4.1.2 Application of the actuator line method

To reduce the computational demand further some simplifications to the physics is required. First the wind turbine is represented using the AL model. The AL model (described in detail later in this chapter) is based on tabulated blade properties and thus do not require the boundary layer of the blades to be resolved in order to find the rotor forces. This increases the size of the smallest relevant scale of the problem from the boundary layer length scale ~10^{-3}m to the length of the airfoil width ~10^0m. A grid resolution study conducted by Keck et al. [37] concluded that the computational cells of ~10^0m is sufficient to capture turbulence scales relevant to wind turbine wakes in atmospheric flows in an LES calculation.

4.1.3 Application of synthetic ABL shear and turbulence

The second simplification is aimed at reducing the need to physically represent the largest scales of the problem. This is achieved by imposing artificial atmospheric turbulence and wind shear by distributed volume forces inside the computational domain (described in detail later in this chapter). As a consequence, the size of the wind farm dictates the computational domain instead of the size of the largest relevant scale in the ABL. If only a few turbines are to be simulated, this method allows the domain to be reduced to ~10^3 m.

A further benefit of imposing the turbulent fluctuations close to the row of turbines is that local grid refinements can be used without loss of modelling fidelity. This means applying the ~10^0 cell size in a region close to the turbines and the wake. Considering a domain shaped like a cube, the grid refinements would be required in approximately ~1% of the domain. The computational grid outside the refinement can be very coarse, and therefore be considered neglectable in this high level estimation. As a consequence this reduces the computational expense by a factor ~10^2.

When all the simplifications described above are applied to a wind farm simulation, the computational grid can be reduced from the initial ~10^{30} to ~10^{10} grid points. In this work most simulations have been conducted over single turbines or rows of turbines resulting in computational grids on the order of ~10^7 to ~10^8 grid points.

4.2 Actuator line model

The fundamental idea behind the AL method is to model the turbine rotor as three rotating lines containing distributed body forces, $\boldsymbol{f}$, in the unsteady incompressible N-S equations, eqs. (4.1) and (4.2).

$$\frac{d\boldsymbol{V}}{\partial t} + \boldsymbol{V} \cdot \nabla \boldsymbol{V} = -\frac{1}{\rho}\nabla p + \nu \nabla^2 \boldsymbol{V} + \frac{\boldsymbol{f}}{\rho} \tag{4.1}$$

$$\nabla \cdot \boldsymbol{V} = 0 \tag{4.2}$$

The main benefit of the approach is that no physical rotor boundaries, or their resulting boundary layers, needs to be resolved to get an accurate representation of the aerodynamics forces of the blades. The body forces are applied at the AL nodes distributed radially along the three lines. The forces are calculated based on local inflow condition at the AL nodes and tabulated blade data in a blade element momentum (BEM) approach, see figure 4.1.

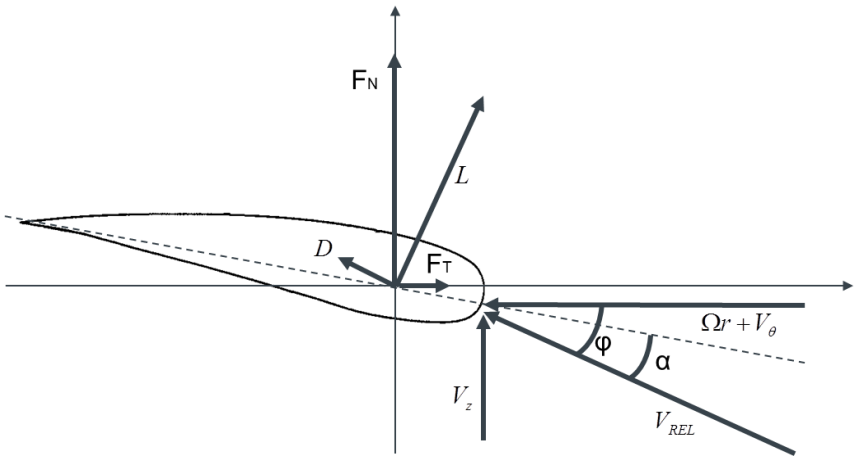

Figure 4.1:shows the properties used to calculate the contribution of the local airfoil section, L and D, to the AL forces in the global coordinate system, F_N and F_T.

The local inflow conditions to the AL node are calculated by finding the inflow angle to the plane of rotation, φ, the local angle of attack, α, and the relative velocity at the AL nodes using eqs. (4.3) - (4.5).

$$\varphi = \arctan\left(\frac{V_z}{\Omega r + V_\theta}\right) \tag{4.3}$$

$$\alpha = \varphi - \gamma \tag{4.4}$$

$$V_{Rel} = \sqrt{V_z^2 + (\Omega r + V_\theta)^2} \tag{4.5}$$

In these equations, Ω is the angular rotation of the rotor, V_z and V_θ is the rotor normal and azimuthal wind speed taken from the global flow field at the actuator node positions, and γ is the local pitch angle of the blade. The lift and drag forces in the airfoil coordinate system, *L* and *D*, is found by eq. (4.6),

$$L, D = \frac{1}{2}\rho V_{Rel}^2 c\big(C_L(\alpha), C_D(\alpha)\big) \tag{4.6}$$

where ρ is the air density, *c* is the chord length and C_L and C_D is the local lift and drag coefficients. A geometrical transformation of the local blade forces gives the forces in rotor coordinate system, eqs. (4.7) and (4.8).

$$F_T = L\sin(\varphi) - D\cos(\varphi) \tag{4.7}$$

$$F_N = L\cos(\varphi) + D\sin(\varphi) \tag{4.8}$$

As a last step the forces at the AL nodes are distributed onto the computational grid. To ensure numerical stability the forces from the AL nodes are applied in a smooth manner using a three-dimensional Gaussian smoothing function eq. (4.9).

$$\eta(d) = \frac{1}{\varepsilon^3\pi^{3/2}} e^{-(d/\varepsilon)^2} \tag{4.9}$$

In this equation η is the three-dimensional Gaussian kernel, *d* is the distance to the actuator node and ε is the force regularisation parameter (corresponds to σ √2 of a 3-dimensional Gaussian distribution) which governs the translation between forces at the AL nodes and the computational grid. ε was given the value of two mesh elements, as suggested by Troldborg [57]. The volume force experienced at a cell in the computational grid due to the ALs can be expressed by eq. (4.10),

$$\boldsymbol{f} = \frac{1}{\Delta V}\sum_{i=1}^{B}\int_0^R \boldsymbol{F}(s) \otimes \eta(d_i)\, ds \tag{4.10}$$

where $\boldsymbol{F}$ is the local force per m of an AL segments, *ds* is the length of the AL segment, d_i is a measure of the distance from the cell centre to the *i*'th actuator line which is used to give the force contribution by the Gaussian kernel, η. ΔV is the volume of the computational cell. The integration is performed along the blades to includes all AL segments and the summation is preformed over the (three) rotor blades.

4.3 Synthetic modelling of atmospheric wind shear

The atmospheric shear and turbulence is generated using the approach proposed by Mikkelsen et al. [147] and Troldborg et al. [148]. Both the mean vertical wind shear and the ambient atmospheric turbulence are modelled by distributed momentum sources in the calculation domain, i.e. $\boldsymbol{f}$ in eq. (4.1).

The method for modelling wind shear can be described as an immersed boundary technique, where volume forces are distributed in the entire domain to give a prescribed arbitrary wind shear profile. The desired wind shear profile may be given in tabulated form including wind veer or as is most common, by a power law coefficient, α, a reference wind speed, U_{amb}, and a reference height, H_{hub}, eq. (4.11).

$$U(z) = \begin{cases} U_{amb}(c_1 z^2 + c_2 z) & z \leq \Delta \\ U_{amb}\left(\frac{z}{H_{hub}}\right)^{\alpha} & z > \Delta \end{cases} \tag{4.11}$$

The model coefficients, c_1 and c_2, are used to control the near wall treatment at distances below Δ. The near wall limit, Δ, is usually taken to be equal to height ten grid cells. The actual turbulent wall boundary layer is not resolved as would be typical for wall bounded flows. Instead, equidistant mesh is preserved near the wall and the velocity profile is prescribed using a numerically well posed parabolic fit.

The description of the desired wind shear profile is used as input to a precursor calculation executed in an empty domain. The calculation of the forces is based on the discretized form of the volume integrated N-S equations, eq. (4.12).

$$A_p V_p^{t+\Delta t} + \sum_i A_i V_i^{t+\Delta t} = S_p + f_p \tag{4.12}$$

The subscript *p* refers to the studied computational cell and the subscript *i* refers to the neighbours of the studies computational node. *V* is the velocity component in the studied direction and *A* is the weighting coefficients. *S* is the source term containing the pressure gradient force and body forces, and *f* is the added body force included to yield the desired velocity. By rearranging the terms in eq. (4.12), and replacing the velocity at *p* by the desired velocity *U(z)* from eq. (4.11), an equation for the force to apply at cell *p* can be found, eq. (4.13)

$$f_p = A_p U(z) + \sum_i A_i V_i^{t+\Delta t} - S_p \tag{4.13}$$

The calculation in the empty domain is run until a steady converged flow field is reached, and the corresponding force field is stored and used later in the AL calculations to include effects of wind shear.

4.4 Synthetic modelling of atmospheric turbulence

The atmospheric turbulence is modelled by imposing fluctuating volume forces in a plane located upstream of the rotor. The forces are found via prescribed three-dimensional velocity fluctuations, generated with the Mann turbulence model (Mann [42, 43]). The grid used to generate the Mann turbulence does not generally match the CFD gird used in the LES simulation (for practical reasons the Mann grid is usually coarser). As a consequence the fluctuations at the location of the nodes in the CFD grid are found by interpolation in the Mann turbulence box. The Interpolation is carried out in two-dimensions in-plane due to the difference in resolution or location of the nodes, but also between the planes of the Mann turbulence box as the Mann planes are generally not aligned with the location of the turbulence plane in the CFD grid. A consequence of the interpolation process is that less turbulence is realized in the CFD domain than prescribed by the imposed synthetic turbulence in the high frequency part of the turbulence spectra (this is shown in figure 4.3). To compensate for the reduced turbulence due to interpolation the velocity fluctuations are scaled by a *turbulence amplification factor*, eq. (4.14),

$$u_i' = u_{i,Mann}' C_{Turb\ amp.} \tag{4.14}$$

in which u_i' is the turbulent local velocity fluctuation in direction *i* and $C_{turb\ amp}$ is the turbulence amplification factor. The fluctuations are introduced to the CFD simulation as volume forces according to one-dimensional momentum theory, eq. (4.15).

$$f_i' = \dot{m} u_i' + \rho A \varepsilon \frac{du_i'}{dt} \tag{4.15}$$

Here *A* is cross-sectional area of the cell in the computational grid, ρ is the air density and $\dot{m}$ is the local mass flow though the cell. As with the force terms of the AL model, the forces need to be introduced into the CFD calculations in a smooth manner to maintain numerical stability. The forces are therefore distributed in the flow direction by a one-dimensional Gaussian smoothing function. The regulatory distributions parameter, ε, is selected to have the same value as in the AL force smearing and is thus equivalent to two grid cells. The volume force experienced at a computational cell in the computational domain is described by eq. (4.16),

$$\boldsymbol{f} = \frac{1}{\Delta V} \boldsymbol{f}' \otimes \frac{1}{\varepsilon\sqrt{\pi}} e^{-(d/\varepsilon)^2} \tag{4.16}$$

where *d* is the distance in flow direction from the centre of the computational cell to the node in the turbulence plane causing the fluctuating force, and ΔV is the volume of the computational cell.

4.5 Post-processing of actuator line data

The LES AL simulations are used to study the wake dynamics to enable further development and calibration of the DWM model. A key assumption in the DWM model is that there is a split in the effect of ambient turbulence of different length scales. Small-scale turbulence is assumed to affect the wake deficit evolution in the MFoR, and large scales dictates the wake meandering. The methods to model these two effects in the DWM model are separated and assumed independent of each other. The wake deficit evolution, without meandering effects, is governed by the steady-state thin shear layer equations and is a function of input conditions and downstream position. The dynamic large scale effects of wake meandering is superimposed on top of the resulting wake deficit. In order to validate these two components of the DWM model individually the dynamics of the wake meandering needs to be extracted from the AL simulations.

Wake meandering is defined as the stochastic movements of the wake deficit due to large scale turbulence. In this work the wake meandering is quantified as the standard deviation of a time series of the wake centre position. The wake centre position is found by calculated the centre of gravity (COG) of the wind speed deficit as proposed by Mikkelsen et al. [149]. The procedure of calculating the COG starts by analysing high resolution and high frequency data in planes perpendicular to the mean flow direction, in this work 10Hz data of 0.04R in-plane resolution is used. The wind speed deficit is filtered by a threshold value, $C_{Threshold}$, to reduce the effect of small-scale turbulence by eq. (4.17).

$$\widehat{U}_{Def} = \begin{cases} 0, & \frac{(U(z)-u)}{U(z)} < C_{Threshold} \\ \frac{(U(z)-u)}{U(z)}, & \frac{(U(z)-u)}{U(z)} \geq C_{Threshold} \end{cases} \tag{4.17}$$

where *u* is the instantaneous local axial velocity from the EllipSys3D calculation, *U(z)* is the imposed mean shear as a function of height. The COG is calculated by integrating the filtered deficit in a circular region around the centre line of the wake (i.e. the axis that starts at the hub of the turbine) and two rotor diameters in radial direction, eq. (4.18)

$$COG_i = \frac{1}{A}\int_0^{2R} \widehat{U}_{Def} r_i \, dA \tag{4.18}$$

Where the subscript *i* indicate if lateral or vertical meandering is studied, r_i is the location of the filtered deficit value and *A* is the total integration area.

Knowing the wake centre position at each time step enables for a detailed study of the wake deficit evolution in a Lagrangian coordinate system, i.e. following the wake centre. This is referred as the wake deficit in the MFoR. To be directly comparable to the DWM deficit module, the wake properties are averaged in azimuthal direction over angular segments of thickness corresponding to the grid resolution of the AL simulations (0.04R). The main benefit in analysing the wake in this manner is that it gives a one to one comparison to the DWM deficit module.

4.6 Summary of research article I: Synthetic Atmospheric Turbulence and Wind Shear in Large Eddy Simulations of Wind Turbine Wake

4.6.1 Research objective:

To verify that the method used to impose synthetic atmospheric shear and turbulence as distributed volume forces in the EllipSys3D AL model is appropriate for wind turbine wake simulations.

4.6.2 Motivation:

In order to use the EllipSys3D AL model for wake investigations and DWM calibration/validation, it is required to validate the ability of the proposed method for imposing synthetic atmospheric turbulence in the simulations. The AL method has been validated in terms of rotor induction (Troldborg [57], Ivanell [58] and Sørensen and Shen [112]) and wake wind speed and turbulence distribution (Troldborg et al. [57, 150] and Larsen et al. [151]). However, a detailed study of the capability of the synthetic turbulence methods and their interactions with the wake turbulence has not yet been conducted. Furthermore, no guidelines are available for the model parameters to apply in the synthetic turbulence implementation to yield desired turbulence intensity in the domain, or the distance required from the turbulence-plane for the imposed turbulence to reach a fully developed stage.

4.6.3 Method:

The investigation consists of two studies. The first study is aimed at verifying the ability of the body force method to generate and maintain stable atmospheric turbulence in an empty computational domain. A part of this study is also to derive guidelines for the appropriate turbulence amplification factor and vertical shear to apply in order to reach a desired turbulence intensity level, as well as the distance required for the imposed turbulence to reach a fully developed stage. The performance is verified by extracting the turbulence intensity as a function of downstream position, and by comparing the spectral distribution of turbulent energy to the imposed Mann turbulence fluctuations.

In the second study, the body force methods are applied in a series of simulations containing a wind turbine represented by actuator lines to verify the wake interaction with the imposed turbulence. Simulations are conducted in a range of the most common operational conditions; wind speeds of 5-15 m/s and turbulence intensities from 6-14%. The resulting turbulent intensity and spectral distribution, as well as the meandering of the wake are validated with field data.

4.6.4 Main results and Conclusions:

Based on the calculations conducted in an empty computational domain it is concluded that the synthetic body force method is capable of generating stable, realistic atmospheric turbulence in flat terrain under neutral stratification. Figure 4.2 show the development of turbulence intensity as a function of downstream distance. It can be seen that the imposed turbulence is lower than prescribed initially but recovers as the flow progresses downstream. This reason for the lower turbulence levels close to the turbulence-plane is that the smaller scales contain less energy than prescribed due to interpolation and grid effects. This can be seen in figure 4.3 by comparing the realized turbulence at 0.5R (blue line) to the imposed turbulence (black line). The energy level in these scales is corrected automatically in the flow-solver by the turbulent energy cascade as the flow evolves with downstream distance.

In terms of guidelines for using the synthetic atmospheric turbulence method the following recommendations are given based on the empty domain study:

- The power-law shear coefficient should be selected to have a value close to the desired turbulence intensity, i.e. $\alpha = 0.10$ for TI = 0.10, in order to yield correct turbulence levels after equilibrium is reached.
- The most appropriate value of the turbulence amplification factor was found to be 1.15. The basis for the evaluation was the distance required for the imposed turbulence to reach the desired turbulence intensity level.
- With the setting suggested above, equilibrium between turbulence and wind shear was achieved after about 6 R (~150 cells) behind the turbulence plane see table 4.1.
- At the location where the turbulent fluctuations are introduced, a reduced amount of energy is seen in the smaller turbulent length scales. As the flow develops this imbalance in the turbulent energy spectra is corrected by the turbulence cascade process in the EllipSys3D model, and a correct turbulent energy spectra is seen at 3.5 R (~90 cells) behind the turbulence plane.

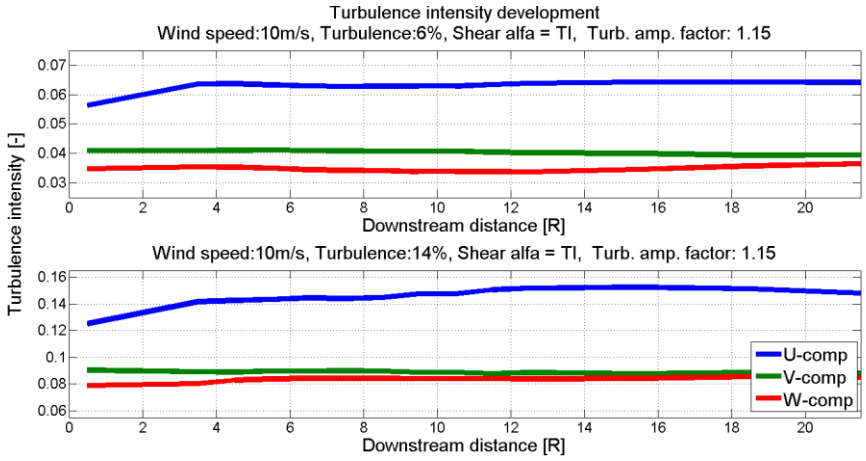

Figure 4.2: Evolution of turbulence intensity of the different velocity component at hub height (H_{Hub} = 2R) as a function of downstream distance in an empty simulation domain.

Table 4.1: Comparison of turbulence intensity at 6.5R compared to 10-20R using the suggested setting for wind shear and turbulence amplification factor.

WS	Target TI	Realized TI at 6.5R	Realized TI at 10-20R	Ratio of TI at 6.5R to 10-20R	Ratio of TI at 10-20R to target TI
5	6	5.47	5.85	0.94	0.98
5	14	11.18	13.68	0.82	0.98
10	6	6.29	6.38	0.99	1.06
10	10	11.68	11.58	1.01	1.16
10	14	14.44	14.93	0.97	1.07
15	6	5.27	5.29	1	0.88
15	14	12.76	12.77	1	0.91

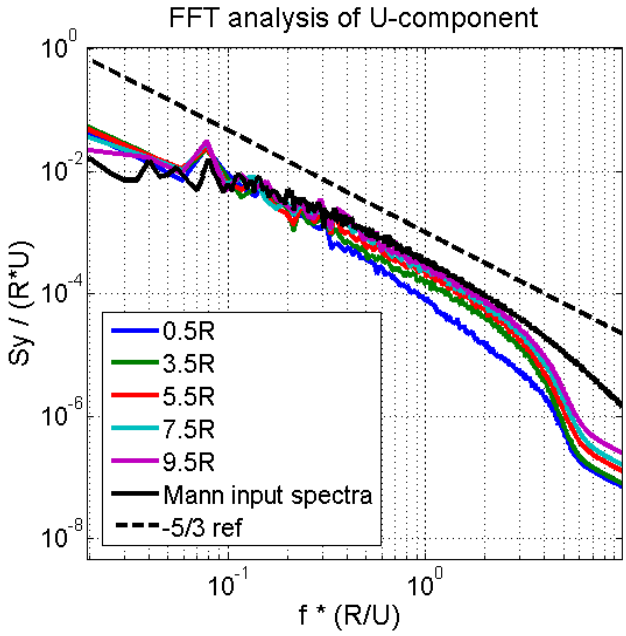

Figure 4.3: The recovery of energy in the small-scales due to the energy cascade in the flow-solver. The black line represents the spectral distribution of the synthetic turbulence being imposed on the flow field.

The second study to verify the wake evolution using an AL model combined with the synthetic atmospheric turbulence showed good agreement with field data. As can be seen in figure 4.4, the average turbulence intensity at hub height from the AL model deviated less the one percentage point (pp) from the field data for distances 4-17R. Figure 4.5 show the turbulent energy spectra for the free stream and the wake region from both AL model and field data from the Alsvik site. The meandering characteristics are difficult to verify due to the low availability of field data, but are extracted and shown in figure 4.6 as a function of ambient turbulence intensity and downstream distance to serve as a reference value for further studies. The reference data included comes from a LIDAR measurement campaign on the NM80 turbine courtesy of Bingöl et al. [30] and measurements in the PRISME wind tunnel courtesy of España et al. [55].

Based on these results it is concluded that the body force method can be used to simulate wake turbulence development in flat terrain and neutral atmospheric conditions for the common range of ambient conditions experienced by a wind turbine.

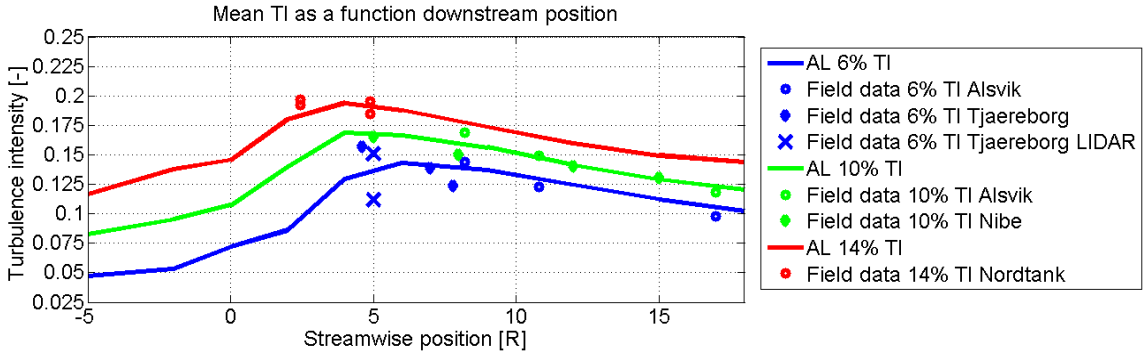

Figure 4.4: Comparison of integrated turbulence intensity extracted from the AL simulations to measurement data from Alsvik, Tjæreborg, Nibe and the Nordtank turbine. The zero location of the x-axis refers to turbine position.

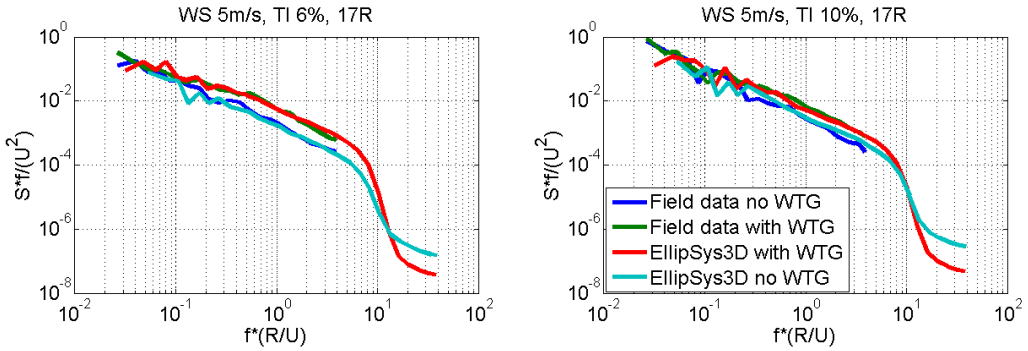

Figure 4.5: Comparison of turbulent energy spectra extracted from AL simulations to measurements from the Alsvik wind farm.

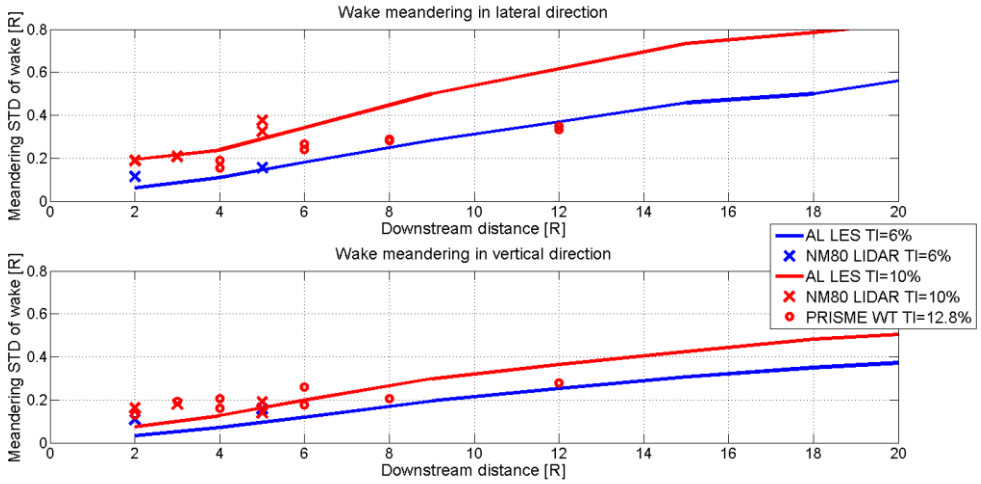

Figure 4.6: the magnitude of the wake meandering, defined as the standard deviation of the wake centre in vertical and lateral direction, as a function of turbulence intensity and downstream distance. The reference data comes from a LIDAR campaign (X) and wind tunnel data from the PRISME wind tunnel (O).

Finally an investigation was conducted to estimate the transport velocity of the wake deficit. It is suggested by Larsen et al. [52] that the process of wake meandering can be modelled by treating the wake as a passive tracer in the atmospheric flow. Under the passive tracer assumption the wake deficit is transported in streamwise direction by the mean velocity and translated horizontally and vertically by large-scale atmospheric turbulent fluctuations.

The hypothesis that the lateral and vertical movements of the wake centre are due to large scale turbulent fluctuations are supported by the experimental results of España et al. [55] and by field measurements by Bingöl et al. [30] and Trujillo et al. [31]. The second hypothesis of the passive tracer assumption, related to the transport velocity of the wake, has not been verified to the same extent. Bingöl et al. [30] applied a wake transport velocity based the Jensen model (Jensen [134]) to correlate the large scale movements in the wake to the wind direction changes of a meteorological mast upstream of the turbine.

In this work the wake transport velocity was investigated by studying time series of the wake centre position at two downstream sampling planes, figure 4.7. By shifting one of the time series by a varying time offset, it is possible to obtain the time offset which yields the maximum correlation. The time offset corresponds to the transport time between the sampling planes. The wake transport velocity is found by dividing the distance between the sampling planes with transport time. The transport velocity (solid lines) for a range of cases is presented in figure 4.8. The dashed line represents the mean velocity in the wake and serves as a reference value. From this investigation it is concluded that the wake transport velocity lies between mean velocity of the wake deficit and the ambient wind speed (which is 1 in figure 4.8).

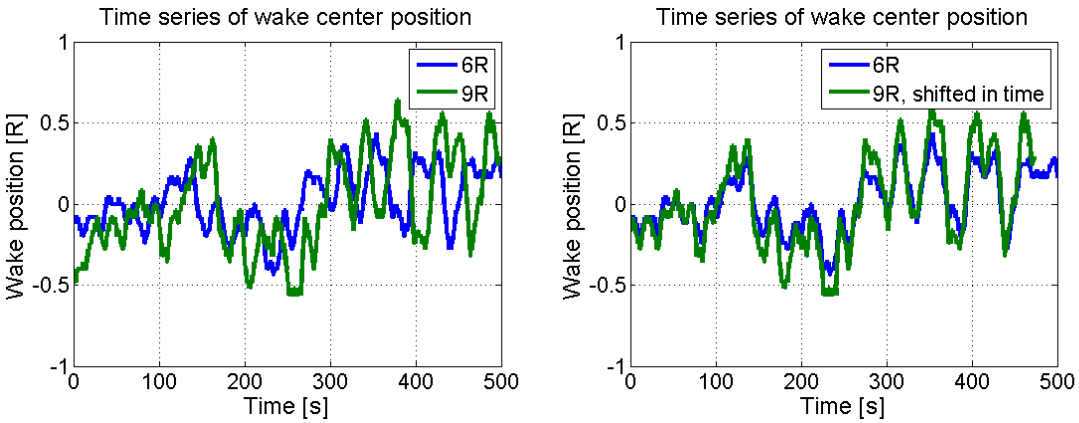

Figure 4.7: The left figure shows the centre position of the wake deficit as a function of time at two sampling planes. The right figure shows the same time series of wake centre position, but including a time offset to find the best correlation between the time series.

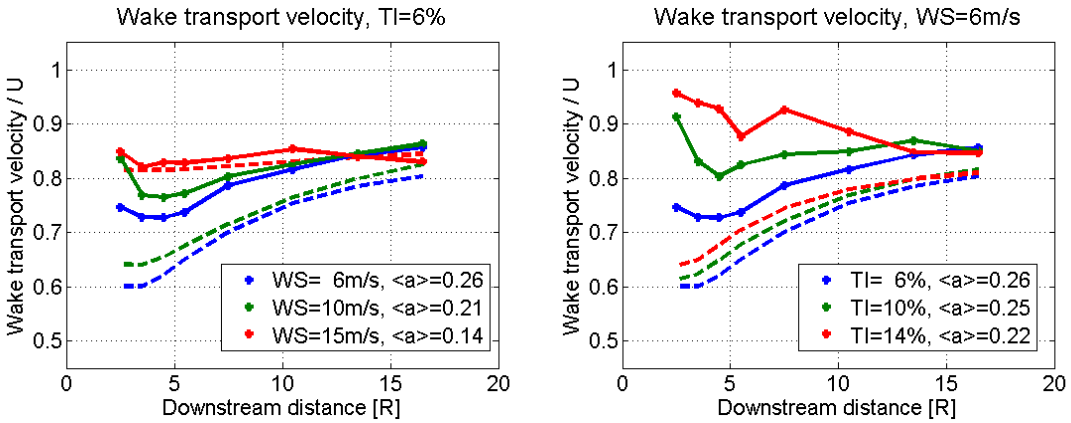

Figure 4.8: The wake transport velocities (solid lines) and the mean velocity of the wake deficit (dashed lines) are depicted as a function of downstream position. The left figure show the effect of different ambient wind speed (or rotor induction) at 6% turbulence intensity and the right figure show the influence of turbulence intensity at 6m/s wind speed.

4.6.5 Post-publication update:

In a later study of the wake meandering in the DWM method, it was seen that applying a wake transport velocity of 80% of the free stream velocity, as opposed to 100%, affected the shape of the evolution of wake meandering in DWM, see figure 4.9. In the beginning the wake meandering increase due to the longer transport time to reach a specific downstream location (i.e. the deficit experience more fluctuations to reach the same downstream location). In the far-wake region the wake meandering is seen to decrease. This reduction is a consequence of the fact that the wake deficit now moves relative to the frozen turbulence field which generated the meandering. This causes the wake deficit to experience different a realization of large scale eddies during the meandering process. This will in turn reduce the standard deviation of the wake centre displacement; the difference is similar to the reduction in variation of independent compared to dependent samples.

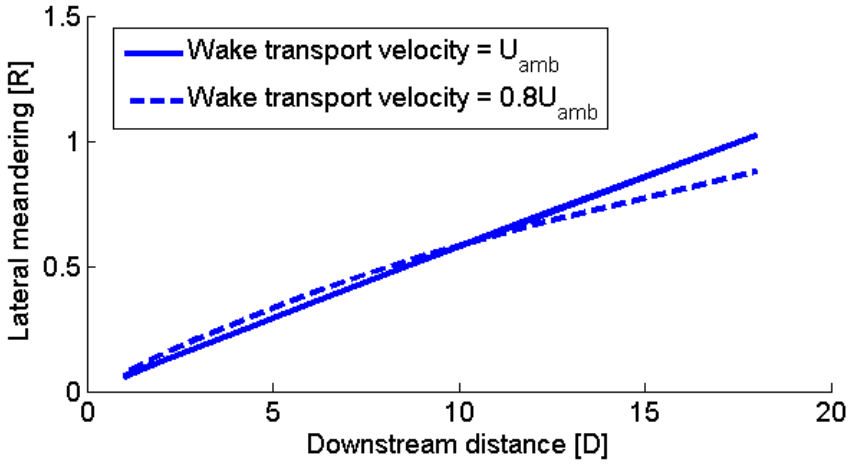

Figure 4.9: wake meandering in the DWM model using a wake transport velocity of 80% (dashed lines) and 100% (solid lines) of the ambient wind speed.

5 Research topic 2: Turbulence formulation of the DWM model

This chapter contains summaries of the journal publications aimed at improving the turbulence formulation of DWM model. The baseline DWM model implementation used as reference in the conducted research consists of the modules described by Madsen et al. [32]. The research activities conducted in the PhD project is based on a gap analysis of the DWM model capabilities and the demand of the wind industry. Four main aspects were selected for further research:

- Improve the spatial turbulence distribution in a single wake
- Improve the modelling of ABL effects on wake turbulence and wake deficit evolution
- Create a method to handle multiple wake deficits and build-up of turbulence over a row of turbines
- Incorporate the effect of atmospheric stability on wake deficit evolution and meandering

The article summaries have the following format: 1) Short description of the research objective, 2) Motivation of the significance of the correction or additional functionality, 3) The research method applied, and 4) The main results and conclusions. The full version of the research papers are found in the back of the thesis.

5.1 Summary of research article II: Implementation of a Mixing Length Turbulence Formulation into the Dynamic Wake Meandering Model

5.1.1 Research objective:

The objective is to improve the spatial distribution of Reynolds stresses in the wake deficit of the DWM model. This is achieved by including the effect of local turbulent velocity scales to model a two-dimensional eddy viscosity distribution in the wake.

5.1.2 Motivation:

In the DWM version previous to this article the eddy viscosity model was based on a single turbulent velocity and length scale in an entire wake cross section in accordance with the method proposed by Ainslie [62, 63]. This yields a one-dimensional eddy viscosity, invariant in cross-flow direction, which is appropriate only after the wake has reached a near Gaussian shape. As Ainslie applied a Gaussian velocity profile as the inlet condition to the model, the single velocity scale was an appropriate selection. In the DWM model, however, the inlet boundary condition is based on the real axial induction profile resulting from an aeroelastic model of the studied turbine. This yields an inlet velocity field which does not vary in a smooth manner in radial direction. Instead, it generates a distinct shear layer which requires local velocity scales to be accurately modelled. Furthermore, a study conducted with the LES AL model showed that the “eddy viscosity” (as estimated from the LES flow field) required between 6-15D to reach a radially invariant stage. It also showed that the eddy viscosity in the shear layer at 3D is on the order of twice as large as the eddy viscosity in the rest of the wake for cases with low ambient turbulence.

5.1.3 Method:

First the wake turbulence was investigated using the LES AL model. The effect on the Reynolds stress distribution in the wake with ambient mean wind speeds ranging from 5 to 15m/s and turbulence intensities of 6 to 14% was evaluated. As the objective is to develop a new eddy viscosity closure for the DWM model deficit module, it is desirable to be able to estimate the azimuthally averaged RANS eddy viscosity distribution in the MFoR from the LES AL simulations. The azimuthally averaged wake deficit in the MFoR is found by the approach described in section 4.5.

Two different methods were used to estimate the eddy viscosity: 1) the Johnson-King equation (see Menter [152]), and 2) the direct definition of eddy viscosity as the product of the turbulent length and velocity scales. The turbulent length scale in the later method is taken to be 0.16R based on a tabulated value from Varseeg and Malalasekera [153]. The turbulent velocity scale is estimated as the square-root of the turbulent kinetic energy. Both methods resulted in eddy viscosity distributions which were not invariant with radial position until 6-15D downstream the turbine. A clear peak in eddy viscosity was seen in the regions with large velocity gradients, thus suggesting that using the local velocity scale in the eddy viscosity calculations should be a better approximation compared to a global velocity scale for the whole cross-section of the wake. This clearly motivates why a two-dimensional eddy viscosity model is required to model the wake development.

The ansatz for developing the new eddy viscosity closure is based on keeping Ainslies formulation for the atmospheric turbulence, as well as the "*filter functions*" (F_1 and F_2) which are required to compensate for the initial non-equilibrium between the velocity and the turbulence field behind the rotor. Thus only the contribution to the eddy viscosity in the wake generated by the wake shear layer is considered. The most straight-forward manner to achieve a local turbulent velocity scale is to apply Prandtl's mixing length model. According to Pope [106] the local turbulent velocity scale in the mixing length model is based the product of the turbulent length scale and the local mean strain-rate. In the DWM model, the local mean strain-rate is equal to the local velocity gradient *du/dr*. Keeping the assumption of one characteristic length scale (l^*) for each cross section of the wake, equal to half the wake width, the turbulent velocity scale distribution is given by eq. (5.1).

$$u^* = l^* \cdot \left|\frac{\partial u}{\partial r}\right| \tag{5.1}$$

This yields an eddy viscosity due to the shear layer in the wake given by eq. (5.2), and a total wake eddy viscosity in the wake evolution given by eq. (5.3).

$$\nu_{T,Shear} = l^{*2}\left|\frac{\partial u}{\partial r}\right| \tag{5.2}$$

$$\nu_T = F_1 k_{amb} TI_{amb} + F_2 k_2 l^{*2}\left|\frac{\partial u}{\partial r}\right|\left(\frac{1}{U_{amb}\cdot R}\right) \tag{5.3}$$

Here U_{amb} and TI_{amb} refer to the ambient mean wind speed and turbulence intensity at hub height. R refers to the radius of the turbine. k_{amb} and k_2 are model coefficients used to calibrate the deficit model (note that the k_{amb} includes a length scale based on a hub-height of 2R. Furthermore in the article summarized by this section, the notation k_1 is used for this constant; however, in the thesis k_1 denotes

the same model constant without the length scale included, see eq. 5.24). F_1 and F_2 are filter functions included to limit the turbulence in the wake before equilibrium between the wind and turbulence field is achieved.

5.1.4 Main results and Conclusions:

By conducting a least-square recalibration to the AL reference data (details on the recalibration procedure is described in chapter seven), using both the modified and the unmodified DWM model, it is concluded that the new eddy viscosity formulations gives a better fit. The criterion used to evaluate the goodness of fit is the standard error (STE) defined as:

$$\mathrm{STE} = \sqrt{\frac{1}{n_c}\sum_{c=1}^{n_c}\left[\frac{1}{n_{c,d}}\sum_{d=1}^{n_{c,d}}\left(\frac{1}{n_{c,d,r}}\sum_{r=1}^{n_{c,d,r}}\left(\bar{U}_{c,d,r}^{ACL}-\bar{U}_{c,d,r}^{DWM}\right)^2\right)\right]} \tag{5.4}$$

The indexes c, d, and r correspond to cases (i.e., variations in inflow conditions), downstream distance and radial position, respectively. The constants, n_c, $n_{c,d}$, and $n_{c,d,r}$, represent the number of cases, number of cross-sections, and number of data points per cross-section, respectively. In this calibration, the constants are equal to four flow cases (wind speeds of 10 m/s and 15 m/s combined with turbulence intensities of 6% and 14%), four cross-sections for each case (3, 6, 9, and 12D downstream the wake generating rotor) and 80 points per cross-section. The STE of the unmodified DWM model was 0.0245 compared to 0.0179 for the new eddy viscosity formulation. This corresponds to a reduction in STE of ~27%. The comparison between the DWM model and the EllipSys3D AL calibration data is shown in figure 5.1.

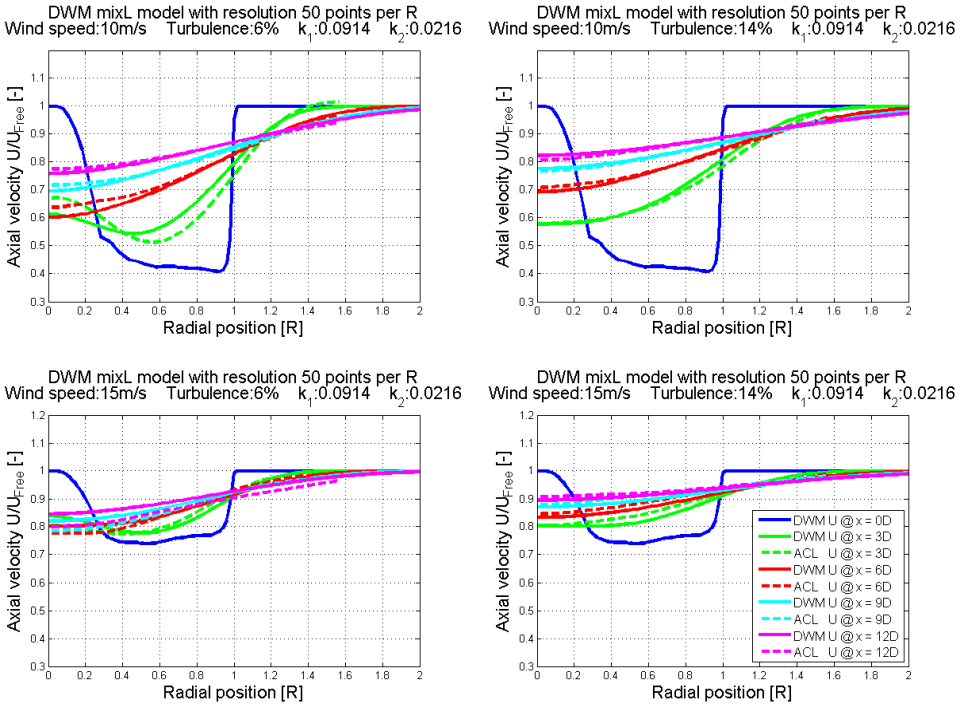

Figure 5.1: The resulting DWM velocity field in the MFoR compared to AL calibration data from wind speeds of 10m/s (top row) and 15m/s (bottom row) and turbulence intensities of 6% (left column) and 14% (right column).

5.1.5 Post-publication update:

Two modifications have been made to the work presented in this article after it was published.

Modification 1: A numerical instability caused by the implementation of the inlet boundary condition and the selected equation to calculate the radial velocity component was found. This instability was removed by selecting a different finite difference scheme to solve the radial velocity.

Modification 2: A blending function has been implemented to ensure that the eddy viscosity does not go towards zero in regions with low mean flow velocity gradients (see eq. (6.6)). This is an issue described by Schlichting [94] as a possible problem when modelling axisymmetric wakes with a mixing length model due to the singularity in the wake centre. The corrected eddy viscosity function is a blend between the derived mixing length formulation and the original Ainslie model. The switch is designed so that the eddy viscosity in a flow region where the eddy viscosity of the mixing length model is smaller than the Ainslie model, the Ainslie eddy viscosity closure is used. This increases the eddy viscosity in regions of low mean flow gradients, but for the largest part of the flow the mixing length eddy viscosity is larger than the Ainslie model.

After these modifications were implemented into the DWM model, the model was recalibrated and a second analysis was conducted to investigate the effect of the improved turbulence formulation. The conclusion is that the results presented in the article do not change significantly, and that the mixing length eddy viscosity model reduces the STE of the DWM model by 13% when compared to the AL data.

5.2 Summary of research article III: Two Improvements to the Dynamic Wake Meandering Model: Including the Effects of Atmospheric Shear on Wake Turbulence and Incorporating Turbulence Build-Up in a Row of Wind Turbines

5.2.1 Research objective:

There are two objectives of this article: 1) to incorporate the effect of ABL shear on the local strain-rate in the wake deficit. This will in turn affect the turbulent stresses and the evolution of the wind speed distribution in the wake. 2) to propose a method to couple the increased turbulence intensity level experienced by a turbine operating in waked conditions to the downstream wake evolution of the wake-affected turbine (see figure 1.3).

5.2.2 Motivation:

In the current DWM formulation, only the velocity gradients of the wake deficit are taken into consideration when calculating the turbulent stresses in the wake. An undesirable consequence of this formulation is that the turbulent stresses go towards zero as the wake deficit recovers. The result is unrealistically low turbulent stress levels in the far-wake region and regions where the wake deficit gradients are small. An appropriate turbulence formulation should result in ambient turbulence conditions after the wake deficit has fully recovered. The proposed method is to include a strain-rate contribution from the atmospheric vertical wind shear in the calculation of the turbulent stresses.

The wake-added turbulence formulation of the DWM model is currently calculated by an analytical expression based on the wake deficit depths and gradients (for details see Madsen et al. [41]). More importantly, the increased turbulence level is assumed to only influence the loads of the wake-affected turbine. No coupling exists between the wake-added turbulence and the wake evolution behind a wake-affected turbine. Consequently, the wake evolution of all turbines along a row will be based on ambient turbulence level.

The method proposed in this paper suggests a physically consistent formulation, where the wake-added turbulence at a downstream rotor is calculated based on the Reynolds stresses in the wake deficit calculation. Furthermore, the average turbulence intensity level at the downstream rotor is used as initial condition for the subsequent wake evolution. This method results in a more realistic wake evolution over a row of wind turbines, and enables the DWM model to capture the build-up of turbulence intensity over a row of turbines.

5.2.3 Method:

ABL shear correction:
The basic idea is to incorporate the effect of the ABL shear on the wake deficit evolution by basing the calculations of the turbulent stresses on a corrected local strain-rate, rather than on the wake deficit gradient alone. Since the wake deficit calculations are carried out in an axisymmetric frame, it is required to theoretically combine the contribution of the two velocity gradients at all location over an annulus into an azimuthally averaged value. This value is then applied as that as the representative strain-rate in the DWM calculation.

As the ABL shear is expressed in Cartesian coordinates (du/dz) and the wake deficit gradient is expressed in axisymmetric coordinates (du/dr). Thus, an appropriate method is required to combine the two gradients to find the representative strain-rate. To illustrate the proposed method, the magnitudes of the two velocity gradients are drawn as a function of azimuthal position for some arbitrary radial location in the wake in figure 5.2. The wake deficit gradient (dashed lines) has a constant value as a function of azimuthal angle since the DWM model assumes axisymmetric flow. The atmospheric shear gradient (dotted lines) is a sinusoidal function over the azimuth as the ABL shear is assumed linear over the cross section of the rotor. The combined local gradient (solid line) is the sum of the two contributions. Since the deficit calculation in the DWM model assumes an axisymmetric flow field, the representative value for the strain-rate to apply is the mean value in azimuthal direction. This corresponds to the average height of the combined curve in figure 5.2.

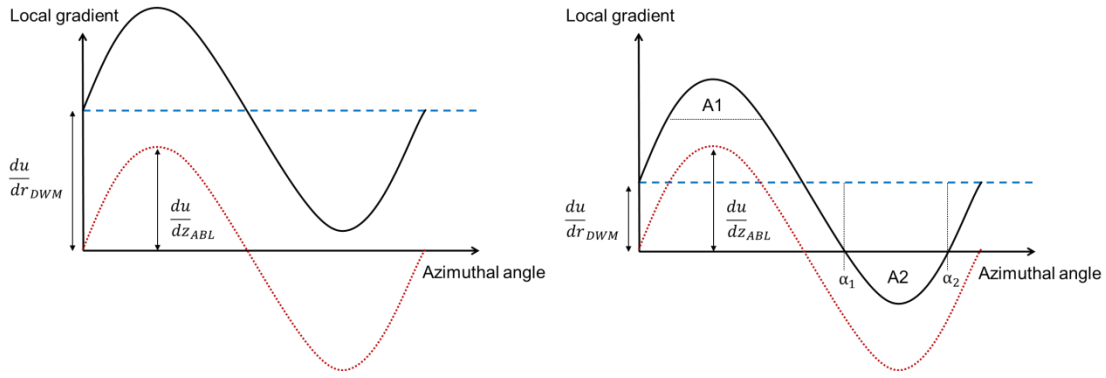

Figure 5.2: Conceptual description of how the local representative velocity gradient (solid line) is calculated given the atmospheric shear (dotted line) in Cartesian coordinates (du/dz) and the wake deficit gradient (dashed line) in polar coordinates (du/dr).Figure 5.2a (to the left) illustrates a case where the magnitude of the wake deficit shear is larger than the atmospheric shear, and figure 5.2b (to the right) a case where the atmospheric shear is larger.

When the magnitude of the atmospheric shear is larger than the wake deficit gradient, a part of the lower wake will experience turbulent stresses acting in the opposite direction compared to the rest of the wake (*A2* in figure 5.2b). Since the DWM model is based on an axisymmetric flow field, this situation cannot be handled in a strictly physically manner. Instead, the key feature to capture for the wake diffusion is the total magnitude of turbulent stresses. This magnitude is found by calculating the azimuthal average of the absolute value of local velocity gradient. This gradient is then used to calculate the turbulent stresses. The geometrical interpretation of this concept is that the representative gradient to apply in the stress calculations corresponds to the total area between the combined curve and the x-axis in figure 5.2b, divided by *2π*. The representative gradient can thus be calculated using the equations

$$A_{Total} = \begin{cases} 2\pi \frac{du}{dr_{DWM}} & ,if \quad \left|\frac{du}{dr_{DWM}}\right| \geq \frac{du}{dz_{ABL}} \\ 2\pi \frac{du}{dr_{DWM}} + A1 + A2 \,, if & \left|\frac{du}{dr_{DWM}}\right| < \frac{du}{dz_{ABL}} \end{cases} \tag{5.5}$$

$$A1 = A2 = \int_{\alpha_1}^{\alpha_2} \left(\frac{du}{dz_{ABL}} \cdot \sin(x)\, dx\right) - (\alpha_2 - \alpha_1)\frac{du}{dr_{DWM}} \tag{5.6}$$

$$\frac{du}{dr_{Total}} = \frac{A_{Total}}{2\pi} \tag{5.7}$$

The angular locations where the effect of the atmospheric shear in cylindrical coordinates is larger than the wake deficit shear, α_1 and α_2, are found by *arcsin*$(\frac{du}{dr_{DWM}} / \frac{du}{dz_{ABL}})$ and π-α_1 respectively. The total mean gradient in the radial direction, as calculated by eq. (5.7), is used to calculate the turbulent stresses in the wake to incorporate the effect of the ABL shear on the wake diffusion. Rather than using the total velocity gradient in the turbulent stress term of the momentum equation, eq. (6.1), since the momentum equation is only meant to solve for wake velocity and not a combined wake-atmospheric velocity, a scaled eddy viscosity, ν'_t, is introduced as

$$\nu_t' = \nu_t \cdot \frac{\frac{du}{dr_{Total}}}{\left|\frac{du}{dr_{DWM}}\right|}. \tag{5.8}$$

The original eddy viscosity is scaled at every computational node by the ratio of the corrected gradient with atmospheric shear effects to the wake deficit velocity gradient in the DWM solution. This has the desired effect of applying the appropriately scaled turbulent stresses as seen by eq. (5.9).

$$\tau_{stress\ DWM} = \nu_t' \cdot \frac{du}{dr}_{DWM} \rightarrow \nu_t \cdot \frac{\frac{du}{dr}_{Total}}{\left|\frac{du}{dr}_{DWM}\right|} \cdot \frac{du}{dr}_{DWM} \rightarrow \nu_t \cdot \frac{du}{dr}_{Total} \tag{5.9}$$

Wake-added turbulence and turbulence over a row of turbines:
The proposed method is based on re-calculating the turbulent shear stress in the DWM wake deficit into a mean turbulence intensity at the downstream rotor position. This is done by first approximating the turbulent stress in streamwise direction using the relations,

$$\tau_{Shear} = -\overline{u'w'} = u'_{rms} w'_{rms} C_{u'w'} = u'u' \left(\frac{w'_{rms}}{u'_{rms}}\right) \cdot C_{u'w'} \tag{5.10}$$

where the coefficient $C_{u'w'}$ and the ratio w'_{rms}/u'_{rms} describe relationship between the standard deviation of axial and radial fluctuations in the wake. These relations are different in the wind turbine wake compared to atmosphere turbulence due to the significantly smaller length scale and increased anisotropy of wake turbulence. In this work, the correlation coefficient has been given the value 0.3, and the ratio w'_{rms}/u'_{rms} has been set to unity based on the findings of Larsen et al. [145]. Rearranging the terms in eq. (5.10) yield an expression for the normal stress in flow direction and taking the square-root of the same expression yields the streamwise velocity fluctuations,

$$\overline{u'u'} \approx \frac{1}{C_{u'w'} \cdot (w'_{rms}/u'_{rms})} \cdot -\overline{u'w'} \tag{5.11}$$

$$TI_{DWM\ MFoR} = \max\left(\sqrt{\frac{1}{C_{u'w'} \cdot (w'_{rms}/u'_{rms})} \cdot \tau_{stress\ DWM}}\ , TI_{amb}\right) \tag{5.12}$$

where the max-operator and second term of eq. (5.12) is included to ensure that the turbulence intensity approximation in the MFoR never assumes a value smaller than the ambient turbulence intensity (this is needed close to the wake-axis and outside of the deficit). Eq. (5.12) yields a local value of wake turbulence intensity for each computing node in the DWM deficit domain, $TI_{DWM\ MFoR}$. However, for running multiple turbine simulations with the DWM model, it is more practical to use average wake turbulence intensity as a single turbulence intensity value is a required input to the deficit calculation. The DWM deficit module outputs the wind speed and turbulence distribution in the meandering frame of reference (i.e without any large scale movements). The meandering can be considered as a series of wake-segments, where each of the wake centres has a stochastic offset in lateral and vertical direction according to some statistical distribution of the large scale turbulence. If this distribution of the meandering is known, it is possible to calculate the average wind field and turbulence intensity at the downstream rotor by calculating the convolution between the deficit (both wind speed and variance, i.e. the square of $TI_{DWM\ MFoR}$ from eq. (5.12)) in the meandering frame of reference and the distribution of the wake centre displacements in the vertical and lateral direction due to wake meandering as follows:

$$\theta_{DWM\ FFoR} = \iint \theta(y - y_m, z - z_m)_{DWM\ MFoR} \cdot PDF_m(y_m, z_m)\, dy_m dz_m. \tag{5.13}$$

In this equation, θ represent the distribution of wind speed or variance in the meandering frame of reference, y-y_m and z-z_m are the local coordinates in the meandering frame of reference and PDF_m is the probability density function describing the meandering distribution. The subscripts *FFoR* and *MFoR* refer to fixed and meandering frame of reference, respectively. This results in a wind speed and turbulence intensity distribution in the fixed frame of reference. The average turbulence intensity and wind speed distribution to apply as "ambient conditions" at the downstream rotor is found by calculating the area weighted mean value of the properties from the rotor centre to width of the initial DWM wake, R_w. The initial width of the wake is calculated by eq. (6.7) by applying the rotor radius as r_t value. The averaged wake turbulence intensity (TI_{WTG}) and wind speed distribution (U_{axisym}) at the downstream rotor to apply as inlet conditions are found using the equations

$$U_{axisym}(r) = \frac{1}{2\pi\Delta r}\int_0^{2\pi}\int_{r-\frac{\Delta r}{2}}^{r+\frac{\Delta r}{2}} U_{DWM\ FFoR}(y_{WTG} + r\cos(\alpha), z_{WTG} + r\sin(\alpha))\, dr\, d\alpha \tag{5.14}$$

$$TI_{WTG} = \frac{1}{2\pi R_w}\sqrt{\int_0^{2\pi}\int_o^{R_w} TI^2_{DWM\ FFoR}(y_{WTG} + r\cos(\alpha), z_{WTG} + r\sin(\alpha))\, dr\, d\alpha} \tag{5.15}$$

The mean turbulence intensity level given by eq. (5.15) represents the mean turbulence intensity in the scales which affect the wake deficit evolution (roughly corresponding to eddies smaller than 2D according to Larsen et al. [52]). This is therefore the appropriate value to use when coupling the turbulence intensity of the wake to the downstream wake evolution of a wake-affected wind turbine. However, to find the total turbulence intensity at a downstream turbine, which is relevant to loads or when comparing to reference data, a contribution due to the meandering of the mean velocity field needs to be included. This is referred to as the "apparent turbulence intensity" (see chapter 2) in the FFoR due the wake meandering and calculated as,

$$TI_M(y,z) = \sqrt{\iint (U(y-y_m, z-z_m)_{MFoR} - U_{FFoR}(y,z))^2 \cdot PDF_m(y_m, z_m)\, dy_m dz_m} \tag{5.16}$$

where the first term can be thought of as the distribution of wind speeds at location (y, z) due to the meandering deficit and the second term represents the mean wind speed in the FFoR. The contribution of eq. (5.15) and (5.16) can be considered to be independent due to the split in scales, which means that the total turbulence intensity in the FFoR can be found by eq. (5.17).

$$TI_{tot\ FFoR} = \sqrt{TI_M^2 + TI^2_{DWM\ FFoR}} \tag{5.17}$$

5.2.4 Main results and Conclusions:

The effect on wake turbulence by including the ABL shear contribution in a simulation run with a wind speed of 8m/s and a turbulence intensity of 14% is shown in figures 5.3 and 5.4. Figure 5.3 shows the local amplification of the turbulent stress given by the second term in eq. (5.8). The atmospheric shear correction has an influence on the turbulent stresses close to the centre axis of the wake and outside the wake shear layer relatively close to the rotor. As the wake deficit recovers, and the strain-rate due to the wake is reduced, an effect on the turbulent stresses occurs throughout the whole wake deficit. The effect of the atmospheric shear correction can be seen in figure 5.4. The effect of atmospheric shear on the turbulence level is small over the first 5D downstream of the turbine. At 5D it starts to increase reaching about 30-100% higher average turbulent stress levels in the region from 15D to 40D.

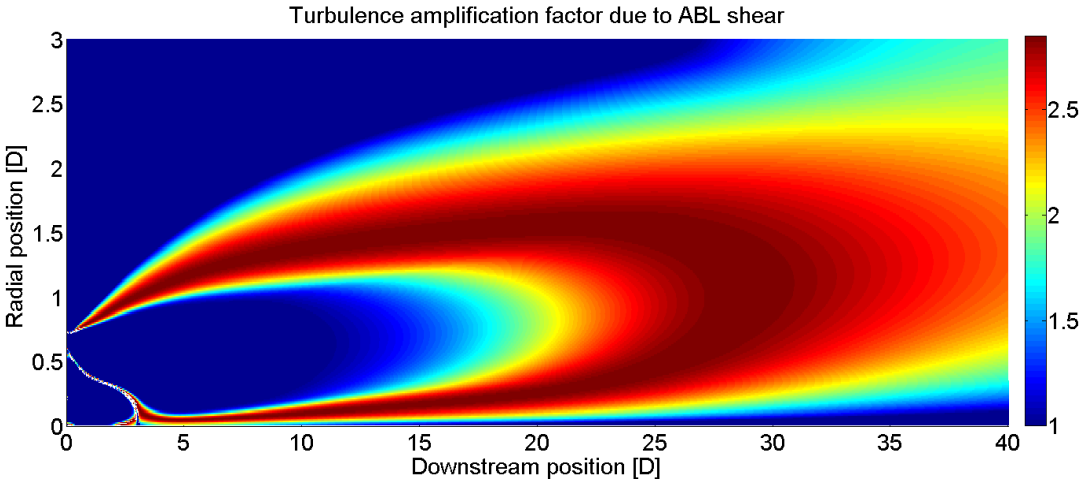

Figure 5.3: The local amplification of turbulent stresses due to the atmospheric shear contribution as given by eq. 5.8 as a function of radial and downstream position. The x-axis of the figure lies on the centre line of the wake. The ambient wind speed for the displayed case is 8m/s, and the turbulence intensity is 14%.

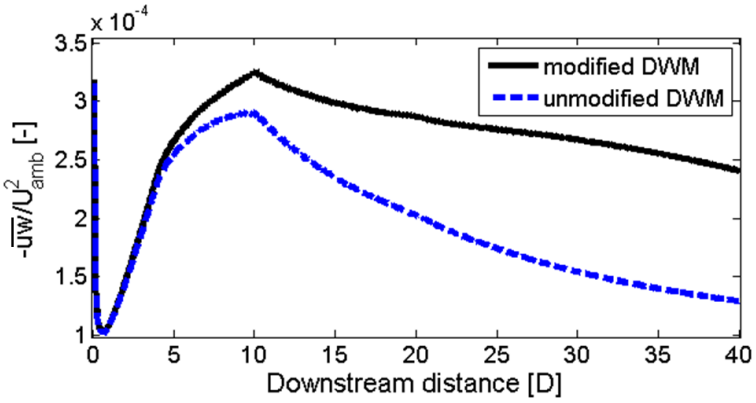

Figure 5.4: Compares the mean turbulent shear stress level in the unmodified DWM model to the shear corrected DWM model as a function of downstream position. The integration is carried out from the rotor centre to 3D in radial direction.

Validation of the resulting mean turbulence level in the wake

The method described by eqs. (5.10)-(5.12) and (5.15) for estimating the turbulence intensity in the wake of a single turbine using the DWM model based on the turbulent stresses, is validated by comparing the mean turbulence intensity in the wake as function of downstream distance to the Ellpisys3D AL model calculations of Keck et al. [36]. The analysis is performed in the MFoR to isolate wake turbulence from the meandering processes. The wake turbulence agrees well with the actuator line model for all the tested cases as shown in Figure 5.5. The largest deviations between the models are seen in the near-wake, at distances closer than two rotor diameters. These deviations are expected as it is outside the region where the DWM equations are valid. In the region where the DWM deficit formulation is valid (i.e. downstream distances larger than 3D), the modified DWM model slightly over-predicts the turbulence intensity between 4 and 8D behind the rotor. The over-prediction is on the order of 0.5-1.0 percentage point (pp, i.e ΔTI in %).

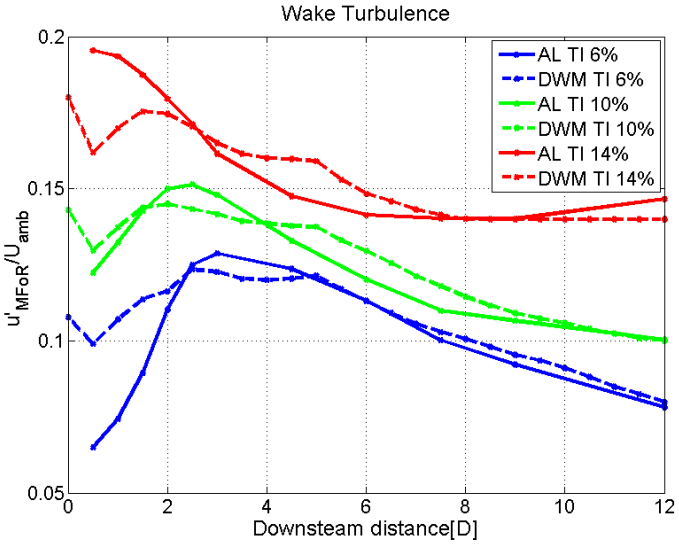

Figure 5.5: The DWM (dashed lines) and the EllipSys3D AL (solid lines) model predicted turbulence intensity in the meandering frame of reference as a function of downstream distance from the wake-generating wind turbine.

The effect of the proposed DWM model improvements

The influence of the proposed atmospheric shear contribution and turbulence build-up is examined by simulating flow through a row of eight wind turbines. For the simulated cases the wind speed is 8m/s, the turbulence intensity is 6% and the mean flow direction is along the row of turbines. Two different turbine spacings, 6D and 10D, are studied.

Figure 5.6 shows the effect on power output of the individual turbines as the various effects in the DWM model are enabled and disabled. The solid black lines represent the modified DWM model including the effects of ABL shear and turbulence build-up and the solid yellow lines represent the unmodified DWM model. The black dashed or dotted lines are results obtained by the modified DWM model after disabling one of the functionalities at the time: ABL shear contribution (dotted lines), turbulence build-up over the row of turbines (dot-dashed lines) and wake meandering (dashed lines). The yellow dashed lines represent the unmodified DWM model without meandering.

By comparing the power output for the row of turbines using the modified DWM model (solid black lines) to the output if turbulence build-up is not taken into consideration (dashed black lines), it is apparent that the effect of turbulence build-up is sensitive to turbine spacing. At 6D-spacing, the reduction of wake loss due to turbulence build-up is on the order of two times the effect of wake meandering (dot-dashed black lines). At 10D-spacing, the effect of turbulence build-up on the wake loss is only about 55% of that caused by meandering. The effect on wake loss caused by the ABL shear contribution to the strain-rate in the wake deficit is about 5% and 20% of the effect of wake meandering at 6D and 10D respectively. Compared to the total power losses due to wake effects of the unmodified DWM model (yellow lines), the inclusion of wake-added turbulence and turbulence build-up over the row of turbines reduced the predicted wake losses by 9% for the 6D case and 6% for the 10D case. The atmospheric shear contribution to turbulence in the DWM model further reduces the power loss by approximately 0.8% at 6D spacing and 1.5% for the 10D case.

These findings suggest that the proposed DWM model improvements have significant effects on the DWM deficit development. They do not only influence the wake turbulence (which is the direct effect), but they also affect the mean wind speed and thereby power predictions. Table 5.1 shows the development of turbulence intensity and wind speed along the rows for the two presented cases. The results suggest that an equilibrium wind speed is reached already at the second or third row inside the park. The turbulence requires much longer distance to become fully developed, and an equilibrium value is not reached before the fifth or sixth row. This suggests that an approach in which only the nearest upstream wake deficit affects a given turbine might be an acceptable simplification in terms of velocity; however, for an accurate turbulence representation, the influence of more upstream wakes should be considered.

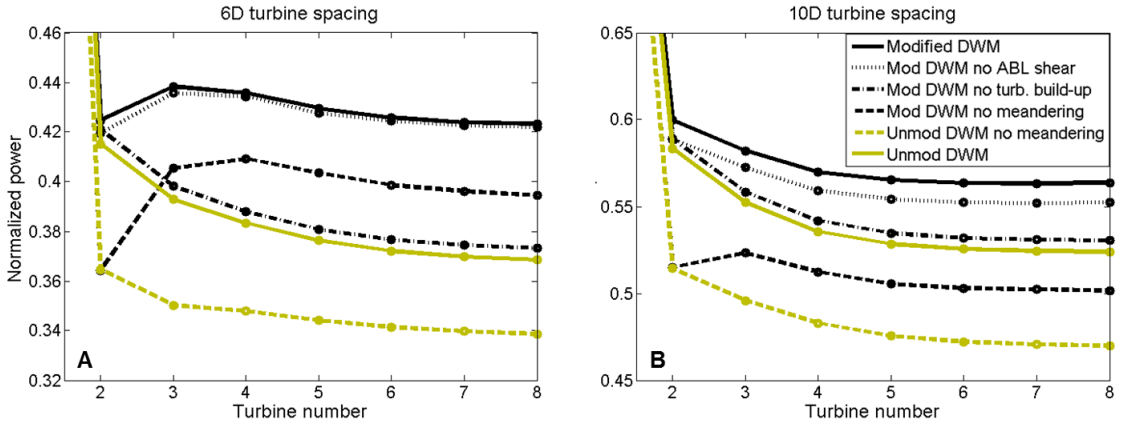

Figure 5.6: The individual effect of the DWM model functionalities by showing the predicted power output of eight wind turbines operating in a row aligned with the mean wind direction at 6D (A) and 10D (B) spacings with various effects enabled.

Table 5.1: The development of turbulence intensity [%] and wind speed [m/s] over the row of wind turbines with the proposed atmospheric shear effect and wake turbulence build up. The ambient conditions for both cases were 8m/s wind speed and 6% turbulence intensity.

Mean wind speed [m/s]

	WTG 1	WTG 2	WTG 3	WTG 4	WTG 5	WTG 6	WTG 7	WTG 8
6D	8.00	5.90	6.00	6.00	5.97	5.95	5.95	5.95
10D	8.00	6.65	6.62	6.57	6.55	6.54	6.54	6.54

Turbulence intensity [%]

	WTG 1	WTG 2	WTG 3	WTG 4	WTG 5	WTG 6	WTG 7	WTG 8
6D	6.0	12.1	13.4	13.9	14.3	14.5	14.6	14.7
10D	6.0	9.7	10.1	10.3	10.4	10.5	10.6	10.6

Validation of DWM flow field with the proposed corrections

To investigate the effect of the proposed ABL shear correction and the coupling of wake turbulence, a set of simulations was performed over two rows of seven and eight wind turbines mimicking the conditions at two of the rows in the Lillgrund offshore wind warm. The simulations were conducted with the modified DWM model, the unmodified DWM model and an AL implementation in OpenFOAM (see

Churchfield et al. [80]). The AL data was used as reference value in the estimation of the STE (see eq. (5.4)). Comparing the wind speed and turbulence distributions of the two DWM model implementations, the modified version demonstrated a reduction in standard error of ~30% in terms of mean wind speed and ~40% in terms of turbulence intensity, see table 5.2. After the turbulence coupling, the STE between the DWM model and the reference AL simulations for all eight turbines was 0.46m/s and 1.73pp of turbulence intensity. These numbers are of the same order of magnitude as the STE of a single wake.

The improved agreement between the modified DWM model and the OpenFOAM model can also be observed visually by comparing the turbulence and velocity fields after the seventh and eight turbine in row B, depicted in figure 15.7. From the figure it is clear that the unmodified DWM model underestimated the turbulence intensity level (5.7b), and consequently over predicted the wake deficit for turbine operating in multiple wake conditions (5.7d). The improvements by using the modified DWM model, quantified in table 5.2, are clearly shown by comparing figures pairwise, i.e. 5.7a to 5.7b and 5.7c to 5.7d for turbulence and wind speed respectively.

Table 5.2, the STE (see eq. (5.4)) in terms of mean wind speed and turbulence intensity level as a function of turbine position for the modified DWM and unmodified DWM models compared to the OpenFOAM AL model. The left table corresponds to row B and the right table to row D on the Lillgrund wind farm.

	STE WS unmod DWM [m/s]	STE TI unmod DWM [%]	STE WS mod DWM [m/s]	STE TI mod DWM [%]
WTG 1	0.38	2.11	0.38	2.11
WTG 2	0.51	2.39	0.46	1.81
WTG 3	0.63	2.88	0.40	1.93
WTG 4	0.69	3.48	0.47	2.21
WTG 5	0.80	3.41	0.48	1.78
WTG 6	0.86	2.80	0.55	2.02
WTG 7	0.98	3.21	0.69	1.83
WTG 8	1.02	4.24	0.61	1.18
Mean	**0.73**	**3.07**	**0.51**	**1.86**

	STE WS unmod DWM [m/s]	STE TI unmod DWM [%]	STE WS mod DWM [m/s]	STE TI mod DWM [%]
WTG 1	0.60	2.10	0.60	2.15
WTG 2	0.46	1.70	0.43	1.28
WTG 3	0.20	1.54	0.17	1.05
WTG 4	0.55	2.67	0.40	1.50
WTG 5	0.65	3.01	0.43	1.55
WTG 6	0.71	3.62	0.44	1.70
WTG 7	0.68	3.38	0.32	1.88
Mean	**0.55**	**2.58**	**0.40**	**1.59**

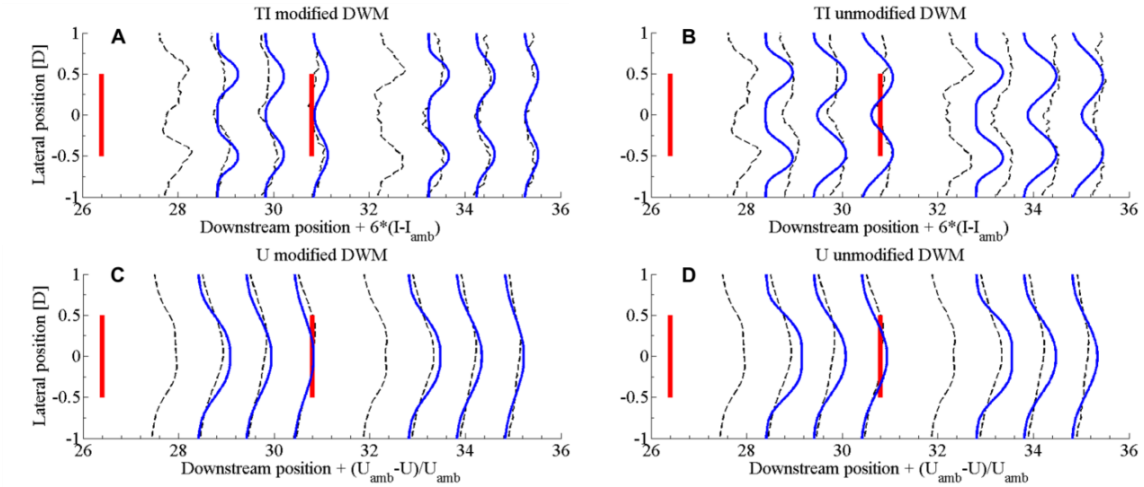

Figure 5.7: Top view of the flow field after the 7th and 8th turbine of row B at the Lillgrund wind farm. The modified (A and C) and unmodified (B and D) DWM models (solid thin lines) are compared to OpenFOAM AL results (dashed lines).

5.3 Summary of research article IV: On Atmospheric Stability in the Dynamic Wake Meandering Model

5.3.1 Research objective:

The objective is to investigate the effect of atmospheric stability on the turbulent length scale of the ABL, quantify the effect of the shift in length scale on the wake evolution, and finally formulate a method to include the effects of atmospheric stability on wake deficit evolution and wake meandering in the DWM model.

5.3.2 Motivation:

The fact that atmospheric stability has an effect on wind turbine loads and power production is well known in the wind power community (see section 2.3.2). There is a consensus that an unstable atmosphere leads to reduced wake effects on power production, to higher turbulence intensities and affects the turbine loads. However, in most investigations the effect of turbulence intensity is not separated from the atmospheric stability. As the turbulence intensity is correlated with atmospheric stability, it is difficult to isolate and quantify the effects of atmospheric stability on wake evolution due to the "noise" from the change in turbulence intensity that will affect the result. On this background the present investigation is based on studying the atmospheric stability effects, while maintaining the turbulence intensity level constant. This is achieved by conducting a series of AL-LES simulations in OpenFOAM in neutral and in very unstable atmospheric conditions (stable atmosphere is currently not handled by the OpenFOAM implementation of the AL model), where the turbulence intensity is maintained constant by calibrating the surface roughness. This allows for a detailed study of the effect on turbulence and wake evolution due to the shift in turbulent length scale.

To illustrate the effect of atmospheric stability on wake simulation with the DWM model, consider the effects of a variation in atmospheric stability while maintaining the turbulence intensity level constant. This isolates the effect of the atmospheric length scale, which have three effects for the DWM model:

1. The ABL shear which ties into the DWM deficit equation via eq. (5.8) would increase with an increasing degree of atmospheric stability. Short length scale results in larger vertical velocity gradients.

$$\frac{du}{dz}_{ABL} \cong \frac{u^*_{ABL}}{l^*_{ABL}} \tag{5.18}$$

2. The turbulent energy in scales larger than 2D, affecting the wake meandering, would decrease with an increasing degree of atmospheric stability.

3. For a given turbulence intensity the amount of energy in scale smaller than 2D, which is assumed to affect the wake deficit evolution, would increase with an increasing degree of atmospheric stability as shorter length scales results in a larger portion of the turbulent energy in the small-scales, see figure 5.8.

An analysis of field data from the OWEZ and the North Hoyle offshore wind farms supports the hypothesis that the length scale of the ABL turbulence is important for the wake recovery of wind turbines. In this analysis a sufficient amount of field data are available to enable binning over wind speed, turbulence intensity and atmospheric stability class. The effect of atmospheric stability can therefore be studied independent of turbulence intensity. The results shows that loss of power

production due to wind turbine wakes under very stable atmospheric conditions (positive Monin-Obukhov lengths < 50) is on the order of 15% higher compared to wake losses in a very unstable atmosphere (negative Monin-Obohov lengths > -100) for the same mean wind speed, turbulence intensity and turbine spacings.

5.3.3 Method:

The approach taken is to capture the effect of non-neutral atmospheric stability in the DWM model based on the fundamental assumption of the split in scales. Following the concept that large scale eddies influence the wake meandering and small eddies affect the wake deficit evolution, it is logical to interpret the turbulent length scale of the ABL turbulences as a parameter governing the distribution of turbulent energy between the wake meandering and the wake deficit evolution. The turbulent length scale for an unstable atmosphere is larger than for a neutral or stable atmosphere. The effect of this shift in turbulent length scale on the spectral distribution of turbulent energy is illustrated in figure 5.8, where the leftmost figures show the ambient turbulence spectra in a very unstable (top row) and very stable (bottom row) atmosphere.

Based on the passive tracer analogy, the energy content in the turbulence scale which affects the wake meandering (middle figures) is found by spatially averaging the turbulent fluctuations over the rotor disc. Mathematically, this can be expressed by a convolution between the ambient turbulence and the rotor disc. In this work, the convolution is carried out in Fourier space as a multiplication between the turbulence spectra and the "*jinc*" (which is the Fourier transform of a circular disc of normalized area, Goodman and Gustafson [68]). The "*jinc"* function is given by eq. (5.19), and is included in the leftmost figures of figure 5.8 (black line) to illustrate which part of the turbulence energy spectra that contributes to wake meandering.

$$jinc\left(\sqrt{k_2^2+k_3^2}\cdot R\right)=\frac{2\cdot J_1\left(\sqrt{\boldsymbol{k_2^2+k_3^2}}\cdot R\right)}{\sqrt{\boldsymbol{k_2^2+k_3^2}}\cdot R} \tag{5.19}$$

J_1 is a Bessel function of the first kind (Goodman and Gustafson [68]), $\boldsymbol{k}$ is the wave number and R is the rotor radius. The turbulent energy in scales which affects the wake deficit evolution (rightmost figures) is found by subtracting the scales dictating wake meandering from the ambient turbulence spectra.

From figure 5.8 it can be seen that the atmospheric turbulence spectra in an unstable atmosphere (top row) has a smaller portion of energy in the scales affecting the wake deficit evolution (right figures), and a larger portion of the turbulent kinetic energy in the wake meandering scales (middle figures) compared to the stable case (bottom row).

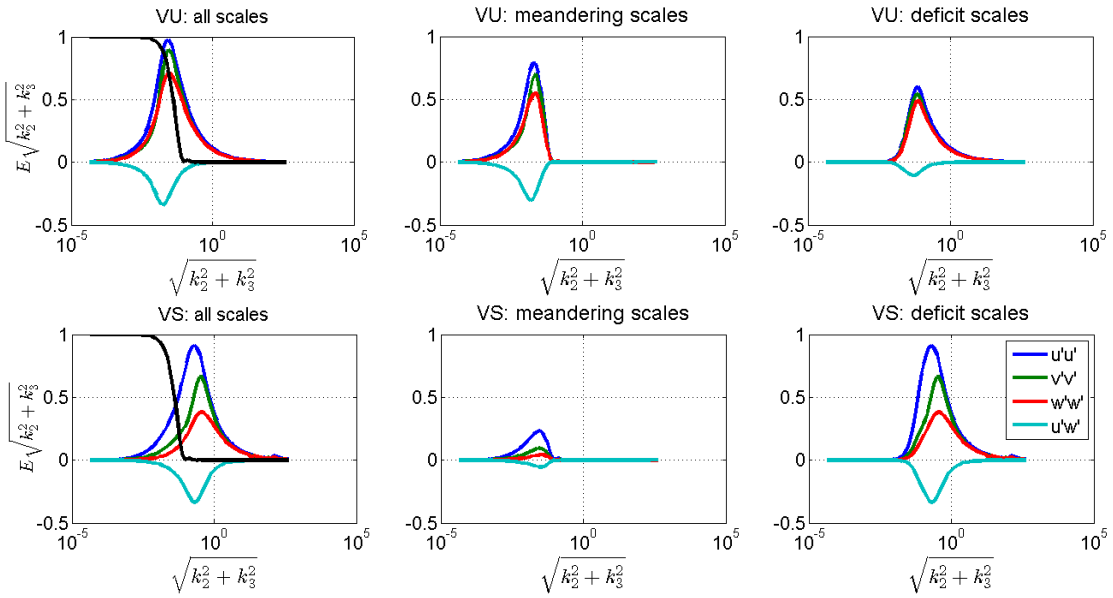

Figure 5.8: The turbulent energy spectra for very unstable (top row) and very stable (bottom) atmospheric conditions found using the Mann model with the parameters suggested by Peña et al. [44]. The left figures show the turbulent energy spectra in all scales, the middle figures show the turbulent scales which affect the wake meandering and the right figures show the turbulence which affect the wake deficit evolution in MFoR. The black line in the left figures show the "jinc" function applied to separate the turbulence affecting the wake meandering and the wake deficit evolution.

To use the proposed method one needs to know the ambient turbulence spectra under various atmospheric stability conditions. In this work the ambient turbulence spectra are generated using the Mann turbulence model (Mann [42], [43]). The Mann turbulence model is derived to generate atmospheric turbulence in neutral stratification. However, Peña et al. [44] showed that with appropriate parameter selection the Mann model can be used to generate atmospheric turbulence with characteristics approximating those of non-neutral atmospheric turbulence.

By utilizing the Mann turbulence model with the input proposed by Peña et al. [44], and applying the "*jinc*" function as described above, the amount of turbulent energy in the wake meandering and wake deficit scales as a function of atmospheric stability are known. The next step is to estimate the effect on the ABL shear, wake deficit evolution and wake meandering. The effect of atmospheric stratification on the ABL shear is estimated by finding the integral length scale and velocity scale of the ambient turbulence and solving eq. (5.18). The integral length scale can be found based on the spectral tensor in the Mann model. As the Mann spectral tensor, $\boldsymbol{\Phi}_{ij}(\boldsymbol{k})$, is the Fourier transform of the (idealised) correlation function of the turbulence, the correlation function of the turbulence may thus be found as inverse Fourier transform of the spectral tensor,

$$R_{ij}(\boldsymbol{r}) = \int_{-\infty}^{\infty} \boldsymbol{\Phi}_{ij}(\boldsymbol{k}) e^{-i\boldsymbol{k}\cdot\boldsymbol{r}} d\boldsymbol{k} \; = \overline{u_i(\boldsymbol{x}) u_i(\boldsymbol{x}+\boldsymbol{r})} \tag{5.20}$$

From this follows that the integral turbulent length scale in any direction can be found by eq. (5.21).

$$L_i = \int_0^{R_{ii}(r)>0} \frac{R_{ii}(r)}{R_{ii}(0)} dr \tag{5.21}$$

The velocity scale of the atmospheric turbulence can in principle be derived from the correlation function in eq. (5.20), however as the ambient turbulence intensity is an input parameter to the DWM model, it is more practical to relate the turbulence velocity scale to the turbulence intensity. This is achieved by integrating the energy content of the normal stress in flow direction, $\overline{u'u'}$, and the shear stress, -$\overline{u'w'}$, in the Mann turbulence spectra. The ratio of the two Reynolds stresses is thus a function of atmospheric stability and can be used to calculate the turbulent velocity scale in all atmospheric stability classes from the ambient turbulence intensity by eq. (5.22).

$$u^*_{ABL} = \left[\left(TI^2_{AMB} * \frac{-\overline{u'w'}}{\overline{u'u'}}\right)\right]^{1/2} \tag{5.22}$$

The principle to find the effect of atmospheric stability on the wake deficit evolution is similar to that of finding the ABL shear, the only difference is that the turbulence scales are calculated based on the small-scale turbulence left after subtracting the turbulent energy which affects the wake meandering (i.e. the spectra in the rightmost figures in figure 5.8). This means that the integral length scale, l^*_{DEF}, is based on eqs. (5.20) and (5.21), but that spectral tensor is replaced by the filtered spectral tensor, $\boldsymbol{\Phi}_{ij}(\boldsymbol{k})_{DEF}$, after the "inverted *jinc* function" has been applied, see eq. (5.23).

$$\boldsymbol{\Phi}_{\mathrm{ij}}(\boldsymbol{k})_{\mathrm{DEF}} = \boldsymbol{\Phi}_{\mathrm{ij}}(\boldsymbol{k})\left(1 - \left(\frac{2\cdot J_1\left(\sqrt{k_2^2+k_3^2}\cdot R\right)}{\sqrt{k_2^2+k_3^2}\cdot R}\right)^2\right) \tag{5.23}$$

Furthermore, the turbulent velocity scale, u^*_{DEF}, is found by eq. (5.22), with the difference that the spectral integration to find the normal stress, $\overline{u'u'}$, and the shear stress, -$\overline{u'w'}$, now is based on the spectral integration of the "deficit scales". The contribution to eddy viscosity in the DWM model is found by applying relevant the length and velocity scales together with the conventional filter functions and calibration constants.

$$v_{T,AMB} = F_1 k_1 u^*_{ABL,\lambda<2D} l^*_{ABL,\lambda<2D} \tag{5.24}$$

The wake meandering in the DWM model is calculated based on the turbulent eddies experienced by a circular disc by the oncoming wind field, see Larsen [52]. This approach is motivated by the assumption that the wake acts as a passive tracer in turbulence field, i.e. the movements of the wake is completely dictated by the large scale turbulent functions of the oncoming flow. Based on this assumption, the effect of atmospheric stability can be included directly by using the Mann turbulence corrected for non-neutral atmospheric turbulence by Peña et al. [44] as input to the meandering algorithm.

The effect of applying the proposed corrections in the DWM model is verified by a comparison to OpenFOAM AL simulation data. The simulations are conducted to mimic the conditions along rows of turbine from the offshore wind farms of OWEZ, which consists of 36 V90-3MW turbines, and North Hoyle, which consists of 30 V80-2MW turbines, see table 5.3.

Table 5.3: list of conducted simulations cases to study the effect of atmospheric stability on ambient turbulence characteristic and wind turbine wake evolution.

Case	Turbine	WS	TI	L	Nr WTG	Spacing
N-N.H. row A	V80	8m/s	6.12%	-∞	4	11D
U-N.H. row A	V80	8m/s	6.16%	-83.6	4	11D
N-N.H. row B	V80	8m/s	6.12%	-∞	4	10D
U-N.H. row B	V80	8m/s	6.16%	-83.6	4	10D
N-N.H. row C	V80	8m/s	6.12%	-∞	5	4.4D
U-N.H. row C	V80	8m/s	6.16%	-83.6	5	4.4D
N-OWEZ row A	V90	8m/s	6.12%	-∞	3	13D
U-OWEZ row A	V90	8m/s	6.16%	-83.6	3	13D
N-OWEZ row B	V90	8m/s	6.12%	-∞	3	11D
U-OWEZ row B	V90	8m/s	6.16%	-83.6	3	11D

The AL simulations used in this work is based on 800s of simulation time. The length of the simulation is a trade-off between reaching stable statistics and the time required to run the simulations (the investigated cases require approximately 500,000 CPU-hours for a simulation time of 600s). Compared to the time scale of the most energy containing turbulent scales, 800s is relatively short, and as a result the most important scales of an unstable atmosphere is only realized a few time. The relatively short simulation time of the AL model causes two main sources of uncertainty; 1) misalignment of the wake centre and 2) spatial inhomogeneity of wind speed and turbulence in the simulation domain. The total uncertainties due to the short simulation times are estimated to 0.12m/s and 0.60pp in neutral conditions and 0.18m/s and 0.92pp in very unstable conditions, for wind speed and turbulence intensity respectively. For more details on the uncertainty estimation see Keck et al. [39, 45].

The accuracy of the DWM model is evaluated by the STE method (see eq. (5.4)). As the STE metric is based on the root-mean-square difference between the flow field in the DWM model and the AL model, the uncertainty in the AL simulations will influence the STE linearly. It should therefore be noted that the uncertainty represent approximately 36% the STE in terms of wind speed and 47% of turbulence intensity of the results presented in table 5.4.

5.3.4 Main results and Conclusions:

The results presented show that atmospheric stability influences the wake effects experienced in a wind farm even when maintaining the ambient turbulence intensity constant. This means that the effect atmospheric stability has on the turbulent length scale is important for wind farm dynamics, and that turbulence intensity alone is not sufficient to describe wake dynamics in the atmospheric boundary layer. Specifically the presented data show that atmospheric stability affects the length scale of the atmospheric turbulence, and that this shift in length scale influences both the wake meandering and the wake deficit evolution. The wake meandering of the DWM model in a very stable atmosphere, quantified as the standard deviation of the wake centre, is found to be ~40% lower in lateral direction and ~56% lower in vertical direction compared to neutral atmospheric conditions at the same ambient turbulence intensity. The same comparison performed in a very unstable atmospheric conditions shows that the wake meandering is ~40% larger in lateral direction and ~76% larger in vertical direction. The OpenFOAM AL model predicted that the wake meandering in a very unstable atmosphere increase with as much as ~99% in lateral direction and ~107% in vertical direction, compared to neutral stratification.

The eddy viscosity term, which governs the wake deficit evolution in the DWM model, is relatively constant when comparing neutral and unstable stratification. In stable stratification, however, the eddy viscosity is seen to be ~50% lower. This is due to the smaller length scale of the turbulence in the stable atmosphere which causes a less effective transport of turbulent momentum and thereby lower deficit diffusion.

Table 5.4 show the STE of five unsteady cases calculated with both the modified (DWM B) and the unmodified (DWM A) versions of the DWM model compared to OpenFOAM AL simulations. The study is conducted to verify that the suggested correction increases the ability to predict the flow field under unstable atmospheric conditions. By comparing the results it can be concluded that the atmospheric stability correction reduces the average STE by ~19% in terms of wind speed and ~28% in turbulence intensity.

Table 5.4: The STE (eq. 5.4) of the DWM model without (A) and with (B) the atmospheric stability correction compared to the OpenFOAM simulations for the unsteady simulations listed in table 5.3.

	STE WS DWM A [m/s]	STE WS DWM B [m/s]	Ratio B/A	STE TI DWM A [%]	STE TI DWM B [%]	Ratio B/A
N.H. row A	0.53	0.39	0.74	2.9	2.0	0.69
N.H. row B	0.60	0.45	0.75	3.4	2.4	0.71
N.H. row C	0.71	0.63	0.89	2.1	2.0	0.95
OWEZ row A	0.48	0.40	0.83	2.0	1.2	0.60
OWEZ row B	0.52	0.43	0.83	1.7	1.1	0.65
Mean	**0.57**	**0.46**	**0.81**	**2.4**	**1.7**	**0.72**

To illustrate the effect of the atmospheric stability correction the velocity and turbulence intensity profiles behind the two first turbines in the *"U-N.H. row A"* case are plotted in figure 5.9. It can be seen that the velocity deficit of the modified DWM model is shallower and wider, and that the average turbulence intensity is higher, which result in a better agreement with the reference AL data.

Wake-loss as a function of atmospheric stability

Figure 5.10 shows the effect on power production in single wake operation as a function inflow angle and atmospheric stability. The ambient wind speed is 8m/s and the turbulence intensity is 6%. The two turbines are located 7D apart. It can be seen that for this configuration the power deficit is 45% deeper in a very stable atmosphere (0.58) compared to a very unstable atmosphere (0.4) when the incoming flow is aligned with the axis of the two turbines. The difference decreases with increasing inflow angle to the turbines, and at mean wind direction exceeding ~7^{o} the power deficit is independent of atmospheric stability.

Assuming a uniform wind distribution, the depicted case yields a reduction in annual energy production (AEP) of 1.7%, 1.6% and 1.4% for very stable, neutral and very unstable atmospheric conditions, respectively (under the assumption that no power loss is experienced in the 330^{o} not shown in the figure). The increase in turbulence intensity in the sector ± 10^{o} is 5.7, 5.1 and 4.9pp (i.e. ΔTI in %) for very unstable, neutral and very stable atmospheric conditions, respectively. In terms of power production, the same trends as in the case presented in figure 5.10 are seen for a range of turbulence intensities and turbine spacing (see Keck et al. [39]), i.e. that the wake in stable stratification cause a larger power loss at the second turbine and that the neutral case is closer to the very stable case than

the very unstable case. The average difference in AEP for the tested cases is 0.22% from very stable to neutral and 0.33% from neutral to very unstable stratification. Considering the effects on wake-added turbulence, however, the influence of atmospheric stability is more complex. This is a consequence of the difference in downstream evolution of the two components of the wake-added turbulence, small-scale shear generated turbulence and apparent turbulence due to wake meandering, with atmospheric stability.

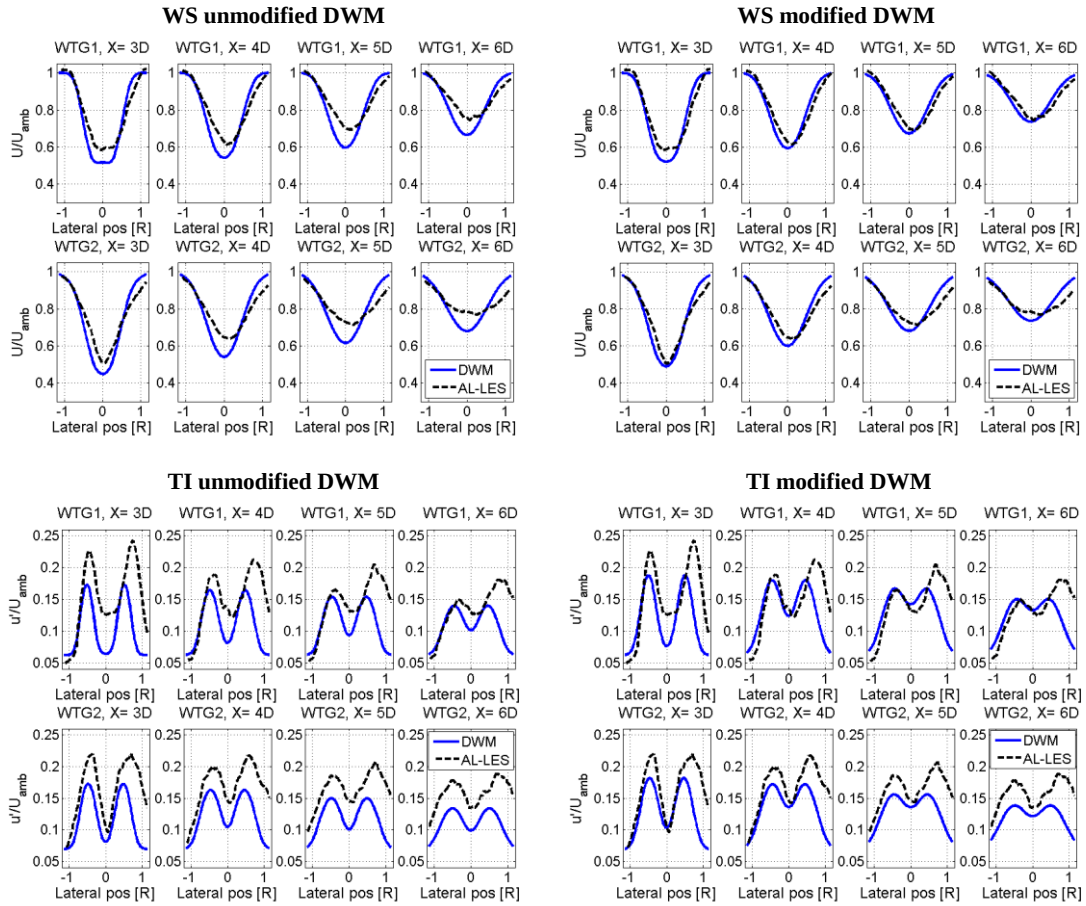

Figure 5.9: Velocity (top) and turbulence intensity (bottom) distribution at hub height 3, 4, 5 and 6D (from left to right) behind the two turbines in the "U-N.H. row A" case. The top row of each figure depicts the result behind the first turbine and the bottom row shows the result behind two turbines.

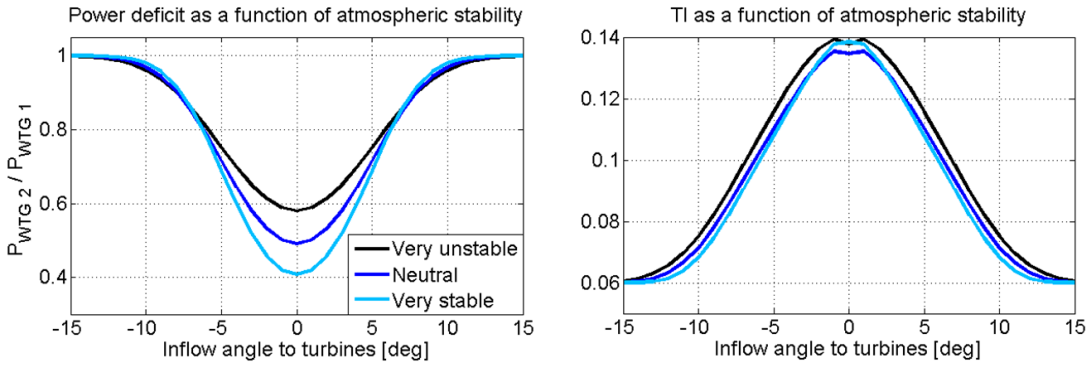

Figure 5.10: Power deficit (left) and turbulence intensity distribution (right) as a function of the atmospheric stability and inflow direction simulated with the DWM model.

Table 5.5 shows a comparison of the effect in terms of power production of a row of turbines due to atmospheric stability. By comparing the average wake losses in the table, it is seen that the AL model predicts a larger difference in wake loss due to atmospheric stability than the DWM model and the field data. The wake losses in very unstable conditions are seen to be 45% smaller compared to neutral conditions. The corresponding number for the DWM model is 10% and it is 6% for the field data. However, it should be noted that the power production in neutral atmosphere for the *N.H 10D* case is an outlier and influences the field data result, see table 5.5. Excluding the *N.H 10D* case yields a 13% difference between unstable and neutral atmospheric conditions instead of the current 6%. This large difference in the AL simulations is attributed to the large increase in wake meandering as a function of atmospheric stability. Comparing the average wake losses in very stable conditions and neutral conditions, the DWM model predicts 12% higher losses and the field data show 13% higher losses.

Table 5.5: Average power production of the wake-affected turbines in the North Hoyle and OWEZ simulations compared to field data. The ambient conditions in all cases are wind speed of 8m/s and a turbulence intensity of 6.2%.

	Field data-VS	DWM-VS	Field data-N	AL-N	DWM-N	Field data-VU	AL-VU	DWM-VU
OWEZ 11D	0.62	0.57	0.71	0.55	0.61	0.72	0.74	0.67
OWEZ 13D	0.74	0.63	0.79	0.59	0.67	0.81	0.66	0.70
N.H 4.4D	0.39	0.28	0.44	0.35	0.35	0.54	0.48	0.38
N.H 10D	0.62	0.53	0.69	0.58	0.59	0.65	0.77	0.64
N.H 11D	0.66	0.56	0.67	0.55	0.61	0.70	0.70	0.67
Mean of COL	0.61	0.51	0.66	0.52	0.57	0.68	0.67	0.61

Saturation level of wind speed and turbulence intensity over a row of turbines

An investigation was also conducted to study the equilibrium level of wind speed and turbulence intensity in the flow through a row of wind turbines in various atmospheric conditions. The purpose of this investigation is to give suggestions for strategies of handling multiple wakes in engineering wake models. The turbulence build-up effect was studied by comparing the flow field through the row of turbines in the AL simulations. The flow field behind five turbines are plotted together based on the downstream distance to the closest wake-emitting turbine, see figure 5.11. The same effect are also studied using the DWM model with ambient wind speed of 8m/s and 6% turbulence intensity for turbine spacings of 4D, 6D and 10D in very stable, neutral and very unstable atmospheres.

The conclusion of the study is that a combined velocity deficit behind a row of turbines can be approximated by the deficit behind a single turbine if the flow is aligned with the row of turbines. The average error associated with using a single wake deficit is 0.13m/s (corresponding to 8.8% of the average reduction in mean velocity) compared to using the combined deficit after eight turbines. The same approach cannot be applied to model the turbulence intensity over a row of turbines. The increase in turbulence intensity at the second rotor is approximately 75% of the increase seen at the eighth turbine. A recommended “rule-of-thumb” approach may be to use the value at the fifth turbine as the saturation level of turbulence intensity over the row. The average error associated with this choice is 0.25pp (which represents 3.2% of the average wake-added turbulence of 7.8pp) compared to the value at the eighth turbine.

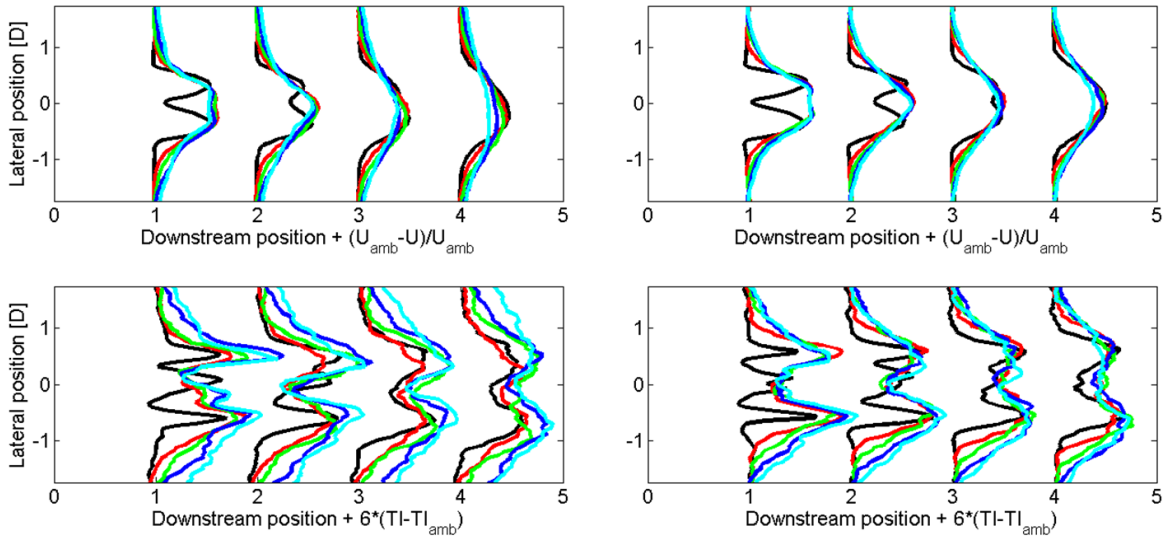

Figure 5.11: The velocity field (top figures) and turbulence field (bottom figures) from the "N-N.H. row C" case (left figures) and the "U-N.H. row C" case (right figures) behind a single turbine (black lines), compared to flow field behind two, three, four and five turbines (red, green, blue and cyan lines).

6 Technical description of the DWM model

6.1 Final version of the DWM model

The aim of this chapter to give a comprehensive description of the final version of the DWM model, including model augmentations proposed in the previous chapter, to serve as a support document for implementation of the DWM model. This first section gives a summary of the workflow in the DWM model as well as references to the research articles containing the background for the current formulation. The subsequent sections contain detailed descriptions of the wake deficit model, the method to calculate the wake meandering, power production (if the DWM model is used as a standalone flow-solver) and multiple wake simulation.

The version of the DWM model presented by Madsen et al. [32] is the baseline for the research activities presented in this thesis. The fundamental functionality is to a large extent kept unchanged. The main changes, as described in the research summary in chapter 5, are:

1. The two-dimensional eddy viscosity model (Keck et al. [37])
2. The strain-rate contribution from the ABL shear in the wake deficit calculation (Keck et al. [39])
3. The method to model multiple wakes and wake-added turbulence (Keck et al. [39])
4. The inclusion of atmospheric stability effects on the deficit and wake meandering (Keck et al. [45]).
5. The wake meandering applied is based on the same principles as proposed by Larsen et al. [52], however, a wake transport velocity equal to 80% of the free stream velocity (as proposed by Keck at al. [36]) is employed rather than using the full free stream velocity as proposed by Larsen et al. [52].

The DWM model is originally designed to be coupled with an aero-elastic software to allow for predictions of loads and power production of wake-affected turbines. However, the model can also be used as a standalone flow-solver to simulate power production as well as the distribution of wind speed and turbulence intensity inside a wind farm (as is done in Keck et al. [39, 45]). This may be more practical for research studies, or for simulating the flow field in a wind farm. The workflow of these two configurations is the same apart from the method used to calculate the power production of the wake-affected wind turbines. If the DWM model is coupled to an aero-elastic solver, the power production (and loads) will be based on the time average of the response of the aero-elastic model due to the instantaneous flow field at the turbine position (step 4a). The DWM model operated as standalone will instead base the power production directly on the mean flow field (step 4b). The workflow of the DWM model is shown in figure 6.1, and can be summarized in five steps:

1. Define the input conditions for the wake-emitting turbine
   i. Average axisymmetric wind speed distribution and average turbulence intensity over the rotor (including upstream wake effects if the turbine is operating in waked conditions)
   ii. Turbine specific rotor induction and hub height
   iii. Atmospheric stability condition
2. Calculate the wake deficit evolution in the MFoR (i.e. solve the axisymmetric N-S equation for the wake deficit). This yields the steady-state velocity and turbulence intensity profile as a function of downstream position (see section 6.1.1).

3. Calculate the stochastic wake meandering of the wake centre position to find the time dependent velocity and turbulence intensity field in the FFoR (see section 6.1.2).

4a. If the DWM model is coupled to an aero-elastic model, the dynamic loads and power production of the wake-affected turbines are calculated by the aero-elastic model based on the transient velocity and turbulence fields in the FFoR (see section 6.1.3).

4b. If instead the DWM is used as standalone flow-solver, the power production is based on the mean flow field at the wake-affected rotor. The mean flow field is found by applying the effect of wake meandering statistically in a field model (see section 6.1.4).

6. For simulations containing more than two turbines, the average inflow velocity and turbulence field at the wake-affected turbine in Cartesian coordinates are calculated (either by the aero-elastic code of the field model). The flow field in Cartesian coordinates is thereafter transformed into an axisymmetric flow field, which is applied as boundary conditions in the subsequent wake deficit calculation of the wake-affected turbine (see section 6.1.5).

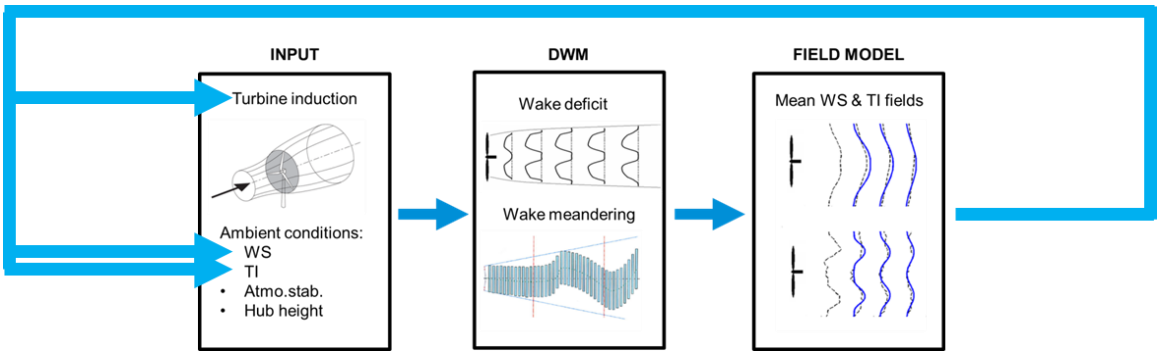

Figure 6.1: Schematic description of the workflow in the DWM model for a multiple wake simulation.

6.1.1 Wake deficit model

The wake deficit in the DWM model is governed by the steady state, axisymmetric thin shear layer approximation of the N-S equations in which momentum is governed by,

$$u\frac{\partial u}{\partial x} + v\frac{\partial u}{\partial r} = \frac{1}{r}\frac{\partial}{\partial r}\left(\upsilon_T r\frac{\partial u}{\partial r}\right) \tag{6.1}$$

and continuity is maintained through

$$\frac{1}{r}\frac{\partial}{\partial r}(rv) + \frac{\partial u}{\partial x} = 0 \tag{6.2}$$

In these equations, the velocity components u and v are in the mean flow (x) and radial (r) directions, respectively, and υ_T is the eddy viscosity. The benefit in using the thin shear layer approximation is a significantly reduced computational cost. This is achieved by omitting the pressure gradient term, approximating the flow as axisymmetric, and by assuming that the velocity gradients in streamwise direction are much smaller than those in radial direction. The fact that the pressure gradient term is neglected means that no pressure-velocity coupling is required. Furthermore, as the flow is assumed to be axisymmetric, only one component of the momentum equation needs to be solved and the other velocity component is given by the continuity equation (which is otherwise unused as there is no pressure-velocity coupling).

Turbulence closure in the wake deficit calculation is obtained by an eddy viscosity formulation, eq. (6.3). The eddy viscosity consist of two contributions: 1) a contribution due to the ambient turbulence, see eq. (6.4), and 2) a mixing length description of the turbulence due to the shear layer of the wake deficit, see eq. (6.5). The eddy viscosity due to the wake deficit includes a correction to avoid underestimating the turbulent stresses as the velocity gradient of the deficit, $\left|\frac{\partial u}{\partial r}\right|$, approaches zero. This is achieved by blending the classical Prandtl mixing length model (first term of eq. (6.5)) with a modified expression based on the average velocity gradient over the deficit (second term in eq. (6.5)) using the max operator.

$$\upsilon_T = \upsilon_{T\,AMB} + \upsilon_{T\,WAKE} \tag{6.3}$$

$$\upsilon_{T\,AMB} = F_1 k_1 u^*_{ABL,\lambda<2D} l^*_{ABL,\lambda<2D} \tag{6.4}$$

$$\upsilon_{T\,WAKE} = F_2 k_2 \cdot max\left(l^{*2}\left|\frac{\partial u}{\partial r}\right|, l^*(1-U_{MIN})\right) \tag{6.5}$$

In eq. (6.4), $u^*_{ABL,\lambda<2D}$ and $l^*_{ABL,\lambda<2D}$ represent the length and velocity scales of the part of ambient turbulence which affect the wake deficit evolution (roughly corresponding to eddies smaller than 2D). In eq. (6.5) *l** represents the mixing length of the wake turbulence (*l** is taken equal to half the width of the wake) and U_{MIN} is the lowest axial velocity in the wake cross section and is thus a function of downstream distance alone. The max operator is included in the eddy viscosity formulation to avoid underestimating the turbulent stresses at locations where the velocity gradient of the deficit, $\left|\frac{\partial u}{\partial r}\right|$, approaches zero. The model constants, k_1 and k_2, are used to calibrate the deficit model. F_1 and F_2 are empirical filter functions included to govern the development of turbulent stresses.

The filter functions, F_1 and F_2, in the DWM model are required to model the evolution of turbulence before the mean velocity field and the turbulence field have reached a state of quasi-equilibrium. This is a consequence of applying an eddy viscosity closure which does not include a transport term for the turbulent kinetic energy. Without filter functions, the turbulence field would be in quasi-equilibrium with the local strain-rate directly at the rotor. This would result in un-physically high turbulence levels close to the rotor, as the mean velocity field changes faster than the turbulence field when the air passes the rotor. The filter functions correct for two fundamentally different effects. The F_1 function is included to compensate for the effect on turbulence caused by the boundary condition treatment in the DWM model. To account for the pressure effects, the velocity field applied at the inlet boundary of the DWM model includes the effects of deceleration and expansion due to the pressure field recovery (see eqs. (6.9) and (6.10)). This generates artificially large velocity gradients in the near wake region (i.e. in the wake-region before the pressure field on a wind turbine has recovered). The role of the F_1 filter function is to reduce the effect of the DWM boundary condition on the turbulent stresses due to ambient turbulence, to avoid unphysical turbulence diffusion of the deficit in the near wake. The length over which the F_1 function acts is taken to be 2D, which is equal to the distance required for the pressure to recover behind the turbine according to Crespo et al. [15] and Sanderse [59]. The F_2 function, apart from the 2D near wake treatment, also governs the development of turbulence generated by the wake shear layer. The length required for the turbulent stresses to reach quasi-equilibrium with the mean velocity field is on the order of 10D based on AL simulations. The details and motivation for this turbulence formulation are given by Keck et al. [37].

Before the eddy viscosity from eq. (6.3) is applied in eq. (6.1) it is scaled to include a strain-rate contribution due to the ABL shear, du/dz_{ABL} by

$$\frac{du}{dr}_{Total} = \begin{cases} \frac{du}{dr}_{DWM} & , \left|\frac{du}{dr}_{DWM}\right| \geq \frac{du}{dz}_{ABL} \\ \frac{du}{dr}_{DWM} + \frac{1}{\pi}\int_{\alpha_1}^{\alpha_2}\left(\frac{du}{dz}_{ABL}\cdot\sin(x)\,dx\right) - (\alpha_2-\alpha_1)\frac{du}{dr}_{DWM} & , \left|\frac{du}{dr}_{DWM}\right| < \frac{du}{dz}_{ABL} \end{cases} \quad (6.6)$$

$$\nu_t' = \nu_t \cdot \frac{\frac{du}{dr}_{Total}}{\left|\frac{du}{dr}_{DWM}\right|}. \quad (6.7)$$

where du/dr_{DWM} is the wake velocity gradient in the wake deficit modelled by the DWM model, du/dr_{TOTAL} is the total velocity gradient with the ABL shear contribution included, and α is the angular locations where the effect of the atmospheric shear in cylindrical coordinates is larger than the wake deficit shear. α_1 and α_2, are found by $arcsin(\frac{du}{dr}_{DWM} / \frac{du}{dz}_{ABL})$ and π-α_1 respectively. The details of this correction can be found in Keck et al. [39]. Applying the scaled eddy viscosity from eq. (6.7) in eq. (6.1) yields the desired effect of basing the turbulent stresses in the DWM wake deficit calculation by the ABL shear corrected strain-rate.

$$\tau_{stress\,DWM} = \nu_t' \cdot \frac{du}{dr}_{DWM} \rightarrow \nu_t \cdot \frac{\frac{du}{dr}_{Total}}{\left|\frac{du}{dr}_{DWM}\right|} \cdot \frac{du}{dr}_{DWM} \rightarrow \nu_t \cdot \frac{du}{dr}_{Total} \quad (6.8)$$

The system of equations given by eqs. (6.1) - (6.7) is solved using a finite-difference scheme, in which a second-order central-difference scheme in the radial direction and a first-order upwind scheme in the mean flow direction are applied. As information only moves downwind along the mean flow direction, a solution can be obtained by "marching" downstream, solving each axial position sequentially. For each location along the mean flow axis, the calculation of the velocity field can be summarized as:

1. Solve the momentum equation for the streamwise velocity component at all radial positions explicitly, using the value for radial velocity component and eddy viscosity from the previous location upstream. This yields a tri-diagonal equation system where all the coefficients are known, which can be efficiently solved.
2. Once the streamwise velocity at the present axial position is known, the corresponding radial velocity and the eddy viscosity can be computed using eqs. (6.2) and (6.3)-(6.7) above.
3. March to the next downstream location and repeat steps 1-3.

6.1.1.1 The boundary condition in the wake deficit model

Omitting the pressure gradient term in the governing equations has the consequence that the near-wake region, where pressure is recovering and significant gradients are present, will not be accurately represented by the DWM model. The inaccuracy in this region is considered acceptable since the near-wake region is not of primary interest when modelling intra-turbine wake effects, as long as the far-wake calculation remains accurate. In the DWM model the effect of the pressure gradient is considered to be negligible at a distance of 3D behind the turbine. This location is referred to as the *point of DWM validity*. The inlet boundary condition (just behind the rotor) is designed to artificially account for the effect of the neglected pressure gradient in such a manner that the resulting flow field after 3D is accurately represented. This is done by including the pressure induced deceleration, and the resulting stream tube expansion, of the fluid at the rotor disc. The boundary condition is based on the turbine-specific averaged axial induction *a*. The pressure effects are approximately accounted for by scaling the

turbine induction both in depth and in width by the factors f_U and f_R, respectively. The resulting inlet velocity distribution, U_{BC}, as a function of radial position applied in the DWM deficit calculations is given by,

$$U_{BC}(r_{BC}) = U_{amb}(1 - (1 + f_U)a(r_{rot})) \tag{6.9}$$

$$r_{BC} = r_{rot}\sqrt{\frac{1-\bar{a}}{1-(1+f_R)\bar{a}}} \tag{6.10}$$

where U_{amb} is the ambient wind speed at hub height, r_{rot} is the radial coordinate of the induction vector at the rotor and $\bar{a}$ is the average induction over the rotor plane. According to BEM theory, the lowest velocity in the wake should correspond to a wake deficit of twice the induction at the rotor. This corresponds to both f_U and f_R being equal to unity. However, from the AL simulations it can be observed that the minimum velocity in the wake occurs approximately 1D behind the rotor and that the double induction, $2a$, is not realised in turbulent inflow ($\sim 1\text{-}1.85a$ is the minimum velocity observed and this occur ~1D behind the rotor, see figure 2.10).

In this work, the approach to find the f_U and f_R coefficients is based on a least-square calibration to AL results. The calibration of the boundary condition conducted in this work relies on minimizing the STE at (and after) the point of DWM validity (i.e. 3D into the computational domain). This is the most important aspect of the boundary condition in the DWM model, as the results in the near-wake region are not used. The coefficients which result in the smallest STE error at 3D are f_U=1.10 and f_R=0.98. The improvement in terms of STE by applying the suggested f_U and f_R factors compared to applying f_U=1 and f_R=1 is on the order of 5%.

Applying an f_U larger than unity, and the fact that f_U and f_R assume different values in the DWM deficit calculation may seem counter-intuitive. Applying an f_U which is larger than the f_R means that less mass passes through the inlet plane of the DWM model after the pressure effects has been accounted for. A likely explanation as to why this improves agreement with AL reference data after the point of DWM validity, is that the artificially large velocity gradient due to the boundary conditions treatment results in a large transfer of mass into the wake (and the domain through the upper boundary) of the DWM model in the near wake. By prescribing a lower mass flow in the wake, this effect is counter-balanced by the selected f_U and f_R coefficients. Similar results were obtained in the DWM model calibration carried out by Madsen et al. [32], where the derivation of the boundary condition is based on the BEM assumption of full induction. In the calibration stage, however, a correction is applied where the r_{wake} values are reduced by $1\text{-}0.45\overline{a_{rot}}$. For a mean induction of 0.2 this reduces the r_{wake} by 9%.

6.1.1.2 Wake-added turbulence

The wake-added turbulence formulation in the DWM model is designed to account for the increased level of small-scale turbulence experienced at a wake-affected turbine. The increased turbulence level has two effects: 1) it increases the fatigue loads of the wake-affected turbine (although the meandering deficit is generally speaking a larger effect), and 2) it affects the rotor induction and the wake diffusion of the wakes emitted from wake-affected turbines. The turbulent stresses in a single wake are already accounted for by the eddy viscosity formulation, eq. (6.3). The wake-added turbulence in the current implementation of the DWM model is calculated based on the turbulent stresses in the wake deficit calculation as,

$$TI_{DWM\ MFoR} = \max\left(\sqrt{\frac{1}{C_{u'w'}*(w'_{rms}/u'_{rms})}\cdot\tau_{stress\ DWM}}\ , TI_{amb}\right) \tag{6.11}$$

where the coefficient $C_{u'w'}$ and the ratio w'_{rms}/u'_{rms} describes the relationship between axial and radial turbulent fluctuations in the wake. These relations are different compared to atmosphere turbulence due to the significantly smaller length scale and the increased degree of anisotropy of wake turbulence. In this work, the correlation coefficient is given the value 0.3, and the ratio w'_{rms}/u'_{rms} is set to unity based on the findings of Larsen et al. [145]. The first term under the "max-operator" represent the turbulence intensity which acts in the DWM deficit calculation. The second term is a correction to ensure that the local turbulence intensity used to estimate the wake-added turbulence at a downstream turbine always assumes a value equal to or greater than the ambient turbulence intensity, TI_{amb}. The correction is required for two reasons: 1) to remove regions of low turbulence in the wake deficit, and 2) to set the ambient turbulence value at all radial nodes outside of the wake deficit before adding the effect of wake meandering to find the turbulence in the FFoR at a downstream turbine. The regions of low turbulence inside the wake of the DWM model are linked to regions of low velocity gradients, which, in combination with the eddy viscosity closure, result in very low turbulent stresses. In nature, turbulent energy is transported, both radially and axially, and as a result the turbulence never goes below the ambient turbulence level. These processes are not included in the DWM model. The effect of the correction can be seen in figure 6.2.

For details of this formulation see the section "improved wake-added turbulence formulation" in Keck et al. [39]. Eq. (6.11) yields a local value of wake turbulence intensity in the wake deficit for each computing node in the DWM domain, $TI_{DWM\ MFoR}$.

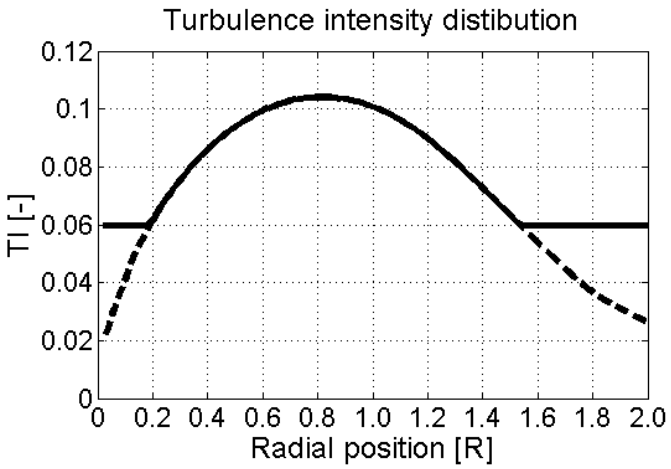

Figure 6.2: Effect of the turbulence correction applied by eq. (6.11) at a cross section 8D downstream of the wake-emitting turbine. The dashed line represents the turbulence applied in the DWM deficit calculation, and the solid line shows the corrected turbulence used to estimate the turbulence level at downstream turbines.

6.1.2 Wake meandering

The DWM deficit model, described in the previous section, outputs a steady-state wind speed and turbulence intensity distribution in the MFoR. To conduct simulations of the flow field in the FFoR (e.g. at a downstream wind turbine), the effect of large scale wake meandering of the wake deficit must be accounted for. The wake deficit calculation can be thought of as generating a "tube" of wake deficit profiles as a function of downstream distance from the wake-emitting turbine. The wake meandering is added by dividing this tube into disc shape wake-segments, and stochastically translate each of these wake-segments in lateral and vertical direction. A location downstream of the wake-emitting turbine in the FFoR, would thus experience a cascade of wake-segments where the centre of the wake-segment have a stochastic offset relative to the mean wind direction due to wake meandering, see figure 6.3.

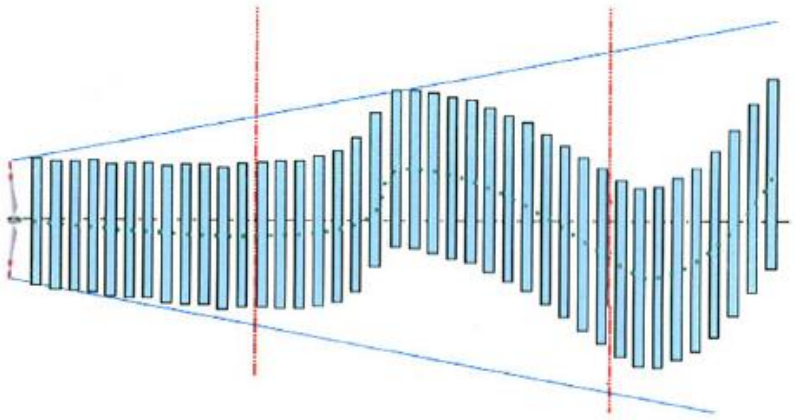

Figure 6.3: Schematic illustration of the wake meandering as applied in the DWM model.

The process of combining the steady-state wake deficit with the transient wake meandering in the DWM model, relates to the split in scales, which is based on the presumption that the two effects can be considered mutually independent. This implies that the wake deficit profiles in two neighbouring wake-segments are independent of each other, i.e. no streamwise mixing occurs between the wake-segments in the meandering process.

The movements of the wake-segments in the DWM model are based on the passive tracer assumption (Larsen et al. [52]). This means that the meandering of the wake is dictated by the turbulent fluctuations of the ambient flow. The instantaneous wake movements can be found by averaging the turbulent fluctuations acting on a cross section of the wake at that moment. As a consequence, the wake meandering will be unaffected by small turbulence scales (as they even out over the cross section of the wake), and thus essentially be governed by the large scale structures of the ambient turbulence. The numerical method used in this work to calculate wake meandering paths based on the principle described above can be summarized in six steps:

1. Use the Mann turbulence model (Mann [42, 43]) to generate random Fourier coefficients in three dimensions. These coefficients will represent the Fourier transform of a three dimensional incompressible frozen turbulence field.
2. Incorporate the effect that wake meandering is governed by the average of all fluctuations over the wake cross section. This is done mathematically by multiplying the generated Fourier coefficients with the "*Jinc*-function" (this is the Fourier transform equivalent of the process of averaging over a circular disc, see eq. (5.19) and Goodman and Gustafson [68]). This multiplication in Fourier space is equivalent to the convolution of the random turbulent velocity field, described by the Fourier coefficients in step 1, and a circular disc in physical space.

3. Release wake-segments at the wake-emitting turbine at a frequency of 1Hz. The wake-segments travel downstream with a velocity of 80% of the ambient wind speed (based on the findings of Keck et al. [36]), this is referred to as the "*wake transport velocity*" (U_{wake}). The frozen turbulence box travel along the flow with the ambient wind speed. Consequently, the wake deficit travels at a negative speed of -20% of the ambient wind speed relative to the frozen turbulence field.
4. Calculate the fluctuating velocities in streamwise, lateral and vertical direction (u'_{wake}, v'_{wake} and w'_{wake}) of all emitted wake-segments at each time step based on their position in the turbulence box. To avoid interpolation as the wake-segments move relative to the turbulence box, which otherwise causes a reduction of turbulent energy, the velocity at the location of the wake-segment is found by applying the definition of inverse Fourier transform (which is continues and can be used to find the velocity at any location in the field, contrary to the inverse fast Fourier transform (IFFT) which generates turbulent fluctuations in a box of fixed spatial resolution).
5. Update the position of the wake-segment at every time step (*dt=1s*) according to eqs. (6.12-6.14).

$$dx = (U_{wake} + u'_{wake})dt \tag{6.12}$$

$$dy = v'_{wake}dt \tag{6.13}$$

$$dz = w'_{wake}dt \tag{6.14}$$

6. Finally, when all the wake-segments have reached the desired downstream distance, the wake meandering is scaled by a factor determined by the square root of the ratio of the expected meandering energy to the total captured meandering energy. This ratio is a function of the dimensions of the turbulence box chosen.

The numerical method described above generates time series of wake centre position in lateral and vertical direction at any cross section downstream of the wake-emitting turbine.

6.1.3 DWM coupled to an aero-elastic solver

The dynamic flow field of the DWM model can be directly coupled to an aero-elastic turbine model. This is achieved by superimposing the meandering wake deficit onto the input flow field in the aero-elastic solver. As a consequence of the DWM formulation, the wake deficit profile at the wake-receiving turbine will be invariant in time (i.e. the distributions of wind speed and turbulence in the wake deficit are time invariant and functions of downstream distance from the wake-emitting turbine alone). The dynamic effect is therefore created by the wake meandering represented as a time series found by eqs. (6.13) and (6.14). The aero-elastic model computes both the power production and structural response of the wake-affected turbine.

6.1.4 DWM as a standalone flow-solver

When employing the DWM model as a standalone flow-solver, it is more computationally efficient to include the effect of the wake meandering on the flow field in a statistical manner, as opposed to using time series generated by the description in section (6.1.2). To this end, the standard deviation of the wake meandering time series is extracted from simulation (with the underlying assumption that the wake meandering has a Gaussian distribution), and stored for future use in a "lookup-table". To enable the execution of the DWM calculations presented in this thesis (and the articles on which it is based), wake meandering statistics for a range of ambient wind speeds, turbulence intensities and atmospheric

stabilities as well as hub heights and downstream distances have been extracted and stored. The standard deviation of the wake centre position is based on 50 time series of 600s of data each.

6.1.4.1 Flow field model

Knowing the distribution of the wake meandering, it is possible to calculate the average wind field and turbulence intensity in the FFoR as the convolution of the deficit in the MFoR (both wind speed and variance, i.e. the square of $TI_{DWM\ MFoR}$ from eq. (6.11)) and the distribution of the wake centre in the vertical and lateral direction due to wake meandering as follows:

$$\theta_{DWM\ FFoR}(y,z) = \iint \theta(y-y_m, z-z_m)_{DWM\ MFoR} \cdot PDF_m(y_m,z_m)\, dy_m dz_m \tag{6.15}$$

In this equation, θ represent the wind speed or variance, y-y_m and z-z_m are the local coordinates in the MFoR and PDF_m is the probability density function for the meandering distribution. The subscripts *FFoR* and *MFoR* refer to fixed and meandering frame of reference.

The turbulence intensity ($TI_{DWM\ FFoR}$), found by eq. (6.15), represents the turbulence intensity in the FFoR due to small-scale ambient turbulence and the turbulence generated by the wake shear layer. This is the turbulence which affects the wake deficit evolution of a wake-receiving turbine. The wake meandering itself, however, also has a contribution to the "*apparent turbulence*" experience at a location in the FFoR, TI_M (see Madsen et al. [32] and Vølund [29]). This contribution comes from the variation of mean wind speed experienced at a fixed location caused by the moving wake deficit. If the time series of wake meandering is applied into an aero-elastic simulation, this effect is accounted for automatically (as is the transition from MFoR to FFoR). When using the DWM model as a standalone flow-solver to study the flow field in the FFoR, however, this effect has to be explicitly accounted for. This contribution is calculated by eq. (6.16), where the first term can be thought of as the distribution of wind speeds at location (y*, z)* due to the meandering deficit and the second term is the mean wind speed in the FFoR.

$$TI_M(y,z) = \sqrt{\iint \left(U(y-y_m, z-z_m)_{MFoR} - U_{FFoR}(y,z)\right)^2 \cdot PDF_m(y_m,z_m)\, dy_m dz_m} \tag{6.16}$$

Due to the split in scales, the contributions to the turbulent fluctuations given by eq. (6.16) and (6.17) can be assumed to be uncorrelated. As a consequence the total turbulence intensity level in fixed frame of reference can be calculated as,

$$TI_{tot\ FFoR} = \sqrt{TI_M^2 + TI_{DWM\ FFoR}^2} \tag{6.17}$$

6.1.4.2 Estimating power production

In the absence of an aero-elastic model, the power production is estimated based directly on the mean inflow wind field. However, since the instantaneous power production is a nonlinear function of the local wind speed (cubic in the wind speed region where wake effects are most pronounced), the time averaged wind speed field cannot be used directly for power estimations. To approximately account for dynamic effects on power production due to partial wake operation caused by meandering, a dedicated velocity field for power estimation is calculated using the equation,

$$U_{power\ FFoR} = \sqrt[3]{\iint U^3(y-y_m, z-z_m)_{DWM\ MFoR} \cdot PDF_m(y_m,z_m)\, dy_m dz_m} \tag{6.18}$$

where again y-y_m and z-z_m are the local coordinates in the meandering frame of reference and PDF_m is the probability density function for the wake meandering. $U_{power\ FFoR}$ is the cube root of the mean value of the cube of the wind speed field in the FFoR. When this quantity is applied for power estimation, the effect that instantaneous power production is based on the local wind speed to the power of three is captured. By applying $U_{power\ FFoR}$ in eq. (6.20) an expression for the velocity field for power estimation as a function of radial position, $U_{power}(r)$, is found. Using the wind field corrected for power estimation, the power production of the turbines may be estimated using the equation,

$$P_{WTG} = \int_0^R \left[(4a(r) \cdot (1 - a(r))^2) \cdot \frac{1}{2} U_{power}^2(r) \cdot U_{power}(r)\, 2\pi r\, dr \right] \cdot f_{mek} \tag{6.19}$$

where a is the azimuthally averaged rotor induction and r is the radial coordinate. The first term in the integration is an estimation of the coefficient of power (C_p), followed by the kinetic energy per unit mass at the rotor, mass flow, and a factor for system losses from mechanical power to electricity. f_{mek} is the coefficient of mechanical to electrical power and is estimated to be 0.9. Note that a refers to average turbine induction, and is not scaled by f_U and f_R as in the DWM model boundary condition.

6.1.5 Multiple wake calculations

The first step when conducting multiple wake calculations is to find the mean flow properties to apply as inlet boundary conditions at the wake-affected turbine. The mean wind speed and the turbulence intensity at a downstream wind turbine are found either using the aero-elastic software, or by applying eq. (6.15). However, as the wake meandering (and thereby the flow field in the aero-elastic model and eq. (6.15)) is expressed in Cartesian coordinates, and the wake deficit calculations of the DWM model requires a steady-state axisymmetric velocity field as input, a transformation is required to couple the oncoming velocity field to the wake-affected turbine. This is achieved by calculating the average axisymmetric velocity field (U_{axisym}) at the downstream rotor over annular sections (in this work a dr = 0.04R is used),

$$U_{axisym}(r) = \frac{1}{2\pi\Delta r} \int_0^{2\pi} \int_{r-\frac{\Delta r}{2}}^{r+\frac{\Delta r}{2}} U_{DWM\ FFoR}(y_{WTG} + r\cos(\alpha), z_{WTG} + r\sin(\alpha))\, dr\, d\alpha \tag{6.20}$$

where y_{WTG} and z_{WTG} are the coordinates of the rotor centre of the wind turbine in the FFoR, r is the radial coordinate and α is an angle used to integrate over the angular segment. By using eq. (6.20), the velocity in the far-field of the deficit calculation of a wake-affected turbine is still equal to the ambient wind speed at the site (or the first turbine in the row).

The turbulence closure of the DWM model does not allow the use of a non-homogeneous turbulence intensity distribution as boundary condition in the calculation of the wake deficit evolution of the wake-affected turbine. This is a consequence of applying an eddy viscosity closure with no transport equation for turbulent kinetic energy. Instead, the effect of increased turbulence intensity at a wake-affected turbine is included by applying the average turbulence intensity over the rotor disc as “ambient turbulence intensity” in the subsequent deficit calculation, see eq. (6.21). The integration is carried out

from the rotor centre to the width of the initial DWM wake at the wake-affected rotor, R_w. The initial width of the wake is calculated by eq. (8) by applying the rotor radius as r_{rot} value.

$$TI_{WTG} = \frac{1}{2\pi R_w}\sqrt{\int_0^{2\pi}\int_o^{R_w} TI^2_{DWM\ FFoR}(y_{WTG} + r\cos(\alpha), z_{WTG} + r\sin(\alpha))\ dr\ d\alpha} \quad (6.21)$$

The large scale turbulence is assumed to be unaffected by the presence of the wind turbine wakes. This means that the wake-added turbulence does not influence the ABL shear or the wake meandering. Consequently, both the ABL shear and the wake meandering are based on the ambient conditions for all simulated turbines.

In the conventional DWM model configuration where the DWM model is coupled to an aero-elastic model, the temporal and azimuthally averaged induction of the aero-elastic calculation is applied in the calculation of the subsequent deficit calculation. When the DWM model used as a standalone flow-solver, however, the rotor induction of the wake-affected turbine is based on tabulated induction vectors as a function of the mean wind speed and, to a lesser extent, turbulence intensity at the rotor as,

$$a(r) = fun(U_{WTG}, TI_{WTG}) \quad (6.22)$$

The mean wind speed at the wake-receiving rotor used to find the rotor induction (U_{WTG}) is found by eq. (6.23).

$$U_{WTG} = \frac{1}{2\pi R_w}\int_0^{R_w} U_{DWM\ FFoR}\ dA \quad (6.23)$$

The induction vector of the downstream turbine is superimposed onto the mean flow field found by eqs. (6.9) and (6.10).

It should be noted that Larsen et al. [40] presented an alternative method for including multiple wake in aero-elastic calculations. This method is based on assuming that 1) the wakes may be treated as independent of each other, and 2) that the effect of multiple wake deficits at a downstream turbine may be modelled by only the deepest deficit at that instance in time and space. The aero-elastic model would then have two, or more, meandering wake deficits of different origin (and thereby shape) super imposed on the input flow field. The rotor will then experience the instantaneously lowest velocity at all locations. This method has not been applied in the research presented here and it is only mentioned as an alternative option for future development.

7 Calibration and validation of the DWM model

7.1 Calibration of the DWM model

As with all engineering models, calibration of the model coefficients to some reliable data source is essential to achieve high model performance. This can be field data, experimental data or, as in this case, data from higher-order models. The calibration of the DWM model is required to find appropriate values for the eddy viscosity coefficients (k_1 and k_2), the eddy viscosity filer functions (F_1 and F_2) and the upstream boundary condition scaling parameters (f_U and f_R).

7.1.1 Calibration procedure

The calibration is based on minimizing the standard error (STE) of the DWM flow field compared to analog flow field extracted from EllipSys3D AL calculations. The STE is defined as the root-mean-square of the difference in mean velocity between the results from the AL simulations and the DWM model, see eq. (5.4). The calibration dataset consists of EllipSys3D AL data from six flow cases with wind speeds of 6 and 10 m/s each combined with turbulence intensities of 6, 10, and 14%. The calibration is carried out in three steps, all based on the gradient-based simplex method of Lagarias et al. [154] and outlined in the Matlab User Guide [155].

Step 1: Calibrate the boundary condition

The DWM inlet boundary condition is calibrated to yield a velocity field as close as possible to the EllipSys3D AL mean velocity field at 3D behind the rotor. As discussed earlier, this is necessary in order to account for the effects of omitting the pressure gradient on the wake deficit development in the DWM model. The pressure gradient effects (expanding and reducing the velocity of the initial deficit caused by turbine induction) are captured by the scaled inlet boundary condition. The boundary condition is, therefore, a function of four model parameters: the inlet deficit modification parameters f_U and $f_{R,}$ together with the eddy viscosity constants and the filter functions from 0-3D, $k_1F_{1,0\text{-}3D}$ and $k_2F_{2,0\text{-}3D}$.

Step 2: Calibrate the F_2 filter function

The F_2 filter function is included in the DWM model to govern the development of turbulence generated by the wake shear layer. Such a function is required as turbulence closure in the DWM model is achieved by a zero-equation eddy viscosity model. Since no transport equation is modelled, the turbulence is calculated based on the local mean strain-rate. As the air passes the rotor the mean flow field over the rotor changes abruptly, and steep mean flow gradients are created close to the turbine. The turbulence, on the other hand, requires distance to reach equilibrium with the mean flow. In many cases this is on the order of 6-10D downstream of the turbine. This effect is captured by the F_2 function. The F_1 function is included as a part of the inlet boundary treatment to include the pressure field in the DWM model. The function is required before the pressure field behind the rotor has recovered, which usually occurs within 2-3D of the wake-emitting turbine. No additional calibration is made to the F_1 function, which is assumed to follow the suggestion given in Madsen et al. [32].

The F_2 filter function is found by using the k_1, the f_U and f_R parameters from step 1, and subsequently running the simplex optimization to find the optimum value of k_2F_2 at different downstream positions. The calibration is performed at downstream distances 3, 4.5, 6, 7.5 and 9D against single EllipSys3D AL

mean velocity cross sections. This yields the optimum value of k_2F_2 at five locations in the wake. By dividing the k_2F_2 values by the far-wake value of k_2, it is possible to find the value of the F_2 filter function which yields the smallest STE. Since it is desired to have a smoothly increasing filter function which reaches unity in the far-wake, the F_2 function is constructed by fitting an exponential saturation function through the five points.

The applied filter functions are given by eqs. (7.1) and (7.2), respectively, and are plotted in figure 7.1. The F_1 filter function varies linearly from 0-1 over the first two diameters of flow to compensate for the boundary conditions treatment of the DWM model. The F_2 filter function consists of two parts; the first part is related to the boundary condition treatment, and the second part to the development of shear layer generated turbulence in the wake.

$$F_1 = \begin{cases} x/2 & x < 2D \\ 1 & x \geq 2D \end{cases} \tag{7.1}$$

$$F_2 = \begin{cases} 0.035 & x < 2D \\ 1 - 0.965e^{-0.35(x-2)} & x \geq 2D \end{cases} \tag{7.2}$$

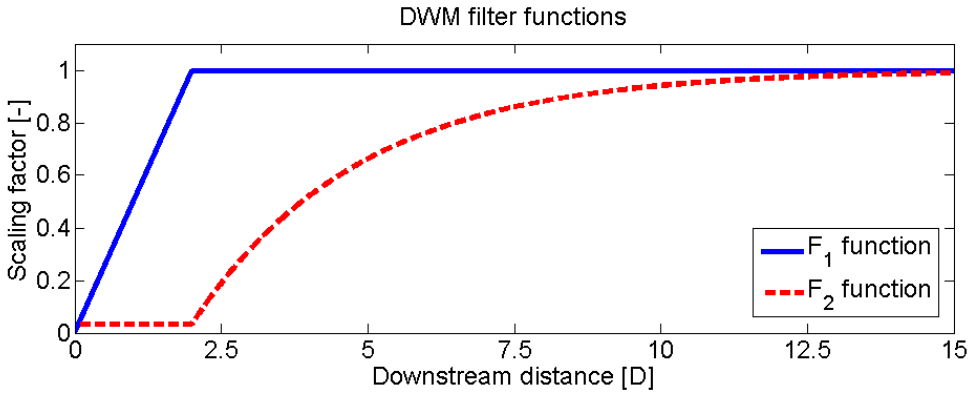

Figure 7.1: Filter functions applied in the DWM calculations.

Step 3: Global calibration of k_1, k_2, f_U and f_R

In this step, simplex optimization is performed on the four model parameters using the entire EllipSys3D AL dataset including all cases and all cross section, and also using the filter function found in step 2. The values k_1, k_2, f_U and f_R found previously, which were used to develop the F_2 filter function, are used as initial condition to the optimization algorithm. This step fine tunes these model parameters.

It should be noted that after the calibration of the DWM model coefficients and filter functions, the values are assumed to be valid for all cases. There is no site, turbine or wind farm specific recalibration and no sensitivity to Reynolds number (as the thin shear layer approximation of the N-S equation is derived for "high" Reynolds numbers).

7.1.2 Calibration results

The DWM calibration performed by Keck et al. [39] gave the following values for the model coefficients: f_U = 1.10, f_R = 0.98, k_1 = 0.587 and k_2 = 0.0178. The STE of the calibration optimum was 0.0162. The DWM velocity field and wake turbulence evolution is compared to the calibration data in figure 7.2 and 7.3.

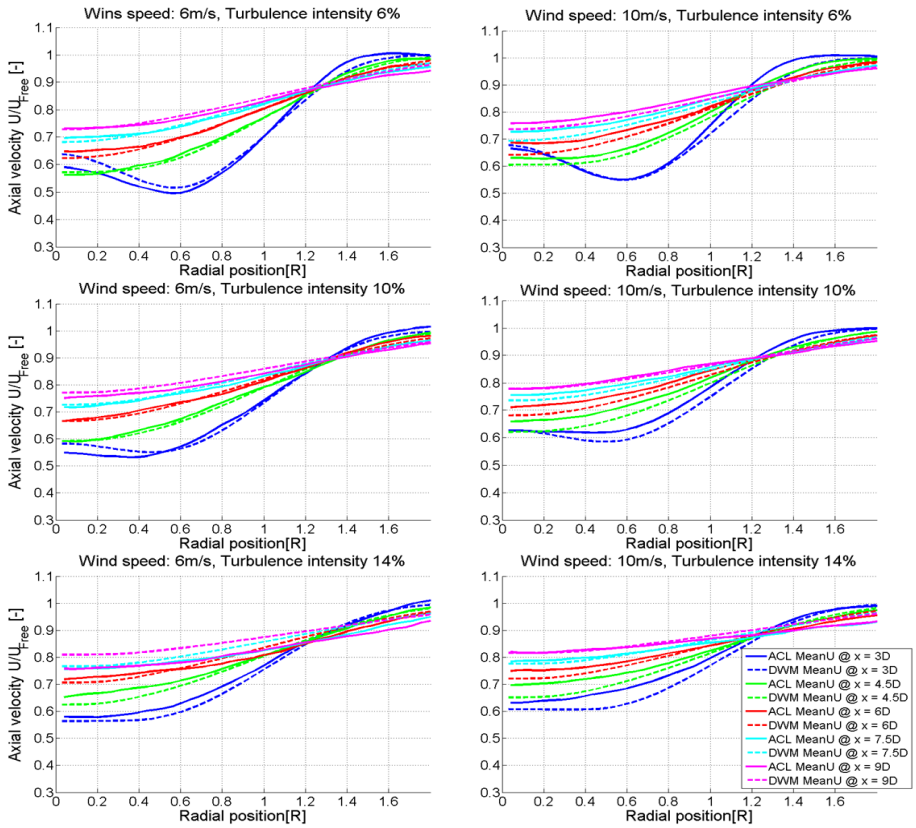

Figure 7.2: Result of DWM (dashed lines) calibration of the wind speed distribution in the MFoR to the EllipSys3D AL database (solid lines). The top represent cases where the wind speed is 6m/s and the bottom row 10m/s. The columns from left to right represent ambient turbulence intensities of 6, 10 and 14% respectively.

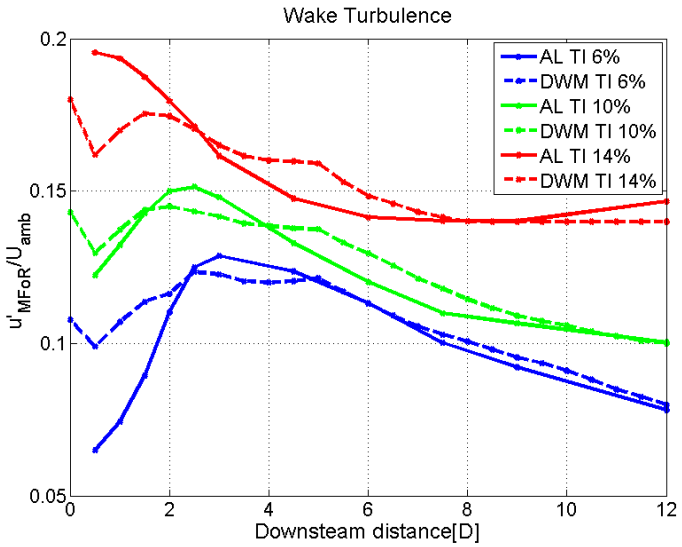

Figure 7.3: The DWM (dashed lines) and the EllipSys3D AL (solid lines) predicted turbulence intensity in the meandering frame of reference as a function of downstream distance from the wake generating wind turbine.

7.2 Validation of the DWM model

This section presents a summary of the validation efforts undertaken to quantify the accuracy of the DWM model utilized as a standalone model after including the results of the research summarized in chapter 5. The details of the standalone DWM model formulation are found in chapter 6.

7.2.1 Validation data

Two sources of data have been used for DWM model validation; 1) field data to validate power production and 2) OpenFOAM AL simulations to validate wind speed and turbulence distributions as well as power production. The data represents six different wind farms:

- **Lillgrund**, field data from Dahlberg [156] and AL data from Churchfield et al. [80].
- **OWEZ**, field data from Albas [157] and AL data from Keck et al. [45].
- **North Hoyle**, field data from Albas [157] and AL data from Keck et al. [45].
- **Nysted**, field data from Barthelmie and Jensen [48]
- **Horn Rev**, field data from Hansen et al. [49]
- **Wieringermeer**, field data from Schepers [46]

The AL simulations have been setup to mimic the average conditions at the wind farms. In addition to the wind farm data listed above, AL simulation conducted by Lee et al. [81] containing two NREL 5MW turbines (Jonkman et al. [158]) has also been used. All the reference data used for validation are listed in table 7.1. For the listed field data cases, the field data contain the average power output of the individual turbines, and the AL data consist of the mean wind speed and turbulence intensity at hub height extracted at cross section located every 1D downstream of the first turbine in the array.

Table 7.1: The field and AL simulation data used for DWM model validation. The information in parentheses and the bin size information only apply to the field data.

Case:	Source	Turbine	WS [m/s]	TI [%]	stability	Bin size [°]	Nr WTG	Spacing [D]
Lillgrund row B	Field, CFD	SWT-2.3-93	8	6.1	N	±1.5	4	11.0
Lillgrund row D	Field, CFD	SWT-2.3-93	8	6.1	N	±1.5	4	10.0
N.H. row A	Field, CFD	V80	8 (±2)	6.2 (±0.1)	N, VU, (VS)	unknown	5	11.0
N.H. row B	Field, CFD	V80	8 (±2)	6.2 (±0.1)	N, VU, (VS)	unknown	5	10.0
N.H. row C	Field, CFD	V80	8 (±2)	6.2 (±0.1)	N, VU, (VS)	unknown	6	4.4
OWEZ row A	Field, CFD	V90	8 (±2)	6.2 (±0.1)	N, VU, (VS)	unknown	4	13.0
OWEZ row B	Field, CFD	V90	8 (±2)	6.2 (±0.1)	N, VU, (VS)	unknown	4	11.0
Wieringermeer	Field	N80	6-12	1-15	N	±5	2	3.8
Horns Rev	Field	V80	6-12	2.5-13	N	±5	2	7.0
Nysted	Field	SWT-2.3-93	6-12	2-12	N	±5	2	10.3
NREL 5MW 5.4%	CFD	NREL 5MW	8	5.4	N	n/a	2	7.0
NREL 5MW 10.1%	CFD	NREL 5MW	8	10.1	N	n/a	2	7.0

7.2.2 Validation method

The power predictions of the DWM model for all cases where there are AL results available are carried out by using the same input data for as the AL model, and comparing the mean power output of the individual turbines. The variation in ambient conditions within the collection of the field data from Nysted, Horns Rev and Wieringermeer wind farms, however, requires the average of a series of DWM calculations to be used in the comparison. Seven DWM simulations are conducted for each turbulence intensity to cover wind speeds between 6 and 12m/s (1m/s increments). The simulations are run with a mean directional offset of 2.5^{o} to include the effect of the bin size used in the field data. This procedure was repeated for seven turbulence intensities ranging from 4 to 16% (2% increments), see figure 7.14.

The wind speed and turbulence intensity distribution predicted by the DWM model are validated against simulation data from the OpenFOAM AL model. The validation is conducted in FFoR (as opposed to the calibration which was performed in the MFoR), which means that both the effects of wake deficit and wake meandering are validated together. The difference between the DWM model and the OpenFOAM AL model predictions is quantified using the STE metric, see eq. (5.4). As the STE metric is based on the square difference at each calculation node, it is sensitive to the effects of misalignments of the mean path of wake meandering as well as inhomogeneous inflow. Consequently, the STE will increase with the uncertainty due to these effects, even if the shape and magnitude of the mean profiles are correct. Both of the aforementioned sources of uncertainty are present in the AL simulations, see figure 7.4 and 7.5.

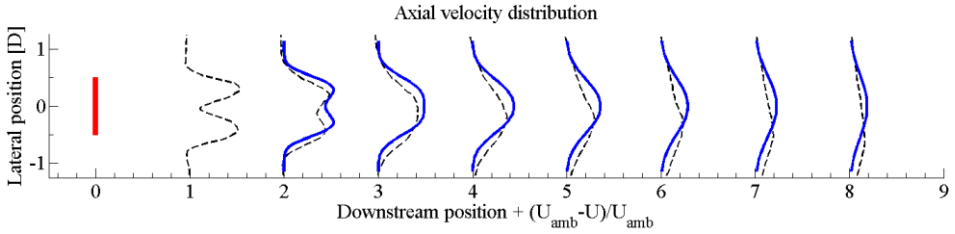

Figure 7.4: The misalignment of the wake deficit of the DWM model (solid lines) and the AL model (dashed lines) behind the first turbine for the unsteady version of the "N.H. row B" case. This misalignment is the main contributor to the resulting STE in this case.

As a consequence of the relatively short simulation times, the above mentioned sources of uncertainty in the OpenFOAM simulation for the cases conducted in neutral atmospheric stratification is on the order of 0.12m/s in wind speed and 0.60pp in terms of turbulence intensity. The uncertainty of the unstable cases is higher due to the increased length scale of the atmospheric turbulence. This cause more wake meandering and generates larger degree of inhomogeneity of the ambient wind speed and turbulence in the computational domain. The uncertainty for the unstable cases is estimated to be 0.18m/s in wind speed and 0.92pp in turbulence intensity. See Keck et al. [39, 45] for details.

The duration of the AL simulation is a trade-off between computational cost and uncertainty in the resulting flow field. As a "standard" AL simulation over a wind farm requires on the order of 500,000 CPU-hours to simulate the flow field for a 10 minute period, the simulations times were required to be kept around 10-15minutes to maintain acceptable time consumption with the computational resources available.

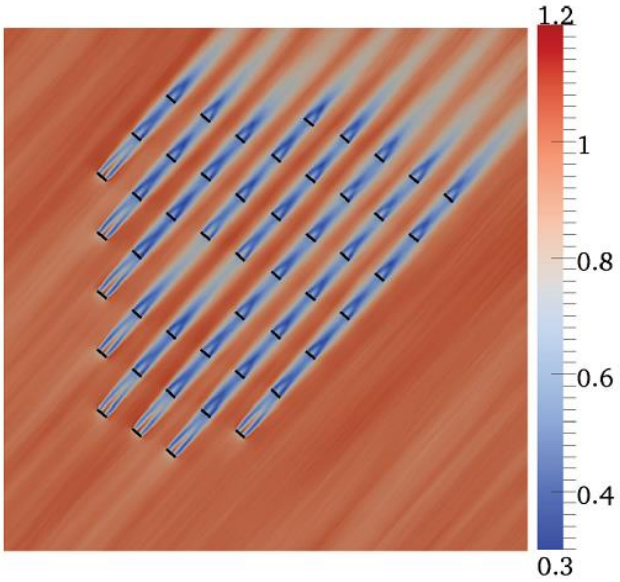

Figure 7.5: The mean wind speed distribution in the OpenFOAM AL simulation of the Lillgrund wind farm. The streak of higher and lower velocity contributes to the STE.

The main source of uncertainty in this validating the DWM power and flow field to the OpenFOAM AL results, however, comes from possible differences in the input turbulence fields to the DWM and the AL simulations. The input turbulence fields for the two models are generated by fundamentally different methods. The ABL turbulence of the DWM in this work is estimated using the Mann turbulence model with the input parameters suggested by Peña et al. [44] (see section 6.1.2), whereas the ABL turbulence applied in the OpenFOAM AL simulations is found by allowing LES turbulence to reach a fully developed stage in precursor calculation executed in an empty domain (Churchfield et al. [159]). The turbulent energy spectra of the applied input velocity field are shown in figure 7.6. From the figure it is seen that the turbulence spectra corresponding to the simulations in neutral stratification are in fair agreement for all wave number above the cut-off frequency of the OpenFOAM precursor simulation. For the unstable case, however, the OpenFOAM model contains more turbulent energy in the large scales of the lateral turbulence spectra, compared to the turbulence applied in the DWM simulation. The higher turbulence level are seen in the range of k_1 0.002 to 0.006, corresponding to turbulent eddies of 1 to 3km in size. In this range the turbulent energy level of the OpenFOAM simulations is approximately four times as high as the Mann turbulence of the DWM model. The peak energy level in the lateral spectra of OpenFOAM turbulence is seen at k_1= 0.003 (2km). The corresponding wave number in the Mann spectra turbulence is k_1= 0.02 (250m). The findings are consistent with the findings presented by Larsen et al. [50] for using the Mann turbulence model with calibrated input parameters to simulate unstable atmospheric conditions.

The difference in turbulent length scales of the OpenFOAM and the Mann turbulence modelling in unstable stratification will have two main consequences for the conducted research: 1) the OpenFOAM data will contain more wake meandering in lateral direction than the DWM model (this is confirmed by table 6 in Keck et al. [45] that the lateral meandering in the OpenFOAM simulations are ~40% higher), and 2) the average flow field will be uncertain as the most energy containing eddies are only realized ~3 times over the conducted simulations (i.e. 2km eddy at 8m/s takes ~4min, the simulations are 10min). In the same simulation the scales of the Mann turbulence containing most energy is realized ~20 times, which is a more appropriate value to obtain statistically significant mean flow field characteristic.

Further investigations are needed to explain these differences in input turbulence and to quantify their effect on the comparison between the OpenFOAM AL and the DWM model.

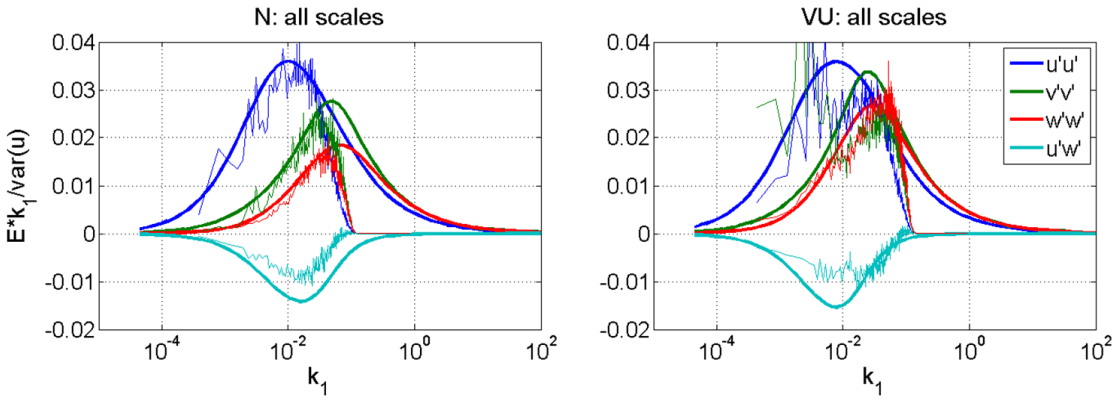

Figure 7.6: The turbulence energy spectra of the wind field generated by Mann model (thick lines) compared to the wind field generated with by precursor simulation in the OpenFOAM AL method (thin lines) for neutral (left) and unstable (right) atmospheric stratification.

7.2.3 Validation results

7.2.3.1 Flow field

The STE metric in terms of wind speed and turbulence intensity profiles for all AL OpenFOAM simulations are presented in tables 7.2 and 7.3. The STE calculations include all available data from cross sections located 3D or further downstream of the wake-emitting turbine (e.g. if the turbine spacing is 7D, the STE is based on data from 3D, 4D, 5D and 6D behind the turbine).

The simulation of the two 5MW NREL reference wind turbines resulted in an average STE between the AL and the DWM velocity fields of 0.29 m/s in terms of for wind speed and 0.9pp in terms of turbulence intensity, see figure 7.7. The main deviation seen in the velocity field is due to the effect of wake rotation in combination with the atmospheric shear profile captured by the OpenFOAM code. This causes the low speed air from the lower part of the computational domain to be lifted into the wake region on the right side of the turbines (as viewed from the front). This effect cannot be captured by DWM model as the atmospheric shear profile is super imposed after the wake deficit calculation.

The STE for the Lillgrund simulations in terms of wind speeds are 0.51 m/s for row B and 0.40 m/s for row D. The corresponding numbers for the turbulence intensity are 1.86pp for row B and 1.59pp for row D. The STE for the simulations carried out in neutral atmospheric conditions for the OWEZ and North Hoyle wind farms in terms of wind speeds is 0.36 m/s and 1.50pp in terms of turbulence intensity. An illustration of the agreement of the velocity and turbulence field in neutral stratification from the OWEZ and Lillgrund simulations, respectively, can be seen in figure 7.8 and 7.9. The average STE of all the simulated cases in neutral stratification is 0.38m/s for wind speed and 1.41pp for turbulence intensity. By comparing the results from the different cases, it can be concluded that the STE increase for smaller turbines spacings. This is due to two factors: 1) the results of the DWM wake deficit generally agree

better at downstream distances larger than 4D, and 2) the STE calculation is less sensitive to misalignment of the wake centre, of the AL results relative to the mean wind direction specified in the DWM model, as the wake gradients are smaller. Furthermore, it can also be seen that the average STE over the rows of wind turbines does not increase with the number of turbines (this effect is more clear in table 2 of Keck et al. [39] publication).

Table 7.2: The STE of the DWM model under neutral stratification compared to the conducted AL simulations.

Cases:	Nr. turbines	Spacing	STE WS [m/s]	STE TI [%]
NREL 5MW 5.4%	2	7D	0.27	0.9
NREL 5MW 10.1%	2	7D	0.32	0.8
N.H. row A	4	11D	0.31	1.6
N.H. row B	4	10D	0.35	1.3
N.H. row C	5	4.4D	0.57	2.2
OWEZ row A	3	13D	0.40	1.2
OWEZ row B	3	11D	0.28	1.2
Lillgrund row B	8	4.4D	0.51	1.9
Lillgrund row D	7	4.4D	0.40	1.6

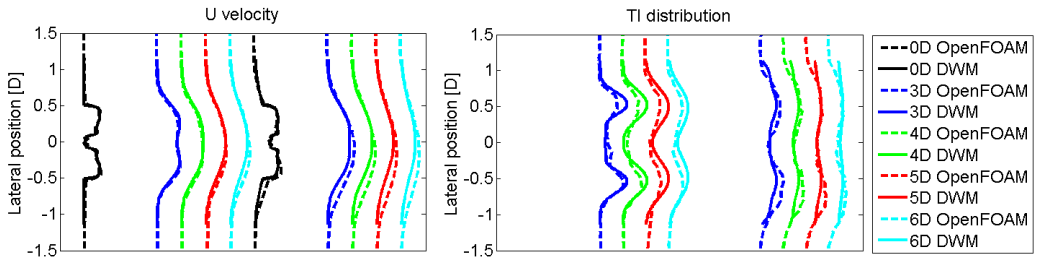

Figure 7.7: Comparison between the mean velocity field (left) and TI field (right) from the DWM model (solid lines) and the OpenFOAM AL simulations (dashed lines) for the "NREL 5MW 5.4%" case.

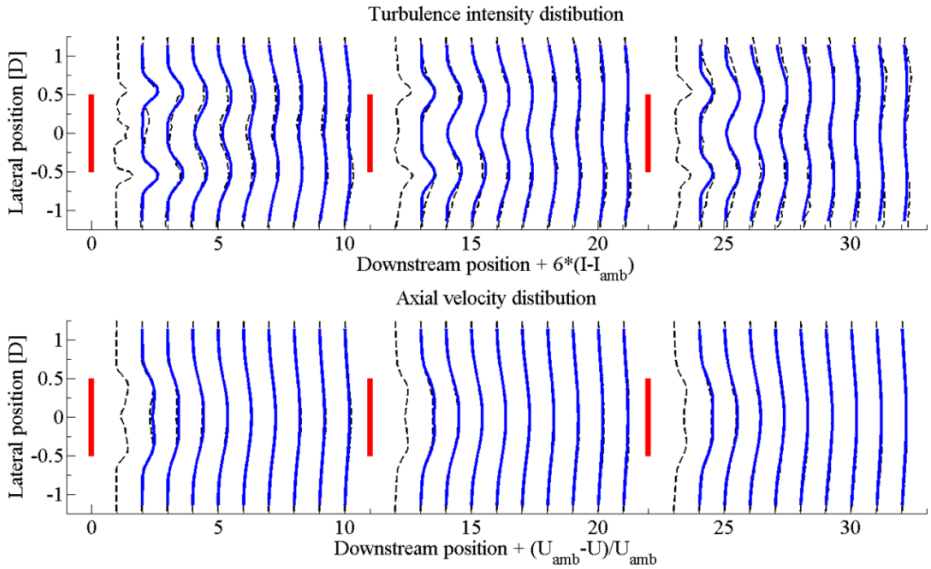

Figure 7.8: Comparison of the turbulence intensity (top) and velocity (bottom) distributions for the "OWEZ row B" case in neutral stratification of the AL model (dashed lines) and the DWM model (solid lines). The thick solid red lines show the rotor positions.

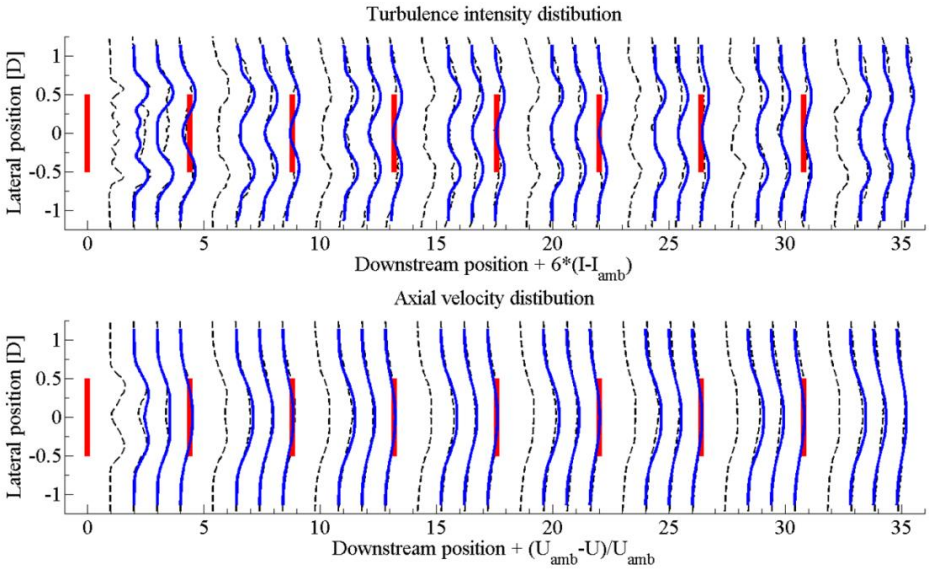

Figure 7.9: Comparison of the turbulence intensity (top) and velocity (bottom) distributions for row B of the Lillgrund wind farm of the AL model (dashed lines) and the DWM model (solid lines). The thick solid red lines show the rotor positions.

The average STE of the all simulated cases in unstable stratification is 0.45m/s for wind speed and 1.74pp for turbulence intensity. This is 25% and 16% higher for wind speed and turbulence intensity, respective, compared to neutral stratification. A large portion of the increase in the STE for the unstable cases compared to the neutral cases, is due to the difference in inflow turbulence as shown in figure 7.6. The difference in amount of large scale energy in the lateral component between the input turbulence to the DWM and the OpenFOAM AL model causes the wake meandering of the OpenFOAM model to be ~40% higher than the meandering observed using the DWM model (Keck et al. [45]). Figures 7.10 and 7.11 show a comparison of the flow field in the DWM and the AL models behind the 2nd turbine of the "OWEZ row B" case in neutral (top figures) and unstable atmospheric conditions (bottom figures). Overall the shape of both the wind speed and turbulence intensity are in fair agreement for both atmospheric conditions. However, it can be seen that the wake deficit of the DWM model for the unstable atmosphere is slightly deeper and more narrow compared to the AL simulations. It can also be seen that the turbulence distribution is wider, and that the magnitude of turbulence intensity is higher (the difference in the far-wake is about 2pp in turbulence intensity), in the AL simulations. These effects are attributed to the larger wake meandering.

The agreement between the flow field in DWM and AL models for the unstable simulation of the "N.H. row C" case is shown in figure 7.12. The STE of this case increases less in unstable conditions compared neutral condition than the other cases. This is probably due to the fact that wake meandering plays a smaller role for closely spaced turbines. The shape of the velocity and turbulence distribution in the DWM model agrees better with the AL data for this case compared to the unstable cases at larger turbine spacings, but the same trends as observed in figure 7.10 and 7.11 can still be seen. The most noticeable improvement, however, is that the average magnitude of turbulence intensity is in better agreement with the AL data, which can be seen by comparing the turbulence distributions in unstable atmospheric conditions at the two turbine spacings, see figures 7.11 (bottom) and 7.12 (top).

Table 7.3: The STE of the DWM model under very unstable stratification compared to the conducted AL simulations.

Cases:	Nr. turbines	Spacing	STE WS [m/s]	STE TI [%]
N.H. row A	4	11D	0.39	2.0
N.H. row B	4	10D	0.45	2.4
N.H. row C	5	4.4D	0.57	2.0
OWEZ row A	3	13D	0.40	1.2
OWEZ row B	3	11D	0.43	1.1

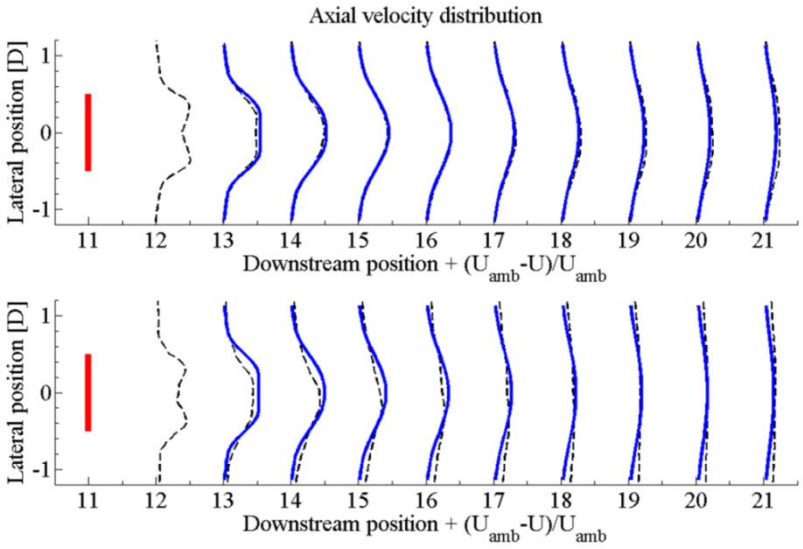

Figure 7.10: Close-up of the velocity field behind the 2nd WTG in the "OWEZ row B" case of the DWM and the OpenFOAM AL model. The top figure show wake deficit evolution in neutral atmospheric stability and the bottom figure shows wake deficit evolution in very unstable atmospheric conditions.

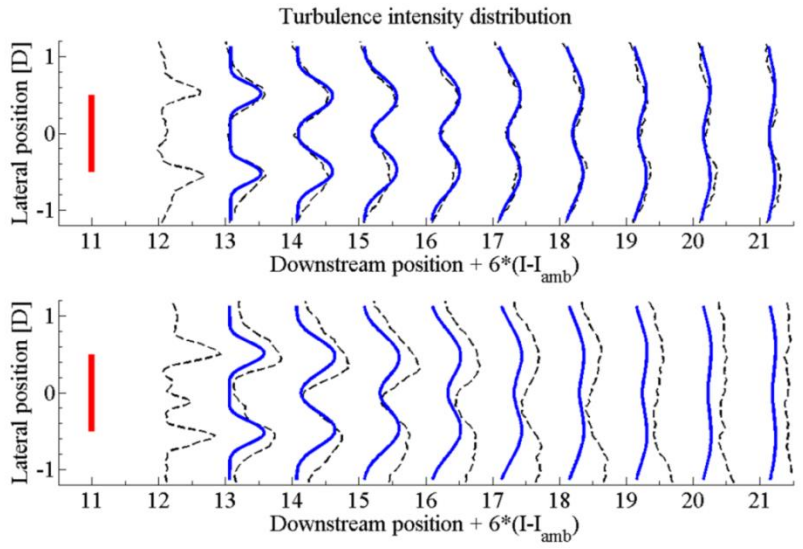

Figure 7.11: Close-up of the turbulence field behind the 2nd WTG in the "OWEZ row B" case of the DWM and the OpenFOAM AL model. The top figure show turbulence evolution in neutral atmospheric stability and the bottom figure shows turbulence evolution in very unstable atmospheric conditions.

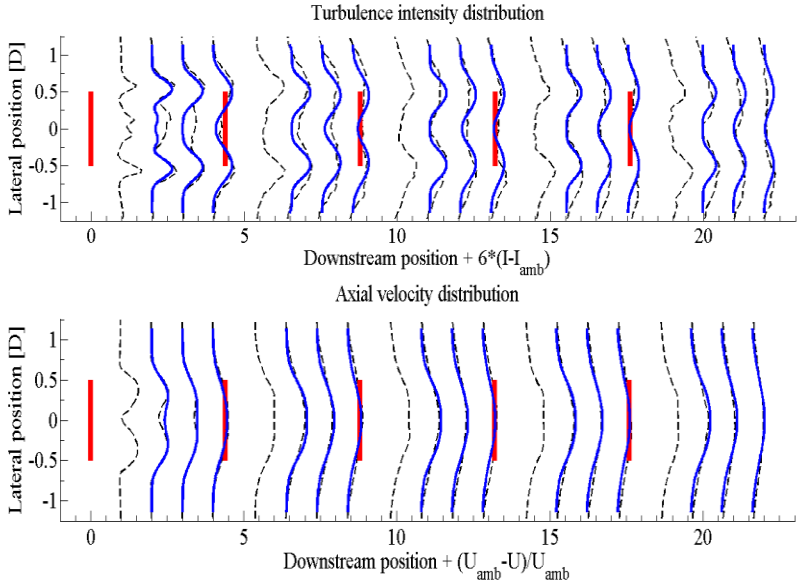

Figure 7.12: Comparison of the turbulence intensity (top) and velocity (bottom) distribution for the "N.H. row C" case for unstable atmospheric stratification between the AL model (dashed lines) and the modified DWM model (solid lines). The red thick solid lines indicate the rotor positions.

7.2.3.2 Power production

The power predictions made by the DWM model at the Lillgrund wind farm agree well with those of the OpenFOAM AL and the full scale field measurements as shown in figure 7.13. The main deviation is that the power estimation for the fourth turbine in row D (right figure), i.e. the turbine with a larger separation to the upstream turbine, the DWM model experiences a larger increase than the OpenFOAM AL model and the field data does. It can also be seen that both the DWM model and the OpenFOAM AL model over-predict power production of the last three turbines in the rows. There is no fundamental explanation as to why the OpenFOAM AL and modified DWM models do not reproduce the power production from the field data in the rear part of the wind farm. The DWM model code is run with exactly the same input as the OpenFOAM simulation, which is a neutrally stratified atmosphere with a wind speed of 9.0 m/s and a turbulence intensity of 6.2%. Although the simulations match the observed average inflow wind speed and turbulence intensity for this wind direction, the difference in predictions for the rear of the wind farm may come from the fact that the field data was collected over many months. Over that time period, there was undoubtedly a range of atmospheric stability and wind speed conditions, unlike in the fixed condition defining the simulations, all of which affects wake propagation and power production. The field data is only binned by wind direction and thus includes a range of ambient wind speeds (all below the wind speed corresponding to rated power) and turbulence intensities.

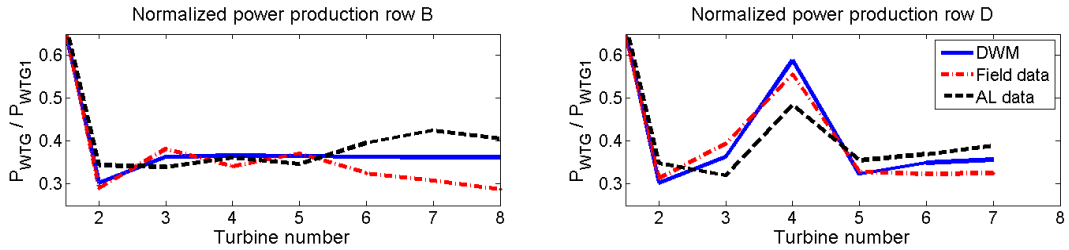

Figure 7.13: Power production over row B and D of the Lillgrund wind farm, spacing 4.4D. The dashed lines are OpenFOAM results, dot-dashed lines are field data and solid lines are the DWM prediction.

The data from the Nysted, Horns Rev and Wieringermeer wind farms are used to validate the ability of the DWM model to capture the wake loss of a single wake situation at a large range of ambient turbulence intensities. Figure 7.14 shows that, in general, the DWM model predicts the power losses for three turbine spacings well over the whole range of inlet turbulence intensities. The difference between the field data and the DWM predictions are in the order of ~5%. The wake effects at larger spacings seem to be slightly overestimated. For small spacings, especially at very low turbulence intensities, the wake effect is underestimated.

Figure 7.15 presents the power production at the North Hoyle wind farm for three atmospheric stability classes (very stable, neutral and very unstable from left to right). The rows of the figure are associated with different turbine spacing (11D, 10D and 4.4D, top to bottom). From the results it can be seen that the field data show consistently lower wake losses compared to the numerical results. This is believed to be due to the use of large bin size of the field data. It could also be a consequence of filtering the field data on two dependent variables (turbulences intensity and atmospheric stability) which may result in selecting special events (such as wind speed ramp-ups etc…). Furthermore, the AL model results for very unstable conditions display too low power loss and increased level of uncertainty, which may be a consequence of the large amount of wake meandering and the relatively short simulation time (see section 7.2.2). Especially, the 10D case (middle row, right column) which is seen to yield a 30% lower wake loss compared to the 11D case of the same ambient conditions (top row, right column). The AL simulations in neutral atmospheric stratification are seen to agree well with the DWM results.

Unfortunately, this means that evaluating the absolute level of the wake losses in a non-neutral atmosphere is difficult based on the reference data available. However, it can be seen that the relative effect of atmospheric stability is captured well by the DWM model when compared to field data. The loss of production of the wake-affected turbines at North Hoyle and OWEZ is seen to be 13% higher for the field data at very stable conditions compared to neutral conditions (at the same turbulence intensity level). The analog number for the DWM model is 12%. The wake loss in very unstable conditions is seen to be 10% lower for the DWM model and 6% lower for the field data (13% if the case at 10D from North Hoyle is removed, which could be considered an outlier, as the wake losses in unstable stratification exceeds the wake losses in neutral stratification and is almost comparable to the very stable case.)

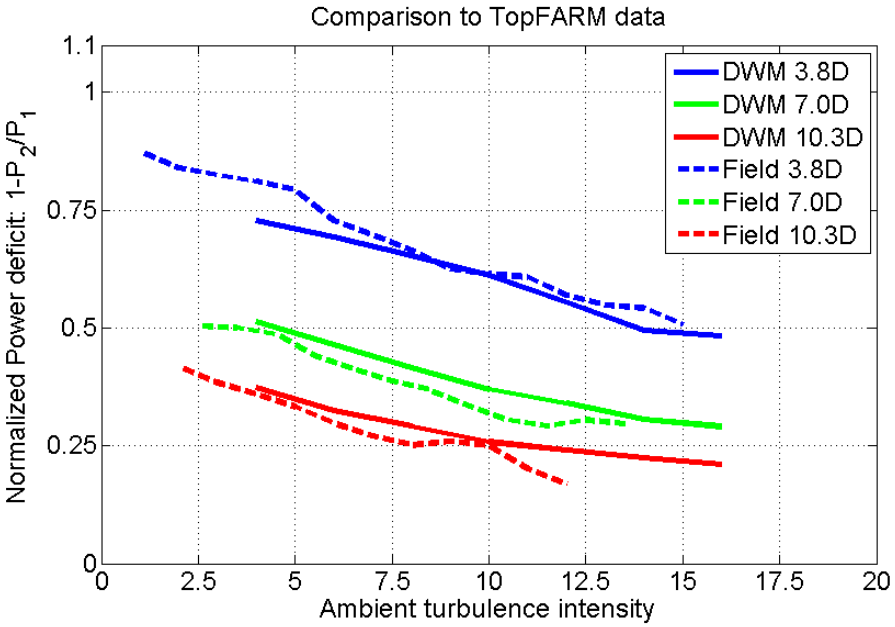

Figure 7.14: Power loss due to wake operation as predicted by the DWM model and observed in field data from three different sites in non-complex and offshore conditions. The wake loss is presented as a function of ambient turbulence intensity and turbine spacing.

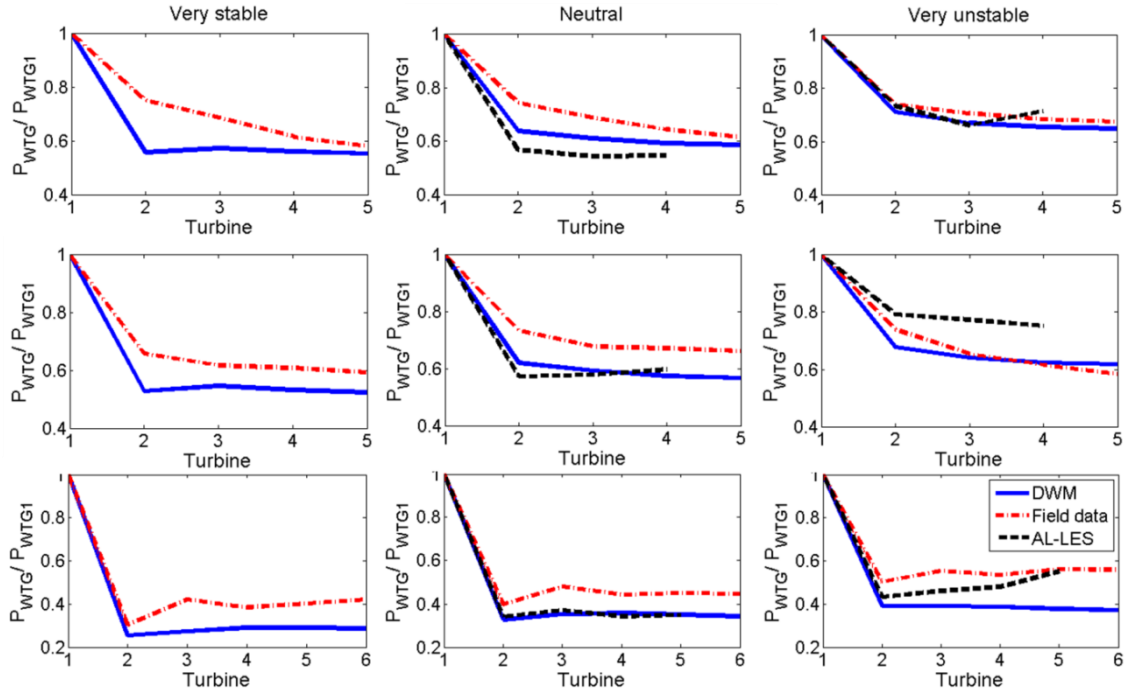

Figure 7.15: The power production for all turbines in the rows from the simulations cases at the North Hoyle wind farm compared to field data. The ambient conditions in all cases are wind speed of 8m/s and a turbulence intensity of 6%. Each column represent an atmospheric stability class (very stable, neutral and very unstable from left to right) and the rows show different turbine spacing (11D, 10D and 4.4D from top to bottom).

Figure 7.16 illustrates the effect on power loss due to wakes as a function of atmospheric stability as simulated by the DMM model. As before, the effect of atmospheric stability is isolated by conducting all simulations with the same ambient wind speed (8m/s) and turbulence intensity (6%). It is clearly shown that the atmospheric stability has an effect on the power production of a row of wind turbines even when the turbulence intensity is kept constant. For the 6D case the stable atmosphere increases the wake loss by 9.8%, while the unstable case reduces wake loss by 5.4%, compared to neutral atmospheric stratification. For the turbines spaced 10D apart the wake loss is increase of 10.9% for stable, and a reduction of 11.7% in unstable stratification, compared to neutral atmospheric stratification.

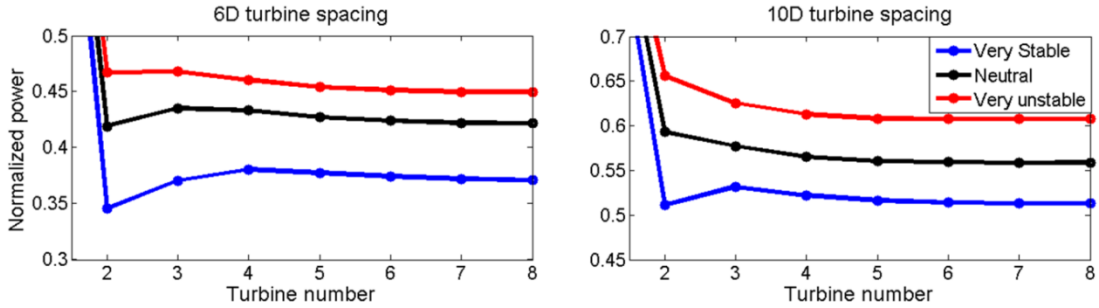

Figure 7.16: Effect of atmospheric stability on power production of a row of eight turbines. The ambient conditions are maintained constant at a wind speed of 8m/s and a turbulence intensity of 6%

Figure 7.17 show that atmospheric stability also changes the composition of the wake turbulence. The wake turbulence composition is shown for a cross section 6D downstream of the first turbine, and the simulations are conducted for an ambient wind speed of 8m/s and a turbulence intensity of 6%, under very stable (left), neutral (middle) and very unstable atmospheric conditions (right). As seen from eq. (6.18), the total turbulence experienced as a downstream rotor (TI_{Tot}) consists of small-scale turbulence ($TI_{Small\text{-}scale}$) and the apparent turbulence created by the meandering of the wake deficit (TI_M). In figure 7.17 it can be seen that the relative contribution to the turbulence intensity due to wake meandering (red dashed lines) is approximately twice as large in the very unstable case (right figure) compared to the very stable case (left figure). The increased amount of turbulence in meandering scales will affect the loads of the wake-receiving turbine (Crespo et al. [15], Vølund [29], Madsen et al. [32] and Sathe et al. [71]), whereas the small-scale turbulence mainly will affect the wake deficit evolution of the wake-affected turbines.

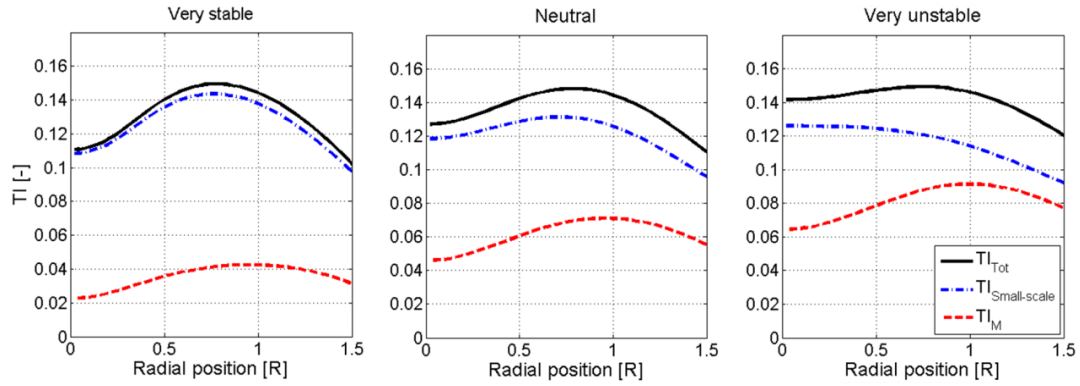

Figure 7.17: The composition of turbulence intensity in the wake as a function of atmospheric stability 6D behind a wake-emitting turbine.

7.2.4 Benchmark of the DWM model to other wake models

The main purpose of this section is to benchmark the power production and the loads of the DWM model with the other engineering models available for modelling wake effects of a wind turbine.

7.2.4.1 Power production

The power production as predicted by the DWM model when utilized as a standalone wake model (see chapter 6) is compared to field data and results from the Jensen 'wind pro' model (Jensen [134] and Katic et al. [135]), the Larsen model (Larsen [160]) and the FUGA model (Ott et al. [144]). The field data and simulation data of the reference models presented in figures 7.18 – 7.20 come from the work of Gaumond [161]. The field data in figure 7.21 comes from the TOPFARM project (Larsen [24]).

The DWM calculations are conducted based on the mean ambient conditions of the various sites. The effects of varying bin-width of the inflow direction are incorporated by conducting DWM simulations for each 1 degree wind direction and averaging the results. For the Horns Rev wind farm a uniform 5 degree windowing applied as described by Gaumond [161], to compensate for directional uncertainty and inhomogeneity over the wind farm.

Figures 7.18 shows the power production as a function of relative wind direction for a single wake case from Horns Rev at 7D turbine spacing, 8m/s ambient wind speed and 7% turbulence intensity. The power deficit measured in the field (dots with error-bars) is wider than predicted by any of the wake models. Overall the DWM model (blue line) shows the best agreement with field data. The DWM model under-predicts power production by ~3% in full wake conditions, but otherwise display good agreement with the field data in the ± 7.5degrees sector. The FUGA model (green line) display similar predictions as the DWM model at large inflow angles, but under-predict the power production within the ± 5degrees sector by ~5-10%. The Larsen model (black line) overestimates the power production at all relative wind direction by ~10%. The Jensen model (red line) predicts the lowest power production, and under-predicts the power produced by ~10-15% in the sector ±7.5 degrees.

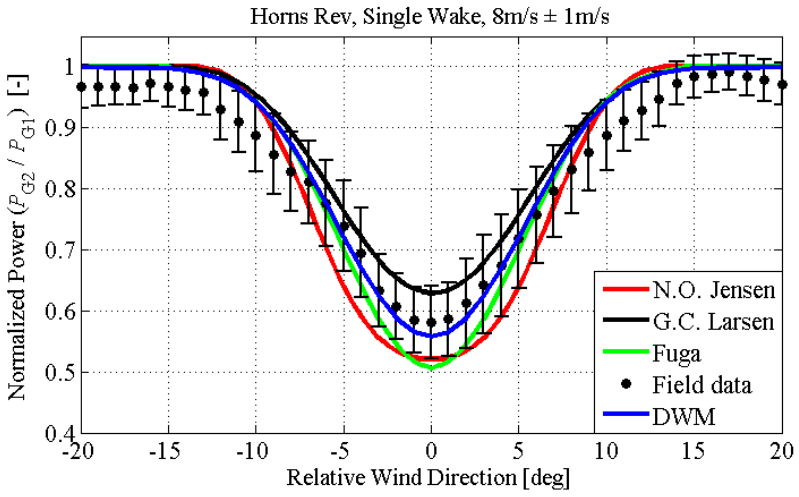

Figure 7.18: Normalized power production as a function of inflow angle for a single wake case at 7D from the Horn Rev wind farm. Courtesy of Gaumond[161].

Figures 7.19 shows the power production as a function of relative wind direction for a single-wake case (left) and a double-wake case (right) from the Lillgrund wind farm at 4.3D turbine spacing, 8m/s ambient wind speed and 7% turbulence intensity. In the double-wake situation it should be noted that the DWM model simulations only includes a single row of turbines, whereas the reference data from Gaumond [161] includes the whole wind farm. The studied turbine experience wake effects from the other rows at inflow angles larger than ±12 degrees.

In general, the field data from Lillgrund agrees better with the wake model predictions both in terms of wake width and maximum wake depth. Similar trends as those observed in the Horn Rev case are observed at the Lillgrund site for the single-wake case (left figure):

- The power deficit of the DWM model has not bias, and is good agreement with the field data at all inflow angles.
- The FUGA model over-predicts the power production by ~5-10% (note that it under-predicted with similar magnitude for the Horn Ref case)
- The Larsen model over-predicts the power production by ~20-30%
- The Jensen model under-predicts the power production by ~5-10%

For the double-wake cases (right figure):

- Also in the double wake case, the best overall agreement is achieved with the DWM model. The shape of the DWM agrees well with the field data (until the effects of other turbine rows affect the result outside of ± 12degree sector), however, the power production is under-predicted by 5-10%.
- The FUGA model under-predicts the power production in a ± 5degree sector by ~25-35%, and. over-predicts the power production by ~15-20% in partial wake operations.
- The Larsen model under-predicts the power production in the wake when the inflow direction is aligned within ±5 degrees from the turbines by ~10%, but over-predicts the production in partial wake operation by ~15-20%.
- The Jensen model under-predicts the power production in the sector ±7.5 degrees by ~30-35%, but is in fair agreement outside of this region.

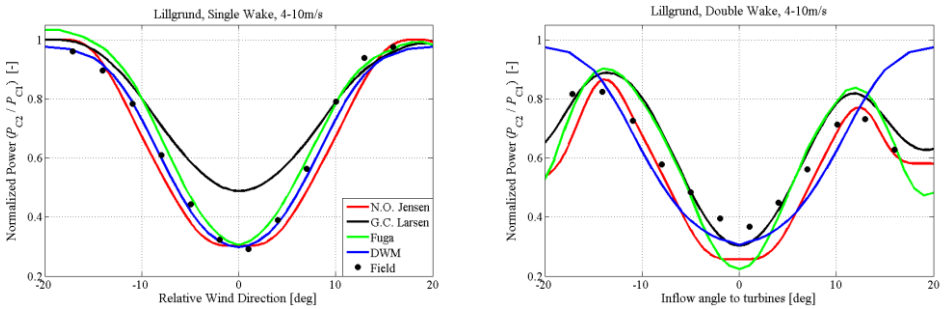

Figure 7.19: Normalized power production as a function of inflow angle for a single wake case at 4.3D (left figure) and a double wake case (right figure) from the Lillgrund wind farm (Gaumond [161)].

Figure 7.20 illustrates the effect of the directional bin size on wake loss in a row of ten turbines. The left figure is based on a ±2.5 degree sector, the middle a ±7.5 degree sector and the right figure on a ±15 degree sector. It should be noted that the power production of the last turbines is affected by the other rows in the wind farm. This effect is included in the reference data from Gaumond [161], but not in the DWM simulations. This effect is seen for the last three or four turbines in the ±7.5 degree sector case and for the last six turbines in the ±15 degree sector case.

In general it is seen that all models predictions improve with larger bin size. This is effect is partially due to reduction in sensitivity of the inflow measurement (and spatial variability) of the field data, as discussed by Gaumond [161]. This is the main explanation for the increased agreement between the DWM model and the field data (for the turbines where the other rows do not influence the result). For the other wake models, however, part of the improved agreement to field data may also be explained by fact that larger bin sizes implicitly includes the effect of wake meandering.

The DWM shows the best agreement with field data (before the effect of the other row influence the results), however, the power production of the wake-affected turbines are under-predicted by ~10-15% and ~5-10% for the ±2.5 and the ± 7.5degree sector case, respectively. This is partially attributed to uncertainty in the incoming wind direction (Gaumond [161] mentions that the wind direction uncertainty of Horn Rev corresponds to a standard deviation of 3.5^{o}), and partially to the fact that the DWM model seems to over-predict the wake effects of the Horn Rev turbine in full wake according to figure 7.18 (the Lillgrund cases presented in 7.13 and 7.20 are in better agreement). The other models over-predict the wake effects in narrow sectors (due to the lack of wake meandering). For the ±15degree sector the Larsen and the Jensen model performs well, and captures the effect of the whole wind farm accurately. The Jensen model also works better for larger directional bins, but over-predicts the wake effects throughout the investigation apart for the last three turbines of the ±15 sector where the wake effects are underestimated.

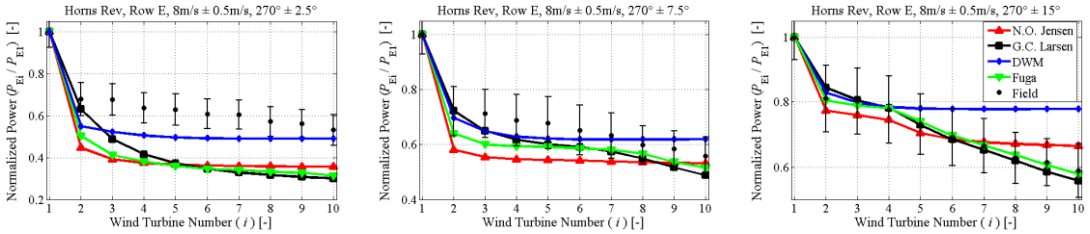

Figure 7.20: Normalized power production using the four models compared to field data at different binning sectors: ± 2.5^{o} (left figure), ± 7.5^{o} (middle figure) and ± 15^{o} (right figure) (Gaumond[161]).

Figure 7.21 shows the wake loss due to a single-wake aligned with the turbines as predicted by the DWM and the Jensen models compared to field data collected at three sites with different turbine spacings 3.8D, 7.0D and 10.3D (the data is descripted in section 7.2.1). The data is collected in an inflow sector of ±5degress relative to the turbines and binned on turbulence intensity. This enables an investigation of the ability of the wake models to capture the wake dynamics under a range of ambient turbulence intensities. For this investigation, the wake decay constant of the Jensen model is calibrated to the field data in figure 7.21 using a least-square method to include the effect of turbulence intensity. In the calibration, the wake decay constant is assumed to have a linear dependence on the ambient turbulence intensity. The best value of the wake decay constant is found to be 72.5% of the ambient turbulence intensity (i.e. *0.725*TI,* which roughly corresponds to the recommended 0.04 at 6% turbulence intensity). Without this calibration the wake effect of the Jensen model is invariant to ambient turbulence intensity.

From figure 7.21 it can be seen that the DWM model (solid lines) captures the effect of turbulence intensity of the wake dynamics in a more realistic manner compared to the Jensen model (dot-dashed lines). The DWM model captures the right trends at all three spacings, and the discrepancies observed in terms of power production are on the order of 5-10%. The wake effects at 3.8D are slightly

underestimated, and at 7.0 and 10.3D the wake effects over-estimated. After the least-square calibration, the effect of the ambient turbulence is captured reasonably well with the Jensen model. The trend of the power loss due to wakes at 3.8D is captured well, but the power production of the wake-affected turbine is over-predicted by ~15-20%. At larger spacings the average power loss is captured better, but instead the trends of ambient turbulence intensity are not captured as well. As a consequence, the wake effects are over-estimated at low turbulence intensities and underestimated at high turbulence intensities for the larger turbine spacings.

The results presented in this section indicate that the (standalone) DWM model captures the power production of wake-affected turbines with higher accuracy than the reference engineering wake models. The results also show that the DWM model captures the trends of varying ambient turbulence intensity better than the Jensen model (even when the Jensen model is calibrated to the validation data).

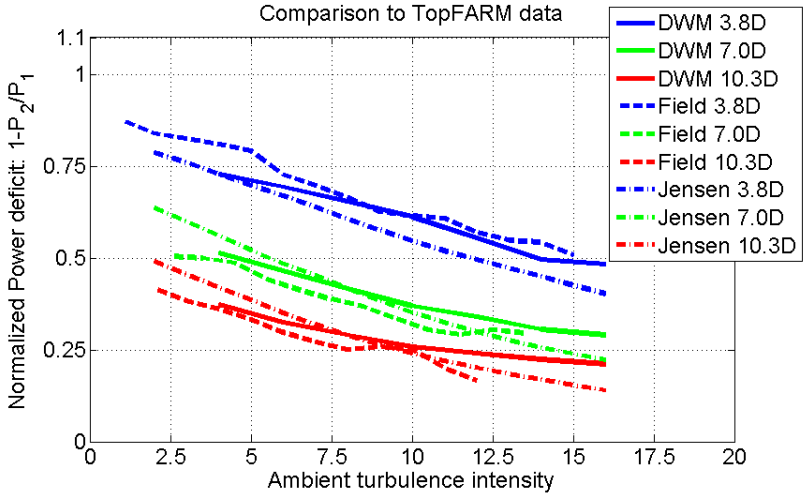

*Figure 7.21: Power loss of the DWM model (solid) and the Jensen model [dot-dashed) compared to field data (dashed), presented as a function of ambient turbulence intensity and turbine spacing. The wake decay constant of the Jensen model is calibrated to be 0.725*TI to capture the effect of ambient turbulence.*

7.2.4.2 Loads

The loads presented in this section come from an internal evaluation of the DWM model conducted at Vestas Wind Systems. The field data from the full-wake cases presented in figure 7.22 comes from the OWEZ wind farm and the partial-wake data presented in figure 7.23 comes from the Høvsøre test site.

Figure 7.22 shows the flapwise fatigue loads of a turbine operating in a single-wake conditions where the wind is aligned with the two turbines as calculated by the DWM model (blue lines) and Frandsen model (red lines), compared to field data (black lines). All loads are normalized with the field data loads at each wind speed. Turbine spacings of 7D (left), 13D (middle) and 23D (right) are investigated. The figures clearly show that the Frandsen model is conservative, and over-predicts the flapwise loads by ~40% on average. The DWM model is within ±10% of the field data for all case in the wind speeds 6-13m/s, and slightly larger at 14m/s.

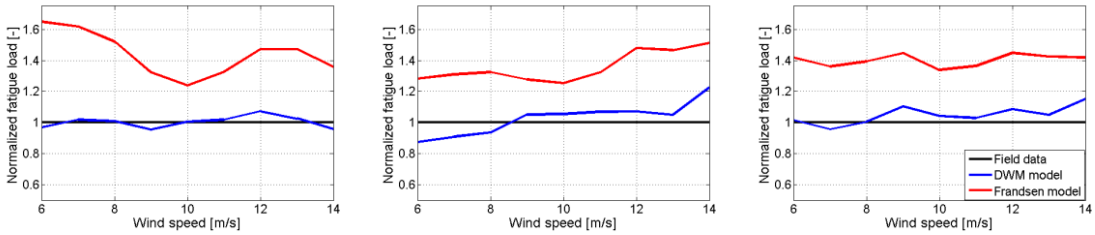

Figure 7.22: Blade flapwise fatigue loads for turbine spacings of 7D (left), 13D (middle) and 23D(right). Courtesy of Vestas Wind Systems.

Figure 7.23 shows the flapwise fatigue loads of a turbine operating in a single-wake conditions where part of the wake hits the downstream turbine (quarter-wake in left figure and half-wake in right figure) at 3D turbine spacing as calculated by the DWM model (blue lines) and Frandsen model (red lines), compared to field data (black lines). All loads are normalized with the field data loads at each wind speed. Also in partial wake operation at close spacings the Frandsen model is over-predicting the flapwise fatigue loads by ~40%. The DWM model is seen to under-predict the loads by on the order of ~10% compared to the field data.

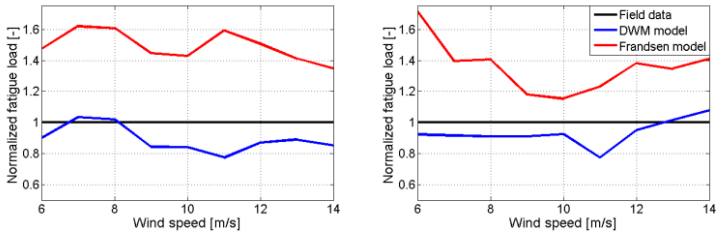

Figure 7.23: Blade flapwise fatigue loads in 25% wake (left), 50% wake (right) at 3D spacing. Courtesy of Vestas Wind Systems.

A more thorough validation of the loads of the DWM model compared to field data is given by Larsen et al. [20, 40]. Although the results presented in this section, and by Larsen et al. [20, 40], looks promising, a systematic validation campaign to cover a wide range of ambient conditions and turbine spacing needs to be undertaken before the DWM model can be used for loads simulations with a reasonable level of confidence.

8 Conclusions

The focus of the research conducted within this PhD project is the treatment of turbulence in the DWM model. The turbulence in the wake of a wind turbine is the most important parameter for wake diffusion, and thus an important parameter to accurately model the distribution of mean velocity. The aim is therefore to capture the most relevant parameters to accurately model the development of wake turbulence and its coupling to the atmospheric boundary layer turbulence in the DWM model. To this end, the research presented in this thesis propose model improvements to: the eddy viscosity closure of the wake deficit, the method to model wake-added turbulence, the intra-turbine coupling of velocity and turbulence, the effect of ABL shear on the wake deficit evolution and the effect of atmospheric stability of the wake evolution.

With the proposed model corrections, the DWM model now contains a physically consistent method for modelling the development of the wind speed and turbulence field as the wind flow through a row of turbines in a wind farm. As the flow field is physically modelled, the DWM model can be used to extract both loads and power estimations from the same model (this is a capability that other engineering models in the wind industry are lacking). As shown in section 7.2.4, the DWM model predicts both power production and wake loads with higher accuracy than the currently available engineering models. This, together with the fact that the computational requirements of the DWM model are maintained sufficiently low, allows wind farm or wind turbine designers to optimize the performance of both power production and loads simultaneously. This may in turn reduce CoE (the potential on the order of ~5% according the TOPFARM project [24]) and contribute to making wind power more competitive. Based on these conclusions, the author considers the DWM model sufficiently mature to be included as an augmentation in the IEC-standard for wake modelling. A proposal for the main effects to consider is given in Appendix A.

The following sections of this chapter will first describe the main contributions and conclusions of the five research projects described in the introduction. This is followed by a section containing suggestions for future research topics for further development of the DWM model.

8.1 Conclusions of the research projects

At the beginning of the research, the capabilities of the DWM model were evaluated and compared to the need of the wind industry. Based on this analysis a list of five research projects were constructed to steer the direction of the research conducted in the PhD period:

- Project 1: Evaluate the turbulence description of the EllipSys3D AL model
- Project 2: The turbulence distribution of a single wind turbine wake
- Project 3: The effect of ABL shear on the Reynolds stresses in the far-wake
- Project 4: Coupling of turbulence over a row of wind turbines
- Project 5: The effect of atmospheric stability effect on wake and wind farm dynamics

The contributions and conclusions based on the individual research projects listed will be given in this section.

8.1.1 Project 1: Evaluate the turbulence description of the EllipSys3D AL model

The first research project was aimed at ensuring that the EllipSys3D AL model is able to model the wake evolution in the ABL for various ambient conditions under neutral atmospheric stability. The project started with a study of the synthetic methods (Mikkelsen et al. [147] and Troldborg et al. [148]) used to generate the ABL turbulence and wind shear in the computational domain, see section 4.3 and 4.4. The ability of the synthetic methods to generate realistic and stable ABL turbulence was verified by allowing the turbulence to evolve in an empty domain. The turbulence intensity level, and the spectral distribution of turbulent energy compared to the theoretical Mann turbulence distribution, after the turbulence had reached equilibrium with the imposed ABL shear was used as evaluation criteria in the study. Based on a parameter study it was concluded that the synthetic turbulence methods were capable of generating realistic turbulence. Furthermore, it was concluded that, with the recommended settings of a power-law shear coefficient equal to the desired turbulence intensity level (i.e. $\alpha = TI_{Taget}$) and a turbulence amplification factor of 1.15 (see Keck et al. [36] for details), the imposed wake turbulence required 150 computational cells to reach a fully developed stage.

A second study was conducted to validate the evolution of turbulence in the wake of a wind turbine represented by actuator lines. The study verified that the AL model, including the synthetic methods to simulate ABL turbulence, captures the evolution of mean turbulence with downstream distance and the spectral distribution of turbulent energy by comparing the results to field data. Also the amount of wake meandering was compared to reference data from a full-scale LIDAR campaign and the PRISME wind tunnel, with fair agreement. (see Keck et al. [36] for further details). Furthermore, an interesting result was also obtained regarding the transport velocity of the wake deficit, which is an important parameter for wake meandering in the DWM model. By synchronizing the time series of the wake centre position in two planes at different downstream locations, it could be shown that the transport velocity of the wake deficit lies between the wake centre speed and the ambient wind speed, and thus is function of rotor induction and downstream position.

8.1.2 Project 2: The turbulence distribution in a single wind turbine wake

By studying the distribution of “eddy viscosity” (estimated from the turbulent fluctuations in LES) in the wake behind the actuator line model, it was observed that the eddy viscosity requires on the order of 6-15D (depending of ambient conditions) to reach a stage where it is invariant with radial position. Based on this observation, the eddy viscosity term which governs the turbulence generated by the wake shear layer (i.e. the right term given by eq. (6.5)) was modified to allow for radially varying eddy viscosity. This was obtained by implementing the standard mixing length model (see e.g. Pope [106]). The improved eddy viscosity model reduced the STE between the velocity field in the DWM model and the AL model by 13% in the meandering frame of reference, and it is therefore concluded to contain a more physically correct description of wake generated turbulence.

At a later stage (after publication), it was noticed that the modified formulation reduced the turbulent stresses in regions of low velocity gradients in an undesirable manner, for example near the wake axis. The reason for this is that the new wake eddy viscosity term goes to zero when the local strain-rate goes to zero. Therefore a blending-function between the modified and the unmodified shear layer eddy viscosity term was introduced, see eq. (6.6). This applied the unmodified eddy viscosity term if the local strain-rate is low. However, it should be noted that any kind of eddy viscosity formulation will yield zero turbulence if there is no local strain-rate. The blending-function simply ensures that the eddy viscosity term itself does not approach zero at locations of low strain-rate.

8.1.3 Project 3: The effect of ABL shear of the Reynolds stresses in the far-wake

The DWM model formulation before this research project neglected the effect of the ABL shear on the strain-rate, and consequently on the turbulent stresses in the wake deficit. The means that the turbulence in the wake deficit was based on the wake gradients alone. This is a good approximation close to the wake-emitting turbine where the wake gradients are much larger than the ABL shear gradient. Further downstream of the wake-emitting turbine, however, the contribution to the strain-rate from the ABL shear is of similar magnitude as the wake deficit (this also happens locally close to the turbine for certain induction profiles and close to the wake-axis). Here the ABL shear contribution to the strain-rate is an important component to maintain realistic turbulence stresses, and thereby wake deficit diffusion.

Based on the conducted research it was concluded that the ABL strain-rate contribution improves the level of turbulent stresses in the far-wake compared to the AL simulations (see figure 8 of Keck et al. [39]), and is thus an important correction for coupling the build-up of turbulence over a row of turbines. There is also a second order effect on the mean velocity field. Furthermore, the effect of the ABL shear contribution will increase in stable stratification, and it is therefore also a component to fully capturing the effect of atmospheric stability in the DWM model.

8.1.4 Project 4: Coupling of turbulence over a row of wind turbines

Previous to this project, the wake deficit evolution of a wake-affected turbine had not been influenced by the increased turbulence level in the oncoming wake. An intra-turbine turbulence coupling was therefore formulated based on approximating the turbulence intensity level at the wake-affected rotor from the turbulent stresses in the oncoming wake (i.e. from the wake deficit calculations of the upstream rotor). This coupling also allowed the turbulence intensity to increase over a row of turbines to reach a saturation level after approximately five turbines (depending of ambient condition and spacing between turbines).

By applying the proposed turbulence coupling and verifying the resulting flow field and power against LES AL simulations and field data, it was concluded that the effect of wake-added turbulence and the build-up of turbulence over a row of turbines is an important parameter for the wake dynamics a wind farm. The improvement quantified using the STE metric showed a 30% reduction in terms of wind speed and 40% in terms of turbulence intensity. Furthermore, it was also shown that after including the turbulence build-up in the DWM model, the STE measure did not increase for the downstream wake-affected turbines compared to the first turbine in the row. The same simulations without the turbulence coupling showed that the STE increased with the number of upstream turbines in the row, both in terms of wind speed and turbulence intensity.

A small study was also conducted to give suggestions for simplified methods of modelling multiple wakes in a wind farm. Two simulations where carried out over a row of eight turbines. The mean wind speed and turbulence intensity at the turbine positions was extracted (without the effects due to rotor induction). The results suggested that it is a feasible approach to approximate the wake deficit of multiple turbines along a row, by the deficit of the closest turbine. The same method cannot be applied for turbulence intensity, however, which was seen to require on the order of five turbines to reach a turbulence level which represented the saturation level of turbulence for the turbine configuration.

8.1.5 Project 5: The effect of atmospheric stability effect on wake and wind farm dynamics

In the fifth research project, the effect of atmospheric stability on the evolution of a wind turbine wake was studied by conducting a series of LES AL simulations. These were conducted in such a manner that the effect of atmospheric stability could be isolated from the effects of turbulence intensity (turbulence intensity is correlated to atmospheric stability in field data). This allowed for the effect of the shift in length scale of the atmospheric turbulence to be investigated separate from the turbulent velocity scale.

The main conclusion of the LES AL study was that modelling the effect of atmospheric stability as an increase in turbulence intensity level alone, is insufficient to capture the effect on the wake physics. The shift in the scale of atmospheric turbulence needs to be accounted for, as it changes the fraction of turbulence energy which affect the wake deficit evolution and the wake meandering. Consequently, the data displayed lower power loss over an array of turbines in a very unstable atmosphere compared to neutral and stable stratification, even though turbulence intensity level was kept constant. Field data showed a ~15% reduced power production of a row of wind turbines in very stable stratification compared to very unstable conditions, when the wind direction was aligned the row of turbines.

A study was also conducted to verify the validity of the approach suggested in the fourth research project for simplified modelling multiple wake deficits (i.e. that multiple wake deficits can be approximated by single deficit of the closest turbine, as long as the wake-added turbulence due to the previous wakes are accounted for in the model). The results of the AL model (and also the modified DWM model) confirmed that the same approach can be used in non-neutral atmospheric conditions.

In a second stage of the project, a method was also proposed to incorporate the effects of atmospheric stability in the DWM model. The method was based on approximating the turbulent length and velocity scales of the whole ABL, the wake deficit and the wake meandering by means of the ambient turbulence spectra. This affects the ABL shear contribution and the eddy viscosity in the deficit calculation, however, the main effect was seen to be the effect of atmospheric stability on the wake meandering.

Including the atmospheric stability effects in the DWM model resulted in a reduction of the average STE compared to AL results of ~19% in terms of velocity distribution and ~28% in terms of turbulence intensity distribution for simulations in very unstable atmospheric conditions. Furthermore, it was seen that the effect of atmospheric stability on the power production of a row of wind turbines agrees well between the DWM model and field data from the rows of wind turbines at the North Hoyle and OWEZ wind farms. Both showed that the very stable stratification leads to ~13% higher wake losses and that very unstable conditions lead to ~8% lower wake losses compared to neutral conditions.

Furthermore, the wake meandering of the DWM model and the actuator line models was in fair agreement in neutral atmospheric conditions. However, due to difference in the input turbulence to the DWM and the OpenFOAM AL models (see Keck et al. [45] for details), the lateral wake meandering in the DWM model for unstable atmospheric conditions is under-predicted compared that to the OpenFOAM AL model by roughly 40%. The vertical wake meandering (and input turbulence spectra) was still in fair agreement. This will influences the comparison of the wake turbulence and velocity distributions in FFoR made in the project, and consequently the STE for the unstable cases are on the order of 20% higher compared to the cases in neutral atmospheric stability.

8.2 Further work

The suggestions for future work is divided into three categories: 1) DWM wake turbulence formulation, 2) DWM functionality, and 3) investigations which could be conducted with the DWM model to increase the understanding of wind turbine wake physics in general.

8.2.1 DWM wake turbulence formulation

As mentioned above, the majority of the research during the PhD project has been focused on the turbulence formulation of the DWM model. Even though the project has led to improvements in both the eddy viscosity closure and the intra-turbine coupling of wake-added turbulence, there are still topics where further research may improve the DWM model further:

1. **The build-up turbulence in the wake deficit calculation:** In the DWM model there is no transport equation for turbulence kinetic energy in the wake deficit. Instead, turbulence build-up is modeled by the F_2 filter function (F_1 should be viewed as part of the inlet boundary treatment and is related to the pressure treatment). The F_2 function thus governs the ratio of realized turbulent stresses in the wake deficit of DWM model, compared to the turbulent stresses if the turbulence was in equilibrium with the local strain-rate (i.e. realized turbulence / "potential turbulence"). In the current formulation, the F_2 function is generic, and thus assumed independent of ambient conditions. From AL simulations, however, it can be seen that the distance required for turbulence in the wake to reach quasi-equilibrium with the wake shear layer is strongly dependent on ambient turbulence intensity, and seems to also have a second order dependence on turbine induction. It would therefore be interesting to either implement a transport equation for turbulence, or model the dependence by creating an F_2 function which depends on ambient conditions.
2. **Conduct further validation of the method to include atmospheric stability effects:** The suggested method to include atmospheric stability effects in the DWM model showed an improved agreement with reference OpenFOAM AL data, and predicted the effect on power production as a function of atmospheric stability well compared to field data. However, there were three main limitations in the validation of the proposed corrections:
    a) The data were only available in planes at hub height, which consequently meant that the deficit and wake meandering had to be evaluated together (as no investigations in the meandering frame of reference was possible).
    b) The turbulent length scale of atmospheric turbulence generated by the OpenFOAM pre-cursor calculation was much larger than that generated by the Mann model with the input parameters suggested by Peña et al. [44] for unstable stratification. This lead to larger wake meandering in the OpenFOAM simulations compared to the DWM model. It also had the consequence that the most energy-containing eddies where realized on the order of five times, which results in a very uncertainty mean flow field.
    c) The OpenFOAM AL model is not currently able to conduct simulations in stable stratification. Therefore only the flow field in neutral and unstable stratifications could be investigated.
3. **Mann model with parameter calibration to emulate non-neutral atmospheric stability:** Based on the comparison with the OpenFOAM input turbulence in unstable atmosphere, it is seen that the turbulence field generated by the Mann model both contains less energy in large length scales and a different ratio between components. As seen in Keck et al. [45], this influences the amount of wake meandering of the turbines, and thus power production and loads of wake-affected turbines. This motivates further investigation to 1) quantify the difference, and 2) develop a modified (Mann) turbulence model which includes buoyancy effects.
4. **The use of frozen turbulence for the wake meandering algorithm:** As described in section 6.1.2, the current formulation to find the wake meandering is based on a passive tracer assumption in a frozen turbulence field generated with the Mann turbulence model. This could potentially cause an overestimation of wake meandering, as the turbulent eddies which generates the wake do not brake-down as in ordinary (dynamic) turbulence. This means that the wake could be overexposed to a single realization of the large scale dynamics (consider the differences between "n

independent samples" to "n multiplied with one sample"). This effect is reduced by allowing the wake deficit to travel at a reduced speed compared to the turbulence box, a wake deficit will then experience different stable turbulent eddies, as opposed to being exposed to the eddies in a plane of the turbulence box for the whole wake trajectory.

8.2.2 DWM functionality

By comparing the functionalities of the DWM model to the list of "key effect for wake evolution", described in chapter two, it is obvious that the current DWM formulation only handles a subset of the parameters. The combination of the model assumptions of the DWM model, and the fact that the computational speed is crucial for the applicability of the DWM for industrial processes, makes some of these effects non-trivial to include in the DWM model. However, finding appropriate "engineering" solutions to the following topics would make the DWM model applicable for a wider range of situations:

1. **Multiple wake simulations where the flow is not aligned with the row of turbines (and non-axial inflow conditions):** As part of research project four, a correction was derived to couple the velocity deficit and turbulence build-up over a row of turbines. This method is strictly only valid in full-wake situations (although fair agreement is seen in the double wake in figure 7.19 also for non-axial inflow). As the wake deficit evolution of the wake-affected turbine is based on an axisymmetric deficit calculation, the effect of a partial wake situation would affect both sides of the emitted deficit in a similar manner. A possible solution may be to divide the rotor into segments and include the oncoming wake effects only in the affected sectors
2. **Near-wake study:** a preliminary investigation shows that the DWM model may be used to predict the flow field already at 2D, as opposed to the 3D currently used as the "point of DWM validity". The applicability in closely spaced turbines should be investigated further and verified for a range of ambient conditions.
3. **Complex terrain:** A correction for the effect of increased turbulence due to complex terrain should be included in the DWM model. The current formulation is conservative in the sense that wake effects are more pronounced in flat terrain. To enable realistic loads and power predictions in complex terrain the increased level of small-scale turbulence should be accounted for.
4. **Deep array:** the recovery of the wake deficits deep inside a wind farm is reduced due to the presence of other wind turbine wakes. Sufficiently deep into the wind farm, kinetic energy is only (or at least mainly) transferred into the wake vertically from the undistributed flow above the wake. A correction for this effect could increase the ability of the DWM model for predicting the loads and power production of very large wind farms.
5. **Mesoscale effects:** To facilitate for a more detailed site specific wind turbine layout, it would be interesting to augment the DWM model so that is can incorporate mesoscale effects. This can be partly achieved by corrections for non-axial inflow and atmospheric stability effects, but an alternative method might be to couple the DWM to a mesoscale model.

8.2.3 DWM investigations of wake physics

As the DWM model contains a large portion of the far-wake physics of a wind turbine, it has reached a maturity level where it can be used for initial studies and parameter sweeps of the wake physics. Suggestions for application with the DWM model:

1. Study the component loads on a wake-affected turbines for possible IEC update of turbine design.
2. Composition of wake turbulence could act as an indication of the severity of wake loads in different situations, see figure 7.17. This concept is based on the observation that the "apparent turbulence" (i.e. the turbulence at a wake-affected turbine caused by the meandering wake deficit) is the most important contributor for loads of wake-affected turbines.
3. Development of control algorithms for wind turbines in farms. The DWM would allow for trade-offs in terms of production and the loads experienced by a turbine.
4. Pending the results of the "near-wake study" suggested above, the DWM could be used to generate improved guidelines for wind sector management in the wind industry.

Bibliography

[1] World Wind Energy Report 2011, http://www.wwindea.org

[2] Wind Energy, The Facts: executive summary, European Wind Energy Association www.ewea.org (2009).

[3] Wind Energy, The Facts: Debunking the myths, European Wind Energy Association www.ewea.org (2009).

[4] Deutch, J., Kadak, K. and Moniz, P. M. et al., Update of the MIT 2003 Future of Nuclear Power. MIT Energy Initiative, 2009.

[5] ExternE, http://www.externe.info/externe_2006/

[6] Vermeer, L. J., Sørensen, J. N. and Crespo, A., Wind turbine wake aerodynamics. Progress in aerospace sciences, 39(6), 467-510, 2003.

[7] Wind Energy, The Facts: Wind Turbine Technology, European Wind Energy Association www.ewea.org (2009).

[8] Lemming, J., Morthorst, P. E., Clausen, N. E. and Hjuler Jensen, P. (2009). Contribution to the chapter on wind power in: Energy technology perspectives 2008, IEA.

[9] Wind Energy, The Facts: Research and Development, European Wind Energy Association www.ewea.org (2009).

[10] Larsen, G.C., Madsen, H.Aa., Bingöl, F. Mann, J., Ott, S.,Sørensen, J.N., Okulov, V., Troldborg, N., Nielsen, M., Thomsen, K., Larsen, T.J. and Mikkelsen, R., Dynamic wake meandering modelling. Risø-R-1607(EN). Risø National Laboratory, Technical University of Denmark, Roskilde, Denmark, 2007

[11] IEC 61400-1, International Standard, Wind turbines – Part 1: Design requirements. 3rd edition, p.73 ff., 2005.

[12] Frandsen, S.T., Turbulence and turbulence-generated structural loading in wind turbine clusters. Risø-R-1188(EN). Risø National Laboratory, Technical University of Denmark, Roskilde, Denmark, 2007.

[13] Thomsen, K., Madsen, H.A., A New Simulation Method for Turbine in Wakes – Applied to Extreme Response during Operation. Wind Energy 2005, 8, pp. 35-47.

[14] Thomsen, K., Madsen, H.Aa., Larsen, G.C. and Larsen, T.J., Comparison of methods for load simulation for wind turbines operating in wake. Journal of Physics: Conference Series, 75. DOI:10.1088/1742-6596/75/1/012072.

[15] Crespo, A., Hernandez, J. and Frandsen, S., Survey of modelling methods for wind turbine wakes and wind farms. Wind energy, 2(1), 1-24, 1999.

[16] Veldkamp HF. Chances in wind energy: a probabilistic approach to wind turbine fatigue design. PhD thesis, Delft Technical University, Delft, 2006, http://www.library.tudelft.nl/ws/search/publications

[17] Schreck S. 2002. The NREL full-scale wind tunnel experiment introduction to the special issue. Wind Energy
5:77–84

[18] Schepers, J.G., Snel, H., Model Experiments in Controlled Conditions – Final Report, ECN, ECN-E-07-042,
Petten, the Netherlands, June 2007.

[19] Duckworth, A. and Barthelmie, R. J., Investigation and Validation of Wind Turbine Wake Models, Wind Engineering, 32(5), 459-475, 2008.

[20] Larsen T.J., Larsen G.C., Madsen H.Aa. and Thomsen K., Comparison of design methods for turbines in wake. Conference proceedings (online), European Wind Energy Conference, Brussels, 31 Marts - 3 April 2008.

[21] Politis, E. S., Prospathopoulos, J., Cabezon, D., Hansen, K. S., Chaviaropoulos, P. K. and Barthelmie, R. J. (2012), Modeling wake effects in large wind farms in complex terrain: the problem, the methods and the issues. Wind Energ., 15: 161–182. doi: 10.1002/we.481
[22] Barthelmie R.J., Hansen K., Frandsen S.T., Rathmann O., Schepers J.G., Schlez W., Philips J., Rados K., Zervos A., Politis E.S. and Chaviaropoulos P.K., Modelling and measuring flow and wind turbine wakes in large wind farms offshore.Wind Energy, 2009. WE-08-0099.
[23] Larsen, G.C. (2010). TOPFARM - next generation design tool for optimization of wind farm topology and operation … background, vision and challenges. The Science of making Torque from Wind. June 28-30, 2010, FORTH, Heraklion, Crete, Greece.
[24] Larsen, G.C., Madsen H.Aa, Troldborg N., Larsen, T.J., Réthoré P.E, Fuglsang P., Ott S., Mann J. and Buhl T., TOPFARM-NEXT GENERATION DESIGN TOOL FOR OPTIMISATION, Wind Energy 13 (2011): 86-99.
[25] Madsen, H.A., Thomsen, K. and Larsen, G.C., 2003, A New method for Prediction of Detailed Wake Loads. Proceedings of IEA Joint Action of Wind Turbines 16th Symposium held in Boulder, USA, May 2003 at NREL, edited by Sven-Erik Thor. pp. 171-188.
[26] Thomsen K. and Madsen H. Aa, new simulation method for turbines in wake - applied to extreme response during operation. In: Proceedings. Delft: Delft University of Technology. 2004. p. 425-432.
[27] Thomsen, K., Madsen H.Aa and Larsen G.C., A new method can predict detailed response for turbines in wind farms, Fact sheet AED-RB-16 (EN), Risoe National Laboratory, Roskilde, Denmark (2003).
[28] Madsen, H.Aa., Thomsen, K. and Petersen, S.M., Wind Turbine Wake Data from Inflow Measurements using a Five Hole Pitot Tube on a NM80 Wind Turbine Rotor in the Tjæreborg Wind Farm. Risø-I-2108(EN), 2003.
[29] Vølund, P., Loads on a horizontal axis wind turbine operating in wake, Journal of Wind Engineering and Industrial Aerodynamics 39, no. 1 (1992): 317-328.
[30] Bingöl, F., Mann, J. and Larsen, G.C., Light detection and ranging measurements of wake dynamics, Part I: One-dimensional Scanning, Wind Energy 13, 51-61, 2010.
[31] Trujillo, J.J., Bingöl, F., Larsen, G.C., Mann, J. and Kühn, M., Light detection and ranging measurements of wake dynamics, Part II: two-dimensional scanning, Wind Energy 14, 61-75, 2011.
[32] Madsen, H.Aa., Larsen, G.C., Larsen, T.J., Troldborg, N. and R. Mikkelsen, Calibration and validation of the Dynamic Wake Meandering model implemented in the aeroelastic code HAWC2. Journal of Solar Energy Engineering, Volume 132, Issue 4, 041014 (14 pages), 2010.
[33] Sørensen, N.N., Michelsen, J.A. and Schreck, S., Navier–Stokes predictions of the NREL phase VI rotor in the NASA Ames 80ft× 120ft wind tunnel. Wind Energy, 5(2-3), 151-169, 2002.
[34] Sørensen J.N. 2011 Aerodynamic aspects of wind energy conversion. Ann. Rev. Fluid Mech., Vol. 43, pp. 427-448
[35] Keck, RE., Mikkelsen, R., Troldborg, N., Investigation of prescribed wind shear and synthetic atmospheric turbulence for rotor wake simulations, Proceedings of Gotland wake conference 2011.
[36] Keck, R.-E., Mikkelsen, R., Troldborg, N., de Maré, M. and Hansen, K. S. (2013), Synthetic atmospheric turbulence and wind shear in large eddy simulations of wind turbine wakes. Wind Energy. doi: 10.1002/we.1631
[37] Keck, RE., Veldkamp, D., Madsen, H.Aa., Larsen, G.C., Implementation of a Mixing Length Turbulence Formulation Into the Dynamic Wake Meandering Model, Journal of Solar Energy Engineering, Volume 134, Issue 2, 021012 (13 pages), 2011.
[38] Panton, R. L. (1996), Incompressible flow. Continuum, 1(1.1), 1-2.
[39] Keck, RE., de Maré M., Churchfield, M.J. Lee, S. Larsen, G. and Madsen H.Aa, Two Improvements to the Dynamic Wake Meandering Model: Including the Effects of Atmospheric Shear on Wake Turbulence and Incorporating Turbulence Build Up in a Row of Wind Turbines, submitted to Journal of wind energy July 2012, accepted with revisions December 2012.

[40] Larsen, T. J., Madsen, H. Aa., Larsen, G. C. and Hansen, K. S. (2012), Validation of the dynamic wake meander model for loads and power production in the Egmond aan Zee wind farm. Wind Energy. doi: 10.1002/we.1563
[41] Madsen, H.A., Larsen, G.C. and Thomsen, K. (2005). Wake flow characteristics in low ambient turbulence conditions. In: proceedings of Copenhagen Offshore Wind 2005.
[42] Mann, J. The spatial structure of neutral atmospheric surface-layer turbulence. Journal of Fluid Mechanics, 273, 141-168, 1994.
[43] Mann, J. Wind field simulation. Probabilistic Engineering Mechanics, Vol. 13, No. 4, pp. 269-282, 1998.
[44] Peña, A., Gryning, S.-E. and Mann, J.: 2010, On the length scale of the wind profil, Quarterly Journal of the Royal Meteorological Society 136(653), 2119–2131.
[45] Keck RE., de Maré M., Churchfield M.J., Lee S., Larsen G. and Madsen H.Aa, On Atmospheric Stability in the Dynamic Wake Meandering Model, submitted to Journal of wind energy January 2013.
[46] Schepers, J. G. (2012). Analysis of 4.5 years EWTW wake measurements. Wind Energy, 2011, 2010.
[47] Barthelmie, R. J., Hansen, K. S. and Pryor, S. C. (2011). Meteorological controls on wind turbine wakes. In: Proceedings. Dutch-Flemish Wind Engineering Association.
[48] Barthelmie, R. and Jensen, L., (2010), Evaluation of wind farm efficiency and wind turbine wakes at the
Nysted offshore wind farm, Wind Energy, 13, pp. 573–586, doi: 10.1002/we.408.
[49] Hansen, K. S., Barthelmie, R. J., Jensen, L. E. and Sommer, A. (2011). The impact of turbulence intensity and atmospheric stability on power deficits due to wind turbine wakes at Horns Rev wind farm. Wind Energy.
[50] Larsen, G. C., Larsen, T. J., Madsen, H. A., Mann, J., Peña, A., Hansen, K. S. and Jensen, L. (2009). The dependence of wake losses on atmospheric stability characteristics. In Euromech Colloquium (Vol. 508, pp. 35-37).
[51] Schmidt, B. J King, GC Larsen, TJ Larsen, Load validation and comparison versus certification approaches of the Risø Dynamic Wake Meandering (DWM) model implementation in GH Bladed, EWEA annual event, Brussels, Belgium 2011.
[52] Larsen, G.C., Madsen, H.Aa., Thomsen, K. and Larsen, T.J., 2008, Wake meandering - a pragmatic approach, Wind Energy 11, 377-395, 2008.
[53] Müller Y., Aubrun S, Loyer S and Masson C., Experimental methodology for the study of the far-wake meandering of a modeled wind turbine, Proceedings of 8th PhD Seminar on Wind Energy in Europe. Zurich Switzerland, 2012.
[54] España G, Aubrun S, Loyer S, Devinant P. Temporal and spatial study of the meandering phenomenon. Proceedings of EuroMech 508. Universidad Politécnica de Madrid: Madrid, Spain, 20–22 October 2009.
[55] España G., Aubrun S., Loyer S., Devinant P., Spatial study of the wake meandering using modelled wind turbines in a wind tunnel.Wind Energy 2011; 14: 923–937.
[56] Eecen P., Wagenaar J.W. and Bot E.T.G, Offshore wind farms: loads and turbulence in wakes. Modeling and validation, Proceedings of Gotland wake conference 2011.
[57] Troldborg, N., Actuator Line Modeling of Wind Turbine Wakes, MEK-FM-PHD 2008-06, Technical University of Denmark, 2008
[58] Ivanell, S., Numerical Computations of Wind Turbine Wakes, PHD thesis, 2009-01, Royal institute of technology, Stockholm, Sweden, 2009
[59] Sanderse, B. Aerodynamics of wind turbine wakes - literature review. Technical Report ECN-E-09-016, ECN, Netherlands, 2009.
[60] Odemark Y. and Fransson J.H.M, *An Experimental study on wake evolution and trailing vortex instabilities,* Proceedings of Gotland wake conference 2011.
[61] Réthoré, P. E. (2009). Wind turbine wake in atmospheric turbulence. Aalborg University, Department of Civil Engineering.
[62] Ainslie, J.F. Calculating the flow field in the wake of wind turbines. Journal of Wind Engineering and Industrial Aerodynamics, 27, pp. 213-224, 1988

[63] Ainslie, J.F., 1986, Wake modelling and the prediction of turbulence properties. Proceedings of the 8th British Wind energy Association Conference, Cambridge 19-21 March 1986. pp. 115-120.
[64] Taylor GJ, Milborrow DJ, McIntosh DN, Swift-Hokk DT. Wale measurement on the Nibe windmills, Proc of the 7th BWEA conference, Oxford, 1985. 27-29 March.
[65] Medici D, Alfredsson PH. Measurements on a wind turbine wake: 3D effects and bluff-body vortex shedding. In Wind Turbine Wakes—Control and Vortex Shedding. Technical Report from KTH Mechanics, Stockholm, 2004; 77–95.
[66] España G, Aubrun S, Loyer S, Devinant P. Wind tunnel study of the wake meandering downstream of a modelled wind turbine as an effect of large scale turbulent eddies. Journal of Wind Engineering and Industrial Aerodynamics 2012; 101: 24–33.
[67] Aubrun S., Müller Y., Loyer S and Masson C. experimental study of the model wind turbine wake dynamics through stereo-PIV measurements, Proceedings of EuroMech 528. Oldenburg, Germany, February, 2012.
[68] Goodman, J. W. and Gustafson, S. C. (1996). Introduction to Fourier optics. Optical Engineering, 35(5), 1513-1513.
[69] Tennekes, H. and Lumley, J. L. (1972). A first course in turbulence. MIT press.
[70] Madsen, H. A., Larsen, G. C., Larsen, T. J., Mikkelsen, R. and Troldborg, N. (2008, March). Wake deficit-and turbulence simulated with two models compared with inflow measurements on a 2MW turbine in wake conditions. In Scientific proceedings. 2008 European Wind Energy Conference and Exhibition, Brussels (BE) (Vol. 31, pp. 48-53).
[71] Sathe A., Mann J., Barlas T., Bierbooms W.A.A.M. and van Bussel G.J.W., influence of atmospheric stability on wind turbine loads, Wind Energy, DOI:10.1002/we.1528.
[72] Stull, R. B. (1988). An introduction to boundary layer meteorology (Vol. 13). Springer.
[73] Obukhov, A.M.,Turbulence in an atmosphere with a non-uniform temperature, Boundary-Layer Meteorology 2, 7-29 (1971).
[74] Monin, A.S., Obukhov, A.M., Basic laws of turbulent mixing in the surface layer of the atmosphere, Tr. Geofiz. Inst., Akad. Nauk SSSR, 151, 163–187, 1954.
[75] Kirchhoff, R.H., Kaminsky, F.C., Wind shear measurements and synoptic weather categories for siting large wind turbines, Journal of Wind Engineering and Industrial Aerodynamics, Volume 15, Issues 1–3, December 1983, Pages 287-297, ISSN 0167-6105, 10.1016/0167-6105(83)90198-8.
[76] Irwin, J.S., A theoretical variation of the wind profile power-law exponent as a function of surface roughness and stability, Atmospheric Environment (1967), Volume 13, Issue 1, 1979, Pages 191-194, ISSN 0004-6981, 10.1016/0004-6981(79)90260-9.
[77] Zoumakis, N. M., The Dependence of the Power-Law Exponent on Surface Roughness and Stability in a Neutrally and Stably Stratified Surface Boundary Layer. Atmosfera (1993), 6, 79-83.
[78] Barthelmie R.J., Frandsen S.T., Hansen K., Schepers J.G., Rados K., Schlez W., Neubert A., Jensen L.E. and Neckelmann S.. Modelling the impact of wakes on power output at Nysted and Horns Rev. In European Wind Energy Conference, 2009.
[79] Wharton, S., Lundquist, J.K., Marjanovic, H., Synergistic effects of turbine wakes and atmospheric stability on power production at an offshore wind farm, LLNL-TR-524756, January 2012
[80] Churchfield, M.J., Lee, S., Michalakes, J. and Moriarty, P.J., A Numerical Study of the Effects of Atmospheric and Wake Turbulence on Wind Turbine Dynamics, Journal of Turbulence, Vol. 13, No. 14, 2012.
[81] Lee, S., A Clifton and P. Moriarty, Wind turbine wakes and turbulence under various atmospheric boundary layers, (manuscript submitted to Computer and Fluids)
[82] A. W. Lavely, G. Vijayakumar, M. P. Kinzel, J. G. Brasseur and E. G. Paterson, Space-time loadings on wind turbine blades driven by atmospheric boundary layer turbulence, AIAA 2011-635, (2011)
[83] Méchali, M., Barthelmie, R., Frandsen, S. and Réthoré, P. E. (2006, October). Wake effects at Horns Rev and their influence on energy production. In European Wind Energy Conference and Exhibition (p. 10).
[84] Troldborg, N., Larsen, G. C., Madsen, H. A., Hansen, K. S., Sørensen, J. N. and Mikkelsen, R. (2011). Numerical simulations of wake interaction between two wind turbines at various inflow conditions. Wind Energy, 14(7), 859-876.

[85] Mikkelsen, R., Sørensen, J. N., Øye, S. and Troldborg, N. (2007, August). Analysis of power enhancement for a row of wind turbines using the actuator line technique. In Journal of Physics: Conference Series (Vol. 75, No. 1, p. 012044). IOP Publishing.
[86] Vermeulen PEJ, Builtjes PJH, Turbulence measurements in simulated wind turbine clusters, Report 82-03003, TNO Division of Technology for Society, September 1982.
[87] Builtjes PJH., and Vermeulen PEJ, Turbulence in wind turbine clusters, Proc. 4th Int. Symposium on Wind Energy Systems, Stockholm, 1982, Vol. 2, pp. 449-464.
[88] Troldborg N, Madsen H.Aa. and Bak C., Experimental and Numerical investigation of wind turbine wake deficit and loads in partial wake operation, Proceedings of Gotland wake conference 2011.
[89] Meyers, J. and Meneveau, C. (2011). Optimal turbine spacing in fully developed wind farm boundary layers. Wind Energy, 15(2), 305-317.
[90] Smith G., Schlez W. and Neubert A., Practical application of wake modelling in large wind farms energy prediction, Proceedings of the Gotland wake conference 2011.
[91] Schlez W., Neubert A. and Cox S., Modelling Very Large Wind Farms Offshore and Onshore, Proceedings of EuroMech 508. Universidad Politécnica de Madrid: Madrid, Spain, 20–22 October 2009.
[92] Andersen S.J., Sørensen J.N. and Mikkelsen R., Low order numerical model of the inherent wake behind an infinitely long row of wind turbines, Proceedings of the Gotland wake conference 2011.
[93] Calaf, M., Meneveau, C. and Meyers, J. (2010). Large eddy simulation study of fully developed wind-turbine array boundary layers. Physics of Fluids, 22, 015110.
[94] Schlichting, H. and Gersten, K. (2004). Boundary-layer theory. Springer.
[95] Snel, H. and Schepers, J. G. (1995). Joint investigation of dynamic inflow effects and implementation of an engineering method. Netherlands Energy Research Foundation ECN.
[96] Mikkelsen, R., Actuator Disc Methods Applied to Wind Turbines, MEK-FM-PHD 2003-02, Technical University of Denmark, 2003.
[97] Sørensen, N. N., Bechmann, A., Réthoré, P. E. and Zahle, F. (2012). Near wake Reynolds-averaged Navier–Stokes predictions of the wake behind the MEXICO rotor in axial and yawed flow conditions. Wind Energy.
[98] Shen, W. Z., Sørensen, J. N. and Yang, H. (2011). Actuator Line/Navier Stokes Computations for Flows past the Yawed MEXICO Rotor. Proceedings of the Gotland wake conference 2011.
[99] Madsen, H. A., Riziotis, V., Zahle, F., Hansen, M. O. L., Snel, H., Grasso, F. and Rasmussen, F. (2011). Blade element momentum modeling of inflow with shear in comparison with advanced model results. Wind Energy.
[100] Hattori, H. and Nagano, Y. (2012). Structures and mechanism of heat transfer phenomena in turbulent boundary layer with separation and reattachment via DNS. International Journal of Heat and Fluid Flow.
[101] Sumner J.,Cabezón D. and Masson C., Prediction of wake effects on wind farm power production using a RANS approach. Part I. Complex terrain: Case studies from Spain. Proceedings of the Gotland wake conference 2011.
102] Jiménez, Á., Migoya, E., Esteban, M., Giménez, D., García, J. and Crespo, A. (2011). Influence of topography and wakes on wind turbulence: measurements and interpretation of results. Wind Energy, 14(7), 895-908.
[103] Helmis CG, Papadopoulos KH, Asimakopoulos DN, Papageorgas PG, Soilemes AT. An experimental study of the near-wake structure of a wind turbine operating over complex terrain. Solar Energy 1995; 54(6):413–28
[104] Hunt j., Mesoscale and turbulence effects on wind farms, Proceedings of EuroMech 508. Universidad Politécnica de Madrid: Madrid, Spain, 20–22 October 2009.
[105] http://www.wrf-model.org/index.php
[106] Pope, S.B. Turbulent Flows. Cambridge University Press, 2000.
[107] Zahle, F. and Sørensen, N.N., Characterization of the unsteady flow in the nacelle region of a modern wind turbine, Wind Energy, 2011:14, pages 271-283, 2011
[108] Zahle, F. and Sørensen, N. N. (2007, August). On the influence of far-wake resolution on wind turbine flow simulations. In Journal of Physics: Conference Series (Vol. 75, No. 1, p. 012042). IOP Publishing.

[109] Réthoré, P-E. M., Troldborg, N., Zahle, F. and Sørensen, N. N., Comparison of the near wake of different kinds of wind turbine CFD models. Abstract from Wake conference, Visby (SE), 8-9 Jun, 2011.
[110] Wußow, S., Sitzki, L. and Hahm, T., 3D-simulation of the turbulent wake behind a wind turbine, In *Journal of Physics: Conference Series* (Vol. 75, No. 1, p. 012033). IOP Publishing, 2007.
[111] Hahm T. and Wußow, S., LES of a turbulent and meandering wake, Euromech Colloquium 508 on Wind Turbine Wakes, Madrid, 20-22 October, 2009. Extended abstract published in ISBN 978-84-7484-220-3, pp. 78-79.
[112] Sørensen, J.N. and Shen, W.Z. Numerical modelling of Wind Turbine Wakes. Journal of fluids Engineering, Volume 124, Issue 2, pp. 393-399, 2002.
[113] Porté -Agel F., Wu Y.-T., Lu H., Conzemius RJ. Large-eddy simulation of atmospheric boundary layer flow through wind turbines and wind farms. J. of Wind Eng. and Industrial Aerodynamics 2011; 99; 154-168
[114] Ivanell, S., Sørensen, J. N., Mikkelsen, R. and Henningson, D. (2009). Analysis of numerically generated wake structures. Wind Energy, 12(1), 63-80.
[115] Jimenez, A., Crespo, A, Migoya, E. and Garcia, J. 2007 Advances in large-eddy simulations of a wind turbine wake. Journal of physics: Conference series, The science of making torque from wind 75 (012041).
[116] Ivanell, S., Mikkelsen, R., Sørensen, J. N., Hansen, K. S. and Henningson, D. (2010). The impact of wind direction in atmospheric BL on interacting wakes at Horns Rev wind farm. TORQUE2010 The science of making torque from wind. Heraklion, Crete, Greece.
[117] Steinfeld, G., Raasch, S., Tambke, J., Peinke, J. and Heinemann, D. (2009, October). Development of a large-eddy simulation (LES) model for modelling the far-wake effects of offshore windfarms. In Proc. Euromech Colloquium 508 on Wind Turbine Wakes.
[118] Migoya, E., Jiménez, A., Manuel, F. and Crespo, A. (2009). Stochastic simulation to study wake meandering using UPMPARK. Euromech Colloquium 508 on Wind Turbine Wakes, Madrid, 20-22 October, 2009. Extended abstract published in ISBN 978-84-7484-220-3, pp. 8-10.
[119] Madsen H. Aa., Mikkelsen R., S Øye, Bak C., Johansen J., A Detailed investigation of the Blade Element Momentum (BEM) model based on analytical and numerical results and proposal for modifications of the BEM model, Journal of Physics: Conference Series. The Science of making Torque from Wind. 2007.
[120] Smaili A., Masson C., On the Rotor Effects upon Nacelle Anemometry for Wind Turbines, Wind Engineering, Volume 28-6, pages 695-714, 2004
[121] Keck, R. E. (2012). A numerical investigation of nacelle anemometry for a HAWT using actuator disc and line models in CFX. Renewable Energy, 48, 72-84.
[122] Sarlak H., Sørensen J. N. and Mikkelsen R., Large Eddy Simulation of Offshore Wind Farm, Proceedings of Gotland wake conference 2011.
[123] Xu, G. and Sankar, L. N. (2000), Computational study of horizontal axis wind turbines, Transactions-American society of mechanical engineers journal of solar energy engineering, 122(1), 35-39.
[124] Voutsinas, S. G. (2006). Vortex methods in aeronautics: how to make things work. International Journal of Computational Fluid Dynamics, 20(1), 3-18.
[125] Glauert H. 1935. Airplane propellers. In Aerodynamic Theory, ed.WFDurand, vol. IV, Division L, pp. 191–269. New York: Springer
[126] Shen WZ, Mikkelsen R, Sørensen JN, Bak C. 2005a. Tip loss corrections for wind turbine computations. Wind Energy 8:457–75
[127] Glauert, H. (1926). The Analysis of Experimental Results in the Windmill Brake and Vortex Ring States of an Airscrew, Rept. 1026. Aeronautical Research Committee Reports and Memoranda, London: Her Majesty's Stationery Office.
[128] Buhl, M.L., Jr. 2004. A New Empirical Relationship between Thrust Coefficient and Induction Factor for the Turbulent Windmill State. NREL/TP-500-36834. Golden, CO: National Renewable Energy Laboratory, September.

[129] Øye, S., Fix dynamisk, aeroelastisk beregning af vindmøllevinge, AFM Report 83-08, Department of Fluid Mechanics, The Technical University of Denmark, 1983.
[130] Hansen MH, Gaunaa M, Madsen HAa. A Beddoes-Leishman type dynamic stall model in state-space and indicial formulations. Technical Report Risø–R–1354(EN), Risø National Laboratory, Denmark, 2004.
[131] Bak, C.; Aagaard Madsen, H.; Johansen, J. 2001. Influence from blade-tower interaction on fatigue loads and dynamics (poster). Wind energy for the new millennium. Proceedings. 2001 European wind energy conference and exhibition (EWEC '01). Copenhagen (DK), 2-6 Jul 2001.
[132] Hansen, M. O. L., 2001, Aerodynamics of Wind Turbines, Earthscan Publications Ltd, Oxford, United Kingdom.
[133] Burton, T.; Sharpe, D.; Jenkins, N.; Bossanyi, E.. (2001). Wind Energy Handbook. West Sussex, England: John Wiley and Sons, Ltd.; pp. 66–68.
[134] Jensen, N.O., A note on wind generator interaction. Risø M 2411. November 1983.
[135] Katic, I., J. Højstrup and N. O. Jensen, 1986: A simple model for cluster efficiency. Proceedings of the European Wind Energy Association Conference and Exhibition, Rome.
[136] Alblas L., Bierbooms W. and Veldkamp D., Power output of offshore wind farms in relation to atmospheric stability, in proceedings of the European Wind Energy Conference and Exhibition (EWEC) 2012.
[137] Wind Atlas Analysis and Application Program (WAsP), Risø National Laboratory, 1987. http://www.wasp.dk/
[138] Mortensen, N. G., Heathfield, D. N., Myllerup, L., Landberg, L. and Rathmann, O. (2007). Getting started with WAsP 9. Risø National Laboratory.
[139] Corbett, J. F., Ott, S. and Landberg, L. The new WAsP flow model: a fast, linearized Mixed Spectral-Integration model applicable to complex terrain. In 2007 European Wind Energy Conference and Exhibition.
[140] Berge, E., Gravdahl, A. R., Schelling, J., Tallhaug, L. and Undheim, O., Wind in complex terrain: a comparison of WasP and two CFD-models, proceedings of the European Wind Energy Conference and Exhibition (EWEC) 2006.
[141] Frandsen, S. (1992). On the wind speed reduction in the centre of large clusters of wind turbines. Journal of Wind Engineering and Industrial Aerodynamics, 39(1), 251-265.
[142] Frandsen, S., Barthelmie, R., Pryor, S., Rathmann, O., Larsen, S., Højstrup, J. and Thøgersen, M. (2006). Analytical modelling of wind speed deficit in large offshore wind farms. Wind Energy, 9(1-2), 39-53.
[143] Larsen, S. E., Ott, S., Peña Diaz, A., Berg, J., Nielsen, M., Rathmann, O. and Ejsing Jørgensen, H. (2011). Wake models developed during the Wind Shadow Project. Roskilde: Danmarks Tekniske Universitet, Risø Nationallaboratoriet for Bæredygtig Energi. (Risø-R-1793(EN)).
[144] Ott, S., Berg, J. and Nielsen, M. (2011). Linearised CFD Models for Wakes. Danmarks Tekniske Universitet, Risø Nationallaboratoriet for Bæredygtig Energi.
[145] Larsen, G.C., Madsen, H.Aa., Larsen, T.J. and Troldborg, N., Wake modeling and simulation. Risø-R-1653(EN). Risø National Laboratory, Technical University of Denmark, Roskilde, Denmark, 2008
[146] Davidson, L. (2011). Fluid mechanics, turbulent flow and turbulence modeling. Div. of Fluid Dynamics, Dep. of Applied Mechanics, Chalmers University of Technology, Göteborg, Sweden.
[147] Mikkelsen, R., Sørensen, J.N. and Troldborg, N., Prescribed Wind Shear Modelling Combined with the Actuator Line Technique. Proceedings of of the 2007 EWEC conference, Milan, 2007.
[148] Troldborg, N., Sørensen, J.N. and Mikkelsen, R., Actuator Line Simulation of Wake of Wind Turbine Operating in Turbulent Inflow. Journal of Physics: Conference Series. The Science of Making Torque from Wind. Technical University of Denmark, Lyngby, August 2007.
[149] Mikkelsen, R., Sørensen, J. N. and Øye, S. (2009, October). Meandering Wake Characteristic Derived from Actuator Line Simulations of Wind Turbine Wakes. In Euromech Colloquium (Vol. 508, p. 29).
[150] Troldborg N., Sørensen, J.N., Mikkelsen, R. D Sørensen, N.N., A simple atmospheric boundary layer model applied to large eddy simulations of wind turbine wakes, manuscript submitted to the journal of wind energy.

[151] Larsen, G.C., Hansen, K.S., Troldborg, N., Mann, J. and Enevoldsen, K., A first attempt to characterize the structure of the wake turbulence using a combined experimental and numerical approach, Conference on Turbulence IV, 2010, Bertinoro (IT), 19-22 Sep. 2010.
[152] Menter, F., R., Two-Equation Eddy-Viscosity Turbulence Models for Engineering Applications, AIAA, vol 32, No. 8, pp. 1598-1605, 1994
[153] Versteeg, H.K. and Malalasekera, W., An introduction to computational fluid dynamics – The finite volume method 2nd ed., 2007
[154] Lagarias, J. C., J. A. Reeds, M. H. Wright and P. E. Wright. Convergence Properties of the Nelder-Mead Simplex Method in Low Dimensions. SIAM Journal of Optimization, Vol. 9, Number 1, 1998, pp. 112–147.
[155] Matlab User Guide, on the topic: Optimizing Nonlinear Functions.
[156] Dahlberg, J.-Å., Assessment of the Lillgrund Wind Farm: Power Performance Wake Effects, [online report] Vattenfall Vindkraft AB, 6_1 LG Pilot Report, Sept. 2009, URL:
[157] Alblas, L., Power output of offshore wind farms in relation to atmospheric stability, Master of science thesis, Faculty of Aerospace Engineering, Delft University of Technology, June 2012.
[158] Jonkman, J., Butterfield, S., Musial, W. and Scott, G., Definition of a 5-MW Reference Wind Turbine for Offshore System Development, TP 500-38060, National Renewable Energy Laboratory, 2008.
[159] Churchfield, M.J., Lee, S., Moriarty, P.J., Martinez, L.A., Leonardi, S., Vijayakumar, G. and Brasseur, J.G., A Large-Eddy Simulation of Wind-Plant Aerodynamics, AIAA paper 2012-537, 50th AIAA Aerospace Sciences Meeting, Nashville, TN, Jan. 2012.
[160] Larsen, G.C., A simple stationary semi-analytical wake model. Risø-R-1713(EN), 2009.
[161] Gaumond M, Evaluation and Benchmarking of Wind Turbine Wake Models, Master thesis Technical University of Denmark, 2012

Nomenclature

Abbreviations:

ABL	Atmospheric boundary layer	
AL	Actuator line	
AMB	Ambient	
BC	Boundary condition	
BEM	Blade element momentum	
CFD	Computational fluid dynamics	
COG	centre of gravity	
DEF	Wake deficit	
DNS	Direct numerical simulation	
DWM	Dynamic wake meandering	
FFoR	Fixed frame of reference (i.e. coordinate system relative to the global)	
fun	function	
IFFT	Inverse fast Fourier transform	
LES	Large eddy simulation	
MFoR	Meandering frame of reference (i.e. coordinate system relative to the wake centre)	
N-S	Navier-Stokes	
N.H.	The North Hoyle wind farm	
OWEZ	The Egmond aan Zee wind farm	
PDF	Probability density function	
pp	Percentage-point, refers to difference in absolute difference in percentages (e.g. ΔTI)	
ROT	wind turbine Rotor	
RANS	Reynolds-averaged Navier-Stokes,	
STD	standard deviation	
STE	standard error, i.e. mean-square-sum of difference reference data and model output	
TI, TI_{TOT}	Turbulence intensity defined as: std(u)/U	[%]
TI_M	Apparent turbulence intensity due to wake meandering	[%]
$TI_{small\text{-}scale}$	Small-scale turbulence intensity due to turbulence generated in wake shear layer	[%]
WS	wind speed	[m/s]
WTG	Wind turbine generator	

Roman letters:

A	Cross sectional area	[m^2]
A_p	weighting coefficients at node p	[kg/s]
a	axial induction factor	[-]
$\bar{a}$	average axial induction factor over the rotor	[-]
B	number of blades	[-]
c	chord length	[m]
c_D	drag coefficient	[-]
c_L	Lift coefficient	[-]
$C_{u'w'}$	correlation coefficient between streamwise and vertical velocity fluctuations	[-]

C_p	Specific heat capacity	[J/kg, K]
$C_{Turb\ amp.}$	Turbulence amplification factor	[-]
$C_{Threshold}$	Threshold value for filtering ambient turbulence	[m/s]
d	distance	[m]
D	Rotor diameter	[m]
D	Sectional drag force	[N/m]
E	Spectral energy density	[m^2/s], [m^3/s^2]
f	frequency	[1/s]
$\boldsymbol{f}$	Body force	[N/m^3]
f_{mek}	Coefficient of mechanical to electrical power	[-]
f_p	Added body force for wind shear at node *p*	[N]
f_R	Factor governing the width of the boundary condition in DWM	[-]
f_U	Factor governing the depth of the boundary condition in DWM	[-]
F_1	DWM filter function to govern effect of ambient turbulence in the wake deficit	[-]
F_2	DWM filter function to govern development of shear layer turbulence	[-]
F_N	Sectional force in normal direction	[N/m]
F_T	Sectional force in tangential direction	[N/m]
H_{Hub}	Hub-height	[m]
k	wake decay constant of the Jensen model	[-]
k	wave number	[1/m]
k_{amb}	DWM constant for eddy viscosity due to AMB turbulence including length scale	[m]
k_1	DWM constant for eddy viscosity due to ambient turbulence	[-]
k_2	DWM constant for eddy viscosity due wake shear layer turbulence	[-]
l.	Turbulent length scale	[m]
L	Monin-Obukhov length	[m]
L	Sectional lift force	[N/m]
$\dot{m}$	massflow	[kg/s]
n_c	number of cases	[-]
$n_{c,\,d}$	number of cross-section per case	[-]
$n_{c,\,d,\,r}$	number of points per cross section	[-]
N	neutral atmospheric stability	[-]
p	pressure	[N/m^2]
P_{WTG}	Power production of the wind turbine generator	[W]
r	radial coordinate	[m]
R	Rotor radius	[m]
R	Specific gas constant	[J/mol, K]
$R_{i,j}$	Correlation function for components *I* and *j*	[-]
S	Stable atmospheric stability	[-]
S_p	Source term at node *p*	[N]
t	time	[s]
T	Temperature	[K]
u	Instantaneous streamwise velocity (x-dir)	[m/s]
u’	Fluctuating about the mean in streamwise velocity (x-dir)	[m/s]
u.	Friction velocity, Turbulent velocity scale	[m/s]
U	Mean velocity in streamwise direction (x-dir)	[m/s]
U_{MIN}	Lowest streamwise velocity in a cross-section of the wake deficit	[m/s]
U	Unstable atmospheric stability	[-]

v	Instantaneous lateral velocity (y-dir)	[m/s]
v'	Fluctuating about the mean in lateral velocity (y-dir)	[m/s]
VS	Very stable atmospheric stability	[-]
VU	Very unstable atmospheric stability	[-]
V_{REL}	Relative velocity to rotor blade	[m/s]
V_θ	Tangential velocity in rotor plane	[m/s]
V_z	Velocity normal to the rotor plane	[m/s]
w	instantaneous vertical velocity (z-dir)	[m/s]
w'	Fluctuating about the mean in vertical velocity (z-dir)	[m/s]
x	streamwise coordinate	[m]
y	lateral coordinate	[m]
z	vertical coordinate	[m]

Greek letters:

α	Angle of attack	[°]
α	Power-law coefficient	[-]
α_1, α_2	Angle in wake where ABL shear than is greater than wake deficit gradient	[°]
ε	force regularization parameter	[m]
ΔV	volume of a computational cell	[m^3]
ϕ	Inflow angle	[°]
γ	pitch angle	[°]
Γ	Circulation	[m^2/s]
λ	Tip-speed ratio	[-]
λ	Wave length	[m]
η	regularization kernel	[-]
ρ	Density	[kg/m^3]
ν	Kinematic viscosity	[m^2/s]
ν_T	Kinematic eddy-viscosity	[m^2/s]
ν'_T	Scaled kinematic eddy-viscosity to include ABL shear contribution	[m^2/s]
ω, Ω	Angular velocity	[rad/s]
τ_{shear}	Turbulent shear stress	[m^2/s^2]
σ	Standard deviation	[-]
θ	Potential temperature	[K]
θ_v	Virtual potential temperature	[K]
Φ	Mann spectral tensor	[m^5/s^2]

Appendix A: Recommendation for IEC-standard

The results presented in this thesis demonstrate that the DWM model is capable of predicting the mean velocity and turbulence field in a simulation of a wind farm operating in the ABL. The ability to capture the flow field inside the wind farm allows the model to predict both the power production and the turbine loads simultaneously, which facilitates consistent design and optimization tool for micro siting. The current standard procedure for wind turbine siting is to first design the layout for optimal power production using one model (commonly the Jensen model (Jensen [134], Katic et al. [135])), then ensure that the site specific loads do not exceed the design loads of the wind turbine using the Frandsen model (Frandsen [12]). This can lead to sub-optimized from a CoE perspective.

The model validation in this thesis (chapter 7) show that the power predictions of the DWM model are in good agreement to field data and higher-order models, and captures the power production and the effect of ambient turbulence intensity and atmospheric stability better than the Jensen model. The limited loads validation performed in this work show that the loads of the DWM model display good agreement with the reference data. A more comprehensive validation of the turbine loads with the DWM model has been undertaken by Larsen el at. [20, 40]. Although the details of that implementation is slightly different compared to the one presented in this thesis, the validation showed that the physical wake description of the DWM model allows for a better representation of the turbine loads than the model currently suggested by IEC-standard. In the author's opinion, the DWM model should therefore be considered to be included as an option in the IEC-standard for both turbine design and wind farm design.

Wind turbine siting

The largest benefits of the DWM model can be utilized by updating the wind turbine siting process. Using the DWM model enables the designer to optimize the farm layout for both loads and power production simultaneously, together with an overall better wake representation, this could significantly lower the CoE of wind energy (according to the TOPFARM project [24] the potential exceeds 5% in reduced CoE). The current approach is to design the wind farm for optimal power production using one model, and subsequently to use a separate model to check that the loads of the turbines in the wind farm does not exceed the design specification. Optimizing only for power production in the first study may result in a sub-optimized layout. For a CoE perspective, a comprehensive wind farm design philosophy including power production, loads and infrastructure could improve the competitiveness of the wind industry. To enable this, the following principal effects need to be accounted for:

- Turbines should be represented based on actual distribution of rotor induction or at least integrated C_T-value.
- The wake deficit (i.e. the reduction of velocity in the wake) should be physically modelled in the computations.
- Dynamic effects due to meandering of the wake deficit should be included as it is the main driver for additional turbine loads in wind farms.
- Increased turbulence level in the wake should be included in the simulations. This has an effect on the turbine loads, but the most important effect may be that the increased turbulence level

influences the wake evolution of the wake-affected turbines, causing less severe wake deficits inside the wind farm.
- The effect of atmospheric stability on the wake evolution should be included. As shown in this thesis, atmospheric stability changes the composition of oncoming turbulence of a wake-affect turbine. This is important for both loads and power production predictions.

Suggestions for methods to incorporate the above listed effects are given in chapter 6.

Individual turbine design

In terms of design of the individual wind turbine, some additional investigations are required before a suggestion for an IEC-standard update can be given. However, with the functionality of the DWM model to represent the wind speed and turbulence distribution, together with the large scale wake meandering inside a wind farm, it is feasible to investigate the effect on component loads by operating in a wind farm compared to solitary operations. The current design process of the individual wind turbine is based on loads of a turbine operating in solitary conditions. The effects of wakes are included in the siting step by scaling the loads of the turbine based on the increased turbulence experienced in a wind farm. For this approach to be adequate, all loads of the turbine are required to scale with similar magnitude when the turbine operates in waked condition. However, the wind field (and loads) experienced by a wind turbine operating inside a farm is different compared to a solitary turbine. This means that relative loads of the various components of the wind turbine may be different inside a wind farm compared to solitary turbines. As a consequence, the current design process could lead to an overly conservative turbine design where some components may be over-engineering.

The suggestion is therefore to investigate whether or not the true loads experienced by a turbine in wake operation do scale similarly. According to the loads investigation presented in figure 2.2, some loads increase more due to wake condition. If the proposed investigation reaches the conclusion that the load-envelope experienced under waked conditions are not a linear scaling of the load in solitary operation, a solution could be to include some load cases based on wind farm situations:
- Including wind farm fatigue load cases based on generic wind farm layout (e.g. 3Dx3D, 6Dx6D, 9Dx9D) and a uniform windrose distribution in flat terrain. This could lead to a better representation of the loads experienced by a wind farm compared to the current practice
- Include extreme loads in wind farm situations. This would require even further analysis to determine the most appropriate load cases.

I: Synthetic Atmospheric Turbulence and Wind Shear in Large Eddy Simulations of Wind Turbine Wake

Wind Energy

WIND ENERGY
Wind Energ. (2013)
Published online in Wiley Online Library (wileyonlinelibrary.com). DOI: 10.1002/we.1631

RESEARCH ARTICLE

Synthetic atmospheric turbulence and wind shear in large eddy simulations of wind turbine wakes

Rolf-Erik Keck[1,3], Robert Mikkelsen[2], Niels Troldborg[3], Martin de Maré[1,3] and Kurt S. Hansen[2]

[1] Rotor Systems, Vestas Wind systems A/S, DK-4000 Roskilde, Denmark
[2] Department of Mechanical Engineering, Fluid Mechanics Section building 403, Technical University of Denmark, DK-2800 Lyngby, Denmark
[3] Wind Energy Department, Risø DTU national Laboratory for sustainable Energy, DK-4000 Roskilde, Denmark

ABSTRACT

A method of generating a synthetic ambient wind field in neutral atmosphere is described and verified for modelling the effect of wind shear and turbulence on a wind turbine wake using the flow solver EllipSys3D. The method uses distributed volume forces to represent turbulent fluctuations, superimposed on top of a mean deterministic shear layer consistent with that used in the IEC standard for wind turbine load calculations.

First, the method is evaluated by running a series of large-eddy simulations in an empty domain, where the imposed turbulence and wind shear is allowed to reach a fully developed stage in the domain. The performance of the method is verified by comparing the turbulence intensity and spectral distribution of the turbulent energy to the spectral distribution of turbulence generated by the IEC suggested Mann model.

Second, the synthetic turbulence and wind shear is used as input for simulations with a wind turbine, represented by an actuator line model, to evaluate the development of turbulence in a wind turbine wake. The resulting turbulence intensity and spectral distribution, as well as the meandering of the wake, are compared to field data. Overall, the performance of the synthetic methods is found to be adequate to model atmospheric turbulence, and the wake flow results of the model are in good agreement with field data. An investigation is also carried out to estimate the wake transport velocity, used to model wake meandering in lower-order models. The conclusion is that the appropriate transport velocity of the wake lies somewhere between the centre velocity of the wake deficit and the free stream velocity. Copyright © 2013 John Wiley & Sons, Ltd.

KEYWORDS

Synthetic Atmospheric Turbulence; Wake modelling; Wake turbulence; LES; Actuator line; Wake Meandering; Wake transport velocity

Correspondence

Rolf-Erik Keck, Wind Energy Department, Risø DTU national Laboratory for sustainable Energy, DK-4000 Roskilde, Denmark.
E-mail: rolf.keck@gmail.com

Received 22 August 2012; Revised 26 March 2013; Accepted 17 April 2013

1. INTRODUCTION

The ability to accurately predict wake effects is critical in the prediction of power and loads of wind turbines in wind farms. Specifically, wind turbine wakes result in a reduction in mean wind speed and increase in turbulence intensity seen by downstream rotors, which tend to both lower the production of the turbine, and increase the effective fatigue loads on the turbine components. The amount by which wake effects affect power and loads on turbines in wind farms, however, depends on several parameters relating to the ambient wind field, including (at least) wind speed, turbulence intensity, turbulent length scale, wind shear, wind veer and stratification. The process of modelling the wake effects in wind farms is further complicated by the fact that the aforementioned ambient parameters are correlated to each other and that the effect on the wake evolution by the individual parameters are non-linear.

Despite the challenging physics of the problem, most engineering descriptions of the wake of a turbine are limited in that they have only been tuned or validated to a few field data campaigns and do not contain a physical description of the distribution of turbulence or dynamics of the wake as it develops in an ambient wind field. Computational fluid dynamics (CFD) methods, on the other hand, can in theory physically model all (or most) of the key physics associated with the ambient wind field and the development of the turbine wakes in the wind farm. Much of the recent focus in CFD modelling of wind turbine wakes has been put on the development of comprehensive large-eddy simulation (LES) models (Crespo,[1]

Porté Agel,[2] Mikkelsen,[3] Troldborg,[4,5] Jimenez,[6] Ivanell,[7] Churchfield *et al.*[8,9] and Lee *et al.*[10]). LES is advantageous over standard Reynolds Averaged Navier Stokes (RANS) models (Rérhoré[11]) in that the large scales of turbulence are resolved physically, without the use of turbulence closure models.

Because of the high computational expense of LES simulations, however, it is not feasible to model all the turbulent scales in a wind farm down to the boundary layer of the turbine blades. Because of this, the actuator disc/line (AD/AL) methods (Ivanell[7] and Sørensen and Shen[12]) have gained popularity in modelling wind turbine rotors in comprehensive wind turbine and farm simulations. Compared with fully resolved CFD modelling of rotor blades, the AL method reduces meshing and computational expense by modelling the blades as body forces. The body forces are based on the local velocity field at the blade sections and tabulated lift and drag values. This eliminates the need to resolve the boundary layer on the blades, resulting in reduced computational times both as a result of fewer mesh elements, but more importantly by the fact that a larger time step can be used without violating the Courant–Friedrichs–Lewy (CFL) constraints.

Given its ability to capture the development of turbulence in the wind turbine wake, rather than statistically model it as in RANS, LES models incorporating AL methods for rotor modelling can be used to generate numerical data of wake dynamics and wake deficit growth in various atmospheric conditions. This data can in turn be used to calibrate and/or validate engineering models. Prior to this, however, the basic components of the LES AL models must be verified and validated against basic theoretical data and field measurements in wind farms. This specific study is aimed at evaluating the synthetic atmospheric wind field description, as proposed by Mikkelsen *et al.*[13] and Troldborg *et al.*[14] in EllipSys3D LES solver for wind farm simulations. The main benefit of imposing synthetic atmospheric wind shear and turbulence by the methods presented here is the ability to generate inlet boundary and initial conditions to wind farm simulations without having to run computationally expensive precursor calculations. Churchfield *et al.*[9] mentions that the precursor calculation in their LES AL wind farm simulation require 37,000 CPU hours per case. The synthetic methods require less than one CPU hour to generate input wind shear and turbulence.

Two previous works (Gilling and Sørensen[15] and Troldborg *et al.*[5]) studied the fundamental aspects of imposing synthetic turbulence and wind shear by body forces inside the computational domain. However, there has not been much comprehensive research directed towards the performance of the methods under the range of ambient conditions important for turbine operation (e.g. ranges of operating thrust, wind speed and turbulence intensity). The main objective of this work is therefore to investigate the capability of the proposed method to model the turbulence development in a wind turbine wake under ambient conditions ranging from wind speeds of 6 to 15 m/s and turbulence intensities from 6 to 14% (defined as the standard deviation of wind speed normalized against ambient mean wind speed, $\overline{u'}/U_{\mathrm{amb}}$). A secondary objective is also to derive best practice recommendations for the model parameters of the synthetic wind field model, i.e. the shear coefficient and the turbulence amplification factor (which is described later in the paper), as well as distance required for the imposed turbulence to reach a fully developed stage.

The first part of the investigation is carried out in an empty computational domain. This has the benefit of isolating the atmospheric turbulence, which enables detailed studies of the appropriate parameter settings and the distance required for the imposed turbulence to reach a fully developed stage. In the second part of the investigation, the results of the empty domain calculations are applied in combination with an AL representation of the wind turbine to verify the wake evolution. The performance of the combined approach is validated against field data from wake measurement campaigns at Nibe, Alsvik, Tjaereborg and the Risø Nordtank turbine.

2. MODEL DESCRIPTION

2.1. Atmospheric wind shear and turbulence

The synthetic method for generating a wind field has been previously implemented by Mikkelsen *et al.*[10] Here atmospheric shear was imposed by distributed volume forces in the unsteady incompressible Navier–Stokes equation in the entire domain, according to equation (1).

$$\frac{\mathrm{d}V}{\partial t} + V\cdot\nabla V = -\frac{1}{\rho}\nabla p + \nu\nabla^2 V + \frac{f}{\rho} \tag{1}$$

The force, $\boldsymbol{f}$, for each computational node is calculated in a precursor simulation without turbines to yield a desired ambient velocity distribution in the domain. The method is capable of prescribing an arbitrarily mean flow field including both wind shear and wind veer. In this investigation, the effects of atmospheric stability and Coriolis force on the flow field are neglected, and the ambient flow field is prescribed as a power-law shear profile; see equation (2).

$$U(z) = \begin{cases} U(H_{\mathrm{hub}})\cdot(c_1 z^2 + c_2 z) & z \le \Delta \\ U(H_{\mathrm{hub}})\cdot\left(\dfrac{z}{H_{\mathrm{hub}}}\right)^{\alpha} & z > \Delta \end{cases} \tag{2}$$

The model coefficients c_1 and c_2 control the near wall treatment below Δ. The near wall limit, Δ, is usually taken to be a distance equivalent to 10 computational cells. The description of the desired wind shear profile in equation (2) is used as

input to a precursor calculation executed in an empty domain. The calculation of the forces is based on an immersed boundary approach where the discretized form of the volume integrated N-S equations (equation (3)) govern the velocity desired at cell centred computational node point p.

$$A_p V_p^{t+\Delta t} + \sum\nolimits_i A_i V_i^{t+\Delta t} = S_p + f_p \tag{3}$$

The subscript i refers to the neighbours of the studied computational node p. V is the velocity component in the studied direction, and A is the weighting coefficients. S is the source term containing the pressure gradient force and body forces, and f is the added body force included to yield the desired velocity. By rearranging the terms in equation (3) and replacing the velocity at p by the desired velocity $U(z)$, an equation for the force to apply at node p can be found:

$$f_p = A_p U(z) + \sum\nolimits_i A_i V_i^{t+\Delta t} - S_p \tag{4}$$

The calculation in the empty domain is run until a steady converged flow field is reached, and the resultant force field is then stored and applied in the subsequent calculations with rotors present.

Atmospheric turbulence on top of the mean shear is included by introducing fluctuating body forces in a plane located close to the turbine by a method proposed by Troldborg *et al.*[14] The forces are found via prescribed three-dimensional velocity fluctuations, generated with the Mann turbulence model (Mann[16,17]). The Mann turbulence model combines an eddy lifetime assumption with rapid distortion theory to transform an isotropic spectral tensor to an anisotropic spectral tensor. The anisotropic spectral tensor depends on three input parameters to characterize the turbulence: rate of dissipation ($\alpha\varepsilon^{2/3}$), turbulent lengths scale (L_{Mann}) and degree of anisotropy (Γ). The Mann turbulence model can be used to generate a three-dimensional box containing random incompressible anisotropic turbulence. In applications, it is customary to interpret the streamwise dimension as time using Taylors hypothesis of frozen turbulence.[18]

The grid used to generate the Mann turbulence generally do not match the CFD grid used in the LES simulation. The grid of the imposed turbulence is chosen to be coarser than the CFD grid to ensure that the CFD grid can resolve the scales of the synthetically generated turbulence. As a consequence, the fluctuations at the location of the nodes in the CFD grid are found by interpolation in the box of synthetic turbulence. The Interpolation is carried out spatially in-plane in two dimensions, and temporally between successive planes in the turbulence box. A consequence of the interpolation process, and the smearing of forces used to introduce the in the CFD domain (described by equations (6) and (7)), is that less turbulence is realized in the CFD domain than prescribed by the imposed synthetic turbulence in the high frequency part of the turbulence spectra (this is shown in Figure 10). To compensate for the reduced turbulence due to interpolation, the velocity fluctuations are scaled by a *turbulence amplification factor*:

$$u'_i = u'_{i,\text{Mann}} * C_{\text{Turb amp.}} \tag{5}$$

Here u_i' is the turbulent local velocity fluctuation in direction i, $C_{\text{turb amp}}$ is the turbulence amplification factor. The fluctuations are introduced to the CFD simulation as volume forces according to one-dimensional momentum theory:

$$f'_i = \dot{m} u'_i + \rho A \varepsilon \frac{\mathrm{d}u'_i}{\mathrm{d}t} \tag{6}$$

In equation (6), A is cross-sectional area of the cell in the computational grid, ρ is the air density and $\dot{m}$ is the local mass flow through the cell. The forces need to be introduced into the CFD calculations in a smooth manner to maintain numerical stability. The forces are therefore distributed in the flow direction by a one-dimensional Gaussian smoothing function. The regulatory distributions parameter, ε, is set to be equivalent to two grid cells. The force experienced at a node in the computational domain is described by equation (7).

$$f = f' \otimes \frac{1}{\varepsilon\sqrt{\pi}} e^{-(d/\varepsilon)^2} \tag{7}$$

Here d is the distance in flow direction from the centre of the computational cell to the node in the turbulence plane causing the fluctuating force.

2.2. Actuator line model

The actuator line model was implemented into the flow solver EllipSys3D (Sørensen[19]) and coupled to FLEX5 (Øye[20]) to allow for aeroelastic calculations by Mikkelsen.[3] The fundamental idea behind the AL method is to model the turbine rotor as three rotating lines containing distributed body forces, $\boldsymbol{f}$, in the unsteady incompressible N-S equations (seen previously in equation (1)). The forces are calculated based on local inflow condition at the AL nodes and tabulated blade data; see Figure 1.

The aeroelastic calculation is based on a two-way coupling between EllipSys3D and FLEX5, and can be described as

- Local field velocities at the position of the AL nodes are extracted from EllipSys3D and passed to FLEX5
- The local velocity triangle at all AL nodes, including elastic or other movement, serves to compute local blade loadings, F_T, F_N, similar to the common blade element momentum (BEM) approach; see Hansen.[21]
- The local blade loadings are re-projected into global coordinates, passed back to the flow solver and applied as a source term in the momentum equation of the LES simulations

The FLEX5 integration is based on a fourth-order Runge–Kutta–Nyströms method; however, only one CFD step is computed for each information transfer, and an Adam–Bashforth extrapolation is applied in order to handle half step computation in FLEX5. Model validation of rotor performance predicted by the applied AL model has been carried out by comparing measured power and experimental C_p coefficient by Troldborg,[4] Ivanell[7] and Sørensen and Shen.[12] Validation of the wake generated by an AL model was conducted by Troldborg *et al.*[4] and Larsen *et al.*[22] Larsen *et al.* conducted the validation to wake measurements in meandering frame of reference (i.e. based on a reference system that follows the wake centre) obtained from a measurement campaign with a backwards facing LIDAR mounted on top of the nacelle (Trujillo *et al.*[23] and Bingöl *et al.*[24]). The mean wind speed and turbulence intensity distributions 2.5 rotor diameters (D) behind the rotor were compared to the field measurements and a high level of agreement over the wake cross section was achieved.

2.3. Numerical setup and computational mesh

The numerical calculations carried out in this work are based on LES filtered N-S equations where the larger eddies in the flow are resolved directly without any turbulence model. Eddies smaller than the grid size, also called sub-grid scales or SGS, are treated by the mixed scale model for SGS eddy viscosity described in Cavar.[25] The convective terms are discretized using a hybrid scheme consisting of a 10% third-order accurate QUICK scheme and a 90% fourth-order accurate central difference scheme (CDS). Pressure–velocity coupling is obtained by using the SIMPLE algorithm. For more information about QUICK or the SIMPLE algorithm, see Versteeg and Malalasekera.[26] The appropriate time step to use in the AL calculations is found by the restriction that the AL should not pass through an entire mesh cell in one time step. This is much more restrictive than the requirement that the CFL number should be lower than unity, since the wind speed is much smaller than the tip velocity of the blade. For the NM80 turbine and the mesh used, this requirement yields a time step equivalent to 175 time steps per rotor revolution based on the target rotor RPM of the turbine controller at a given mean wind speed.

The computational mesh is drastically simplified by representing the turbine rotor as AL lines compared to resolving the physical boundaries of the rotor blades. Furthermore, flat ground is assumed for all the calculations, and the flow close to

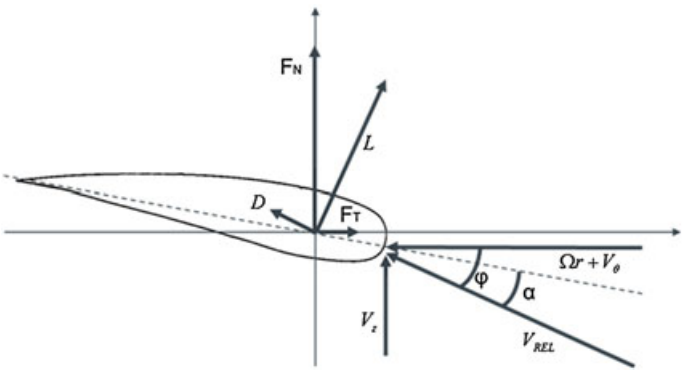

Figure 1. Illustration of the properties used to calculate the contribution of the local airfoil section, L and D, to the AL forces in the global coordinate system, F_N and F_T.

the ground is treated by the expression in equation (2), where the no-slip condition is enforced by source terms and the turbulence production because the wall itself is neglected. As a consequence, no boundary layer needs to be resolved by the computational grid, enabling the use of a Cartesian mesh in the whole domain. All calculations were carried out on a Cartesian grid in a rectangular domain of $10R \times 30R \times 52R$, in width, height and flow direction, respectively; see Figure 2. The origin of the coordinate system is taken to be the lower right corner of the inlet cross section of the domain, i.e. the lower right corner of Figure 2a.

The domain and the computational mesh are designed with the ambition of economizing the computational expense and maximizing the concentration of grid points in the volume of interest. A refined mesh region is constructed to give high spatial resolution where the imposed turbulence of the wake needs to be resolved. The domain outside of the refined region is only designed to maintain the mean flow field properties and allow for high quality data to be obtained in the refinement region. As a consequence, a course grid can be used, which has the result that the design of the outer domain is less sensitive considering the computational expense. Instead, the main consideration is to ensure that the boundaries do not influence the simulation results and that the cross-sectional area of the domain is sufficiently large to avoid blockage effects. To avoid blockage effects, the cross section of the domain is made 95 times larger than the swept area of the ALs (300R2 compared with 3.14R2). The boundary conditions applied are (i) prescribed mean velocity at the inlet, (ii) no slip by forcing terms and wall treatment according to equation (2) on the lower boundary, (iii) cyclic on the lateral boundaries, (iv) prescribed velocity at the top boundary given by equation (2) and (iv) a convective outlet boundary condition. The inlet and the top boundaries contain prescribed velocities that are sensitive for the solution in the domain. Therefore, these domain boundaries are placed 'far away' from the region of interest (i.e. the wake). The inlet boundary is placed 15.5R away from the turbulence plane and 21.5R from the rotor position in order to avoid pressure effects influencing the inlet. The top boundary is placed at a distance of 30R (or 26R away from the wake refinement).

On the basis of a mesh sensitivity study performed by Keck *et al.*,[27] a mesh resolution of 25 points per rotor radius (PPR) in cross-flow direction and 23 PPR in flow direction was found to be sufficient to resolve turbulence scales into the inertial sub-range; see Figure 4. This is required in order to accurately model the SGS stresses by the eddy viscosity model. This resolution was applied in the grid refinement region, i.e. the inner box in Figure 2. Furthermore, the same study also concluded that a refinement region with a cross section of $4R \times 4R$ and a resolution of 25 PPR is adequate to model the wake development and the integrated momentum deficit of the wake; see Figure 3. An effect seen by using a $4R \times 4R$ compared with a $6R \times 6R$ region of refinement was a slight reduction on the wake meandering in the order of 10%. This result is expected as wake meandering is primarily caused by turbulent eddies in the atmospheric boundary layer turbulence, which are larger than the rotor; see España *et al.*[28] The relatively small cross section of refinement region, relative to the size of the eddies that cause the wake meandering, will lead to eddies being affected by the coarser grid outside the refinement. This will in turn subject the eddies to an increased dissipation (by the SGS viscosity) and reduce the life time of the large structures. With a large cross section of the refinement region, this effect is reduced. Due to computational constrain, larger refinement regions than $6R \times 6R$ were not tested in the sensitivity study. Consequently, the results are not grid independent with respect to the size of the refinement region, and a further sensitivity study would be required to fully establish the influence of this parameter on the wake meandering. For the conducted investigation, this effect was not considered important enough to justify the increase of computational time by 125% (from ~10,000 CPU hours to ~22,500 CPU hours) required to capture the extra meandering. (Figure 4)

The turbulence plane used to introduce the velocity fluctuations is located in a cross section of the domain 15.5R downstream of the inlet boundary. The size of the plane is $8R \times 4R$, and it is positioned centrally in lateral direction and starts 0.4R above the ground level in vertical direction (i.e. above the near wall treatment); see dashed line/box in Figure 2. The turbulence plane thus covers the cross section of the grid refinement region and a region surrounding the grid refinement.

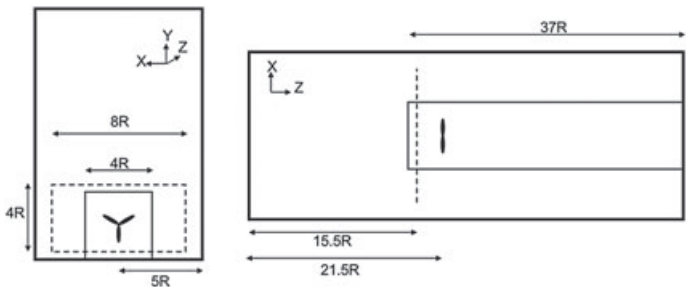

Figure 2. The left figure is an *X–Y* plane showing the cross section of the computational domain, and the right figure is an *X–Z* plane showing the computational domain from above. The outer solid box represents the computational domain. The rotor location is indicated by the solid black body. The dashed line/box indicates where the turbulent fluctuations are applied, and the internal solid box shows the refined region included to maintain the imposed turbulence and limit numerical dissipation.

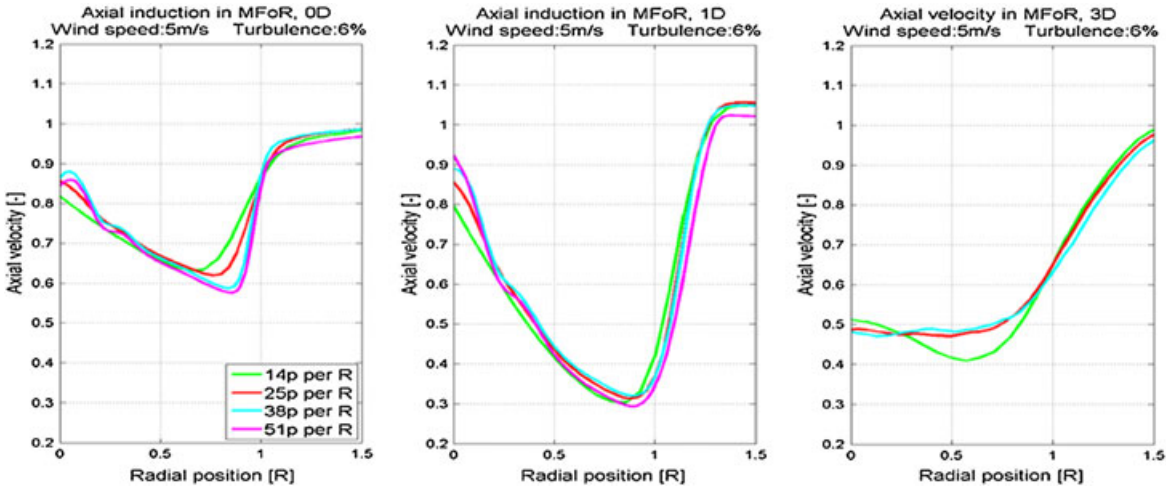

Figure 3. The development of axial velocity for four different AL resolutions: 14, 25, 38 and 51 points per radii (p per R). The left figure is at the rotor plane, the middle figure is at 1D and the right figure is at 3D downstream of the turbine. (The 51 p per R case is missing at 3D as the computational domain was shortened because of computational demand; thus, no data could be extracted at 3D.)

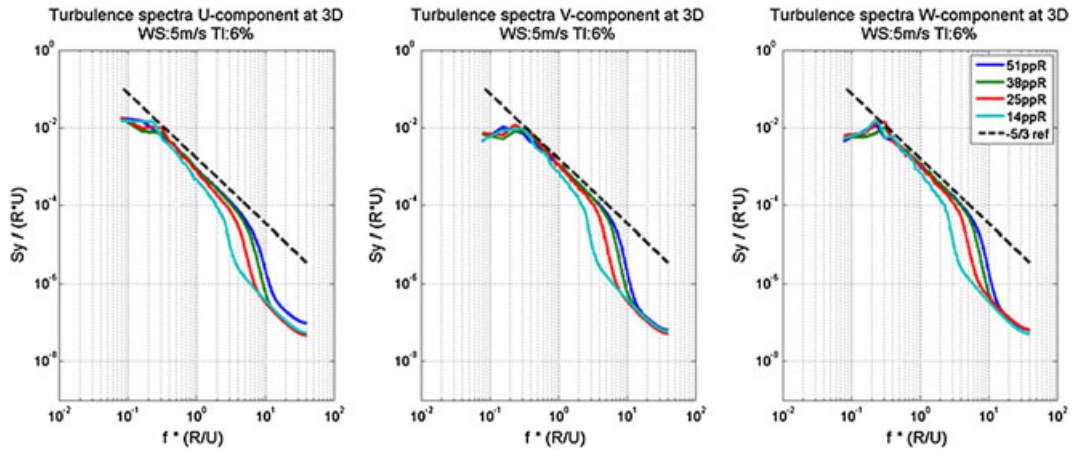

Figure 4. The spectral distribution of turbulent energy for four different grid resolutions in the wake region: 14, 25, 38 and 51 p per R. The figure shows the energy spectra in streamwise, horizontal and vertical directions (left, middle and right figures, respectively).

Turbulent fluctuations are imposed around the grid refinement in order to minimize the reduction of turbulence due to turbulent diffusion close to the edges of the refinement region. No turbulence is imposed far away from the grid refinement region as that turbulence would be exposed to unphysical dissipation due to the course grid resolution.

The location of the rotor in the wake simulations are based on simulations in an empty domain, presented later in this paper. It was found that the imposed fluctuations require about 150 cells to reach a fully developed state. As a consequence, the centre of the rotor is placed 6R behind the turbulence plane at 5R, 2R and 21.5R. The grid refinement is required after the turbulent fluctuations have been introduced to reduce the level of numerical dissipation and to resolve the scales that are important for the wake development. The grid refinements are therefore added to the domain from 3–7R $\times$ 0–4R $\times$ 15–52R. The mesh in the refined region consists of 'near cubic' mesh elements corresponding to 25 PPR resolution in cross-flow direction and 10% elongated mesh elements in flow direction; i.e., for a 40 m rotor radius, the element size is 1.6 m $\times$ 1.6 m $\times$ 1.76 m. Outside of the refined region, the elements are stretched towards the domain boundaries. In total, the mesh consists of 162 blocks of 48 $\times$ 48 $\times$ 48 cells, yielding a total mesh count of ~18 million cells.

2.4. Post processing of wake meandering

For the cases where there is a wind turbine present in the simulation, an important result is the amount of large-scale movement of the entire wake deficit by large turbulent structures, commonly referred to as wake meandering. Wake meandering

is quantified as the standard deviation of the wake centre position over time. The wake centre position is calculated at every time step in planes perpendicular to the mean flow direction as the centre of gravity (COG) of the wake deficit. The procedure of calculating the COG starts with recording high frequency data from planes perpendicular to the mean flow direction; in this work, 10 Hz data have been used. The wake speed deficit is filtered by a threshold value, $C_{\text{Threshold}}$, to reduce the effect of small-scale turbulence by equation (8).

$$\hat{U}_{\text{Def}} = \begin{cases} 0, & \dfrac{(U(z)-u)}{U(H_{\text{hub}})} < C_{\text{Threshold}} \\ \dfrac{(U(z)-u)}{U(H_{\text{hub}})}, & \dfrac{(U(z)-u)}{U(H_{\text{hub}})} \geq C_{\text{Threshold}} \end{cases} \tag{8}$$

where u is the instantaneous local axial velocity from the EllipSys3D calculation, $U(z)$ is the imposed mean shear as a function of height and $U(H_{\text{hub}})$ is the wind speed at hub height. The COG is calculated by integrating the filtered deficit in a circular region around the centre line of the wake (the axis that starts at the hub of the turbine) and 2R in radial direction:

$$COG_i = \frac{1}{A}\int_0^{2R} \hat{U}_{\text{Def}} \cdot r_i \, \mathrm{d}A \tag{9}$$

The subscript i indicate if lateral or vertical meandering is studied, r_i is the location of the filtered deficit value and A is the total integration area. The proposed algorithm cannot solve the problem that it is hard to determine a wake centre in the far-wake where the wake deficit is shallow relative to the turbulent fluctuations. This also means that the meandering statistics in the far-wake are associated with an increased level of uncertainty. (However, the effect of the wake deficit can also be considered small in this region) The appropriate value of the threshold parameter is a balance between being able to filter away the effect of turbulence and still being able to accurately trace the wake. A high turbulence level requires a large value for the threshold parameter; however, this reduces the detectability of the wake as the deficit recovers. In this work, a threshold parameter of 0.2 was used in all studies.

3. DESCRIPTION OF INVESTIGATION

The main objective of this investigation is to evaluate the performance of the method for generating a synthetic ambient wind field, as proposed by Mikkelsen *et al.*[13] and Troldborg *et al.*,[14] when applied in wind turbine wake simulations in neutral stratification and flat terrain. However, before running wake simulations, the input parameters to the method and the appropriate placement of the rotor relative to turbulence plane need to be investigated. This is achieved by running a series of LES simulations in an empty computational domain to allow detailed studies of

1. the relationship between the applied power-law shear coefficient and its balance with the generated turbulence intensity
2. the appropriate value for the 'turbulence amplification factor' (a model coefficient included to yield the right amount of turbulence in the simulations; see equation (5))
3. the distance required for the imposed turbulence to reach a fully developed state after the turbulence plane

The imposed turbulence used for all investigation is based on the Mann turbulence model, Mann.[16,17] The input parameters to the Mann model in terms of turbulent length scale, L_{Mann}, and the degree of anisotropy, Γ, were maintained constant at 47 m and 3.89, respectively. The rate of dissipation, $\alpha\varepsilon^{2/3}$, was calibrated to yield the desired turbulence intensity. As mentioned above, the Mann turbulence grid is coarser than the CFD grid to ensure that the synthetic turbulence can be resolved in the CFD simulations. The Mann turbulence box used to generate the synthetic turbulence in this work is $5\,\text{m} \times 5\,\text{m}$ in cross-flow direction (compared with $1.6\,\text{m} \times 1.6\,\text{m}$ for the CFD grid) and 1, 2 and 3 m in flow direction for the cases of wind speed 5, 10 and 15 m/s, respectively (compared with 1.76 m in the CFD grid). The different resolution in flow direction stems from the fact that all Mann turbulence boxes used in this investigation contains 4096 planes, which has the consequence that different free stream velocities leads to different spatial dimensions to allow for the same amount of simulation time. The important parameter to consider in streamwise direction, however, is the number of CFD time steps taken per Mann turbulence plane. This governs the temporal interpolating and ensures that the streamwise component of Mann turbulence fluctuations can be realized on the CFD grid. In this work, the CFD time step is 10 times smaller than the time between two successive Mann turbulence planes.

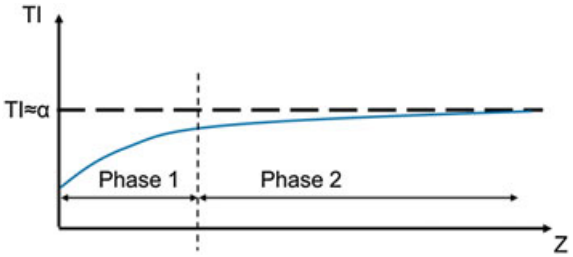

Figure 5. Characteristic development of turbulence intensity in EllipSys3D using the synthetic turbulence method. The solid line represents the realized turbulence in the simulation. In the first phase, the level of turbulence increase rapidly as the imposed turbulence recovers from the interpolation and force smearing process and adapts to the CFD grid. The turbulence level after the first phase is determined by the imposed turbulence level and the turbulence amplifications factors. In phase 2, the turbulence level evolves towards an equilibrium level based on the balance between turbulence production and dissipation.

The empty domain simulations cover wind speeds of 5, 10 and 15 m/s and turbulence intensities of 6, 10 and 14%. The development of the turbulence intensity in the EllipSys3D model for an empty domain follows a clear trend that can be described by two fundamentally different phases: The first phase is related to the turbulence cascade in the flow solver. At the location where turbulence is imposed ($z = 0$ in Figure 5), the turbulence lies below the prescribed level. Initially, it increases rapidly with downstream distance. It takes a few radii for the turbulence to develop to the level specified by the input turbulence and turbulence amplification factor. This initial increase of turbulence cannot be attributed to interactions with the vertical shear profile, as it increases too rapidly and the effect is also seen in simulations with a small amount of vertical shear. The physical explanation is that the cascade process in the flow solver 'corrects' the deficit of turbulent energy in the smaller scales. As mentioned above, the under-realization of small-scale turbulence occurs due to the interpolation and the force smearing processes used when imposing the synthetic turbulence on the CFD grid (see Figure 10). The first phase is thus responsible for the fast initial increase in turbulence depicted in the beginning of Figure 5. After the imposed turbulence 'has adjusted itself' to the grid, the second phase is the development of turbulence to an equilibrium level set by the mean atmospheric shear.

The second phase starts when the energy levels in the small scales are in balance with the large-scale turbulence (i.e. when the spectral distribution has reached a stable form). This means that the turbulence has been fully adjusted to the computational grid. In the second phase, the turbulence continues to develop towards the equilibrium level based on the mean flow properties, dashed line in Figure 5. Since this study is carried out in neutral stratification, i.e. no buoyancy effects are taken into account, the equilibrium level in an empty domain is dictated by the vertical wind shear alone.

The objective of the empty domain study is to find the optimal parameters to apply in the AL model in order to make the development from imposed turbulence to realized fully developed turbulence in EllipSys3D as fast as possible. This is of importance when turbine wake simulations are conducted so that the turbine rotor is placed at the appropriate distance from the turbulence plane.

The second part of the study is aimed at evaluating the evolution of wake turbulence when applying the synthetic turbulence methods. A turbine is placed 6R behind the turbulence plane, and a set of EllipSys3D AL calculations are conducted covering the range of the most common operational conditions for wind turbines, wind speeds of 6, 10 and 15 m/s and turbulence intensities of 6, 10 and 14%. The ability to model the turbulence evolution in the wake is verified by comparing the mean turbulence intensity as a function of downstream distance, the turbulent energy spectra and the wake meandering of the AL model wake to measured field observations. The meandering characteristics are difficult to verify due to the low availability of field data but are extracted and shown as a function of ambient turbulence intensity and downstream distance to serve as a reference value for further studies.

All simulation results from the AL model presented in this section are based on 500 s of simulation time. Ideally, longer simulation time would be desirable as the temporal and spatial variation of turbulence is relatively high for some of the tested cases, but this was not feasible with the restricted computational resources available (a case of 500 s of simulation time take about 5 days with the available computational resources ~10,000 CPU hours). The relatively short simulation time yields an uncertainty in the numerical mean value of wind speed and turbulence. The magnitude of the uncertainty can be estimated by assuming that the atmospheric length scale at hub height is in the order of 100 m; this yields 25, 50 and 75 independent samples at a mean wind speed of 5, 10 and 15 m/s, respectively. To reduce the uncertainty, the flow field is averaged in lateral direction over 80 computational cells (128 m), assuming a lateral length scale of 32 m (using the relation $L_{UY} = \kappa z$ for $z = 80$ m) results in five independent samples. This yields a total of 125, 250 and 375 independent samples for the 5, 10 and 15 m/s cases. The uncertainty of the sample mean and turbulence intensity is estimated by equations (10) and (11); see Vännman and Dunkels.[29]

$$\sigma_{\text{mean } ws} = \frac{\sigma_{ws}}{\sqrt{n}} \tag{10}$$

$$\beta_{TI} = \sqrt{\frac{\chi^2_{84.13\%}(n-1)\cdot\sigma^2_{ws}}{(n-1)}} - \sigma_{ws} \tag{11}$$

where σ_{ws} is the standard deviation of the wind speed (given by the turbulence intensity), n is the number of independent samples and $\chi^2_{84.13\%}(n-1)$ is the scaling value for the 84.13% percentile based on the χ^2 distribution. This choice was made as the χ^2, for high degrees of freedom (>50), approaches the normal distribution and the 84.13% percentile for the normal distribution corresponds to one standard deviation above the mean. The estimates of the uncertainty for wind speed and turbulence can be seen in Table I.

4. DESCRIPTION OF FIELD DATA

This section contains a short description of the field data used to validate the EllipSys3D AL model. Four different sites have been used and the available data is summarized in Table II.

4.0.1. Alsvik

Alsvik is an onshore wind farm in flat terrain that is located approximately 75 m (6R) from the shore of the Baltic Sea in westerly direction. The data used in this paper are collected in wind directions ranging from 210 to 320° (i.e. wind from the Sea); the operational conditions of the turbines can therefore be considered to be close to offshore conditions. The site consists of four 180 kW turbines with a rotor diameter of 23 m and a hub height of 30 m. The layout is setup for studying single wake effects on wind turbines. There are two meteorological masts at Alsvik, which means that the ambient wind is measured accurately by the first mast and the single wake is captured by the downstream mast at distances of 8, 12 and 17R. More information about the Alsvik wind farm can be found in Djerft and Mattson.[30]

4.0.2. Tjæreborg

The site consists of eight 2.5 MW NM80 turbines in flat terrain. The layout of the wind turbines relative to the meteorological mast yields single wake conditions at distances of 4.6, 7.0 and 7.8R. No measurement of the ambient wind conditions is available for the time of the wake measurements; instead, the long-term average condition for the site was used as reference number.

As a part of the TOPFARM project (Larsen *et al.*[31]), a LIDAR equipment was mounted on one of the turbines to characterize the wake properties in a meandering frame of reference. For the period of the LIDAR measurements, a meteorological mast was available to measure the ambient conditions. The wake wind speed and turbulence were measured 40, 80, 120, 160 and 200 m behind the rotor.

Table I. Estimation of uncertainty of the assembly mean wind speed and turbulence intensity due to the limited simulations time.

	WS 5 m/s	WS 5 m/s	WS 10 m/s	WS 10 m/s	WS 10 m/s	WS 15 m/s	WS 15 m/s
	TI 6%	TI 14%	TI 6%	TI 10%	TI 14%	TI 6%	TI 14%
Wind speed [m/s]	0.005	0.012	0.004	0.006	0.009	0.003	0.007
Turbulence intensity [%]	0.37	0.86	0.26	0.44	0.61	0.22	0.50

Table II. Summary of field data used for validation of the EllipSys3D AL model.

	Rotor diameter [m]	Hub Height [m]	Amb. conditions	Wake dist. [R]
Alsvik	23	30	Met mast	8.0, 12.0, 17.0
Tjæreborg	80	59	Long-term ref	4.6, 7.0, 7.8
Tjæreb. LIDAR	80	59	Met mast	0.5, 1.0, 1.5, 2.0, 2.5
Nibe	40	45	WS from production	5.0, 8.0, 12.0, 15.0
Risø Nordtank	41	36	Nacelle anemometer	2.44, 4.88

4.0.3. Nibe experiment

The Nibe site is in the northern part of Jutland in flat terrain close to the coast. The Nibe wake experiment consists of two 630 kW Nibe wind turbines with a rotor diameter of 40 m and hub height of 45 m. The turbines are located 200 m (10R) apart from each other along a north–south axis, and four meteorological masts are located 5, 8, 12 and 15R north of the southernmost wind turbine. For the period used in this paper, only the southern turbine was operational, creating single wake measurements of the wake at the four meteorological masts. No meteorological mast is installed at the site to measure the undisturbed oncoming wind, which means that the ambient conditions have to be estimated. The wind speed is estimated by the power production of the undisturbed wind turbines, and the oncoming turbulence intensity is estimated to 10–15% by Taylor *et al.*[32] The raw data were not available for this analysis; instead, digitalization of the figure presented in the report by Taylor *et al.*[32] has been used. On the basis of the figures representing the data used in this paper, the ambient turbulence is estimated to be 10%.

4.0.4. Risø Nordtank

The 500 kW Nordtank turbine is located south of the Risø Campus in flat terrain consisting mainly of farmland. The turbine has a rotor diameter of 41 m and a hub height of 36 m. A wake measurement campaign similar to the Nibe experiment has been conducted where two meteorological masts were placed 2.44R and 4.88R behind the wake emitting turbine. The ambient conditions are estimated on the basis of nacelle measurements calibrated to a nearby meteorological mast.

5. RESULTS

5.1. Part 1: turbulence evolution in an empty domain

The investigation of the turbulence evolution in an empty domain starts with an initial investigation to determine the influence of the model parameters. On the basis of these initial results, appropriate parameter values are suggested. Finally, a set of simulations are conducted to verify the capability of the synthetic atmospheric shear and turbulence methods by applying the parameter values.

5.1.1. Initial investigation of the model parameters

5.1.1.1 Influence of atmospheric shear coefficient. A set of simulations are conducted to investigate the influence of the wind shear coefficient on the turbulence evolution in the domain. The ambient wind speed in the investigation is 10 m/s, and the turbulence intensities are 6 and 14%. The wind shear coefficient is varied at three levels (0.05, 0.10 and 0.15) while holding the turbulence amplification factor constant; see Table III. The expected result is that the wind shear coefficient should determine the equilibrium level of turbulence in the far-wake of the simulations, as no other mechanism of turbulent production is present since the simulations are conducted in neutral stratification. Figure 6 show the result of the first three cases of Table III. The input turbulence and wind speed of all three cases are the same, and thus, the difference in the evolution of turbulence is caused by the wind shear coefficient alone. This confirms that the wind shear is important for the turbulence levels in the far-wake. The turbulence in Figure 6 does, however, not reach an equilibrium level in the simulated distance of 20R. This is the result of using a too high turbulence amplification value, 1.3 instead of more appropriately 1.15, and as a consequence, a long distance is required for the turbulence to evolve to a state of equilibrium with the vertical shear.

5.1.1.2 Influence of turbulence amplification factor. In the subsequent investigation, the influences of the turbulence amplification factor on the turbulence evolution are tested at levels 1, 1.15 and 1.30 while maintaining the wind shear coefficient constant for a range of ambient conditions; see Table IV. The turbulence amplification factor increase the

Table III. Simulation cases in the investigation of the influence of the wind shear coefficient on the turbulence evolution in the domain.

Wind speed	Target TI	Shear coeff. (α)	$C_{\text{Turb Amp}}$
10	6	0.05	1.3
10	6	0.10	1.3
10	6	0.15	1.3
10	14	0.05	1.3
10	14	0.10	1.3
10	14	0.15	1.3

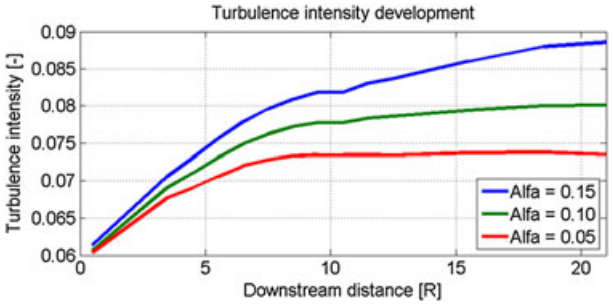

Figure 6. The effect of the atmospheric wind shear on the turbulence evolution in the CFD simulation. By comparing the turbulence level at end of the domain, it is clear that the applied wind shear is important for the equilibrium turbulence value. All cases were executed with the same input turbulence field and turbulence amplification factor of 1.3. (Note that the subsequent study suggests that a turbulence amplification factor of 1.15 should be applied; this is the reason why all the studied cases reach a higher TI than desired.)

Table IV. Simulation cases in the investigation of the influence of the turbulence amplification factor on the turbulence evolution in the domain.

Wind speed	Target TI	Shear coeff. (α)	$C_{\text{Turb Amp}}$
5	14	0.15	1.0
5	14	0.15	1.15
10	6	0.15	1.0
10	6	0.15	1.15
10	6	0.15	1.3
10	14	0.15	1.0
10	14	0.15	1.15
10	14	0.15	1.3
15	14	0.15	1.15
15	14	0.15	1.30

magnitude of turbulence being imposed in the computational domain; see equations (5) and (6). The expected effect is that the turbulence amplification factor will affect the value of the input turbulence and the realized turbulence after the initial increase in turbulence intensity (i.e. the phase one recovery described above, which is due to under-realization of small-scale turbulence close to the turbulence plane; see Figure 10) as is illustrated in Figure 5. This effect is confirmed by the results presented in Figure 7 (cases 6–8 in Table IV), which show that the starting point of the three cases is clearly influenced by the turbulence amplification factor applied. Furthermore, it can be seen that starting point and the initial

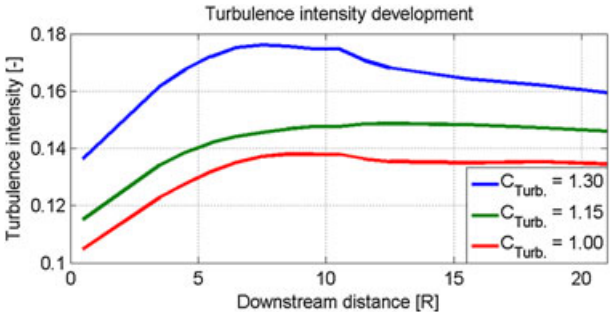

Figure 7. The effect of the turbulence amplification factor on the turbulence evolution in the CFD simulation. It is clear that the applied turbulence amplification factor is an important parameter for the turbulence level at the location where the imposed turbulence has adjusted to the CFD grid (i.e. after phase 1). The figure also shows that this will in turn affect the distance required to reach a stable turbulence intensity level in the CFD domain. All cases where executed with the same shear coefficient of 0.15.

increase of turbulence intensity are important parameters when attempting to achieve a desired stable turbulence intensity value in the simulation domain.

5.1.1.3 Observed behaviour from the initial investigation of model parameters. From the conducted investigation, it was observed that the turbulence intensity level in the domain converges towards a level close to the wind shear coefficient; i.e., $\alpha = 0.10$ yields a fully developed turbulence intensity level of 10%. Furthermore, applying a turbulence amplification factor of 1.15 (in combination with the suggested wind shear setting) seems to give the fastest convergence to a steady turbulence level in the domain. If larger turbulence amplification is applied, the turbulence overshoots and requires a longer distance to decrease to the desired level. In the subsequent section of the empty domain investigation, the evolution of the turbulence intensity and the turbulent energy spectra with downstream distance are investigated on the basis of the suggested parameter values.

5.1.2. Downstream evolution of turbulence with the suggested parameter values

The mean value of turbulence intensity and the development of the turbulent energy spectra were studied as function of downstream position to evaluate where the imposed turbulent fluctuations had reached a fully developed stage. Figure 8 shows the development of turbulence components. As reported by Gilling and Sørensen,[15] the streamwise velocity component experiences the largest reduction in turbulence level when imposed at the turbulence plane and thus requires the longest distance to account for the initial effects in adjusting the imposed turbulence to the numerical grid and the flow solver. This trend is seen consistently in all cases in the investigation. On the basis of this result, only the turbulence intensity and turbulent energy spectra of the streamwise component are investigated when evaluating at what downstream position the synthetic turbulence is fully developed in EllipSys3D.

When applying the suggested shear and turbulence amplification factors, we can see that the turbulence intensity reaches a steady value after 6R (~150 cells) from the turbulence plane. This is shown in Table V where the fifth column represents the ratio of turbulence intensity at 6.5R to the mean turbulence intensity at 10–20R. For wind speeds of 10 and 15 m/s, the average error is ~1%. The result for the '*5* m/s, *6% TI*' case suggests that lower wind speeds might require slightly longer

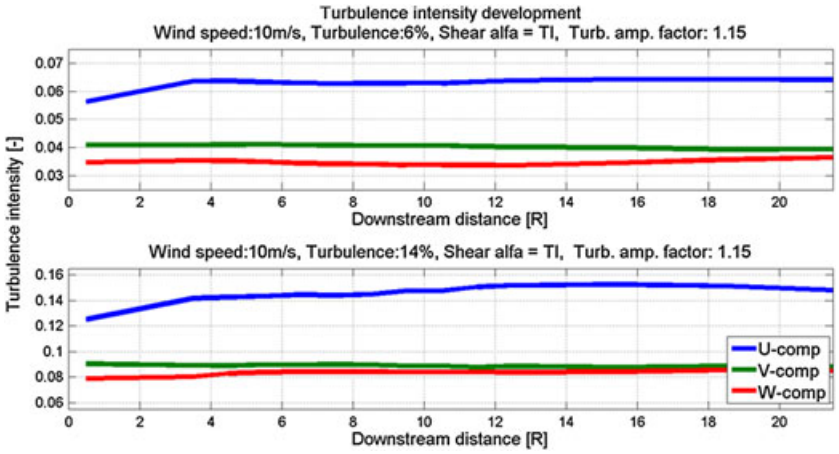

Figure 8. Evolution of turbulence intensity of the different velocity component at hub height as a function of downstream distance in an empty simulation domain.

Table V. Comparison of turbulence intensity at 6.5R compared to 10–20R using the suggested setting for wind shear and turbulence amplification factor.

WS	Target TI	Realized TI at 6.5R	Realized TI at 10–20R	Ratio of TI at 6.5R to 10–20R	Ratio of TI at 10–20R to target TI
5	6	5.47	5.85	0.94	0.98
5	14	11.18	13.68	0.82	0.98
10	6	6.29	6.38	0.99	1.06
10	10	11.68	11.58	1.01	1.16
10	14	14.44	14.93	0.97	1.07
15	6	5.27	5.29	1	0.88
15	14	12.76	12.77	1	0.91

distances to develop. The '*5* m/s, *14% TI*' case should be seen as an outlier in the analysis. As no error was detected in the process of generating the input turbulence, the case was not lifted out of the paper, but it should be noted that the low level of turbulence at 6.5R is likely related to the fact that an unusually low realized input turbulence was achieved (9.52% as opposed to the 14% desired). The last column of Table V, which represents the ratio of realized turbulence in the far-wake to the target turbulence level, shows the relatively high uncertainty in finding the desired turbulence level.

Figure 9 shows the vertical distribution of turbulence intensity in the simulation domain for the cases with a wind speed of 10 m/s. It can be seen that the turbulence in the simulation is almost invariant over the rotor height. The figure also confirms that the suggested parameter settings lead to a stable turbulence with downstream close to the desired turbulence intensity level and that the majority of the recovery due to grid and interpolation effects occurs over the first 3R.

Observing the turbulent energy spectra of the streamwise component, Figure 10, it can be seen that the energy levels in the high-frequency scales (i.e. small eddies) are reduced close to the turbulence plane by comparing the spectra of the imposed Mann turbulence (black line) to the realized turbulence at 0.5R (blue line). This is due to the interpolation and the force smearing effect when imposing the synthetic turbulence onto the CFD grid. An effect can be seen in all non-dimensional frequencies of 0.4 and higher ($f_{\text{Non-Dim}} = f^*R/U$, where $R = 40$ m and $U = 10$ m/s); this corresponds eddies with a length scales of 100 m ($L = U/f = R/f_{\text{Non-Dim}}$) or ~60 CFD cells and smaller. The under-realization of turbulent energy increases with increasing frequency and reaches 80% at $f_{\text{Non-Dim}} = 2$ (eddies of 20 m or ~12 CFD cells). The amount of turbulent energy in these scales recovers rapidly as the flow progress downstream by the energy cascade in the flow solver. At 3.5R, the energy levels in the small scales have recovered in whole spectral range. At this point, the turbulence is considered to be adjusted to the turbulent grid and flow solver; i.e., phase one of the evolution of the imposed turbulence is completed. After 3.5R, the turbulence in seen to increase in all scales; this is the start of the second phase in the turbulence development, where the turbulence level evolves in all scales towards an equilibrium level with the imposed vertical shear.

5.1.3. Conclusions of empty domain investigation

With an appropriate selection of parameter values, the implemented methods for synthetic turbulence and wind shear yield satisfactory results in neutral stratification and flat terrain. On the basis of the conducted numerical investigations, the main findings are as follows:

- The power-law shear coefficient should be selected to have a value close to the desired turbulence intensity, i.e. $\alpha = 0.10$ for $TI = 0.10$, in order to yield correct turbulence levels after equilibrium is reached.

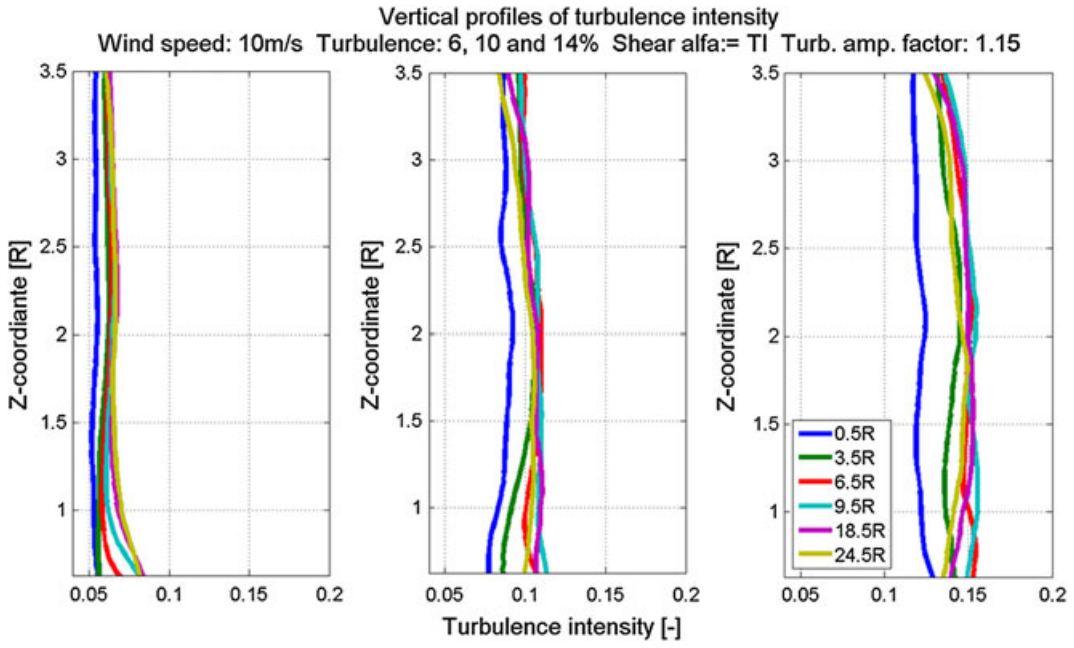

Figure 9. Vertical profiles of turbulence intensity in an empty simulation domain as a function of height above ground level (*y*-axis) and downstream distance (line colour) when applying the suggested values for shear and turbulence amplification factor. The ambient conditions are wind speed of 10 m/s and turbulence intensity of 6, 10 and 14% (from left to right).

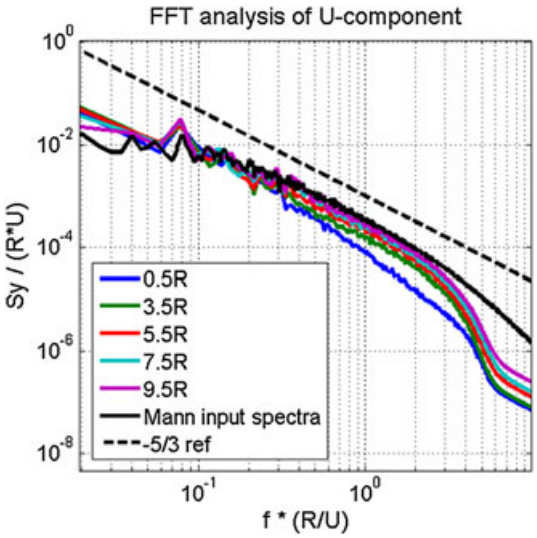

Figure 10. Power spectra of streamwise velocity component at various distances downstream of the turbulence plane. The spectra display a recovery of energy in the small scales due to the energy cascade in the flow solver. The black line represents the spectral distribution of the synthetic turbulence being imposed on the flow field.

- The best value of the turbulence amplification factor was found to be 1.15. The basis for the evaluation was the distance required for the imposed turbulence to reach the desired turbulence intensity level.
- With the setting suggested above, equilibrium between turbulence and wind shear was achieved after about 6 R (~150 cells) behind the turbulence plane.
- At the location where the turbulent fluctuations are introduced, a reduced amount of energy is seen in the smaller turbulent length scales. As the flow develops, this imbalance in the turbulent energy spectra is corrected by the turbulence cascade process in the EllipSys3D model. At distances larger than 3.5 R (~88 cells) behind the turbulence plane, the distribution of turbulent energy assumes the well-known $-5/3$ slope in the inertial sub-range in eddy sizes down to the cut-off due to grid resolution.

5.2. Part 2: turbulent wake evolution

5.2.1. Downstream development of mean value of turbulence intensity

Figure 11 shows the mean value of turbulence intensity at hub height in the wake as a function of ambient turbulence intensity and downstream distance. The presented values in the graph are the mean value of turbulence intensity over a 1.6×0.4D area at hub height, centred on the axis from the hub of the turbine. The solid lines are results from AL simulations, and the dots indicate field data from Alsvik, Tjæreborg, Nibe and the Risø Nordtank wake measurements in similar conditions. It should be noted that the AL simulations are not setup to mimic the specific field data cases. Instead, the idea is to validate that the AL model can in fact capture the correct trend and reasonable magnitude of wake turbulence for a large range of cases. All AL simulations were carried out with the NM80 turbine. This is the same turbine as is used at the Tjæreborg measurement, but the reference data from the other sites are collected with other turbine models. Furthermore,

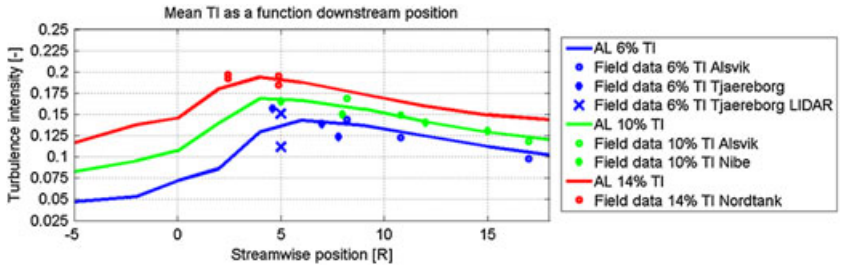

Figure 11. Comparison of integrated turbulence intensity extracted from the AL simulations to measurement data from Alsvik, Tjæreborg, Nibe and the Risø Nordtank turbine. The zero location of the *x*-axis refers to turbine position.

the mean ambient conditions of the field data are not identical to the conditions applied in the AL simulations. The presented AL results are the average of two simulations carried out with wind speeds of 6 and 10 m/s for turbulence intensities of 6, 10 and 14%, whereas the field data are collected at wind speeds ranging from 5 to 11 m/s. This approach is justified as long as the thrust coefficient of the turbines (C_T), and the ambient turbulence intensity level are similar. The C_T is assumed to be similar for the studied turbine for wind speed below rated power. The ambient turbulence intensity of the field data used for the comparison is in the range of ± 1 percentage point from the simulated cases.

Overall, it can be seen that the increased turbulence levels in the wake of the AL simulations is in fair agreement with the reference sources considering the differences in turbine models and ambient conditions. All datasets capture the trend of the wake turbulence in a satisfactory manner, and no bias towards under-prediction/over-prediction of turbulence intensity levels of the AL model is observed. The turbulence intensity of the Nibe (green diamonds) and the Alsvik (blue and green circles) measurements agree well at all observed locations and have an average difference between AL and field data of ~0.5 percentage points. The meteorological mast data from Tjæreborg (blue diamonds) and Risø Nordtank (red circles) measurements are off by ~1 percentage point, and the LIDAR measurements from Tjæreborg (crosses) are off by ~2 percentage points. Part of the discrepancies between field data and LIDAR measurement could be that the analysis of the LIDAR data is performed in a meandering frame of reference (MFoR), which means that the effect of wake meandering is filtered out. Furthermore, the relatively low sampling frequency (0.45Hz) and spatial resolution (10 m $\times$ 5 m) increase the uncertainty of the turbulence measurement using the LIDAR equipment. Overall, the mean deviation between the AL model and the field data is below 1 percentage point and the largest deviation is 2.5 percentage points.

An important result is that the AL model is able to capture the level of turbulence decay in the far-wake. This shows that the parameter suggestions for the atmospheric shear coefficient and the turbulence amplification factor, developed for empty domain simulations, can be applied in wake simulations. This is not an obvious result as the shear settings found to yield turbulence balance in an empty domain might not hold for wake simulation when the turbulence level, and thereby the dissipation, is much higher.

5.2.2. Downstream development of turbulence spectra

The Alsvik site offers an opportunity to validate the development of the auto spectra as a function of downstream position as there are turbines positioned at 8R, 12R and 17R upstream from one of the meteorological masts on site, whereas the other meteorological mast is undisturbed by wake at the wind directions in question.

As all the EllipSys3D AL runs in this work are executed with a turbine of 40 m rotor radius and the turbines at Alsvik is equipped with a rotor of 23 m radius, the data from the two sources need to be non-dimensionalized in order for the turbulent spectra to be compared. The length scale of turbulence can be assumed to depend on R, as the length scale of the turbulence in a neutral atmosphere can be assumed to be proportional to the hub height, and both turbines have a hub height close to 2*R. There are two velocity scales present in the problem, however, $\overline{u'}$ and U. To compare the cases, it is therefore required that the turbulence intensity (u'/U) is comparable.

To improve the statistical significance of the comparison logged data from a 1.6D $\times$ 0.4D surface at hub height, centred on the wake axis, are extracted from the LES simulations. In order to make the comparison as similar as possible, the wind direction sector used to select the field data is recalculated for each distance to ensure that the samples are collected from a sector equivalent to the 1.6D plane used to achieve the numerical results. Figure 12 shows the result of the comparison of turbulence auto spectra extracted from the AL simulations to field data from the Alsvik wind farm. Overall, good agreement is seen for the amount of turbulent energy in all measured scales both in free ambient condition and waked conditions. The largest deviations between the field data and the simulations are seen in the '12R' cases and at dimensionless frequencies between 0.3 and 0.7, where the field data display higher turbulence levels. At the Alsvik site, the three different wake distances represent three different inflow directions. The reason for these discrepancies are not known, however, due to the difference inflow direction compared to the other cases a probably cause is that some terrain effect influence turbulence in the field data.

5.2.2.1 Meandering. The meandering of the wake deficit is an important parameter for wake modelling. The work of Madsen *et al.*[33] showed that it is critical driver for some component loads and power production of turbines operating in waked conditions. On the basis of the conclusions of Larsen *et al.*,[34] the meandering could also serve as a good indication of the development of the large-scale turbulent fluctuations in wake, which are hard to capture by looking at the turbulent energy spectra because there are few realizations of the large scales in the simulations.

The wake meandering in horizontal and vertical direction is depicted as the standard deviation of the wake centre in Figure 14. The wake meandering of the AL model (solid lines) exhibits three documented features:

(1) The wake meandering is proportional to the ambient turbulence intensity as proposed by España *et al.*[28]
(2) The wake meandering in lateral direction is larger than in vertical direction. This is attributed to the larger amount of energy in lateral direction (see Figure 8). This is in agreement with the findings of Larsen *et al.*[34] and España *et al.*[28] where it is proposed that the meandering is proportional to the standard deviation of the cross-flow wind speeds.

(3) The wake meandering increases approximately linearly with downstream distance as described by Crespo *et al.*[1]

Unfortunately, only a limited amount of field data is available to be used for validation of the downstream development of wake meandering. A complication when studying wake meandering in the full scale field experiments is acquiring data of sufficiently high spatial and temporal resolution to find the wake centre with reasonable accuracy. The reference data included here are from a LIDAR measurement campaign on the NM80 turbine and PIV data from the PRISME wind tunnel presented by España *et al.*[28] The LIDAR used can only collect data at distances of up to 200 m, as the rotor has a radius of 40 m; this is equivalent to 5R. The wind tunnel data consist of wake meandering measurements at distances 4, 6, 8 and 12R.

The PRISME wind tunnel measurements were carried out in a 5 m × 5 m × ×20 m test section using a rotor represented by an actuator disc with a diameter of 0.1 m. The model scale is 1:400, which means that the 0.1 m rotor disc represents a rotor diameter of 40 m. The rotor discs used for this comparison are constructed of a metallic mesh of solidities resulting in axial induction of 0.19 and 0.12. For the cases used in this comparison, the hub height was 0.35 m, the wind speed was 3.38 m/s and the turbulence intensity was 12.8%. The instantaneous wake centre position is extracted from the PIV data by finding the outer edges of the wake as the location where '$u = 0.95\,U_{amb}$'. This is achieved by collecting data in two-

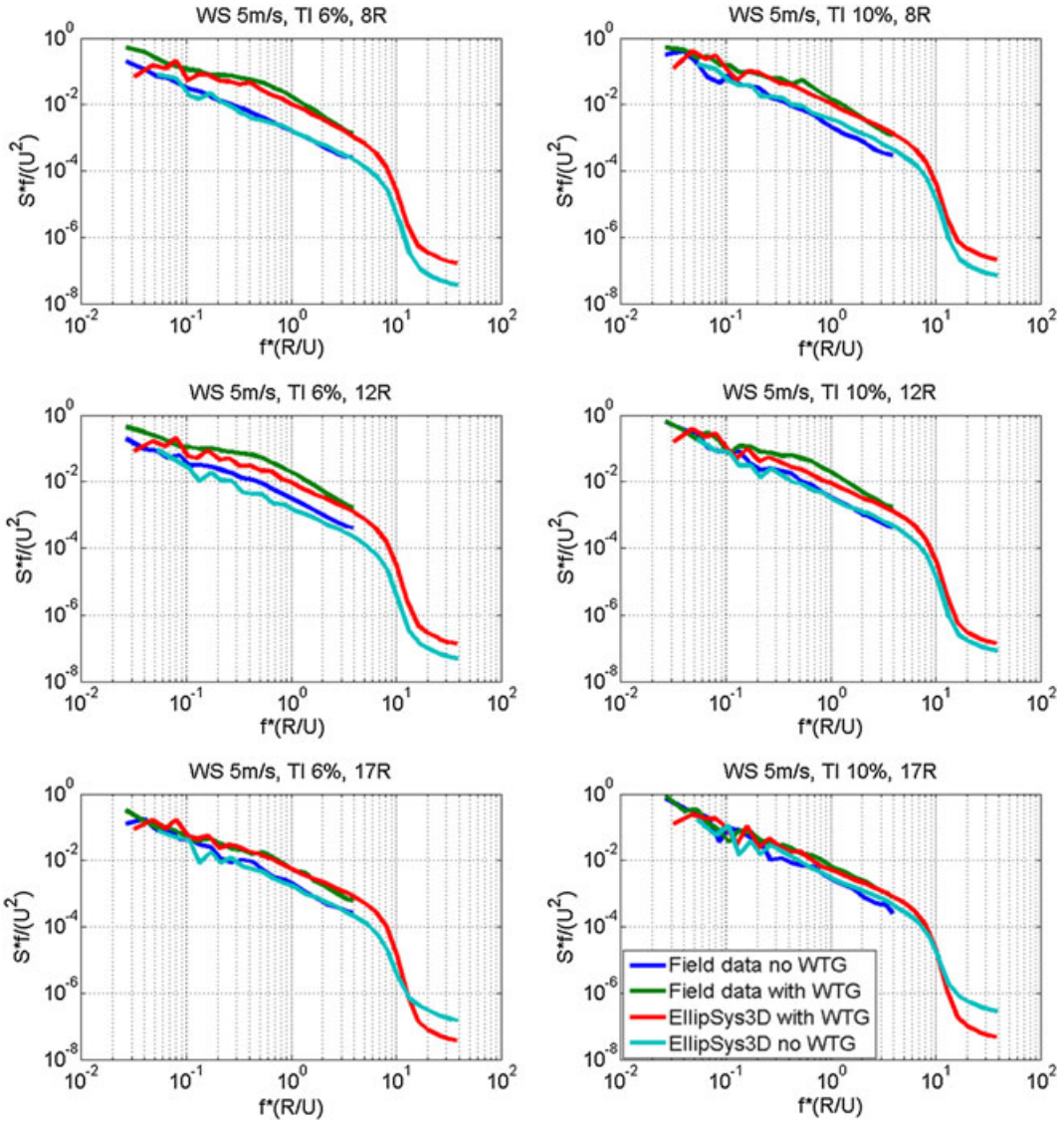

Figure 12. Comparison of turbulent energy spectra extracted from AL simulations to measurements from the Alsvik wind farm.

DOI: 10.1002/we

dimensional cut planes, *X–Y* at hub height for lateral meandering and *X–Z* for vertical meandering, and by applying a binary filter to remove all wind speeds above 95% of the free stream velocity. The wake centre is taken to be located in the middle of the left and right (or upper and lower if vertical meandering is studied) wake edges. For more details, see España *et al.*[28] As the wake meandering is driven by the large-scale fluctuations approaching the rotor, the free stream spectrum of streamwise turbulent energy in the wind tunnel is compared to that of the AL simulations before studying the meandering; see Figure 13. Overall, good agreement is seen. The discrepancies seen in the high frequencies range is due to grid effects on the LES resolved turbulence in the AL simulations. From Figure 13, it seems as if there may be a slightly more turbulent energy in the larger scale for the AL model; however, as few realizations of turbulence in these scales is achieved in the 500 s of simulations time, the comparison of the larger scales in the flow is uncertain.

The reference data sources are compared to the AL simulations in Figure 14. Overall, the LIDAR data and the vertical meandering component of the wind tunnel are in fair agreement with the AL results. The lateral component of the wind tunnel data agrees reasonably well with the AL results in the first 6R behind the rotor, but at larger downstream distances, the lateral meandering is significantly lower in the wind tunnel. The meandering is 40% lower at 8R and 50% lower at 12R. A possible explanation for the larger deviations further downstream could be the difficulty of accurately detecting the wake boundaries in the far-wake. The algorithm used to analyse the wind tunnel data is sensitive to the edges of the wake. Because the COG approach used in the AL simulations (equation (4)) weighs the distance with the depth of the wake deficit, it should be more robust towards the uncertainty of detecting the edges of the wake.

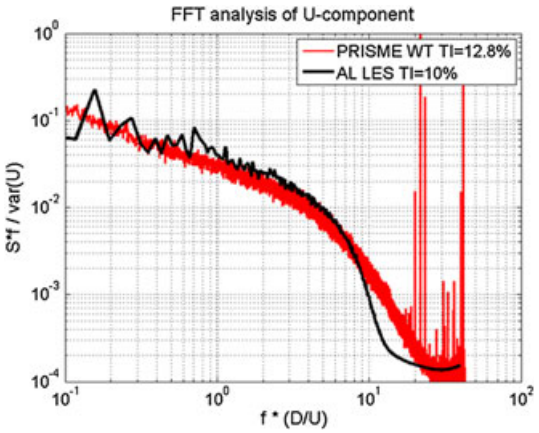

Figure 13. Comparison of the free stream turbulence spectra of the PRISME wind tunnel and the corresponding AL simulation.

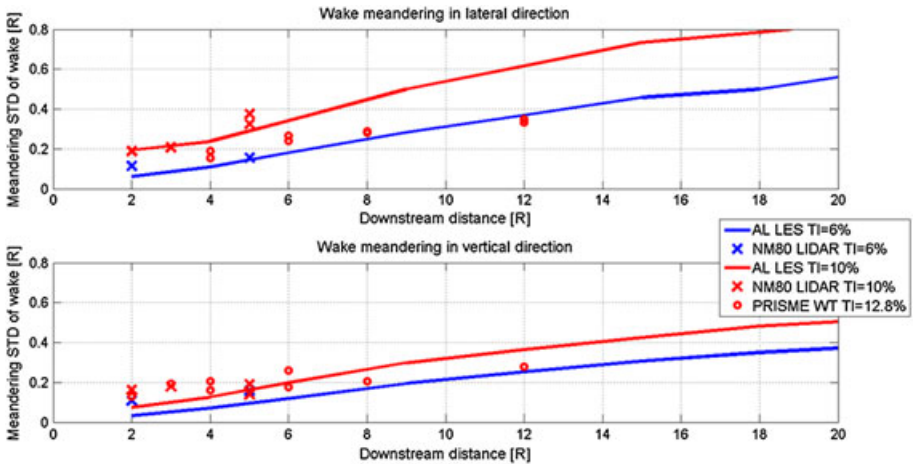

Figure 14. The magnitude of the wake meandering, defined as the standard deviation of the wake centre in vertical and lateral direction, as a function of turbulence intensity and downstream distance. The reference data come from a LIDAR campaign (X), and wind tunnel data from the PRISME wind tunnel (O).

5.2.3. Wake transport velocity

It is suggested by Larsen *et al.*[34] that the process of wake meandering can be modelled by treating the wake as a passive tracer in the atmospheric flow. Under the passive tracer assumption, the wake deficit is transported in streamwise direction by the mean velocity and translated horizontally and vertically by large-scale atmospheric turbulent fluctuations.

The hypothesis that the lateral and vertical movements of the wake centre are due to large-scale turbulent fluctuations is supported by the experimental results of España *et al.*[28] and Aubrun *et al.*[35] In their investigation, the wake meandering was studied in a wind tunnel with anisotropic large-scale turbulence and compared to the meandering observed when applying isotropic small-scale turbulence. Trujillo *et al.*[23] and Bingöl *et al.*[24] also showed that the meandering of the wake deficit was closely correlated to the incoming large-scale fluctuations by using a backwards facing LIDAR mounted on top of the nacelle of a wind turbine.

The second hypothesis of the passive tracer assumption, related to the transport velocity of the wake, has not been verified to the same extent. Bingöl *et al.*[24] applied a wake transport velocity based the Jensen model (Jensen *et al.*[36]) to correlate the large-scale movements in the wake to the wind direction changes of a meteorological mast upstream of the turbine. In this work, the wake transport velocity will be investigated by studying time series of the wake centre position at two downstream sampling planes; see Figure 15. By shifting one of the time series by a varying time offset, it is possible to obtain the time offset that yields the maximum correlation; see Figure 16. This time offset corresponds to the transport time between the sampling planes. To refine the estimate of the transport time between two successive sampling planes, a second-order polynomial is fitted to the three points closest to the highest correlation. The maximum point of the

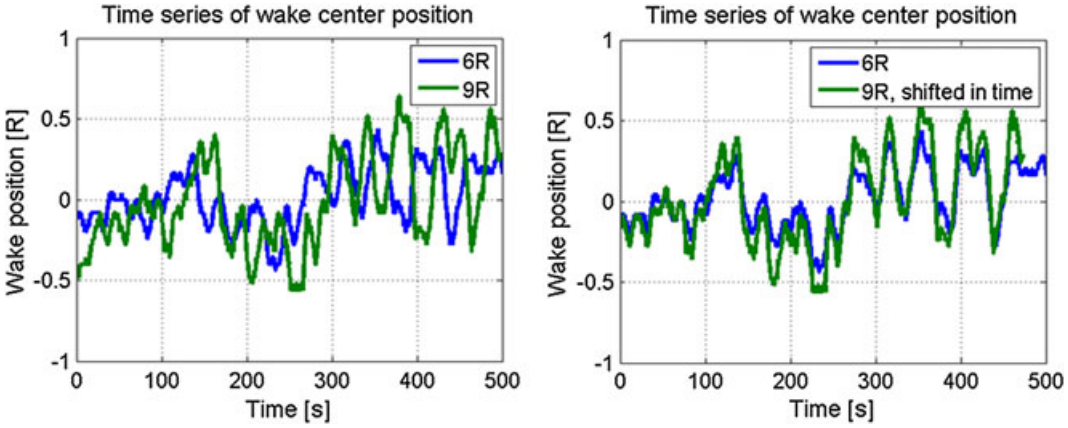

Figure 15. The left figure shows the centre position of the wake deficit as a function of time at two sampling planes. The right figure shows the same time series of wake centre position but including a time offset to find the best correlation between the time series.

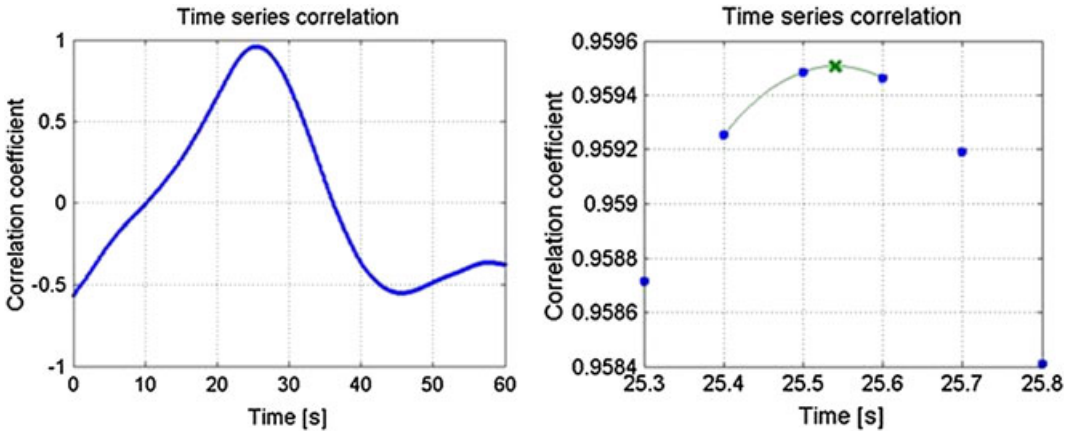

Figure 16. The left figure shows a typical correlation graph between two time signals of the wake centre position at two different sampling planes. The right figure shows the application of the second-order polynomial to estimate the wake transport time with higher resolution than the data sampling frequency. The maximum of that polynomial (X) was selected to represent the wake transport time.

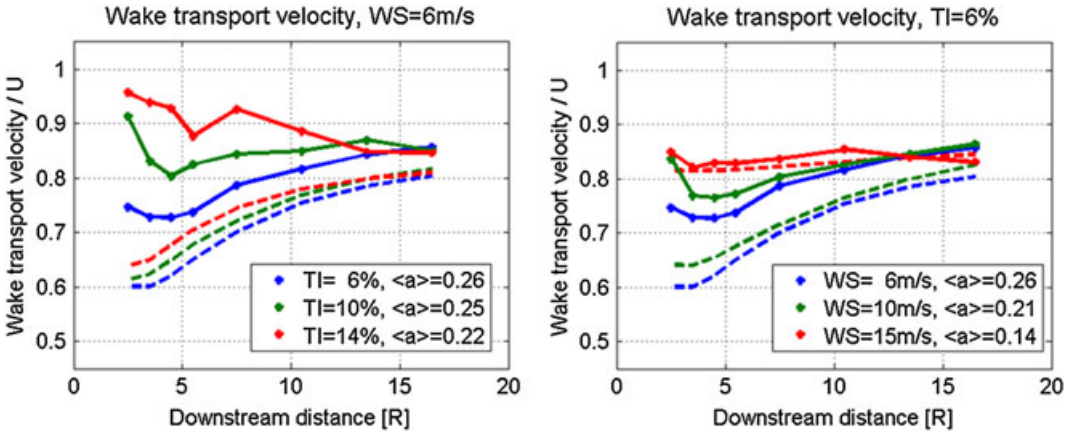

Figure 17. The wake transport velocities (solid lines) and the mean velocity of the wake deficit (dashed lines) are depicted as a function of downstream position. The left figure shows the effect of different ambient wind speed (or rotor induction) at 6% turbulence intensity, and the right figure shows the influence of turbulence intensity at 6 m/s wind speed.

polynomial curve is taken to be the transport time of the wake. The wake transport velocity is found by dividing the distance between the sampling planes with transport time.

The wake transport velocity is calculated as a function of downstream distance by applying the method described above; see Figure 17. To reduce the uncertainty in the analysis, the data presented are the average transport velocity based on the vertical and the horizontal meandering of the wake centre position. This result in an uncertainty of the normalized velocity of approximately 0.02, 0.05 and 0.10 for cases of 6, 10 and 14% turbulence intensity, respectively. Figure 17 also contains the mean velocity of the wake deficit (dashed lines) as a reference to the transport velocity of the wake. This mean velocity is averaged over a wake area given by the BEM assumption of double induction in the far-wake (Hansen[21]); see equation (12), where a was calculated as the mean induction in the rotor plane.

$$A = \frac{1-a}{1-2a}\pi R^2 \tag{12}$$

It is clear from Figure 17 that the wake transport velocity is higher than mean wake velocity but lower than the ambient wind speed.

5.2.4. Conclusions

A general study of the methods applied in EllipSys3D to efficiently model the effect of atmospheric wind shear and turbulence in LES flow field simulations has been conducted. Specifically, the ability to generate and maintain stable realistic turbulence in an empty domain and the capability to accurately model turbulence development in wind turbine wake simulations have been the key focus of the study. The investigations are carried out in neutral stratification and flat terrain. The objective is both to verify the performance of the body force methods and to generate a set of guidelines for future users of the model.

First, a set of simulations was carried out over an empty domain where the effect of the turbulence amplification factor and the applied vertical wind shear on downstream turbulence development was tested. The conclusions of that study was that the body force methods, using synthetic Mann turbulence as input, are capable of generating turbulence, which is maintained at equilibrium with the applied wind shear in EllipSys3D. In agreement with the findings of Gilling and Sørensen[15] and Troldborg *et al.*,[5] the turbulent fluctuations close to the turbulence plane were found to be underestimated. This reason for the lower turbulence levels close to the turbulence plane is that the smaller scales contain too little energy due to interpolation, smearing of the applied forces and grid effects. The energy level in these scales is corrected automatically in the flow solver by the turbulent energy cascade as the flow evolves with downstream distance. With a turbulence amplification factor of 1.15, the distance required for the small scales to recover is minimized. As a consequence of the energy cascade, the spectral distribution of turbulence will be controlled by the flow solver and the computational grid. The turbulence in the CFD simulations will therefore not maintain the spectral distribution of the imposed turbulence.

Further, as seen in a preliminary study by Keck *et al.*[37] and Troldborg *et al.*,[5] the atmospheric shear applied in the simulation was found to be an important parameter for the development of the imposed turbulence. In neutral stratification, the atmospheric shear alone dictates the equilibrium between turbulent stresses and the mean flow field. To achieve the

desired turbulence level in the simulation, it is important to apply the correct wind shear. A power-law shear coefficient equal to the desired turbulence intensity should be applied, e.g. $\alpha = 0.10$ for a target turbulence intensity of 10%

Because it is desirable to have a turbulence field that is approximately fully developed at the rotor, attention has been given to the downstream distance where equilibrium between the turbulence and the imposed shear gradient is reached. With the suggested parameter setting above, the turbulence intensity and spectral distribution approach a fully developed state about 150 computational cells after the turbulence plane.

A second study was conducted to verify the body force methods for simulations with a turbine included. This also serves as a verification of the suggested turbulence parameter settings for wind turbine wake simulations. Considering the uncertainty due to the fact that the field data comes from turbines of different size, that the range of ambient conditions is used and that the AL results are based on a simulation time of 500 s, the overall agreement between the AL model and the field data is good. The trend of the average turbulence intensity is captured well in all cases, as well as the mean difference in wake turbulence intensity between the field data and the AL model in the order of 1 percentage point. Also, the spectral distribution of turbulence energy agrees well between the AL model and the dataset from the Alsvik site. The wake meandering from the AL model agrees with the limited data available, but more validation data are required to draw firm conclusions about the accuracy of the amount of meandering.

Finally, an investigation of the wake transport velocity was conducted on the basis of the AL model data. The results show that the 'transport velocity of the wake', used to model wake meandering in lower-order models, is lower than the free stream velocity. Instead, the appropriate value lies somewhere between the mean velocity of the wake deficit and the free stream velocity.

On the basis of this study, it is concluded that the body force method can be used to simulate wake turbulence development in flat terrain and neutral conditions. The suggested values for the atmospheric shear, turbulence amplification factor and placement of the turbulence plane relative to the rotor are also valid for cases where a wind turbine rotor is included.

REFERENCES

1. Crespo A, Hernández J, Frandsen S. Survey of modelling methods for wind turbine wakes and wind farms. *Wind Energy* 1999; **2**: 1–24.
2. Porté-Agel F, Wu Y-T, Lu H, Conzemius RJ. Large-eddy simulation of atmospheric boundary layer flow through wind turbines and wind farms. *Journal of Wind Engineering and Industrial Aerodynamics* 2011; **99**: 154–168.
3. Mikkelsen R. Actuator disc methods applied to wind turbines, MEK-FM-PHD 2003–02, Technical University of Denmark, 2003.
4. Troldborg N. Actuator line modeling of wind turbine wakes, MEK-FM-PHD 2008–06, Technical University of Denmark, 2008.
5. Troldborg N, Sørensen JN, Mikkelsen RD, Sørensen NN. A simple atmospheric boundary layer model applied to large eddy simulations of wind turbine wakes. Manuscript submitted to the *Wind Energy*, 2013. doi: 10.1002/we.1608
6. Jimenez A, Crespo A, Migoya E, Garcia J. Advances in large-eddy simulations of a wind turbine wake. *Journal of Physics Conference Series* 2007; **75**: 012041; The science of making torque from wind.
7. Ivanell S. Numerical computations of wind turbine wakes. PHD Thesis, 2009–01, Royal Institute of Technology, Stockholm, Sweden, 2009.
8. Churchfield MJ, Lee S, Michalakes J, Moriarty PJ. A numerical study of the effects of atmospheric and wake turbulence on wind turbine dynamics. *Journal of Turbulence* 2012; **13**: N14. doi:10.1080/14685248.2012.668191.
9. Churchfield MJ, Lee S, Moriarty PJ, Martinez LA, Leonardi S, Vijayakumar G, Brasseur JG. A large-eddy simulation of wind-plant aerodynamics, AIAA paper 2012–537. *50th AIAA Aerospace Sciences Meeting*, Nashville, TN, Jan. 2012.
10. Lee S, Clifton A, Moriarty P. Wind turbine wakes and turbulence under various atmospheric boundary layers. Manuscript submitted to *Computer and Fluids*.
11. Réthoré P-E, Wind turbine wake in atmospheric turbulence. PhD th., DEC Thesis No. 22, AAlborg University, 2009.
12. Sørensen JN, Shen WZ. Numerical modeling of wind turbine wakes. *Journal of Fluids Engineering*; **124**: 393–399.
13. Mikkelsen R, Sørensen JN, Troldborg N. Prescribed wind shear modelling combined with the actuator line technique. *Proceedings of the 2007 EWEC conference*, Milan, 2007.
14. Troldborg N, Sørensen JN, Mikkelsen R, Actuator line simulation of wake of wind turbine operating in turbulent inflow. *Journal of Physics Conference Series* 2007; The Science of Making Torque from Wind. Technical University of Denmark, Lyngby, July 2007. IOP Publishing **75**(1): 012063.
15. Gilling L, Sørensen NN. Imposing resolved turbulence in CFD simulations. *Wind Energy* 2011; **14**: 661–676.

16. Mann J. The spatial structure of neutral atmospheric surface-layer turbulence. *Journal of Fluid Mechanics* 1994; **273**: 141–168.
17. Mann J. Wind field simulation. *Probabilistic Engineering Mechanics* 1998; **13**: 269–282.
18. Taylor GI. The spectrum of turbulence. Proceedings of the Royal Society of London. *Series A-Mathematical and Physical Sciences* 1938; **14**(919): 476–476.
19. Sørensen NN. *General purpose flow solver applied to flow over hills*, (Doctoral dissertation, Technical University of Denmark Danmarks Tekniske Universitet, Risø National Laboratory for Sustainable Energy Risø National laboratoriet for Bæredygtig Energi, Wind Energy Division Afdelingen for Vindenergi, Aeroelastic Design Aeroelastisk Design) Ph.D. Thesis, 1995; 2002: 393–399.
20. Øye S. Fix dynamisk, aeroelastisk beregning af vindmøllevinge, AFM Report 83–08, Department of Fluid Mechanics, The Technical University of Denmark, 1983.
21. Hansen MOL. *Aerodynamics of Wind Turbines*. Earthscan Publications Ltd: Oxford, United Kingdom, 2001.
22. Larsen GC, Hansen KS, Troldborg N, Mann J, Enevoldsen K. A first attempt to characterize the structure of the wake turbulence using a combined experimental and numerical approach. *Conference on Turbulence IV, 2010*, Bertinoro (IT), 19–22 Sep. 2010.
23. Trujillo JJ, Bingöl F, Larsen GC, Mann J, Kühn M. Light detection and ranging measurements of wake dynamics, Part II: two-dimensional scanning. *Wind Energy* 2011; **14**: 61–75.
24. Bingöl F, Mann J, Larsen GC. Light detection and ranging measurements of wake dynamics, Part I: one-dimensional scanning. *Wind Energy* 2010; **13**: 51–61.
25. Cavar D. Large eddy simulation of industrially relevant flows, MEK-FM-PHD, 2006–02, Technical University of Denmark, 2006.
26. Versteeg HK, Malalasekera W. *An Introduction to Computational Fluid Dynamics—The Finite Volume Method* (2nd edn), 2007; Longman Scientific and Technical: New York.
27. Keck RE, Veldkamp D, Madsen HAa, Larsen GC. Implementation of a mixing length turbulence formulation into the dynamic wake meandering model. *Journal of Solar Energy Engineering* 2011; **134**: 021012.
28. España G, Aubrun S, Loyer S, Devinant P. Spatial study of the wake meandering using modelled wind turbines in a wind tunnel. *Wind Energy* 2011; **14**: 923–937.
29. Vännman K, Dunkels A. *Matematisk statistik*. Studentlitteratur, 2002.
30. Djerft E, Mattson H. Evaluation of the software program WindFarm and comparisons with measured data from Alsvik. Technical Report TN 2000–30, FFA, Bromma, Sweden, 2000.
31. Larsen GC. TOPFARM—next generation design tool for optimization of wind farm topology and operation … background, vision and challenges. *The Science of Making Torque from Wind*, FORTH, Heraklion, Crete, Greece, June 28–30, 2010.
32. Taylor GJ. Wake measurements on the Nibe wind turbines in Denmark. National Power, ESTU WN 5020, United Kingdom, 1990.
33. Madsen HAa, Larsen GC, Larsen TJ, Troldborg N, Mikkelsen R. Calibration and validation of the dynamic wake meandering model implemented in the aeroelastic code HAWC2. *Journal of Solar Energy Engineering* 2010; **132**: 041014.
34. Larsen GC, Madsen HAa, Thomsen K, Larsen TJ. Wake meandering—a pragmatic approach. *Wind Energy* 2008; **11**: 377–395.
35. Aubrun S, España G, Devinant P. Physical modelling of the far-wake from wind turbines. Application to wind turbines interactions. *European Wind Energy Conference*, Milan, Italy, 7–10 May 2007.
36. Jensen NO. A note on wind generator interaction. Risø M 2411, November 1983.
37. Keck R-E, Mikkelsen R, Troldborg N. Investigation of prescribed wind shear and synthetic atmospheric turbulence for rotor wake simulations. *Proceedings Gotland wake conference*, 2011.

II: Implementation of a Mixing Length Turbulence Formulation into the Dynamic Wake Meandering Model

Rolf-Erik Keck[1]
Rotor Systems,
Vestas Wind Systems A/S,
DK-4000 Roskilde, Denmark;
Wind Energy Department,
Risø DTU National Laboratory for Sustainable Energy,
DK-4000 Roskilde, Denmark
e-mail: roeke@vestas.com

Dick Veldkamp
Rotor Systems,
Vestas Wind Systems A/S,
DK-4000 Roskilde, Denmark

Helge Aagaard Madsen

Gunner Larsen

Wind Energy Department,
Risø DTU National Laboratory for Sustainable Energy,
DK-4000 Roskilde, Denmark

Implementation of a Mixing Length Turbulence Formulation Into the Dynamic Wake Meandering Model

The work presented in this paper focuses on improving the description of wake evolution due to turbulent mixing in the dynamic wake meandering (DWM) model. From wake investigations performed with high-fidelity actuator line simulations carried out in ELLIPSYS3D*, it is seen that the current DWM description, where the eddy viscosity is assumed to be constant in each cross-section of the wake, is insufficient. Instead, a two-dimensional eddy viscosity formulation is proposed to model the shear layer generated turbulence in the wake, based on the classical mixing length model. The performance of the modified DWM model is verified by comparing the mean wake velocity distribution with a set of* ELLIPSYS3D *actuator line calculations. The standard error (defined as the standard deviation of the difference between the mean velocity field of the DWM and the actuator line model), in the wake region extending from 3 to 12 diameters behind the rotor, is reduced by 27% by using the new eddy viscosity formulation.* [DOI: 10.1115/1.4006038]

Introduction

The DWM model is a low fidelity physical wake model continuously developed at Risø DTU since 2003 (see Madsen et al. [1] and Larsen et al. [2]). The idea behind the model is to capture the key features of the wake with regard to wind turbine loads and power production, while maintaining sufficient computational speed for design calculations. Based on field observations, the wake deficit development and the meandering, or large scale turbulent movements, of the wake deficit were identified as being the most important factors for the wind turbine loads. An important observation is the different characteristics and effects of the large scale movements of the wake deficit on the wind turbines as compared to small scale turbulence. This implies that the modeling of turbulence as one number alone, as in the Frandsen model [3], cannot accurately describe the effects of wake operations on a wind turbine. The following example illustrates the importance of turbulent scales.

Consider a turbine that operates in the wake of a neighboring turbine. If two wind fields with similar wind speed and turbulence intensity, but with different characteristic turbulent length scales, were to hit the turbines, the loads would be different. Let us assume that the first wind field has a smaller characteristic length scale, i.e., it has more turbulent kinetic energy in the smaller scales and less in the large scales. Such a wind field would result in a diffusive wake, where the wake deficit recovery is fast, and the large scale movements of the wake are small. The second wind field, with high energy content in the larger scales, displays the opposite wake deficit development. The low amount of small scale energy leads to a stable wake due to the low level of diffusive turbulent mixing, and the energy in the large scales manifests itself as large scale movements of the entire wake.

It is intuitively clear that the loads of these two simplified cases will be different from each other. In the first case, loads due to the wake will be driven mainly by the increased turbulence level of the oncoming air, as in the Frandsen model. In the second case, wake loads are driven by the random movements of a wake deficit with large velocity gradients over the swept rotor disc area. Rather than a general increase of turbulence level, this resembles a series of "extreme" scenarios where parts of the rotor are operating in wake affected inflow conditions with considerably lower wind speeds, while the rest of the rotor sees the unaffected free stream velocity. This example highlights the most important assumption of the DWM model—the split in turbulence scales. Larsen et al. [2] gives a thorough description of the method used to model the meandering in the DWM. A "cut-off eddy size" between small scale turbulence, affecting the wake development, and large scale turbulence, governing the meandering of the whole wake deficit, was assumed at two rotor diameters. The meandering approach is validated by full-scale measurements from the Tellus rotor (see Bingöl et al. [4] and Trujillo et al. [5]). The wake movements were measured by a LIDAR unit mounted on top of the nacelle, which allowed for investigations in the nacelle frame of reference.

The wake deficit model included in the DWM model is heavily influenced by the classical wake model proposed by Ainslie [6,7]. Ainslie uses a thin shear layer approximation of the Navier– Stokes (N–S) equations where turbulent closure was obtained by including a simple eddy viscosity formulation to model the wake flow behind a wind turbine. Madsen et al. [8] identified the need for a physical wake model for detailed investigations of loads on wind turbines, which led to the development of the first version of the DWM model. Further iterations on the model have been conducted in many steps by various authors over the last few years. An overview of the development and the validation efforts can be found in the work by Larsen et al. [9,10]. Two major improvements relevant to this article were implemented by Madsen et al. [11], with the inclusion of rotor added turbulence into the model, and Madsen et al. [12], where the model is implemented in aero-elastic code HAWC2 and validated against actuator disc and line models as well as full-scale data from the Tjæreborg and Tellus experimental campaigns.

The focus of this article is to investigate the description of turbulence in the wake deficit module of the DWM model, i.e., the small scale turbulence. As mentioned above, many investigations have been carried out to improve the DWM model, but so far the description of turbulent eddy viscosity presented by Ainslie in

[1]Corresponding author.

Contributed by the Solar Energy Division of ASME for publication in the JOURNAL OF SOLAR ENERGY ENGINEERING. Manuscript received May 30, 2011; final manuscript received February 6, 2012; published online March 15, 2012. Assoc. Editor: Spyros Voutsinas.

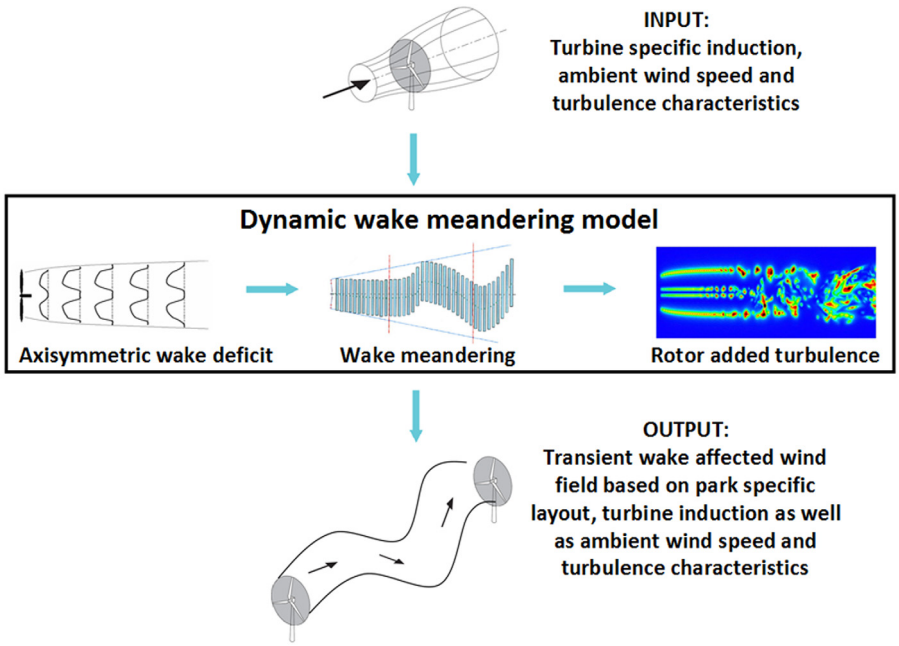

Fig. 1 A high level calculation sequence of the DWM model including required input and delivered output

1986 has not been critically considered. The hypothesis behind this article is that the improved ability to investigate the distribution of turbulence behind the rotor via high-fidelity computational fluid dynamic (CFD) models will give new insight as to how a realistic and inexpensive turbulence model can be formulated. The approach taken is to first investigate the distribution of turbulence in the wake by using ELLIPSYS3D actuator line simulations, described later. The second step is to formulate a reasonable turbulence model based on the results from the actuator line model. The turbulence model needs to be consistent with the purpose of the DWM formulation, i.e., the requirements are that it should be compatible with the boundary condition of the blade element momentum (BEM) theory, and maintain high computational speed for design calculations. Finally, a least-square calibration of the modified DWM model coefficients to actuator line results is performed, as well as a benchmark against the original model.

Current Version of the DWM Model

The current form of the dynamic meandering wake model, as described in Ref. [1], consists of three submodules governing the wake deficit development, the meandering process, and the rotor added turbulence (see Fig. 1). The high level calculation sequence can be described as follows:

(1) The wake deficit development is calculated based on the two-dimensional axisymmetric thin shear layer approximation of the steady Reynolds averaged Navier–Stokes (RANS) equations. Turbulent closure is obtained by using an eddy viscosity formulation that is assumed to be constant in radial direction, and thus dependent only on the downstream position in the wake.
(2) The meandering process is modeled as random displacements of the wake deficit by large scale turbulent fluctuations (with characteristic dimensions of two rotor diameters or larger) perpendicular to the flow direction. The fluctuations are commonly based on low-pass filtered Mann turbulence [13,14], but could also be based on field measurements obtained at a specific turbine site, or on other turbulence models if so desired. In the wake meandering process, it is assumed that the wake deficit development remains unaffected by the meandering and that no axial mixing takes place.
(3) Rotor added turbulence is included to incorporate the effect of added turbulence due to tip, root, and bound vortices as well as shear layer generated turbulence in the wake. It is calculated based on a homogeneous Mann turbulence box in the meandering frame of reference, i.e., the center of the turbulence box is always located in the center of the wake deficit. As a crude approximation, the in-homogeneity of the rotor added turbulence is obtained by scaling the local turbulence based on the depth and the velocity gradient of the wake deficit. The rotor added turbulence is neither assumed to influence the wake deficit development nor the meandering process. Hence, it only affects the flow field experienced at the downstream rotor.

As the current investigation does not require the reader to have a deeper knowledge of all DWM modules, only module 1 will be described in further detail in this chapter. Readers interested in more details regarding modules 2 and 3 are referred to the work by Larsen et al. [3] and Madsen et al. [11].

Wake Deficit Model in DWM. The wake deficit development in the DWM is governed by the steady, axisymmetric thin shear layer approximation of the RANS equations. The main simplifications, as compared to solving the full set of N–S equations, are the absence of a pressure term and the reduction of the momentum equation. This is possible due to the simplification of two-dimensional flows and the assumption that gradients in the flow direction can be neglected as they are much smaller than the gradients in the radial direction. This reduces the computational effort as no pressure–velocity coupling is needed and only one momentum equation needs to be solved (see Eq. (1)). Physically, the consequence of omitting the pressure influence on the wake development is that regions with large pressure gradients, i.e., the near wake, will not be modeled realistically. Accordingly, the DWM should only be considered to give accurate results after the pressure gradients have become small. This can be thought of as at any downstream position after maximum wake induction has occurred. According to Sanderse [15], the maximum velocity

deficits, and thereby the full wake expansion due to the pressure field, are found roughly two diameters behind the rotor.

Turbulence closure is obtained by using a turbulent eddy viscosity formulation which consists of two parts: ambient turbulence and turbulence induced by the shear layer (see Eq. (3)). Both terms in Eq. (3) have the same general form, i.e., a filter function, a model constant, and a term of the governing physical mean flow property. The model coefficients, k, are universal, i.e., they do not change with ambient condition or turbine model. The filter functions F are needed to account for the development of turbulence behind the rotor. The classical eddy viscosity concept is based on the assumption of fully developed turbulence, where the turbulent stresses can be found by looking at the quantities of the mean flow alone. This is not a good approximation in the case of a wind turbine, since wind turbine alters the mean flow properties abruptly and creates large mean flow gradients at the rotor. The turbulence on the other hand, needs a relatively long distance in order to develop to a level where it is in equilibrium with the new mean flow conditions. In the current DWM version, the filter functions are factors between 0 and 1, based on axial position. The idea is that F_2 should counter balance the nonequilibrium between the amount of turbulent kinetic energy and the mean flow properties. F_1 is included to model the delay of significant wake diffusion due to entrainment of the wake.

Thin shear layer momentum equation

$$u\frac{\partial u}{\partial x}+v\frac{\partial u}{\partial r}=\frac{\upsilon_T}{r}\frac{\partial}{\partial r}\left(r\frac{\partial u}{\partial r}\right) \tag{1}$$

The continuity equation for axisymmetric flow

$$\frac{1}{r}\frac{\partial}{\partial r}(rv)+\frac{\partial u}{\partial x}=0 \tag{2}$$

Turbulent eddy viscosity equation

$$\upsilon_T=F_1k_1TI_{\text{amb}}+F_2k_2\frac{b}{R}\left(1-\frac{U_{\min}}{U_{\text{amb}}}\right) \tag{3}$$

Implementation of the Standard DWM Model. The velocity deficit module of the DWM model as described above has been implemented in MATLAB with the purpose of being used as the baseline for the model development. For the implementation, the momentum equation, Eq. (1), is discretized using a second order central difference scheme in radial direction and a first order upwind scheme in flow direction. The selected upwind scheme is sufficient to give good accuracy in the calculations, as very small grid cells can be used without this resulting in long computational time. Thus, grid independence in the solutions is easily achieved. The thin layer approximation of the N-S is a parabolic system, which considerably eases the solving process. A consequence of information only going along the flow direction is that a solution can be obtained by "marching" in the flow direction. For each location along the flow direction, the calculation sequence can be summarized as:

(1) Solve the momentum equation for the streamwise velocity component at all radial positions explicitly, by using the value of the radial velocity component and the eddy viscosity from the previous location upstream. This yields a tridiagonal equation system where all the coefficients are known, which can easily be solved by any tridiagonal matrix algorithm.
(2) Once the streamwise velocity is known, the radial velocity for all radial positions can be updated using the continuity equation, Eq. (2).
(3) The eddy viscosity for all radial positions is updated using Eq. (3) above.
(4) March to the next downstream location and repeat steps 1–3.

The numerical implementation of the DWM deficit module used in this study is not identical to that used by Madsen et al. [1]. Two main modifications are made to the numerical algorithm:

(1) The method for updating the radial velocity component used by Madsen et al. [1] is based on an upwind scheme for all streamwise derivatives. In the present implementation, an alternative central difference scheme is applied to the streamwise derivative when solving Eq. (2) to find the radial velocity component. This improves mass conservation in the solution. The upwind scheme increases the total mass flow by 2.75% over the first 20 rotor diameters of flow, whereas the same test applied to the central difference scheme yields a reduced increase of 1.20%.
(2) The second difference is the treatment of mean flow gradients when calculating the fluxes. In Madsen et al. [1], a five point average filter is applied to the first and second order derivatives when calculating the convective and diffusive fluxes. This is included to ensure numerical stability in the solution. For the present implementation, no such filter is required.

The boundary conditions used for the wake deficit calculations are based on the axisymmetric axial rotor induction of the specific turbine model. This makes the DWM directly compatible with BEM based aero-elastic tools. However, since the pressure term is omitted in the governing equation, the effect of pressure expansion and deceleration of the fluid needs to be taken into account at the boundary. For the standard DWM deficit model, the boundary conditions proposed by Madsen et al. [1] are used. The set of boundary conditions are based on the assumption of full wake induction *at the rotor plane*, i.e., changing the axial velocity to $U_0(1-2a)$, where a denotes the axial induction factor. The pressure driven expansion of the wake deficit is also applied at the rotor plane, and is calculated based on mass conservation of the air volume in each circular BEM element. Since the velocity at the rotor is lower under the assumption of full induction, the wake expands radially. This approach to calculate the boundary condition is consistent with the original BEM assumptions of no radial flow, which results in mass conservation within circular elements, and the idea of full induction $(1-2a)$ as the lowest velocity in the wake. The inlet boundary condition for the radial velocity component is zero radial velocity, which again is consistent with the BEM assumption of independent radial stations. The center of the wake is treated by a symmetry condition, and no velocity gradients (or second derivatives) are used as the boundary conditions as the radius goes to infinity. Finally, no boundary condition is needed for the outlet boundary, as information only moves in the streamwise direction in the model.

For the remainder of this work, the implementation described above will be referred to as the "standard DWM deficit model," which will serve as a baseline for the development of the new turbulent closure description.

The ELLIPSYS3D Actuator Line Model

The ELLIPSYS3D [16] actuator line is a high-fidelity CFD tool used to investigate the flow field and loads of a wind turbine operating in realistic ambient conditions. The model was first put forward by Sørensen and Shen [17] and later implemented into the in-house flow solver ELLIPSYS3D by Mikkelsen [18]. The actuator line model is an aero-elastic, three-dimensional computational model that combines the full set of large eddy simulation (LES) filtered N–S equations with a volume force representation of the wind turbine blades. The volume forces are calculated based on tabulated values of C_L and C_D data and the local flow field at the blades. The main benefit of introducing the effect of the wind turbine blades as a source term in the N–S equations, instead of modeling the real physical boundaries, is that the mesh requirements go down drastically, as the boundary layer does not need to be resolved in order to accurately calculate the forces. The grid

studies performed indicate that resolutions of 25 points for a 40 meter rotor radius yield a far wake that may be considered to be grid independent. The ability to use relatively coarse meshes reduces computational time both directly, since few grid points are solved for, and indirectly, since larger time steps can be used without violating the Courant– Friedrichs–Lewy condition. Compared with solving a fully physical representation of the wind turbine, the actuator line model is at least 1 order of magnitude faster.

The forces exerted on the flow field by the rotor, and consequently the turbine loads, are calculated by using FLEX5 (see Øye [19]). FLEX5 is a state of the art BEM code based on the mode shapes approach. Both the blades and the tower can have as many modes as desired. At every time step, blade, damping, and stiffness matrices are recalculated, which amounts to making the code nonlinear. The FLEX5 model includes the normal engineering corrections applied to BEM: Prandtl tip correction, dynamic wake model and stall, oblique inflow, and meandering wake models. A description of these models can be found in Hansen [20]. The aero-elastic calculation is based on a two-way coupling between ELLIPSYS3D and FLEX5, and can be described as:

- LES calculations in ELLIPSYS3D are used to calculate the flow field in the domain
- the flow field at the position of the actuator lines is extracted and passed to FLEX5
- FLEX5 recalculates the velocity information to local velocity and angle of attack related to the actuator lines
- the local forces (in the airfoil section coordinate system) are found based on the local inflow angle, the pitch and twist of the blade, and tabulated values of C_L and C_D (the dynamic stall model is applied if needed)
- the forces are used to recalculate the deformation of the wind turbine structure and the actuator line positions
- the forces are passed back to ELLIPSYS3D, transformed into the global CFD coordinate system based on the local inflow angle to the airfoil section and applied as a source term in the momentum equation

The model also includes atmospheric turbulence by introducing a mean shear and prescribed turbulent velocity fluctuations close to the rotor. These are also generated by volume force techniques in order to save computational effort.

- Atmospheric shear is included by distributed volume forces in the entire domain. The method to find these forces is to run a presimulation without actuator lines and to find the magnitude of the distributed forces that yields the desired wind shear through an iterative method. For more details, see Mikkelsen et al. [21].
- Atmospheric turbulence on top of the mean shear is included by introducing fluctuating forces in a X–Y plane (Z denotes the flow direction) located a few radii upstream of the turbine (for this work 3.5R was used). The imported turbulence is generated with a Mann turbulence generator. The reason why turbulent fluctuations are introduced near the rotor as opposed to at the inlet boundary is to reduce the mesh requirements. Mesh refinements are thus only required close to the rotor without significant turbulent dissipation in the simulation. For more details, see Troldborg et al. [22].

The ability of these methods to realistically model the atmospheric conditions and maintain the generated turbulence in the wake region, both in magnitude and in spectral distribution, was verified by Keck et al. [23]. Another investigation was carried out by Larsen et al. [24], where the wake predictions of the actuator line model were restricted to only use information from the same measurement points as a field measurement conducted with LIDAR equipment. Both methods used the same postprocessing. The idea was that this would lead to an "apples-to-apples" comparison. The result of the study shows that the actuator line captures both the velocity deficit and the turbulence distribution in the wake very well. Even with the simplified representation of the blades and the computationally low-cost representation of the atmospheric turbulence, the actuator line model is still a high-fidelity model with desirable capabilities for wake studies. More information about the actuator line model and some examples of wake examinations can be found in Mikkelsen [18], Troldborg [25], and Ivanell [26].

Wake Investigations With Actuator Line Simulations. The approach taken to find an improved turbulence formulation in DWM is to first observe the physics of the wake, and then try to develop an adequate model capable of capturing the key properties. This requires a high quality set of data, gathered while controlling the most important properties of the inflow. For this investigation, the ambient wind speed and turbulence level have been the foci. Since it is hard to conduct full-scale measurements of the turbulence properties in the wake of a wind turbine with sufficient resolution in time and space and to control the inflow parameters, a set of ELLIPSYS3D actuator line calculations were conducted to generate a database to support the development of an improved turbulence model in the DWM. Throughout the investigation, the same numerical settings and computational grid were maintained, apart from the wind speeds and the turbulence intensity. These were varied in order to test their influence on the wake turbulence distribution and the wake recovery. Wind speeds at levels 5 m/s, 10 m/s, and 15 m/s, and turbulence intensity levels of 0%, 6%, and 14% were tested. The investigations were carried out on a fully flexible representation of a NM80 80 m diameter rotor.

Numerical Setup. The ELLIPSYS3D actuator line calculations are based on LES filtered N–S equations where the larger eddies in the flow are resolved directly without any turbulence model. Eddies smaller than the grid size, also called subgrid scales or SGS, are treated by an eddy viscosity model. The eddy viscosity treatment of the smaller eddies is justified by the higher level of isotropy, which allows for a universal treatment of the turbulent energy in this part of the energy spectra. The universal treatment of small scales is only valid if the cell size is sufficiently small to resolve scales well into the inertial subrange. This condition was tested and fulfilled for all the simulations performed in the work (see Fig. 2). The dynamics and dissipation of the small eddy scales are modeled by the mixed scale model for SGS eddy viscosity described in Cavar [27]. The model parameters were selected according to the recommendations in the numerical sensitivity study performed by Troldborg [25]. The force regularization parameter, □, which governs the width of the force distribution in the calculation domain, was given the value of two mesh elements. The appropriate time step is found by the restriction that the actuator line should not pass through an entire element in one time step. This is much more restrictive than the requirement that the Courant-Friedrichs-Lewy (CFL) number should be lower than unity, since the wind speed is much smaller than the tip velocity

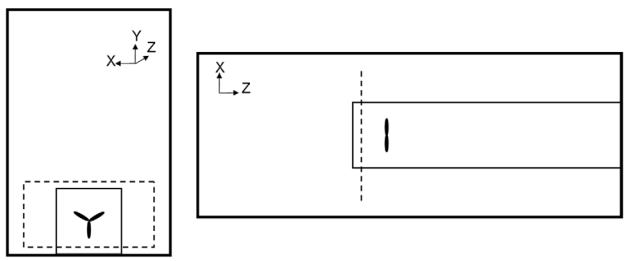

Fig. 2 Sketch of the computational domain. The left figure is an X–Y plane showing the cross-section of the domain, and the right figure is an X–Z plane showing the domain from above. The outer solid box represents the computational domain. The rotor location is indicated by the solid black body. The dashed line/box indicates where the turbulent fluctuations are applied, and the solid box shows the refined region.

of the blade. For the NM80 turbine and the mesh used, this requirement yields a time step equivalent to 175 time steps per revolution. The convective terms are discretized using a hybrid scheme consisting of a 10% third order accurate Quadratic Upwind Interpolation for Convective Kinematics (QUICK) scheme and, a 90% fourth order accurate central difference scheme (CDS). The motivation for using a hybrid scheme is that the low numerical diffusion of the CDS is desired, but using the CDS alone is found to cause numerical instability, or wiggles, in the solution. By combining the CDS and the QUICK schemes these errors are avoided. Pressure–velocity coupling is obtained by using the SIMPLE algorithm. The PISO algorithm was also considered by Troldborg, since it is commonly used with unsteady flows, but it was concluded that SIMPLE gives the same result as PISO does for CFL numbers associated with the actuator line simulation, while using less computational time.

The calculations were carried out on a Cartesian grid in a rectangular domain of $10 \times 30 \times 52R$, in width, height, and flow direction, respectively (see Fig. 2). A refined mesh region was constructed to minimize numerical dissipation in the wake region. This refinement covered the domain from $3–7 \times 0–4 \times 15–52R$. The mesh in the refined region consists of square mesh elements corresponding to 25 cells per turbine radius resolution stretched 10% in flow direction, i.e., for a 40 m rotor radius the element size is $1.6 \times 1.6 \times 1.76$ m. Outside of the refined region, the elements are stretched towards the domain boundaries. In total, the mesh consists of 162 blocks of $48 \times 48 \times 48$ cells, yielding a total mesh count of $\sim 18 \times 10^6$ cells.

The only wind turbine component considered in the simulation is the rotor. The center of the rotor was located at 5, 2, and 19*R*. Flat ground is assumed in all simulations, and an atmospheric shear profile, corresponding to a power law profile of shear exponent of $\alpha = 0.15$, was used. The shear was generated with the approach proposed by Mikkelsen et al. [21]. Atmospheric turbulence was included by a turbulence plane ranging from 1–9, 0.4–4.4, and 15.5*R*, according to the method proposed by Troldborg et al. [22]. An investigation made by Keck et al. [23], conducted after this project, reached the conclusion that the shear level should be set to a value corresponding to the desired turbulence intensity (i.e., $\alpha = \mathrm{TI}$), and that the turbulence plane should be located at least 6*R* in front of the turbine. The justifications for these settings are, first, that the turbulence will strive towards an equilibrium turbulence level dictated by the shear conditions (if atmospheric stability effects are neglected), and, second, that the imported Mann turbulence was found to contain less turbulent energy in the smaller scales. However, it was concluded that as the flow develops with downstream advection in the ELLIPSYS3D model, the spectral distribution is corrected by the energy cascade. Both these processes reach stable conditions over a transport distance of 6*R*. Thus, the settings used in this work will lead to slightly lower turbulence intensity in the near wake, and, for the 6% case, the relatively high shear will cause higher turbulence intensity in the far wake. The turbulence intensity in the simulations, without any rotor influence, was obtained based on simulations performed in an empty domain and using the same computational mesh and input turbulence (see Table 1).

Table 1 Free stream turbulence level in the simulations as a function of downstream distance from the rotor position

Distance	6% turbulence case	14% turbulence case
0*D*	5.79	12.27
3*D*	6.71	13.17
6*D*	7.25	12.66
9*D*	7.34	12.29
12*D*	7.48	12.06

Mesh Sensitivity Study. As mentioned, the selected domain size and adopted model settings (the CDS-QUICK hybrid discretization scheme, the SIMPLE algorithm for pressure–velocity coupling, a force distribution parameter equal to two elements and a simulation time step limited by tip-speed ratio and mesh element size) are based on the numerical sensitivity study performed by Troldborg [25]. It was decided, however, that an additional mesh sensitivity study should be performed to investigate the solution dependency on size and resolution of the refined mesh region. The wind speed and turbulence intensity of the case chosen for the investigation were 5 m/s and 6%, respectively. The case was selected due to it being critical in the sense of having a very high level of rotor induction. Furthermore, some turbulence was desired to evaluate the dissipation of the numerical grid, but not so much as to overshadow the investigated parameters. Four levels of mesh resolution were tested: 14, 25, 38, and 51 points per radius. Two sizes of mesh refined regions were tested with a resolution of 25 points per radius, one with a cross-section of 2×2 rotor diameters and another with a cross-section of 3×3 rotor diameters. The mesh performance was evaluated based on its ability to capture the correct induction of the rotor, on the integrated axial momentum deficit and on turbulence distribution in the wake as well as on its influence on the turbulence spectrum and the meandering of the wake.

Conclusions from the mesh sensitivity study:

- For wake calculations, a resolution of 25 points per rotor radius captures the integrated linear momentum deficit and wake turbulence of the generated wake (see Figs. 3 and 4). To capture the sharp gradients of the induction near the tip region, a resolution of 38 points per radius was required (see Fig. 3). It should be noted that no tip correction was used in the mesh sensitivity study. This could have had an influence on the grid resolution needed to capture the correct tip loads.
- All tested resolutions were fine enough to capture the –5/3 slope in the energy spectrum associated with the inertial subrange. The assumption of isotropic turbulence in the SGS can therefore be considered fulfilled (see Fig. 5). The cutoff between resolved and unresolved scales changes with grid resolution as expected.
- Resolution has no significant effect on the meandering process.
- Increasing the size of the refined region to a cross-section of 3×3, instead of 2×2 turbine diameters, increased meandering of the wake center in the order of 2–3% in the near wake and 10–11% in the far wake. Another effect was that more energy was present in the small scales of the turbulent spectra (see Fig. 6). A plausible explanation could be that the wake in the simulation, which has a smaller refined wake region, leaves the refined region more often. The shear layer would then be drained of small scale turbulent energy that is transferred to the SGS and dissipated.

For the current study, a mesh resolution of 25 points per rotor radius in the refined region was concluded to give sufficient accuracy in the calculations. The effects of increasing the resolved domain were not considered to be important enough to justify the 125% increase in computational time for these calculations, but they are presented here as a reference to upcoming investigations for which wake meandering and small scale energy may be important parameters.

Eddy Viscosity Distribution in Actuator Line Data

As mentioned, the current eddy viscosity formulation in the DWM takes into account the ambient turbulence and the turbulence generated by the wake shear layer. Both terms, however, are described in such a way that the eddy viscosity can only vary in the flow direction. This results in a one-dimensional eddy viscosity expression that is uniform in radial direction. To evaluate if

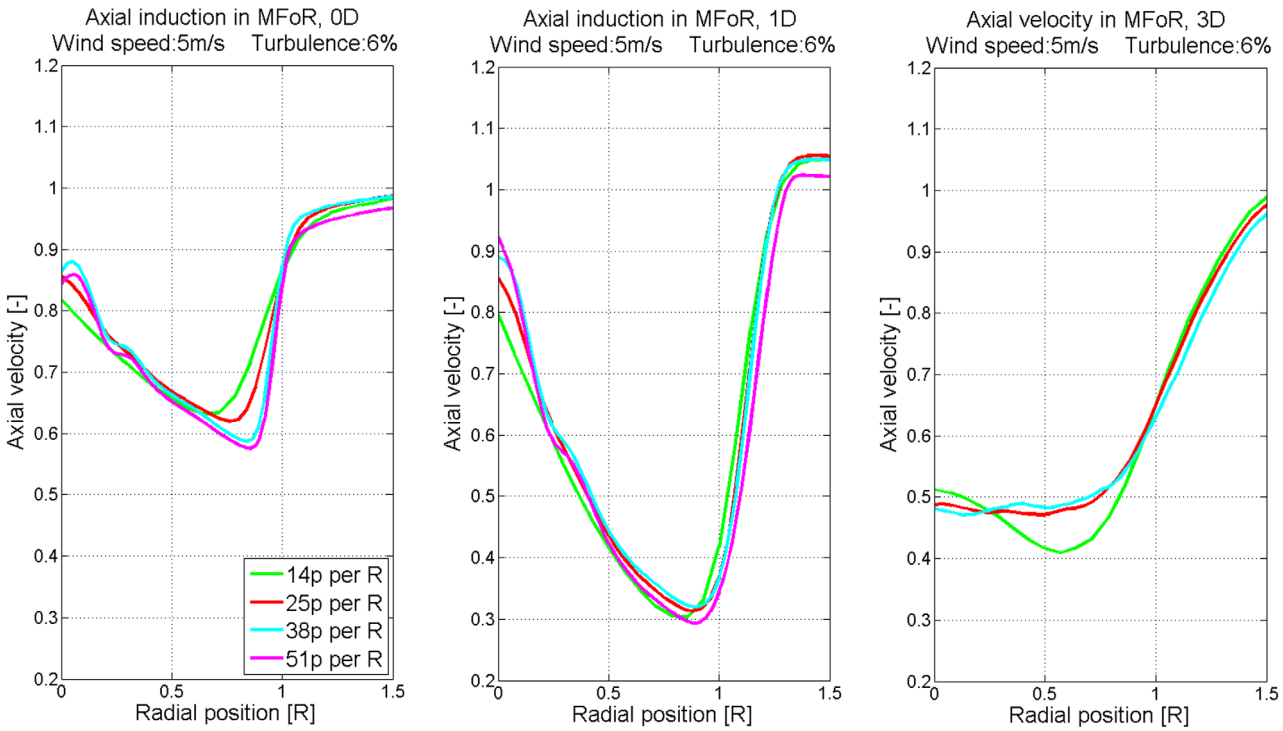

Fig. 3 The development of axial velocity in four different actuator line resolutions: 14, 25, 38, and 51 points per radii (p per *R*). The left figure is at the rotor plane, the middle figure is at 1*D*, and the right figure is at 3*D* downstream of the turbine. The 51 p per *R* case is missing at 3*D* as the computational domain used was too short to extract data so far downstream.

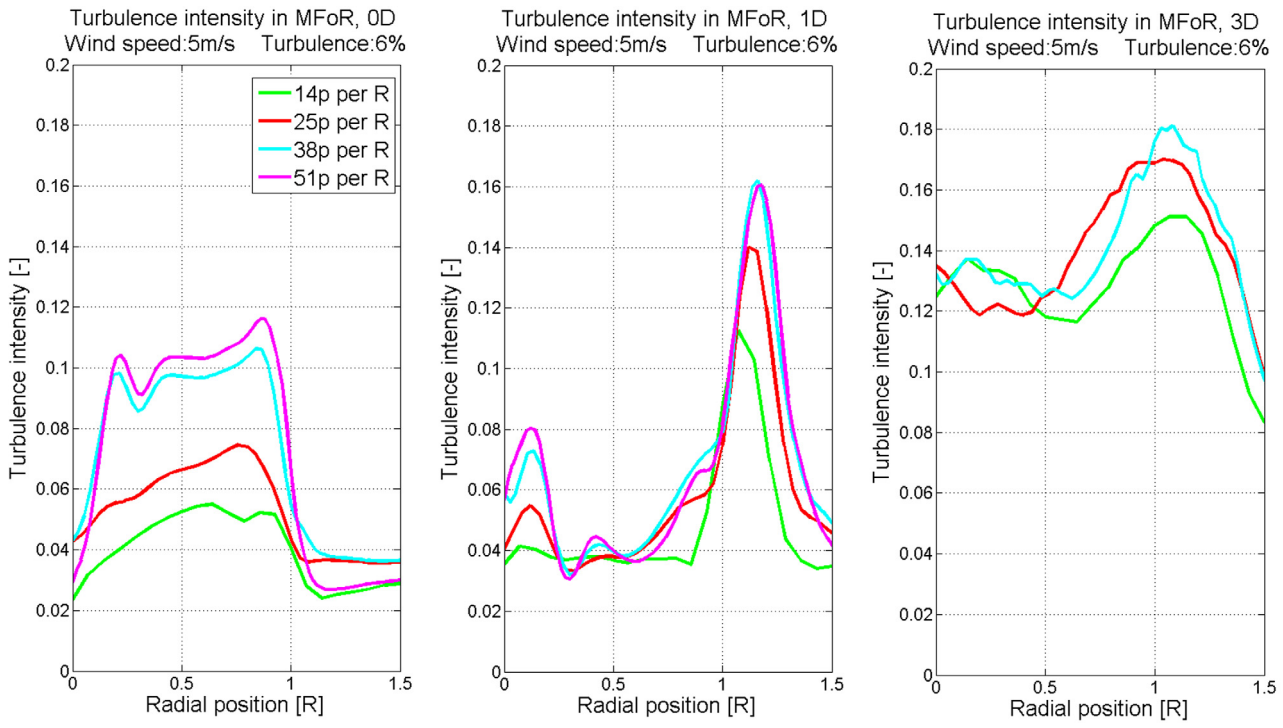

Fig. 4 The development of wake turbulence intensity in four different actuator line resolutions: 14, 25, 38, and 51 points per radii (p per *R*). The left figure is at the rotor plane, the middle figure is at 1*D*, and the right figure is at 3*D* downstream of the turbine. The 51 p per *R* case is missing at 3*D* as the computational domain used was too short to extract data so far downstream.

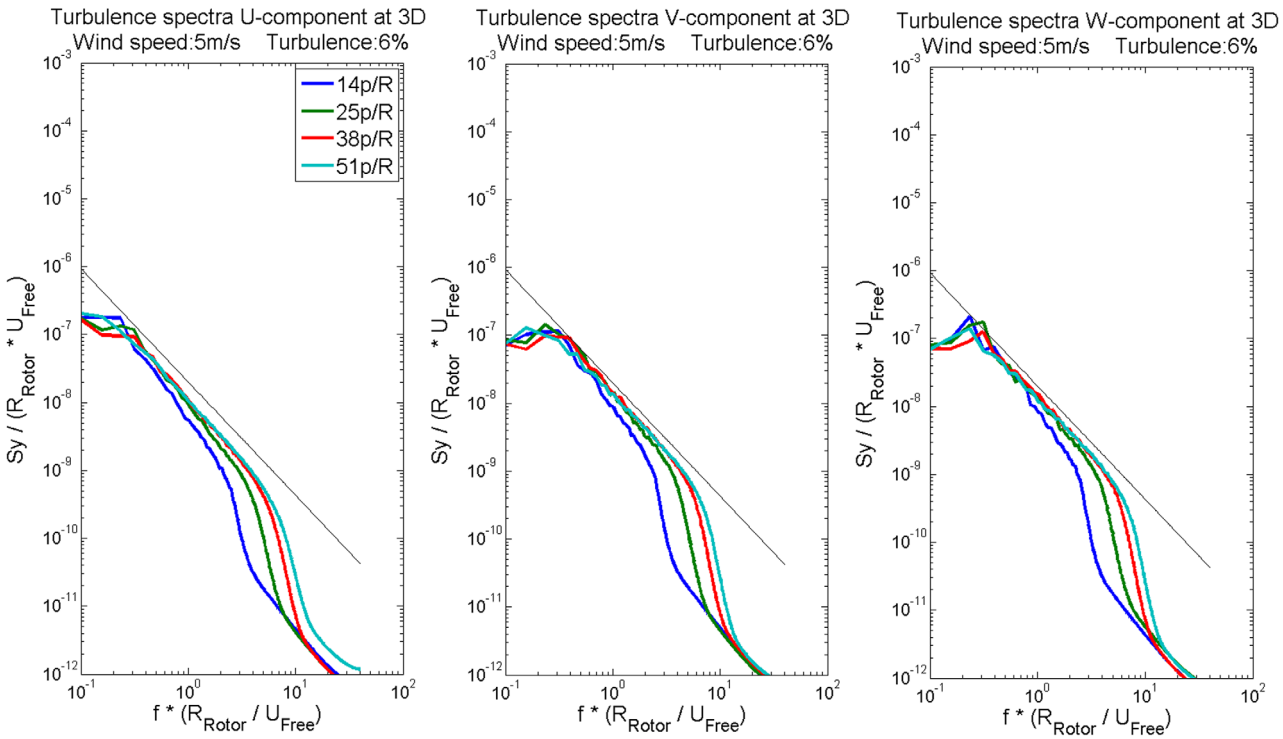

Fig. 5 The development of turbulent energy spectra in four different grid resolutions in the wake region: 14, 25, 38, and 51 points per radii (p per *R*). The figure shows the energy spectra in streamwise, vertical, and horizontal directions (left, middle, and right figure, respectively).

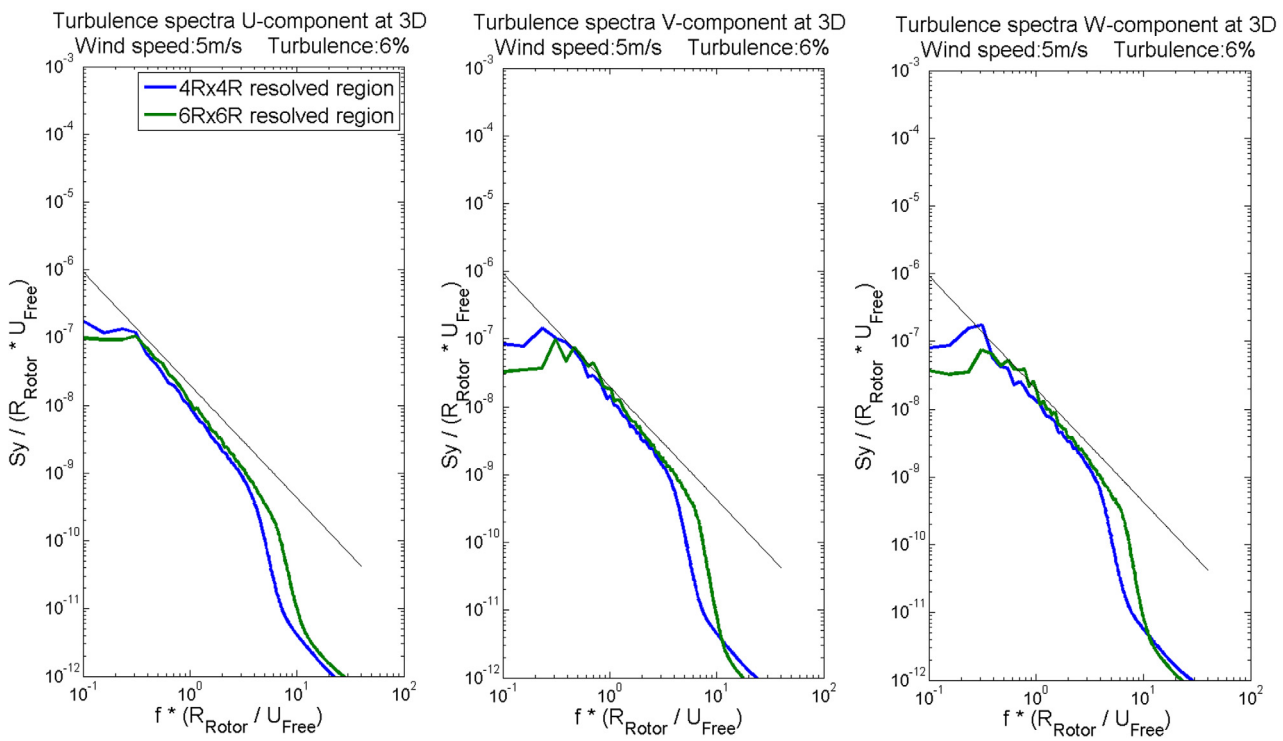

Fig. 6 The development of turbulent energy spectra in two sizes of the wake refined region in the actuator line resolutions: 4 × 4 and 6 × 6 radius. The figure shows the energy spectra in streamwise, vertical, and horizontal direction (left, middle, and right figure, respectively).

this formulation is adequate, the turbulence eddy viscosity distribution in the actuator line calculations will be approximated based on the resulting velocity field and turbulent kinetic energy. Two different methods have been used to approximate the (RANS) eddy viscosity from the LES simulations. The first method is based on the Johnson–King equations (see Menter [28]), and the second method uses a tabulated estimate for the characteristic length scale of the wake, thus enabling an eddy viscosity approximation directly by the eddy viscosity definition (see Eq. (8)). Both approaches are based on the turbulent kinetic energy content of the flow given by Eq. (4)

$$k = 0.5\left(\overline{u_1'^2} + \overline{u_2'^2} + \overline{u_3'^2}\right) \tag{4}$$

The Johnson–King model is evaluated here, since it is especially developed for regions of flow with adverse pressure gradients where the production of turbulent kinetic energy is much larger than the dissipation. Traditionally, it is used to limit eddy viscosity in the shear–stress transport (SST) model in regions of separation; it is not traditionally used for free shear layer flows (here, the SST model used the k-ε model instead). Since both of these conditions are fulfilled in the initial part of the wake, before the pressure has recovered and the turbulence has reached equilibrium with the mean flow, it proves to be an interesting turbulence model for wake flow close to the rotor. The Johnson–King model gives a direct approximation of the turbulent stresses (see Eq. (5))

$$\tau_{\text{Stress}} = \rho \cdot a_i \cdot k \tag{5}$$

The constant a_i is a model constant equal to 0.30. In a two-dimensional flow, the turbulent eddy viscosity, ν_T, is given by dividing the turbulent stresses by the mean flow gradient (see Eq. (6))

$$\nu_T = \frac{\tau_{\text{Stress}}}{du/dr} \tag{6}$$

Combining Eqs. (5) and (6) thus yields the approximation of eddy viscosity by the Johnson–King model

$$\nu_{T,J-K} = \frac{\rho \cdot a_i \cdot k}{du/dr} \tag{7}$$

The second approach is based on the standard definition of the eddy viscosity (see Eq. (8)). The characteristic velocity scale is given by Eq. (9), where k is known from Eq. (4). Versteeg and Malalasekera [29] give a reference value for the characteristic length scales in wakes as per Eq. (10)

$$\nu_T = l^* \cdot u^* \tag{8}$$

$$u^* = k^{1/2} \tag{9}$$

$$l^* = 0.16R \tag{10}$$

Combining Eqs. (8)–(10) gives a second approximation of the turbulent eddy viscosity (see Eq. (11))

$$\nu_{T,V\,M} = 0.16R \cdot k^{1/2} \tag{11}$$

The eddy viscosity of the actuator line model has been evaluated based on Eqs. (7) and (11) (see Fig. 7). Something worth noting in the two approximations is that Eq. (7) (plotted to the left) is linearly dependent on turbulent kinetic energy, whereas Eq. (11) (right set of figures) is proportional to the square root. The difference stems from the fact that the Johnson–King model assumes that the turbulent stresses are directly proportional to the realized turbulence level, while the normal eddy viscosity approach assumes that the turbulent stresses are based on the local ratio of turbulence production and dissipation. Both models predict a similar shape of the turbulence distribution in the wake, apart from the near wake where the Johnson–King model yields a lower eddy viscosity. The absolute level of turbulence seems to be consistently larger for the standard eddy viscosity formulations. This offset could be attributed to the use of a "rule-of-thumb" turbulent length scale, which of course has a large uncertainty when used in a specific application. The absolute level, however, is not of great importance in this investigation, as the focus lies on the regime before reaching a radially uniform eddy viscosity distribution. The downstream distance required for the eddy viscosity to reach a distribution that is independent of the radial coordinate is dependent on the ambient turbulence. For 0%, 6%, and 14% ambient turbulence intensities, wake transport distances of 15, 9, and 6D, respectively, are necessary, before a one-dimensional eddy viscosity is sufficient to describe the eddy viscosity in the wake. It is therefore concluded that an improved turbulence model for the DWM is indeed required.

Development of a Mixing Length Model in DWM

The fundamental idea of using an eddy viscosity formulation to simulate the turbulence in the DWM model is well motivated in our application. First, a computationally inexpensive turbulence model is essential, since the industry requires a fast tool that can be used in aero-elastic calculations of design loads. Second, the flow problem at hand is documented as a flow for which the use of a mixing length model to calculate the eddy viscosity is a good approach (see Versteeg and Malalasekera [29]). It is also reasonable to follow Ainslie's approach in dividing the eddy viscosity contributions that stem from fundamentally different sources, in this case the ambient turbulence and the wake shear layer generated turbulence, as it is natural to assume that they require different treatments. The filter functions need to be kept in order to balance the initial nonequilibrium between the mean flow and the turbulence. In the present study, the filter functions as developed by Madsen et al. [1] are left unchanged. Furthermore, the assumption made by Ainslie that the free stream turbulence affects the whole cross-section of the wake in a similar way is kept. This assumption can be interpreted as the turbulent velocity and length scales associated with the ambient turbulence being invariant across the wake, which means that the eddy viscosity contribution due to ambient turbulence intensity can be seen as constant for a given cross-section.

Hence, the second part of the eddy viscosity caused by the shear layer is the focus for improvement. A natural first approach to develop this formulation is to use a multiple turbulent velocity scale description in the wake. The Ainslie eddy viscosity model is a simple version of the mixing length model, where it is assumed that only one characteristic turbulent length and velocity scale exists at any given downstream distance in the wake, i.e., $l^* = f(x)$ and $u^* = f(x)$. While this assumption reduces the computational demand slightly, it limits the performance in regions with high mean flow gradients. The motivation for Ainslie's choice to use a single velocity scale is based on the fact that Gaussian velocity profiles were used as initial condition in the original wake development model. Since the current DWM uses BEM induction as the input velocity field, multiple velocity scales are required to capture the turbulence distribution in the turbine wake before the flow has reached a state of smooth mean flow gradients. According to Sanderse [15], the downstream distance required before the wake reaches a Gaussian shape can be in the order of 5 diameters depending on rotor induction and ambient conditions.

According to the classical formulation of the mixing length model, the most common approximation is that the local turbulent velocity scale is based on the local strain rate and the turbulent length scale (see Pope [30]). In the DWM model, the local strain rate is equal to the local velocity gradient du/dr. If we keep the assumption of one characteristic length scale for each cross-section of the wake, the turbulent velocity scale distribution is given by Eq. (12)

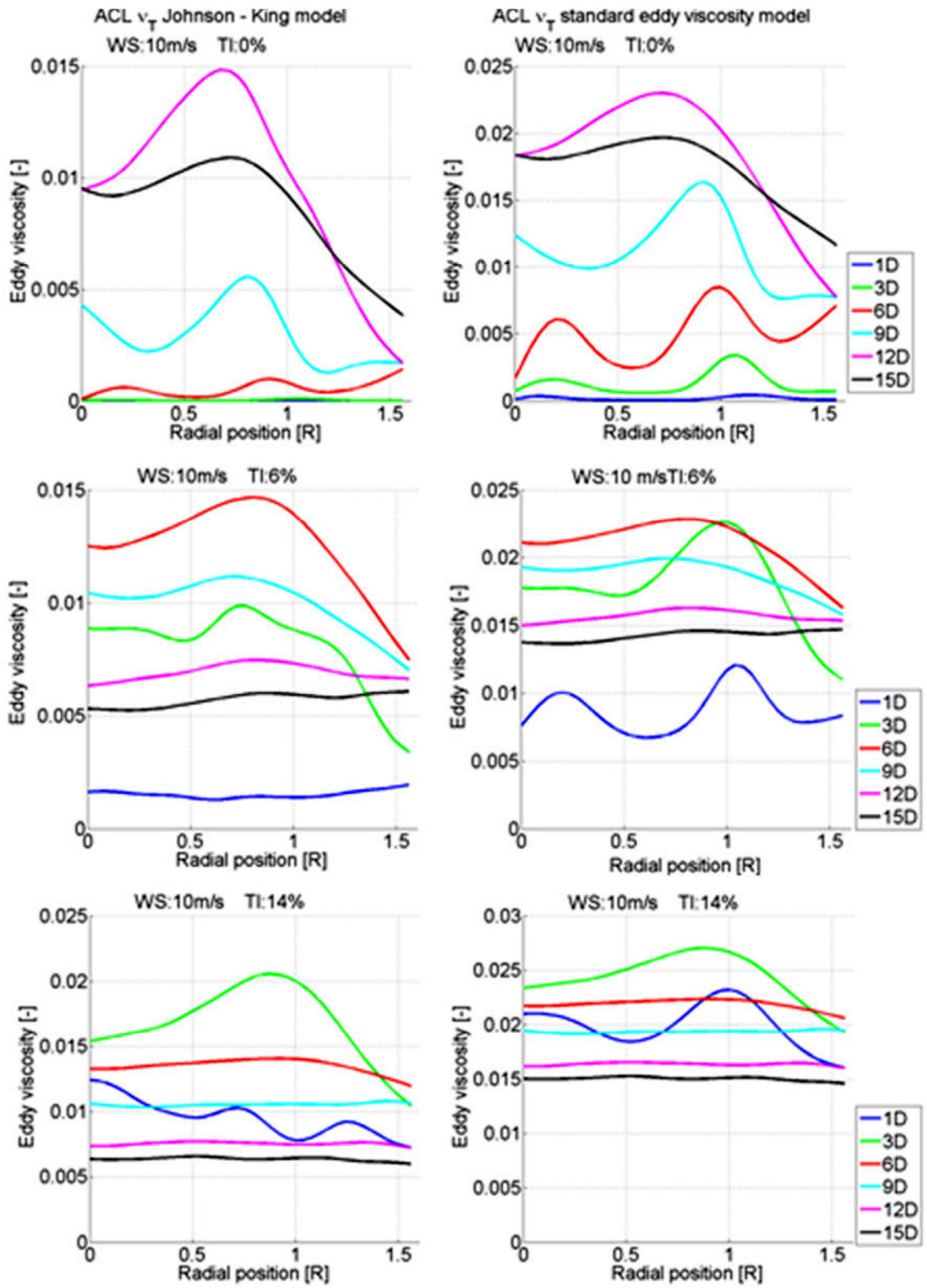

Fig. 7 The development of axisymmetric eddy viscosity from a set of actuator line simulations of an NM80 Turbine. The eddy viscosity is extracted from the turbulent kinetic energy balance ("k") in the simulations based on two different models, the Johnson–King model (left column, Eq. (7)) and the standard eddy viscosity model (right column, Eq. (11)). Radial eddy viscosity profiles are extracted 1, 3, 6, 9, 12, and 15*D* downstream of the rotor, and inflow conditions are wind speed of 10 m/s and ambient turbulence intensity of 0%, 6%, and 14% (top, middle, and bottom row).

$$u^* = l^* \cdot \left|\frac{\partial u}{\partial r}\right| \tag{12}$$

The turbulent length scale l^* in the DWM model is assumed to be equal to half the width of the wake. It is defined as the distance from the center of the wake to the radial position where the axial velocity is 95% of the free stream velocity. The resulting eddy viscosity that governs the shear generated turbulence is thus found by combining Eqs. (12) and (8), which results in Eq. (13)

$$\nu_{T,\text{Shear}} = l^{*2}\left|\frac{\partial u}{\partial r}\right| \tag{13}$$

Using Eq. (13) to replace the second half of the RHS of Eq. (3), while keeping the model coefficient k_2 and the filter function F_2, yields the new eddy viscosity formulation (see Eq. (14))

$$\nu_T = F_1 k_{\text{amb}} TI_{\text{amb}} + F_2 k_2 l^{*2}\left|\frac{\partial u}{\partial r}\right|\left(\frac{1}{U_{\text{amb}} \cdot R}\right) \tag{14}$$

The physical parameters considered are still the ambient turbulence intensity and the shear layer of the wake deficit. The contribution to the turbulent mixing due to free stream turbulence is assumed to be uniform over the cross-section of the wake. Thus, the first term of the eddy viscosity formulation is left unchanged. As dictated by the classical mixing length model, the local velocity gradient, du/dr, and the turbulent length scale, l^*, are used to calculate turbulent mixing due to the shear layer. This leads to a two-dimensional eddy viscosity function, in which the turbulent stresses induced by the shear layer are proportional to the square of the velocity gradient.

Development of Inlet Boundary Condition. A consequence of changing the eddy viscosity formulation is that the inlet boundary condition needs to be modified. Since the turbulent stresses due to the wake shear layer in the mixing length model follows the square of the velocity gradient, a high level of turbulent mixing takes place close to the rotor if full induction is assumed at the rotor plane. If the same inlet boundary condition were applied as in the standard DWM version, this would generate a much too wide and smooth velocity field. As discussed above, the DWM model is only valid after the pressure has recovered. This means that the objective of the applied boundary condition in DWM is to yield a correct flow field after the initial two to three rotor diameters in the computational domain. Consequently, the shape and the depth of the appropriate boundary condition must be a function of rotor induction, wake recovery, and turbulent mixing inside the domain (which in turn is dependent on the turbulence model, the filter functions, and the model coefficients). Therefore, the initial deficit must be selected based on considerations of wake width and total integrated deficit desired in the wake after some reference location. In the discussion below, the inlet boundary condition is constructed so that the DWM velocity field agrees with the actuator line calculations at the cross-sections located more than three rotor diameters behind the rotor. The 3D cross-section is taken to mark the start of the computational domain, where the DWM model can be considered to be correct, and it will be referred to as the "point of DWM validity."

In the present development, the assumption of full wake induction at the rotor plane is kept. A low initial velocity is required, since the omission of the pressure term means that no sink term for the axial velocity exists in the domain. The filter functions, which could have been used to modify the initial turbulent mixing and wake recovery, were left unchanged in this study. Therefore, the only factor that is modified is the wake expansion at the rotor. The width of the wake at the rotor plane was selected to minimize the difference in integrated momentum deficit between the DWM and the actuator line model at the cross-sections located 3, 6, and 9D downstream of the rotor. The integrated momentum deficit is based on an integration of velocity deficit ($U_{amb} - U$) over a disc of 1.8R in radius, centered at the wake center. Using this approach, it turns out that no expansion at the rotor plane is required when using the proposed mixing length model, see Table 2.

The new inlet boundary condition is therefore based on full induction without prescribing any expansion of the wake at the rotor plane. The fact that less wake expansion should be included in the boundary condition for the mixing length model is intuitive when considering the difference between the two turbulence models. The expansion of the wake deficit is a function of the turbulent stresses in the shear layer. In the mixing length model, these stresses are greater compared to the standard DWM model, and therefore, a narrower deficit is required at the inlet boundary to yield the correct width at the point of DWM validity. Another consequence of the new boundary condition is a reduced integrated momentum deficit compared to the boundary condition applied in the standard DWM model. The motivation for applying a reduced deficit lies in the fact that the boundary condition is designed to yield a correct velocity field at, and after, the point of DWM validity. The recovery of the wake in the transport process, from the rotor to the location three diameters downstream, is dictated by turbulent momentum transfer (TMT) into the wake from the free stream via the shear layer. The momentum transfer is a function of shear layer area and the magnitude of the turbulent stresses at the shear layer. This explains why the choice of turbulence model strongly influences the initial recovery of the wake. Approximations of the recovery of the wake deficit due to TMT by the standard DWM and the mixing length DWM models are given by Eqs. (15) and (16), respectively

$$\mathrm{TMT}_{\mathrm{STD,DWM}} \propto 2\pi(1+\alpha_{\mathrm{wake}})R\,dx^*\left(du/dr\right) \tag{15}$$

$$\mathrm{TMT}_{\mathrm{MIXL,DWM}} \propto 2\pi R\,dx^*\left(du/dr\right)^2 \tag{16}$$

The coefficient α_{wake} represents the fraction of wake expansion included at the rotor plane used by the standard DWM model. The first terms are related to the contact area between the wake and the free stream at a cross-section of width dx close to the rotor plane. The second term represents the magnitude of the turbulent stresses, which are proportional to the mean flow gradients. It is clear that there will be significant differences in the wake recovery due to the relative development of wake width and mean flow gradients of the two models. The validity of this approach was verified by comparing the wake width and the axial velocity distribution from the DWM mixing length model with the actuator line simulations in cross-sections located, respectively, at 3, 6, 9, and 12 diameters downstream of the rotor (see Fig. 9). A study of the resulting velocity field, with and without the modified boundary condition, was conducted to quantify the effect of the modified boundary condition. It was concluded, that the new boundary condition improved the fit of the DWM mixing length model to the actuator line model according to the "standard error method," as defined in Eq. (17), by 20%.

Table 2 Comparison of dimensionless integrated momentum deficit of the DWM mixing length model, without initial wake expansion, to that of the actuator line model. The ambient condition for this case was wind speed of 10 m/s and 6% turbulence intensity. Note that no comparison is available at the inflow boundary since a significant part of the rotor induction is still in the pressure field for the actuator line model.

Downstream location	DWM mixing length	Actuator line model
0D	1.673	n/a
3D	1.386	1.580
6D	1.245	1.277
9D	1.148	1.141

Results and Discussion

The model coefficients of the standard DWM and the mixing length DWM model (containing the new eddy viscosity formulation and inlet boundary condition) were calibrated to the actuator line wake data based on the four flow cases with wind speeds of 10 m/s and 15 m/s and turbulence intensities of 6% and 14%. The performance of the DWM models was evaluated based on the average standard error. The standard error is defined as the standard deviation in mean velocity between the actuator line and the DWM models (see Eq. (17))

$$\text{Standard error} = \sqrt{\frac{1}{n_c}\sum_{c=1}^{n_c}\left[\frac{1}{n_{c,d}}\sum_{d=1}^{n_{c,d}}\left(\frac{1}{n_{c,d,r}}\sum_{r=1}^{n_{c,d,r}}\left(\bar{U}_{c,d,r}^{\mathrm{ACL}} - \bar{U}_{c,d,r}^{\mathrm{DWM}}\right)^2\right)\right]} \tag{17}$$

where the indexes c, d, and r correspond to cases (i.e., variations in inflow conditions), downstream distance and radial position,

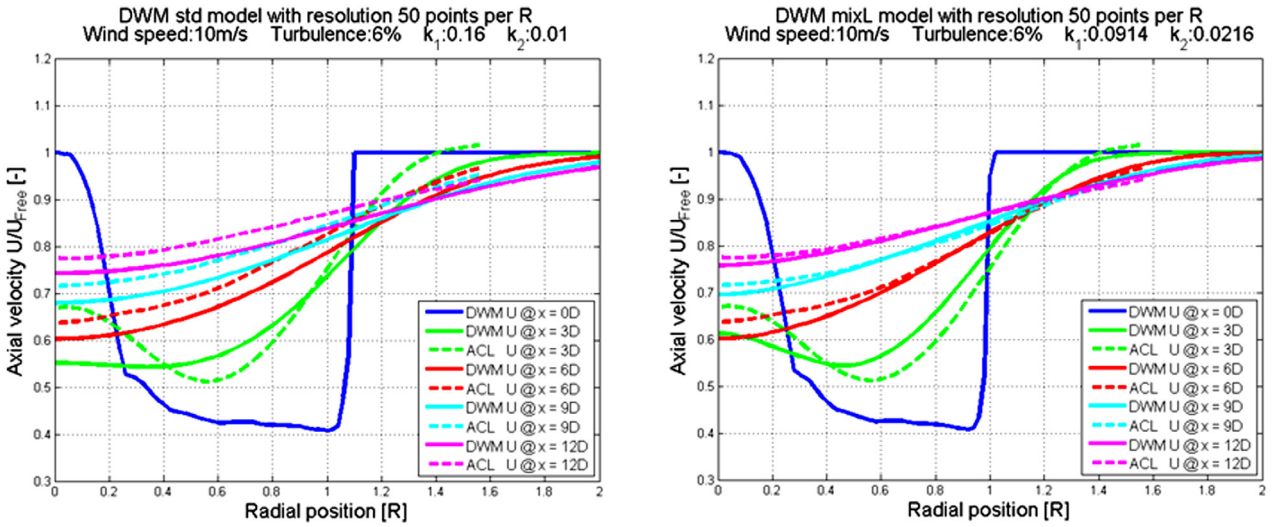

Fig. 8 Comparisons of the mean streamwise velocity distribution between the calibrated standard DWM model (left) and the mixing length DWM model (right) to actuator line data. The mixing length DWM model captures the velocity distribution in the wake better than the standard DWM model. The improvements are especially clear at 3*D*, where the shape of the wake deficit is improved.

respectively. Thus, the constants, n_c, $n_{c,d}$, and $n_{c,d,r,}$ represent the number of cases, number of cross-sections, and number of data points per cross-section, respectively. For this investigation of the DWM models, the constants are equal to four flow cases (wind speeds of 10 m/s and 15 m/s, turbulence intensities of 6% and 14%), four cross-sections for each case (3, 6, 9, and 12*D* behind the rotor) and 80 points per cross-section. The variable $\hat{e}$ is the mean flow velocity as given directly by the models. Note that, statistically, no information was used in creating the mean velocities,$\bar{U}$. Therefore, the sum of the square error should still be divided by the number of computational points, $n_{c,d,r}$, to find the correct variance between the models, as opposed to dividing by $n_{c,d,r} - 1$.

First, the same calibration procedure as proposed by Madsen et al. [1] was used. The basic assumption made in the calibration was that the k_2 coefficient can be found through a calibration of the DWM models to laminar actuator line data. Since the reference data do not contain any influence from ambient turbulence, the results of the DWM model are invariant to the value of the k_1 coefficient (see Eq. (14)). The second step is to keep the value of k_2, and calibrate the k_1 coefficient to the nonlaminar flow cases. By using this calibration method, the standard DWM formulation gave a standard error of 0.0270, and the mixing length DWM had a standard error of 0.0223, which corresponds to a reduction of 17%.

A further reduction in standard error was achieved when an alternative calibration algorithm was used. The first calibration procedure is based on the assumption that the ambient turbulence and the shear layer generated turbulence are independent of each other. In order to examine this assumption, consider the production term in the k-equation. P_k is proportional to the local Reynolds stresses times the mean velocity gradients. For the DWM, this implies that the amount of turbulence generated from the shear layer cannot be assumed to be independent of the ambient turbulence, as the turbulent production is enhanced by the existing turbulent fluctuations. A new calibration was performed, where the best values for k_1 and k_2 were found by a series of iterations. In the first iteration, k_1 was assigned an initial value, which was held constant during the calculations, and a least-square fit of k_2 was calculated. In the second iteration, k_2 was held constant, and an updated value for k_1 was calculated. This was repeated until both values for k_1 and k_2 reached steady values. By using this method, the standard error was further reduced to 0.0245 for the standard DWM and to 0.0179 for the mixing length DWM model. This corresponds to reductions by 9% for the standard DWM model and by 20% for the mixing length DWM model, based on the alternative calibration procedure. Based on the later calibration method, the standard error of the mixing length DWM model is 27% lower than the standard DWM model.

Figure 8 shows the results of the calibration for the case of 10 m/s wind speed and 6% turbulence intensity, which is the case that most clearly illustrates the improvement achieved by modifying the eddy viscosity formulation. Comparing the velocity distribution three diameters downstream of the rotor in the two figures, it can be seen that the new eddy viscosity formulation performs better in regions with steep velocity gradients. This observation is consistently found in all tested flow cases.

A sensitivity study was conducted by varying the model coefficients and recording the changes in standard error. The conclusions of the study was that the modified DWM model is rather insensitive to changes in model coefficients smaller than 10%, which only led to less than a 2% increase in standard error. A second conclusion is that the model is less sensitive to changes in the k_2 coefficient. Changing the value by as much as 30% only increased the standard error by 6%.

An additional study was conducted to investigate the influence of the modified boundary condition. A full model calibration using the iterative calibration procedure (as described above) with and without the modified boundary condition was performed. The standard error when the original boundary condition was used (i.e., with wake expansion at the rotor position) was 0.0223; this should be compared with 0.0179 for the new boundary condition, which corresponds to an improvement of 20%. The large improvement due to the modifications made to the boundary condition motivates further work on the topic. A further improvement could be achieved by optimizing the boundary condition together with the eddy viscosity coefficients and the filter functions, thereby completely controlling the initial turbulent mixing in the model. It would also be interesting to investigate if the boundary condition should be parameterized based on ambient conditions or turbine characteristic, or if a universal boundary condition is sufficient.

The calibrated DWM model shows good agreement with the actuator line data for all the extracted cross-sections (see Fig. 9). Two things should be noted when reading these results. First, the DWM model has been calibrated only to the actuator line model, not to field measurements. The accuracy of the proposed DWM model is therefore dependent on the ability of the actuator line model to

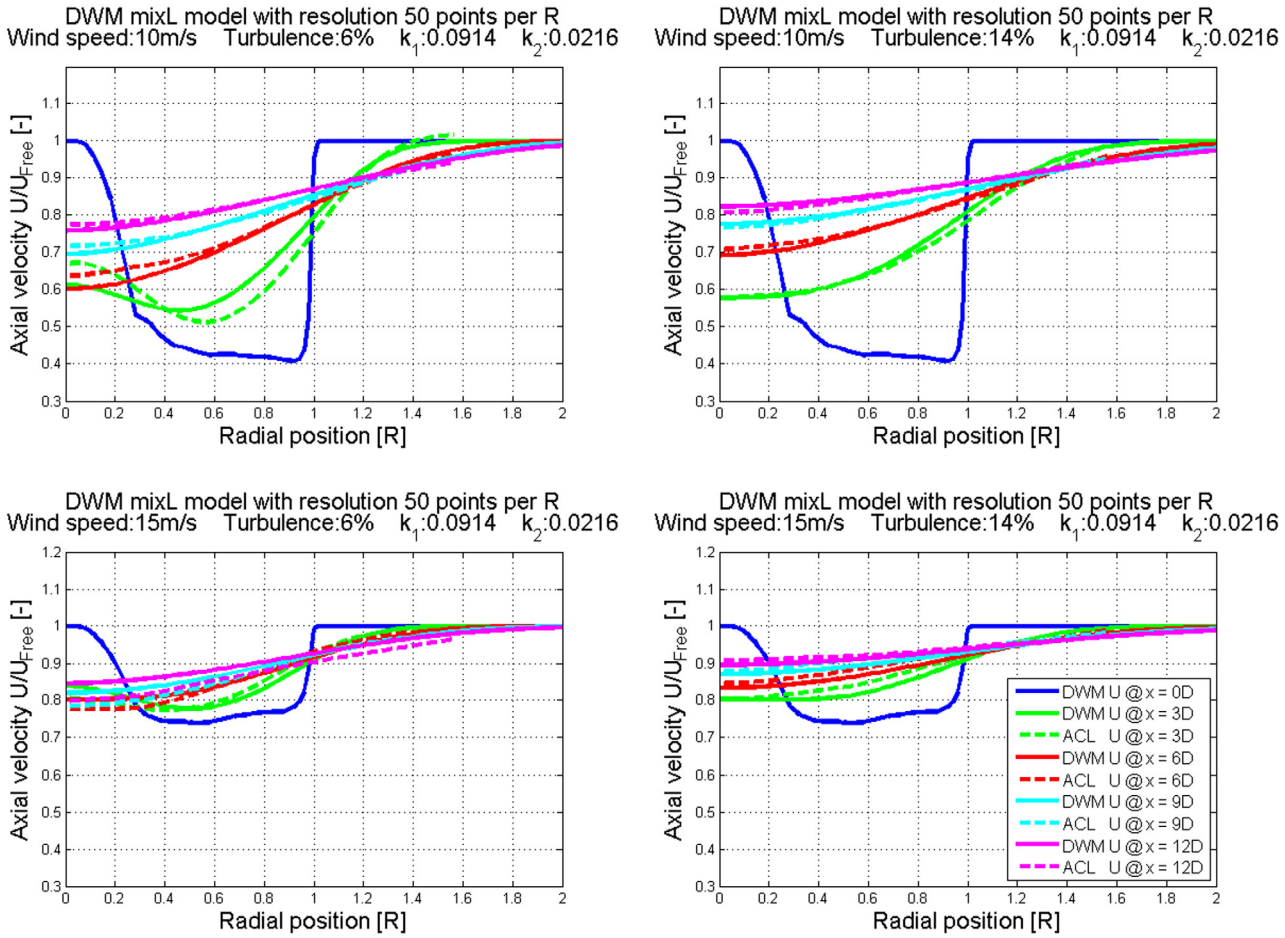

Fig. 9 The result of calibration by least-square fit to actuator line data for the DWM model with the mixing length eddy viscosity by using the iterative calibration method. Overall, a very good agreement is seen for all four cases presented.

predict the flow field in a realistic manner. The authors consider the validations of the actuator line model to field data performed at Risø and DTU by, among others, Troldborg [25] and, most recently, by Larsen et al. [24], to justify the use of the actuator line as a method of development and calibration of lower order models. Second, it should be noted that the same data set has been used for both calibration and verification in this study. However, since only the two parameters governing the turbulent mixing of the DWM model (k_1 and k_2) have been fitted to actuator line data, and good correlation is obtained for all tested operational conditions at various downstream cross-sections in the wake, it is concluded that the high performance of the improved DWM model is a not a consequence of overfitting to the verification data. The DWM model with the improved eddy viscosity formulation does in fact represent the physics of the wake to a high level.

It is important to remember that the measure of the standard error that is used to evaluate the model performance in this work, does not necessarily correspond to an increased ability to predict fatigue loads of the same magnitude. It only refers to the ability of the model to capture the mean flow velocity in a meandering frame of reference (i.e., following the wake movement). For future work, a separate study should be conducted on the effects of the improved ability to model the mean velocity on the ability to accurately model turbine loads.

Table 3 A study of the sensitivity for variations of the k_1 and k_2 coefficients to the standard error. The standard error in the table has been normalized to best fit the calibration above in order to increase readability. It can be seen that the standard error is relatively insensitive to variations; if a coefficient changes by less than 10%, the standard error increases by less than 2%.

		Variation in k_2 coefficient								
		− 30%	− 20%	− 10%	− 5%	0%	5%	10%	20%	30%
Variation in k_1 coefficient	− 30%	1.430	1.336	1.258	1.225	1.195	1.169	1.147	1.111	1.088
	− 20%	1.262	1.187	1.129	1.105	1.085	1.068	1.054	1.036	1.030
	− 10%	1.140	1.084	1.045	1.031	1.020	1.013	1.008	1.007	1.015
	− 5%	1.095	1.050	1.021	1.011	1.005	1.001	1.001	1.007	1.021
	0%	1.063	1.028	1.007	1.002	1.000	1.001	1.004	1.016	1.036
	5%	1.042	1.016	1.005	1.004	1.005	1.009	1.015	1.034	1.058
	10%	1.031	1.015	1.012	1.014	1.019	1.026	1.035	1.058	1.086
	20%	1.041	1.040	1.050	1.058	1.068	1.080	1.093	1.123	1.157
	30%	1.083	1.094	1.114	1.126	1.140	1.154	1.170	1.204	1.241

Conclusions

An improved eddy viscosity model has been developed for the DWM model. The model considers the same physical contributions to the turbulence in the wake as the original Ainslie model, i.e., free stream and shear layer generated turbulence. The main difference is that the eddy viscosity originating from the wake shear layer is based on a local turbulent velocity scale as opposed to assuming a single turbulent velocity scale for the entire cross-section of the wake.

The accuracy achieved with the modified eddy viscosity model is shown by comparing the average wake deficit found with the DWM model to that of the high-fidelity ELLIPSYS3D actuator line calculations. The standard error between the mean velocity field of the DWM and the actuator line model are reduced by 27% by implementing an eddy viscosity formulation based on the mixing length model to calculate the turbulent stresses.

Nomenclature

Variables and Constants

a_i = model constant in the Johnson–King equation equal to 0.30 (s)
α_{wake} = coefficient of wake expansion in the standard DWM model (-)
b = width of half the wake (m)
c = index referring to flow case number (-)
d = index referring to cross-section (-)
k = turbulent kinetic energy (m^2, s^{-2})
k_1 = calibration constant for influence of ambient turbulence (-)
k_2 = calibration constant for shear layer turbulence generation (-)
n_c = number of flow cases (-)
$n_{c,d}$ = number of cross-sections in flow case, c (-)
$n_{c,d,r}$ = number of data points in cross-section d and flow case c (-)
ν_T = turbulent eddy viscosity (m^2, s^{-1})
l^* = turbulent length scale (m)
r = radial coordinate, or radial index (m) or (-)
R = turbine radius (m)
TI = turbulence intensity (-)
TMT = turbulent momentum transfer (kg, m ,s^{-2})
τ_{stress} = turbulent stress (m^2, s^{-2})
u = axial velocity (m, s^{-1})
u_i' = velocity fluctuation (m, s^{-1})
u^* = turbulent velocity scale (m, s^{-1})
U_{amd} = undisturbed free wind speed (m, s^{-1})
U_{min} = minimum speed in the wake deficit (m, s^{-1})
v = radial velocity (m, s^{-1})
x = axial coordinate (m)

Functions

F_1 = filter function to model the delay in turbulent wake diffusion due to entrainment
F_2 = Filter function included to compensate for the initial non-equilibrium between the mean velocity field and the turbulent energy content created due to the rapid change in mean flow gradients over the rotor

References

[1] Madsen, H. Aa., Larsen, G. C., Larsen, T. J., Troldborg, N., and Mikkelsen, R., 2010, "Calibration and Validation of the Dynamic Wake Meandering Model Implemented in the Aeroelastic Code HAWC2," ASME J. Sol. Energy Eng., **132**(4), p. 041014.
[2] Larsen, G. C., Madsen, H. Aa., Thomsen, K., and Larsen, T. J., 2008, "Wake Meandering—A Pragmatic Approach," Wind Energy, **11**, pp. 377–395.
[3] Frandsen, S. T., 2007, "Turbulence and Turbulence-Generated Structural Loading in Wind Turbine Clusters," Risø National Laboratory, Technical University of Denmark, Roskilde, Denmark, Risø-R-1188(EN).
[4] Bingöl, F., Mann, J., and Larsen, G. C., 2010, "Light Detection and Ranging Measurements of Wake Dynamics, Part I: One-Dimensional Scanning," Wind Energy, **13**, pp. 51–61.
[5] Trujillo, J. J., Bingöl, F., Larsen, G. C., Mann, J., and Kühn, M., 2011, "Light Detection and Ranging Measurements of Wake Dynamics, Part II: Two-Dimensional Scanning," Wind Energy, **14**, pp. 61–75.
[6] Ainslie, J. F., 1988, "Calculating the Flow Field in the Wake of Wind Turbines," J. Wind Eng. Ind. Aerodyn., **27**, pp. 213–224.
[7] Ainslie, J. F., 1986, "Wake Modelling and the Prediction of Turbulence Properties," *Proceedings of the 8th British Wind energy Association Conference*, Mar. 19–21, Cambridge, pp. 115–120.
[8] Madsen, H. A., Thomsen, K., and Larsen, G. C., 2003, "A New Method for Prediction of Detailed Wake Loads," *Proceedings of IEA Joint Action of Wind Turbines 16th Symposium*, Sven-Erik Thor, ed., NREL, Boulder, pp. 171–188.
[9] Larsen, G. C., Madsen, H. Aa., Bingöl, F., Mann, J., Ott, S., Sørensen, J. N., Okulov, V., Troldborg, N., Nielsen, M., Thomsen, K., Larsen, T. J., and Mikkelsen, R., 2007, "Dynamic Wake Meandering Modelling," Risø National Laboratory, Technical University of Denmark, Roskilde, Denmark, Risø-R-1607(EN).
[10] Larsen, G. C., Madsen, H. Aa., Larsen, T. J., and Troldborg, N., 2008, "Wake Modeling and Simulation," Risø National Laboratory, Technical University of Denmark, Roskilde, Denmark, Risø-R-1653(EN).
[11] Madsen, H. A., Larsen, G. C., and Thomsen, K., 2005, "Wake Flow Characteristics in Low Ambient Turbulence Conditions," Proceedings of Copenhagen Offshore Wind.
[12] Madsen, H. Aa., Larsen, G. C., Larsen, T. J., Mikkelsen, R., and Troldborg, N., 2008, "Wake Deficit-and Turbulence Simulated With Two Models Compared With Inflow Measurements on a 2MW Turbine in Wake Conditions," *Scientific Proceedings. 2008 European Wind Energy Conference and Exhibition*, Brussels (BE), Mar. 31–Apr. 3, pp. 48–53.
[13] Mann, J., 1994, "The Spatial Structure of Neutral Atmospheric Surface-Layer Turbulence," J. Fluid Mech., **273**, pp. 141–168.
[14] Mann, J., 1998, "Wind Field Simulation," Probab. Eng. Mech., **13**(4), pp. 269–282.
[15] Sanderse, B., 2009, "Aerodynamics of Wind Turbine Wakes—Literature Review," ECN, The Netherlands, Technical Report No. ECN-E-09-016.
[16] Sørensen, N. N., 1995, "General Purpose Flow Solver Applied to Flow Over Hills," Ph.D. thesis, Risø-R-827(EN), Risø National Laboratory, Technical University of Denmark, Roskilde, Denmark.
[17] Sørensen, J. N., and Shen, W. Z., 2002, "Numerical Modelling of Wind Turbine Wakes," ASME J. Fluids Eng., **124**(2), pp. 393–399.
[18] Mikkelsen, R., 2003, "Actuator Disc Methods Applied to Wind Turbines," Technical University of Denmark, MEK-FM-PHD 2003-02.
[19] Øye, S., 1983, "Fix Dynamisk, Aeroelastisk Beregning af Vindmøllevinge," Department of Fluid Mechanics, The Technical University of Denmark, AFM Report No. 83-08.
[20] Hansen, M. O. L., 2001, *Aerodynamics of Wind Turbines*, Earthscan Publications Ltd, Oxford, United Kingdom.
[21] Mikkelsen, R., Sørensen, J. N., and Troldborg, N., 2007, "Prescribed Wind Shear Modelling Combined With the Actuator Line Technique," Proceedings of the 2007 EWEC conference, Milan.
[22] Troldborg, N., Sørensen, J. N., and Mikkelsen, R., 2007, "Actuator Line Simulation of Wake of Wind Turbine Operating in Turbulent Inflow," J. Phys.: Conf. Ser. 75:012063, The Science of Making Torque from Wind, Technical University of Denmark, Lyngby.
[23] Keck, R.-E., Mikkelsen, R., and Troldborg, N., 2011, "Investigation of Prescribed Wind Shear and Synthetic Atmospheric Turbulence for Rotor Wake Simulations," *Proceedings Gotland Wake Conference*.
[24] Larsen, G. C., Hansen, K. S., Troldborg, N., Mann, J., and Enevoldsen, K., 2010, "A First Attempt to Characterize the Structure of the Wake Turbulence Using a Combined Experimental and Numerical Approach," iTi Conference on Turbulence IV, Bertinoro (IT), Sep. 19–22.
[25] Troldborg, N., 2008, "Actuator Line Modeling of Wind Turbine Wakes," Technical University of Denmark, MEK-FM-PHD 2008-06.
[26] Ivanell, S., 2009, "Numerical Computations of Wind Turbine Wakes," Ph.D. thesis, Royal Institute of Technology, Stockholm, Sweden.
[27] Cavar, D., 2006, "Large Eddy Simulation of Industrially Relevant Flows," MEK-FM-PHD 2006-02.
[28] Menter, F. R., 1994, "Two-Equation Eddy-Viscosity Turbulence Models for Engineering Applications," AIAA J., **32**(8), pp. 1598–1605.
[29] Versteeg, H. K., and Malalasekera, W., 2007, *An Introduction to Computational Fluid Dynamics—The Finite Volume Method*, 2nd ed., Longman Group Ltd., London, United Kingdom.
[30] Pope, S. B., 2000, *Turbulent Flows*, Cambridge University Press, Cambridge, United Kingdom.

III: Two Improvements to the Dynamic Wake Meandering Model: Including the Effects of Atmospheric Shear on Wake Turbulence and Incorporating Turbulence Build Up in a Row of Wind Turbines

Two Improvements to the Dynamic Wake Meandering Model: Including the Effects of Atmospheric Shear on Wake Turbulence and Incorporating Turbulence Build-up in a Row of Wind Turbines

Rolf-Erik Keck[1,2], Martin de Maré[1,2], Matthew J. Churchfield[3], Sang Lee[3], Gunner Larsen[2] and Helge Aagaard Madsen[2]

[1] Rotor Systems, Vestas Wind Systems A/S, DK-4000 Roskilde
[2] Wind Energy Department, Risø DTU National Laboratory for Sustainable Energy, DK-4000 Roskilde
[3] National Renewable Energy Laboratory, 15031 Denver West Parkway, Golden, CO 80401-3305 USA

Corresponding author:
Rolf-Erik Keck – rolf.keck@gmail.com

Abstract
The dynamic wake meandering model is an engineering wake model designed to physically model the wake deficit evolution and the unsteady meandering that occurs in wind turbine wakes. The present study aims at improving two features of the model:

1) the effect of the atmospheric boundary layer shear on the wake deficit evolution by including a strain-rate contribution in the wake turbulence calculation.
2) the method to account for the increased turbulence at a wake-affected turbine by basing the wake-added turbulence directly on the Reynolds stresses of the oncoming wake. This also allows the model to simulate the build-up of turbulence over a row of turbines in a physically consistent manner.

The performance of the modified model is validated against actuator line model results and field data from the Lillgrund offshore wind farm. Qualitatively, the modified dynamic wake meandering model is in fair agreement with the reference data. A quantitative comparison between the mean flow field of the dynamic wake meandering model with and without the suggested improvements, to that of the actuator line model, shows that the root-mean-square difference in terms of wind speed and turbulence intensity is reduced on the order of 30% and 40%, respectively, by including the proposed corrections for a row of eight turbines. Furthermore it is found that the root-mean-square difference between the actuator line model and the modified dynamic wake meandering model in terms of wind speed and turbulence intensity does not increase over a row of turbines compared to the root-mean-square difference of a single turbine.

Introduction
The dynamic wake meandering (DWM) model (Madsen et al. [1]) is a reduced-order wake model developed to capture the most important physical effects of wind turbine wake dynamics while maintaining low computational demand, making it suitable for design calculations. The current form of the DWM model consists of three separate parts, which are outlined below and shown in figure 1:

1. A steady-state, axisymmetric wake deficit is calculated based on the thin shear layer approximation to the Navier-Stokes (N-S) equations, as proposed by Ainslie [2, 3].
2. Stochastic, large-scale meandering of the wake deficit is applied. The wake deficit is assumed to act as a passive tracer that is translated horizontally and vertically by large-scale atmospheric turbulent fluctuations (eddies larger than twice the turbine rotor diameter), as suggested by Larsen et al. [4].

3. Small-scale wake-added turbulence is superimposed on the flow field that results from parts 1 and 2. The magnitude of the wake-added turbulence is based on the local depth and the radial gradient of the wake deficit (for further details see Madsen et al. [5]). In the current formulation, the wake-added turbulence only affects the loads at the downstream rotors. No coupling to the velocity and turbulence evolution of the wake of the downstream turbine is included.

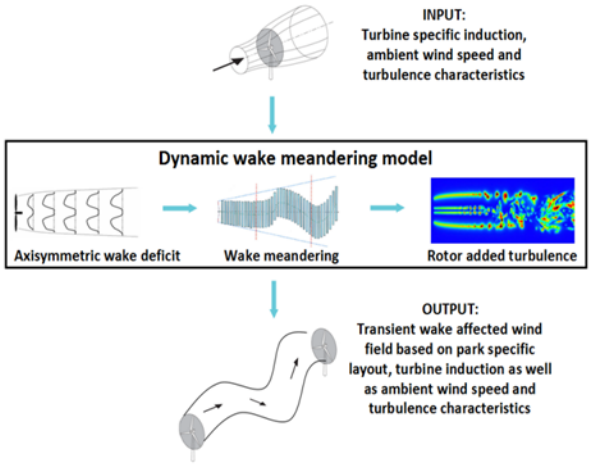

Figure 1, an overview of the workflow of the DWM model.

The resulting wake dynamics are applied as input to an aero-elastic calculation to simulate the effects of operating a turbine in the wakes of others, as described by Madsen et al. [6]. In practice, the shape of the wake deficit is determined by the ambient wind speed and turbulence intensity, along with the turbine induction and distance between the wake-receiving and wake-emitting turbines. The small-scale turbulence is based on the distance from the wake centre, and is superimposed onto the wake deficit in the meandering frame of reference (MFoR). Both of these contributions to the wake effects are time invariant. The dynamic effect in the DWM model is then created by the large-scale translation of the entire deficit, including the small-scale turbulence. The meandering is applied in the vertical and lateral directions only. Finally, the atmospheric shear is taken into account by superimposing the vertical shear profile on the calculated wake dynamics. The downstream rotor will therefore experience a sheared inflow, on which the mean wake deficit and the added small-scale turbulence are superimposed. The location of the wake deficit relative to the rotor is updated at every time step of the aero-elastic simulation.

In the current DWM formulation, the effect of atmospheric shear is added to the mean flow field only once the wake deficit has been calculated. A focus of this article is to include the effect of atmospheric shear-generated turbulence in the wake deficit calculation of the DWM model. This results in a more accurate wake deficit development in the far-wake region, where the vertical atmospheric wind shear is of the same order of magnitude or larger than the wake deficit shear, and therefore, is a non-negligible source of turbulence kinetic energy generation in the wake. The more comprehensive modelling of the far-wake turbulence dynamics also enables a more physically consistent wake-added turbulence formulation based on the turbulent stresses in the wake deficit calculations. Using the improved wake-added turbulence description, we also propose a method to include the wake-added turbulence from upstream wakes in the calculation of the wake deficit of a downstream rotor. This enables the DWM to simulate the mean flow field and the build-up of turbulence over a row of turbines in a more physically consistent manner.

The first section of the article describes the method used to calculate the wake deficit in the DWM model. This is followed by a brief summary of the computational fluid dynamics (CFD) actuator line (AL) models used for validating the proposed DWM model improvements. The two

following sections give the physical motivation and theory for including a contribution from atmospheric shear on the wake turbulence, along with a suggestion on how to practically include the effect in DWM calculations over a row of turbines. Finally, we present the results, discussion, and conclusion of the work.

The deficit calculations in the DWM model

The wake deficit in the DWM model is governed by the steady-state, axisymmetric thin shear layer approximation of the N-S equations in which momentum is given by

$$u\frac{\partial u}{\partial x} + v\frac{\partial u}{\partial r} = \frac{1}{r}\frac{\partial}{\partial r}\left(v_T r \frac{\partial u}{\partial r}\right) \quad (1)$$

and continuity is maintained through

$$\frac{1}{r}\frac{\partial}{\partial r}(rv) + \frac{\partial u}{\partial x} = 0. \quad (2)$$

In these equations, the velocity components u and v are in the mean flow (x) and radial (r) directions, respectively, and ν_t is an eddy viscosity. The main benefit in using the thin shear layer approximation is a significantly reduced computational cost. This is achieved by omitting the pressure gradient term, approximating the flow as axisymmetric, and assuming that the magnitude of the velocity gradients in streamwise direction is much smaller than those in radial direction. The fact that the pressure gradient is neglected means that there is no pressure-velocity coupling, and no need to solve an equation for pressure, which is often the most expensive part of the solution procedure. Further, as the flow is assumed to be axisymmetric, only one component of the momentum equation needs to be solved and the other velocity component is given by the continuity equation (which is otherwise unused, as there is no pressure-velocity coupling). Turbulent diffusion is accounted for with an eddy viscosity formulation, based on the following mixing length model described by the equation

$$v_T = F_1 k_{amb} TI_{amb} + F_2 k_2 l^{*2} \left|\frac{\partial u}{\partial r}\right|. \quad (3)$$

where $\frac{\partial u}{\partial r}$ refers to the axial velocity gradient in radial direction, k_{amb} and k_2 are DWM model constants (the k_{amb} constant includes a length scale based on a hub height equal to the rotor diameter), TI_{amb} and U_{amb} are the ambient turbulence intensity and mean wind speed at hub height, R is the rotor radius, and l^* is the turbulence mixing length. F_1 and F_2 are filter functions included to govern the development of turbulent stresses. The filter functions are required, as no transport equation for turbulent kinetic energy is included in the turbulence closure of the DWM model. Without filter functions, the turbulence field would be in perfect equilibrium with the local strain-rate directly at the rotor. However, in wake modelling, the mean flow field changes abruptly at the rotor, but the process of the turbulence reaching a fully developed stage with the new local strain-rate is relatively long. The F_1 function is included to compensate for the effect on turbulence caused by the boundary condition treatment. To account for the pressure effects in the DWM model, the wake deceleration and expansion is applied at the inlet boundary, see eqs. (4) and (5). This generates unphysical large velocity gradients close to the rotor. Thus, the role of the F_1 filter function is to reduce the effect of the ambient turbulence close to the rotor to avoid this unphysical turbulence diffusion of the wake deficit. Consequently, the length of the F_1 function is taken to be 2 rotor diameters (D), which is roughly equal to the distance required for the pressure to recover behind the turbine according to Sanderse [7]. The F_2 filter function governs the development of turbulence generated by the wake shear layer. This process is seen to be approximately 10 D, based on AL simulations. The details and motivation for this turbulence formulation are given by Keck et al. [8].

The equation system described by eqs. (1–3) is solved using a finite-difference scheme in which a second-order central-difference scheme in the radial direction and a first-order upwind scheme in the mean flow direction are applied. As information only moves along the mean flow direction, a solution can be obtained by "marching" downstream, solving each axial position sequentially. For each location along the mean flow axis, the sequence to find the velocity field can be summarized by:

1. Solving the momentum equation for the streamwise velocity component at all radial positions explicitly using the value for radial velocity component and eddy viscosity from the previous location upstream. This yields a tridiagonal equation system in which all of the coefficients are known.
2. Using eqs. (2) and (3) above to compute the corresponding radial velocity and the eddy viscosity (once the streamwise velocity at the present axial position is known).
3. Proceeding to the next downstream location and repeating steps 1 and 2.

The boundary condition in the DWM model

Omitting the pressure gradient term in the equations has the consequence that the near wake region, where pressure is recovering and significant gradients are present, will not be accurately represented by the DWM model. According to Sanderse [7], this region is usually on the order of 2 D. The inaccuracy in this region is considered to be acceptable because the near wake is not of primary interest when modelling the effects of wakes on turbine operations, as long as the far-wake calculation remains accurate.

In the DWM model, the effect of the pressure gradient is considered to be negligible at a distance of 3 D behind the turbine. This location is referred to as the "point of DWM validity." The inlet boundary condition is designed to artificially account for the effect of the neglected pressure gradient in such a manner that the resulting flow field after 3 D is accurately represented. This is done by including expansion and deceleration of the fluid at the rotor disc. The boundary condition is based on the turbine-specific, azimuthally and time averaged axial induction profile as a function of radial position in the rotor plane, $a(r_{rot})$. This is commonly found from an aero-elastic simulation. The pressure effects are included by scaling the turbine induction profile, both in magnitude (to account for deceleration) and the radial position where the induction is applied (to account for wake expansion), by the factors f_U and f_R, respectively. The resulting inlet velocity distribution, U_{BC}, as a function of wake radius, r_{BC}, that is applied to the DWM calculations is given by

$$U_{BC}(r_{BC}) = U_{amb}(1 - (1 + f_U)a(r_{rot})) \tag{4}$$

$$r_{BC} = r_{rot}\sqrt{\frac{1-\langle a\rangle}{1-(1+f_R)\langle a\rangle}} \tag{5}$$

where $U_{amb}$is the ambient wind speed at hub-height and the $\langle\ \rangle$ operator denotes spatial averaging over the swept rotor disc.

A least square re-calibration to computational fluid dynamics AL data of the model parameters and F_2 filter function was performed with the proposed modification; a description of this is given later. Based on the calibration, the following values were applied in the calculations: f_U = 1.10, f_R = 0.98, k_1 = 0.587 and k_2 = 0.0178. The filter functions used are shown in figure 2.

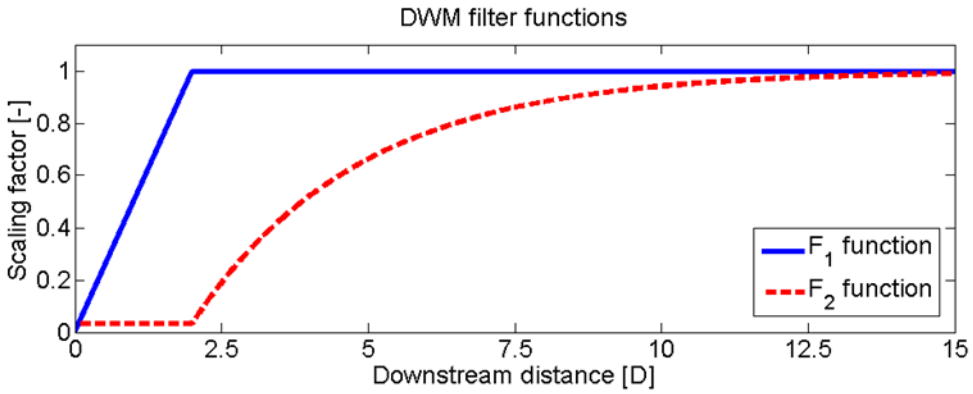

Figure 2, filter functions applied in the DWM calculations.

Actuator line model

The DWM development presented in the article is driven by higher-order CFD predictions using AL turbine models. The fundamental processes that the proposed corrections attempt to mimic have been observed in CFD studies using the AL models, and the DWM model parameters have been calibrated against AL model calculations. The AL models used in this work are based on the formulation of Sørensen and Shen [9]. Each turbine blade is represented as a line along the blade axis, and the line is divided into a number of discrete segments. At each actuator line segment, a lift and drag force is calculated based on the local angle of attack, chord length, actuator width, and airfoil type using tabulated airfoil lift and drag properties, which are usually corrected for three-dimensional effects. These actuator forces are projected onto the CFD flow field as volumetric body forces, in this case, using a three-dimensional Gaussian projection. The body force field enters into the Navier-Stokes equations and creates the main effects of a turbine on the flow field, including axial induction, wake formation, and generation of blade tip and root vortices. The main benefit of the AL model is that the high grid resolution necessary to model the boundary layer of the blades is avoided. This significantly lowers the computational expense because fewer computational cells are required, which also allows for larger time steps without violating the Courant–Friedrichs–Lewy condition.

Two different implementations of the AL model are used for DWM development and validation in this work:

- The Ellipsys3D [10] AL model developed at the Technical University of Denmark (DTU) by Mikkelsen [11] and Troldborg [12].
- The OpenFOAM [13] implementation developed at the National Renewable Energy Laboratory (NREL) by Churchfield et al. [14].

There are many similarities between the two implementations of the AL models. They are both incorporated into large-eddy simulation (LES) solvers and solved over relatively coarse computational grids, with a resolution such that 50–60 grid cells span the turbine rotor. LES is an unsteady CFD method that solves the filtered Navier-Stokes equations, resolving the larger, energy-containing turbulent scales and modelling the effect of the remaining smaller scales.

The main difference between the models lies in the treatment of atmospheric shear and turbulence. The DTU implementation imposes a volumetric body force on the incompressible Navier-Stokes equations that generates a desired atmospheric shear and turbulent fluctuations. Shear is imposed by prescribing a volume force field over the entire domain. The magnitude of the volume forces is determined through a precursor calculation in which no turbines are included, and any desired profile can be prescribed as outlined by Mikkelsen et al. [15]. The atmospheric turbulence is imposed through fluctuating volume forces within a thin region located a few radii upstream of the wind turbine. The magnitude and fluctuations of the volume forces are based on a pregenerated turbulence field, which is translated into a force field by

one-dimensional momentum theory, as described by Troldborg et al. [16]. Keck et al. [17] validated this method for simulations of a wind turbine, represented by the EllipSys3D AL model, wake in natural atmospheric turbulence to field and wind tunnel data. The validation campaign comprised of validation of the evolution of turbulence intensity, turbulence spectra and wake meandering as a function of downstream distance for a range of common operating conditions.

The NREL implementation also solves the incompressible Navier-Stokes equation for motion, but thermal effects are accounted for through a Boussinesq buoyancy term. This term allows for the modelling of atmospheric stability (in this work, however, all simulations were carried out in neutral stratification). Rather than using a force field to create the atmospheric shear and turbulence, these effects are generated by running precursor atmospheric boundary layer calculations in a horizontally periodic turbine-free domain. After the turbulent boundary layer has developed to a quasi-equilibrium state, velocity and temperature information at the upstream boundaries are stored at every time step. This data is then used in the turbine simulations as time-dependent inlet boundary conditions. The benefit over the DTU implementation is that the shear and turbulence used for the wind turbine simulation are generated directly from the Navier-Stokes equations and that buoyancy effects on the turbulence production can be captured. The disadvantage is that the method is significantly more computationally expensive. The details of this method are outlined by Churchfield et al. [14].

Figure 3 shows a comparison of the input turbulence spectra in neutral stratification to the EllipSys3D AL model (prescribed by the Mann model (Mann [18] and [19]), thick lines), to that of the OpenFOAM AL model (generated by the precursor, thin lines). The input turbulence spectra of the normal stress components are in fair agreement for all scales above the spectral cut-off due to the grid size of the LES precursor calculations. The largest deviation is seen for the shear stress component (cyan line), which is lower in the OpenFOAM precursor compared to that of the Mann model.

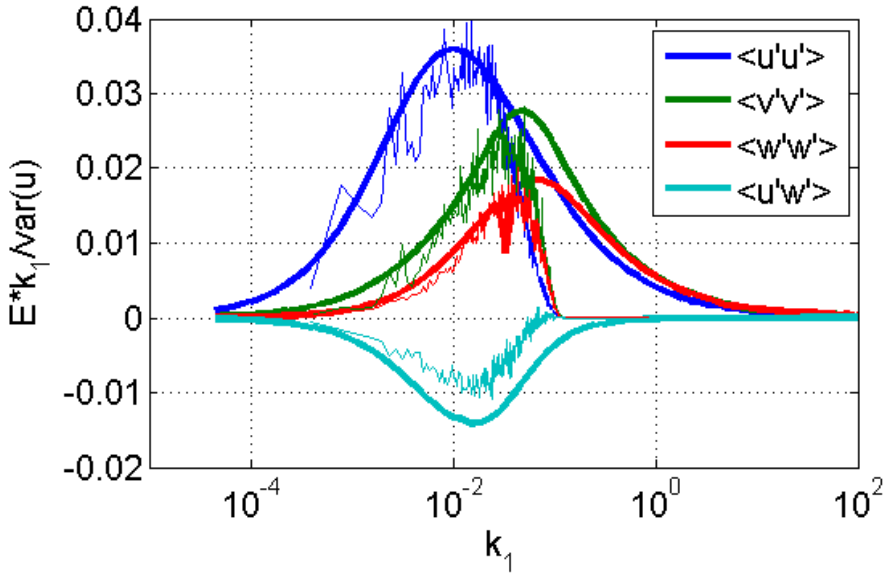

Figure 3, turbulent energy spectra of the input wind field to the EllipSys3D AL model (thick lines) and the OpenFOAM AL model (thin lines).

Figure 4 shows the wake meandering resulting from the two models for a single turbine with a rotor diameter of 80m, represented as ALs, operating in 8m/s wind speed and 6% turbulence intensity. The wake meandering is quantified as the standard deviation of the wake centre. The method selected to find the wake centre in the two models is slightly different due to the

availability of data. In this work, the EllipSys3D AL simulations are setup to allow for analysis in the MFoR (i.e. in a coordinate system following the centre of the wake, which allows for studies of the wake deficit evolution). This requires storing planes of data in whole cross-sections of the wake and calculating the wake centre as the centre of gravity of the wake deficit at each time step. This procedure to find the wake centre in the EllipSys3D simulations is described in Keck at al. [17]. The OpenFOAM calculations are setup to be used as validation of the DWM model in the fixed frame of reference (FFoR, i.e. relative to a fixed location and therefore affected by both wake deficit evolution and wake meandering). To facilitate an analysis in the FFoR, data was stored in a lateral plane and in a vertical plane, with a joint axis aligned with the mean wake axis (i.e. the axis extending into the wake from the hub of the wind turbine in the mean wind direction). The wake centre position is found as the location where a simplified wake shape gives the best fit with the instantaneous wake deficit, see Keck et al. [20] for more details. The first algorithm has higher accuracy, but increases the amount of data that needs to be stored by an order of magnitude and the analysis to find the wake centre is more time consuming, relative to the second algorithm. Since it is not critical to the analysis of this study to accurately quantify the wake meandering of the OpenFOAM AL simulations (we are only interested in the resulting flow field at hub-height), the inexpensive second algorithm is applied to the OpenFOAM simulations. From figure 4 it is seen that the two models yields similar magnitude of wake meandering in both lateral (solid lines) and vertical (dashed lines) direction. This is expected as the input turbulence spectra in figure 3 are in fair agreement in large scales which dictates the meandering.

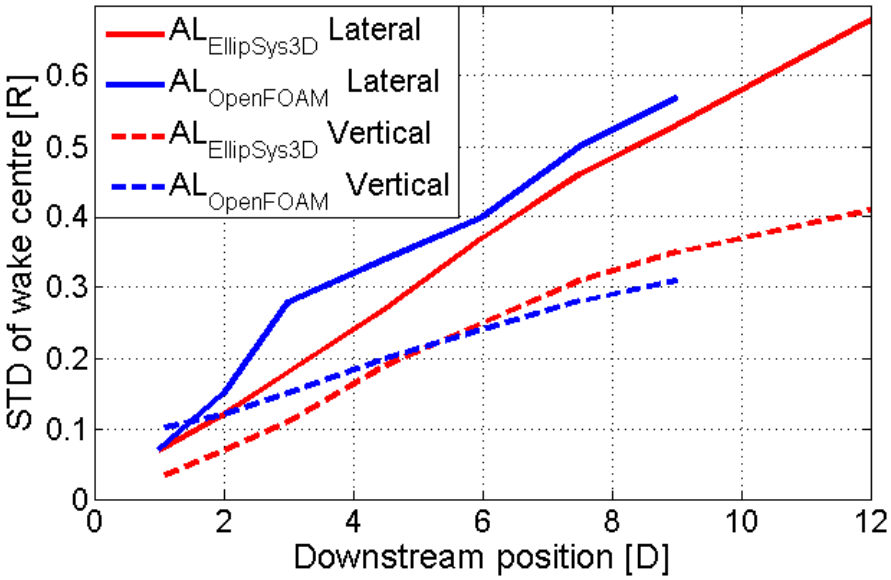

Figure 4, wake meandering downstream of a single turbine operating in 8m/s wind speed and 6% as modeled by the EllipSys3D AL model (red lines) and OpenFOAM AL model (blue lines). The wake meandering is quantified as the standard deviation of the wake centre, and normalized against rotor radius.

Atmospheric shear contribution to turbulence in the DWM deficit model

In the DWM model, the turbulent stresses are calculated based on the zero-equation eddy viscosity model shown in eq. (3). In a zero-equation eddy viscosity model, there is no transport equation for turbulent kinetic energy to maintain an integrated balance of production and dissipation. Instead, the eddy viscosity is directly proportional to the local mean flow gradients. Further, in all eddy viscosity models, the turbulent stresses are calculated as the product of the

eddy viscosity and the local velocity gradients. As a consequence, it is very important for the calculation of the turbulent stresses to apply the correct total mean velocity gradient in the model.

In the current formulation, only the wake deficit gradient is considered when calculating the turbulent stresses in the DWM model. This limitation has the undesirable effect that, as the wake deficit recovers, the turbulent stresses approach zero, resulting in unrealistically low turbulent stress levels in the far-wake region. An appropriate turbulence formulation should result in ambient turbulence conditions after the wake deficit has fully recovered. The proposed method is to include a strain-rate contribution from the atmospheric vertical wind shear when calculating the turbulent stresses. A difficulty, though, is that atmospheric shear is not axisymmetric, but the DWM model wake deficit formulation is.

The magnitude of the atmospheric shear gradient should be expressed as a function of ambient turbulence intensity to fit with the existing DWM input parameters. An appropriate dimensionless wind shear value can be found by estimating the non-dimensional characteristic velocity and length scale, u^*_{ABL} and l^*_{ABL}, of the atmospheric turbulence, and using the relation

$$\frac{du}{dz}_{ABL} = \frac{u^*_{ABL}}{l^*_{ABL}}. \tag{6}$$

The velocity scale is based on the neutral atmospheric turbulence spectra, as calculated by the model proposed by Mann [18] and [19]. To be compatible with the DWM model parameters, the atmospheric velocity scale is formulated as a function of ambient turbulence intensity. This is achieved by relating the normal stresses (given by the turbulence intensity level) to the shear stresses in the atmosphere (which yield the velocity scale), through integration of the turbulent energy in the atmospheric turbulence spectra,

$$u^*_{ABL} = \left[\left(TI^2_{amb} \cdot \frac{-\overline{u'w'}}{\overline{u'u'}}\right)\right]^{1/2} \tag{7}$$

where TI_{amb} is the ambient turbulent intensity and $\overline{u'u'}$ and $-\overline{u'w'}$ are the normal and shear stresses of the atmospheric turbulence, respectively. The overbar denotes time averaging. The atmospheric length scale is estimated using Monin-Obukhov scaling given by Ratto [21],

$$l^*_{ABL} = \frac{\kappa z}{R} \tag{8}$$

where κ is the von Kármán constant, z is the height above the ground level, and R is the rotor radius. This atmospheric shear is calculated at a reference height of 100 m, and it is considered to be linear and have one uniform value in the whole simulation domain (i.e., it is invariant in downstream direction and height). Further, it is also assumed to be unaffected by the presence of the wake deficit. The effect of the atmospheric shear is to increase the local strain-rate, and thereby, the turbulent stresses in regions of low wake deficit gradients. This is typically the far-wake region, but also may include the regions close to the wake centreline and the rotor for nearly uniform induction profiles.

The strain-rate to apply in the DWM calculations should be a function of radial and axial position, where each value corresponds to the azimuthally averaged axial velocity gradient with respect to radial direction (as the deficit is based on two-dimensional calculation, variations in azimuthal directions cannot be captured). As the atmospheric shear is expressed in Cartesian coordinates (*du/dz*) and the wake deficit gradient is in axisymmetric coordinates (*du/dr*), an appropriate method is required to combine the two gradients to find the representative strain-rate. To illustrate the proposed method, the local radial gradient of axial velocity of the two velocity gradients is drawn as a function of azimuthal position for some arbitrary radial location in the wake deficit in figure 5. The wake deficit gradient (dashed lines) has a constant value as a function of azimuthal position, as the DWM model assumes axisymmetric flow. The contribution due to the atmospheric shear gradient (dotted lines) is a sinusoidal function over the azimuth, as

linear atmospheric shear is assumed over the cross section of the rotor. The combined local gradient (solid line) is the sum of the two contributions. Since the deficit calculation in the DWM model assumes an axisymmetric flow field, the representative value for the strain-rate to apply is the mean value in azimuthal direction. This value corresponds to the average height of the combined curve in figure 5.

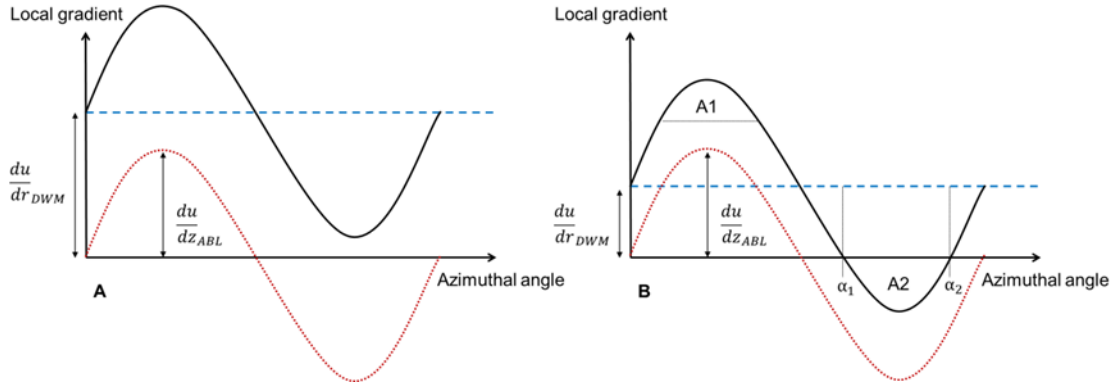

Figure 5a and b, conceptual description of how the local representative velocity gradient (solid line) is calculated given the atmospheric shear (dotted line) in Cartesian coordinates (du/dz) and the wake deficit gradient (dashed line in axisymmetric coordinates (du/dr).Figure 3a (left) illustrates a case in which the magnitude of the wake deficit shear is larger than the atmospheric shear, and figure 3b (right) illustrates a case in which the atmospheric shear is larger.

An important observation is that when the magnitude of the wake-deficit gradient is larger than the atmospheric shear, the mean effect of the atmospheric gradient is zero, as shown in figure 5a. This is the same as saying the integral of the total local gradient is equal to the integral of constant wake deficit gradients. In this region, no correction due to atmospheric shear is required. The correction should therefore only give a nonzero contribution when the magnitude of the atmospheric shear gradient is larger than the wake deficit gradient.

When the magnitude of the atmospheric shear is larger than the wake deficit gradient, a part of the lower wake (*A2* in figure 5b) will experience turbulent stresses acting in the opposite direction compared to the rest of the wake. Since the DWM model is based on an axisymmetric flow field, this situation cannot be handled in a strictly physically manner. Instead, the key feature to capture for the wake diffusion is the total magnitude of turbulent stresses. This magnitude is found by calculating the azimuthal average of the absolute value of local velocity gradient at each radial position. This gradient is then used to calculate the turbulent stresses. The geometrical interpretation of this concept is that the representative strain-rate to apply in the stress calculations corresponds to the average (absolute) distance between the combined curve and the x-axis in figure 5b. The representative strain-rate can thus be calculated using the equations

$$A_{Total} = \begin{cases} 2\pi \frac{du}{dr_{DWM}} & , \quad \left|\frac{du}{dr_{DWM}}\right| \geq \frac{du}{dz_{ABL}} \\ 2\pi \frac{du}{dr_{DWM}} + A1 + A2\,, & \left|\frac{du}{dr_{DWM}}\right| < \frac{du}{dz_{ABL}} \end{cases} \tag{9}$$

$$A1 = A2 = \int_{\alpha_1}^{\alpha_2} \left(\frac{du}{dz_{ABL}} \cdot \sin(x)\, dx \right) - (\alpha_2 - \alpha_1) \frac{du}{dr_{DWM}} \tag{10}$$

$$\frac{du}{dr_{Total}} = \frac{A_{Total}}{2\pi} \tag{11}$$

For a given radial position, the azimuthal section of the deficit in which the atmospheric shear contribution is larger than the wake deficit shear, i.e. between α_1 and α_2, are found by

arcsin($\frac{du}{dr_{DWM}}$ */* $\frac{du}{dz_{ABL}}$*)* and *π-α₁*, respectively. The strain-rate, as calculated by eq. (11), is used to calculate the turbulent stresses in the wake to incorporate the effect of the atmospheric shear on the wake diffusion. Rather than using the total velocity gradient in the turbulent stress term of the momentum equation, eq. (1), and because the momentum equation is only meant to solve for wake velocity and not a combined wake-atmospheric velocity, a scaled eddy viscosity, ν'_t, is introduced as

$$\nu'_t = \nu_t \cdot \frac{\frac{du}{dr_{Total}}}{\left|\frac{du}{dr_{DWM}}\right|}. \tag{12}$$

The original eddy viscosity is scaled at every computational node by the ratio of the corrected gradient with atmospheric shear effects to the wake deficit velocity gradient in the DWM solution. This has the desired effect of applying the appropriately scaled turbulent stresses, τ, in the wake deficit calculation

$$\tau = \nu'_t \cdot \frac{du}{dr_{DWM}} = \nu_t \cdot \frac{\frac{du}{dr_{Total}}}{\left|\frac{du}{dr_{DWM}}\right|} \cdot \frac{du}{dr_{DWM}} = \nu_t \cdot \frac{du}{dr_{Total}} \tag{13}$$

A correction is included to ensure numerical stability in regions with wake deficit velocity gradients close to zero. Because the total mean velocity gradient according eq. (11) never approaches zero, numerical instabilities occur in the scaling of the eddy viscosity, as the last term of eq. (12) approaches infinity. This is solved by the application of a Wiener filter, [21]

$$\frac{1}{\frac{du}{dr_{DWM}}} \approx \frac{\frac{du}{dr_{DWM}}}{\left(\frac{du^2}{dr_{DWM}} + k_{wiener}\right)} \tag{14}$$

where $\frac{du}{dr_{DWM}}$ is the azimuthally average wake deficit gradient and k_{wiener} is the Wiener constant. The value of the Wiener constant is selected based on the size of the atmospheric shear and the radial resolution of the DWM model, Δr_{DWM}. These properties are used to define the constant as they represent the magnitude of the nominator and the discretization error of the wake deficit gradient, which both influence the sensitivity of the eddy viscosity scaling factor

$$k_{wiener} = 2\frac{du}{dz_{ABL}} \cdot \Delta r_{DWM}^2. \tag{15}$$

The effect of the proposed corrections on wake turbulence in a simulation run with a wind speed of 8 m/s and turbulence intensity of 14% is shown in figures 6 and 7. Figure 6 shows the local amplification of the turbulent stress given by second term of eq. 13. As described above, the turbulent stresses are not scaled at locations where the wake deficit gradients are larger than the atmospheric gradient. This is shown in the figure by the dark core in the majority of the wake region for the first 12D downstream of the rotor. The atmospheric shear correction influences the turbulent stresses close to the centre axis of the wake and outside the wake shear layer relatively close to the rotor. As the wake deficit recovers and the strain-rate caused by the wake is reduced, an effect on the turbulent stresses near occurs throughout the whole wake deficit. The effect of the atmospheric shear correction on the turbulent stresses is shown in figure 7. The averaging is carried out from the centre of the wake to 3 D in radial direction. The effect of atmospheric shear on the turbulence level is small over the first 5 D downstream of the turbine. At 5 D, it starts to increase, reaching about 30% to 100% higher average turbulent stress levels in the region from 15 D to 40 D.

The computational time to find the wake deficit in the DWM model increases by ~15% by including the atmospheric shear contribution, from 2.25 to 2.64 seconds, when calculating the flow field over the first 15 D on a standard laptop. As the DWM model is designed to be used

with aero-elastic software, this increase in computational time is negligible compared to the time consumed by the aero-elastic software.

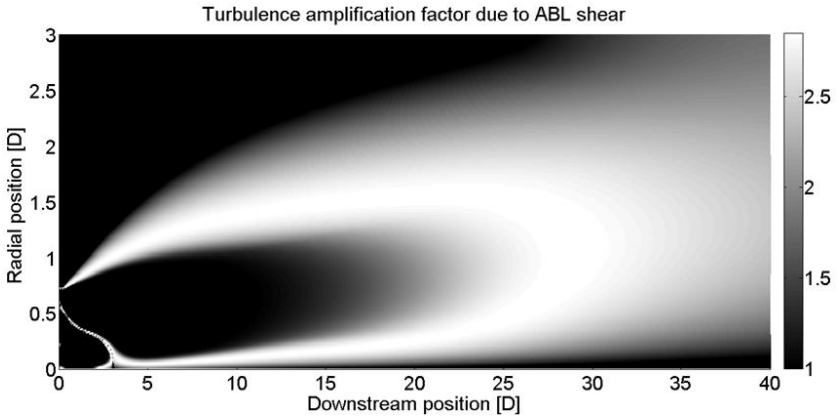

Figure 6, the local amplification of turbulent stresses caused by the atmospheric shear contribution, given by the second term of eq. (12) (i.e. $\frac{\frac{du}{dr_{Total}}}{\left|\frac{du}{dr_{DWM}}\right|}$), as a function of radial and downstream position. The x-axis of the figure lies on the centreline of the wake. The ambient wind speed for the displayed case is 8 m/s and the turbulence intensity is 14%.

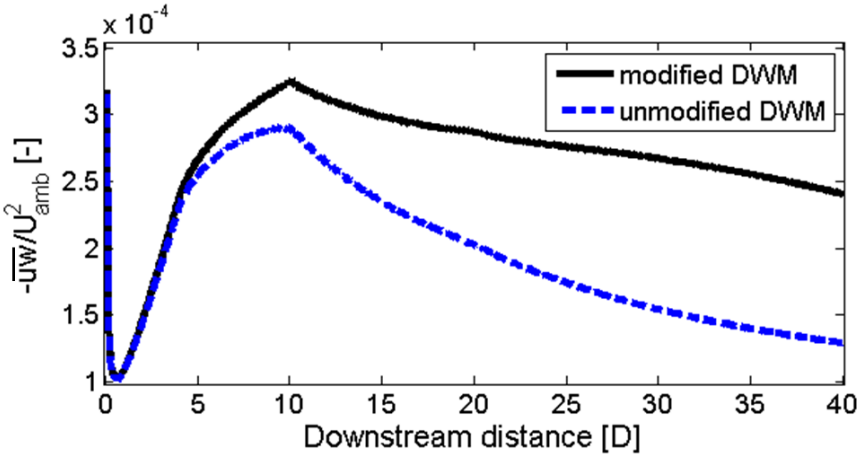

Figure 7, the normalized turbulent shear stress level, spatially averaged over the wake from the centre of the wake to 3 D in radial direction, as found by the unmodified DWM model (dashed blue line)and the shear corrected DWM model (solid black line)as a function of downstream position. The overbar operator refers to time averaging for the Reynolds stresses.

DWM calibration

After the atmospheric shear contribution to the turbulence stresses is implemented in the DWM model, a recalibration is required. This recalibration ensures that the newly implemented correction actually provides a better fit to higher-order CFD AL models (i.e., that more physics is captured), and to find the appropriate values for the model coefficients and the upstream boundary condition scaling parameters. The basis of the calibration is to minimize the average standard error (STE) of the DWM flow field compared to results extracted from Ellipsys3D AL simulations. The reason that the DWM model is calibrated to the EllipSys3D AL results, and not the OpenFOAM AL model, is that data from the EllipSys3D AL simulations are available in

planes covering the whole cross-section of the wake. Having planes of the data covering the wake cross-section enables calibration of the wake deficit formulation in the DWM model to be conducted in the MFoR, thus removing the influence of wake meandering. This procedure is described in keck et al. [17]. The STE is defined as the standard deviation in mean velocity between the actuator line and the DWM models

$$STE = \sqrt{\frac{1}{n_c}\sum_{c=1}^{n_c}\left[\frac{1}{n_{c,d}}\sum_{d=1}^{n_d}\left(\frac{1}{n_{c,d,r}}\sum_{r=1}^{n_{c,d,r}}\left(\bar{U}_{c,d,r}^{ACL}-\bar{U}_{c,d,r}^{DWM}\right)^2\right)\right]} \quad (16)$$

where the indexes *c*, *d*, and *r* correspond to cases (i.e., variations in inflow conditions), downstream distance and radial position, respectively. The constants, n_c, $n_{c,d}$, and $n_{c,d,r}$, represent the number of cases, number of cross sections, and number of data points per cross section, respectively. In this calibration, the constants are equal to six flow cases (wind speeds of 6 m/s and 10 m/s, turbulence intensities of 6%, 10% and 14%), five cross-sections for each case (3, 4.5, 6, 7.5, and 9 D behind the rotor) and 80 points per cross section (radial coordinates from the rotor centre to 1.6 R). The calibration is carried out in three steps, all based on the gradient-based simplex method of Lagarias et al. [23], which is also outlined in the Matlab User Guide [24].

Step 1: Calibrate the boundary condition

The DWM inlet boundary condition is calibrated to yield a velocity field as close as possible to the Ellipsys3D AL mean velocity field at 3 D behind the rotor. As discussed earlier, this is necessary in order to account for the effects of the omitted pressure gradient on the wake deficit development in the DWM model. The pressure gradient effects (expanding and reducing the velocity of the initial deficit caused by turbine induction) are captured by the scaled inlet boundary condition. The boundary condition is, therefore, a function of four model parameters: the inlet deficit modification parameters f_U and $f_{R,,}$ along with the eddy viscosity constants and the filter functions from 0–3 D, $k_1{*}F_{1,\,0\text{-}3D}$ and $k_2{*}F_{2,\,0\text{-}3D}$.

Step 2: Calibrate filter functions F_2

The F_2 filter function is included in the DWM model to govern the development of turbulence generated by the wake shear layer. Such a function is required, as the turbulence closure of the DWM model is a zero-equation eddy viscosity model. Because no transport equation is modelled, the turbulence is calculated based on the local mean flow gradient. The mean flow field over the rotor changes very abruptly, and steep mean flow gradients are created very close to the turbine. The turbulence, on the other hand, requires distance to reach equilibrium with the mean flow. In many cases, this is on the order of 6 to 10 D downstream of the turbine. This effect is captured by the F_2 function. The F_1 function is related to the treatment of the pressure field in the boundary conditions of the DWM model. The pressure field recovers in the first two rotor diameters downstream of the turbine. Therefore, no additional calibration is made to the F_1 function (see eq. (17)), which is assumed to follow the suggestion given in Madsen et al. [1].

The F_2 filter function is found by using the k_1, the f_U and f_R parameters from step 1, and running the simplex optimization to find the optimum value of $k_2{*}F_2$ at different downstream positions. The calibration is performed at 3, 4.5, 6, 7.5, and 9 D against single Ellipsys3D AL mean velocity cross sections. This yields the optimum value of $k_2{*}F_2$ at five locations in the wake. Since it is desired to have a smoothly increasing filter function that reaches unity in the far-wake, an F_2 filter function is constructed by fitting an exponential saturation function through the five points. The applied filter functions are given by eqs. (17) and (18), respectively, where *x* refers to the downstream position expressed in rotor diameters relative to the wake-emitting turbine. The F_1 filter function varies linearly from 0-1 over the first two diameters of flow to compensate for the boundary conditions treatment of the DWM model. The F_2 filter function consists of two parts; the first part is related to the boundary condition treatment, and the second part to the development of shear layer generated turbulence in the wake.

$$F_1 = \begin{cases} x/2 & x < 2D \\ 1 & x > 2D \end{cases} \quad (17)$$

$$F_2 = \begin{cases} 0.035 & x < 2D \\ 1 - 0.965e^{-0.35(x-2)} & x > 2D \end{cases} \quad (18)$$

Step 3: Global calibration of k_1, k_2, f_U and f_R
In this step, simplex optimization is performed on the four model parameters using the entire Ellipsys3D AL dataset with all cases and all cross sections, and also using the filter function found in step 2. The values k_1, k_2, f_U and f_R found previously, are used as initial conditions to the optimization algorithm. This step fine tunes these model parameters.

The STE with the atmospheric shear contribution to turbulence included is 5.3% smaller than for the existing DWM model, which is reduced from 0.017 to 0.016. This reduction is an indication that the atmospheric shear contribution does capture a relevant physical process of the wake dynamics and recovery.

Improved wake-added turbulence formulation
After including the contribution of the atmospheric shear gradient in the calculation of the turbulent shear stresses in the DWM deficit calculations, the far-wake stresses are maintained at realistic levels. This makes it is possible to formulate an expression for wake-added turbulence, which is consistent with the simplified Navier-Stokes solution that govern the velocity deficit. We propose that after including the correction for atmospheric turbulence, the wake-added turbulence at a downstream rotor should be based on turbulent shear stresses used in the wake deficit calculations of the upstream, oncoming wake. This would result in a more realistic build-up of turbulence intensity over a row of turbines, compared to using the ambient turbulence intensity level to prescribe the wake evolution, as is the current standard method. The most straightforward method for coupling the wake turbulence of the upstream rotor to the inflow of the downstream rotor is through the turbulence stresses of the oncoming wake. This requires the turbulent stresses in the deficit calculation to be expressed as a local estimation of the turbulence intensity before being applied in the DWM calculations for the next rotor. This can be achieved by approximating the turbulent stresses in the normal direction based on the turbulent shear stresses using the relation,

$$-\overline{u'w'} = u'_{rms} w'_{rms} \cdot C_{u'w'} \quad (19)$$

where $C_{u'w'}$ is the correlation coefficient between axial and radial velocity fluctuations, and u' and w' is the axial and radial fluctuations in the wake respectively. The over-bar denotes time averaging and the subscript *rms* refers to the root-mean-square of the fluctuating components over time. Rewriting the radial velocity fluctuations as,

$$w'_{rms} = \frac{w'_{rms}}{u'_{rms}} u'_{rms} \quad (20)$$

inserting eq. (20) into eg. (19) and rearranging the terms yields,

$$-\overline{u'w'} = u'_{rms} \cdot u'_{rms} \frac{w'_{rms}}{u'_{rms}} \cdot C_{u'w'}. \quad (21)$$

By using the fact that the axial fluctuations are perfectly correlated with themselves *(*i.e. $u'_{rms} u'_{rms} = \overline{u'u'}$*)*, eq. (21) can be arranged to estimate the streamwise component of the Reynolds stress as,

$$\overline{u'u'} = \frac{1}{C_{u'w'} \cdot (w'_{rms}/u'_{rms})} \cdot -\overline{u'w'}. \quad (22)$$

The correlation coefficient, $C_{u'w'}$, and the $\frac{w'_{rms}}{u'_{rms}}$ ratio of wake generated turbulence is different compared to atmospheric turbulence due to the higher degree of isotropy and short turbulent length scale. In this work, these properties have been given the values of 0.3 and unity, respectively, based on the findings of Larsen et al. [25]. Inserting the dimensionless DWM shear stresses into eq. (22) and taking the square root yields an approximation of the turbulence intensity in the DWM model (left term under the max-operator in eq. (23)). As the output of eq. (23) will be used to estimate the turbulence at downstream rotors in a FFoR, a correction is included to ensure that the turbulence intensity in the wake region always assumes a value that is equal or greater than the ambient turbulence intensity (TI_{amb}). This correction is required for two reasons: 1) to remove regions of low turbulence in the wake deficit (these exist at the wake axis due to symmetry effects on the mean gradient), and 2) to set the ambient turbulence value at all computational nodes outside of the wake deficit (where the deficit model does not contain any turbulent stresses) before adding the effect of wake meandering to find the turbulence at a downstream turbine. The effect of this correction can be seen in figures 8 and 9.

$$TI_{DWM\ MFoR} = \max\left(\sqrt{\frac{1}{C_{u'w'}\cdot(w'_{rms}/u'_{rms})}\cdot\tau_{stress\ DWM}}\ , TI_{amb}\right). \tag{23}$$

Eq. (23) yields a local value of wake turbulence intensity for each computational node in the DWM domain, $TI_{DWM\ MFoR}$. The DWM deficit module outputs the wind speed (eq. (1)) and turbulence distribution (eq. (23)) in the MFoR (i.e., without any large-scale movements). The meandering can be viewed as a series of wake segments in which the wake centre has a stochastic offset in lateral and vertical direction according to some statistical distribution. If this distribution of the meandering is known, it is possible to calculate the average wind field and turbulence intensity at the downstream rotor by calculating the convolution between the deficit (both wind speed and variance, i.e. the square of $TI_{DWM\ MFoR}$ from eq. (23)) in MFoR and the distribution of the wake centre in the vertical and lateral direction due to wake meandering as follows

$$\theta_{DWM\ FFoR} = \iint \theta(y - y_m, z - z_m)_{DWM\ MFoR}\cdot PDF_m(y_m, z_m)\, dy_m dz_m. \tag{24}$$

In this equation, θ represents the wind speed or variance distribution in the MFoR; y-y_m and z-z_m are the local coordinates in the MFoR; and PDF_m is the probability density function for the meandering distribution. In this work, a Gaussian distribution is used to describe the meandering of the wake deficit. The standard deviation of the wake deficit location in lateral and vertical direction is extracted from Ellipsys3D AL calculations, where the wake centre is taken to be the centre of gravity of the wake deficit in a plane perpendicular to the mean flow. The subscripts *FFoR* and *MFoR* refer to the fixed and meandering frame of reference. Eq. (24) results in a wind speed and variance distribution in FFoR.

Using the DWM model to conduct simulations over a row of wind turbines, the flow field in FFoR is used to find the turbulence intensity and velocity distribution to apply as “ambient conditions” at the downstream rotor. However, as the deficit calculation of the DWM model is based on an axisymmetric formulation, the flow field in FFoR needs to be transformed using eqs. (25) and (26), before it can be applied as boundary conditions at the subsequent rotor. The input velocity field to the wake-affected turbine is a function of radial coordinate (r), whereas the input turbulence intensity is a single number representing the mean value over a cross section of the wake (due to the eddy viscosity model, it is nontrivial to couple the turbulence distribution in the oncoming wake to the subsequent wake deficit evolution).

$$U_{axisym}(r) = \frac{1}{2\pi\Delta r}\int_0^{2\pi}\int_{r-\frac{\Delta r}{2}}^{r+\frac{\Delta r}{2}} U_{DWM\ FFoR}(y_{WTG} + r\cos(\alpha)\,, z_{WTG} + r\sin(\alpha))\, dr\, d\alpha \tag{25}$$

$$TI_{WTG} = \frac{1}{2\pi R_w}\sqrt{\int_0^{2\pi}\int_o^{R_w} TI^2_{DWM\ FFoR}(y_{WTG} + r\cos(\alpha)\,, z_{WTG} + r\sin(\alpha))\, dr\, d\alpha} \tag{26}$$

R_w is the initial width of the wake deficit in the DWM model and is calculated by eq. (5) by applying the rotor radius as r_{rot} value. The mean turbulence intensity level given by eq. (26) represents the mean turbulence intensity in the scales that affect the wake deficit evolution (roughly corresponding to eddies smaller than 2 D, according to Larsen et al. [4]). This is, therefore, the appropriate value to use when coupling the turbulence intensity of the wake to the downstream evolution of the wake-affected wind turbine. However, to find the total turbulence intensity at the downstream turbine (in FFoR), which is relevant to loads or when comparing to reference data, a contribution that is caused by the meandering of the mean velocity deficit needs to be included. This is referred to as the "apparent turbulence intensity",

$$TI_M(y,z) = \sqrt{\iint (U(y-y_m, z-z_m)_{MFoR} - U_{FFoR}(y,z))^2 \cdot PDF_m(y_m, z_m)\, dy_m dz_m} \quad (27)$$

where the first term can be thought of as the distribution of wind speeds at location *"y, z"* due to the meandering deficit and the second term represents the mean wind speed in FFoR. The contribution of eq. (24) and (27) can be considered as independent because of the split in scales, which means that the total turbulence intensity in FFoR can be found by eq. (24):

$$TI_{tot\ FFoR} = \sqrt{TI_M^2 + TI_{DWM\ FFoR}^2}\ . \quad (28)$$

A method for applying the DWM model to a row of wind turbines

An investigation using the DWM model, including the new formulation for atmospheric shear contribution and wake-added turbulence, was conducted for a case of eight turbines aligned with the wind direction. The goal of the investigation was to quantify the effect of the DWM model improvements on the power prediction along a row of turbines.

The first rotor experiences the ambient wind speed and turbulence intensity. For the downstream turbines, new inflow conditions need to be calculated using eqs. (24–26), and will include the wake deficit, wake meandering and an increased small-scale turbulence level. The resulting inflow conditions will be a function of the upstream turbine's operational characteristics, the ambient conditions, and the distance between the turbines.

The mean wind speed and turbulence intensity, eqs. (25) and (26), are used to find the appropriate induction and turbulent mixing in the eddy viscosity model for the downstream rotors. The mean wind speed as a function of radial position, given by eq. (25), is also used to keep track of the mean flow field over the entire row of turbines. The induction of the turbine (including the scaling of the deficit by f_U and f_R according to the DWM boundary condition according to eq. (4) and (5)) is linearly superimposed onto the oncoming averaged wind field. The resulting flow field is used as the inlet boundary condition in the DWM model deficit calculation, and is thus a combination of the incoming non-uniform wind and turbine induction. The same procedure is used at the subsequent rotors in the row.

Using this method, both the reduction in mean wind and the increase in turbulence intensity are being built up over the row of turbines. It is, however, assumed that the scale of the increased turbulence in the wake deficit is sufficiently small to avoid affecting the large-scale wake meandering. Therefore, the meandering statistics are not changed over the row of turbines, and are maintained based on the larger scale fluctuations in the ambient winds for all turbines in the row.

The implementation of the DWM model used to investigate the effects of the atmospheric shear contribution to turbulence and the build-up of turbulence over a row of turbines is not coupled to an aero-elastic software. Therefore, power is estimated directly from the oncoming flow field. Because the instantaneous power production is a function of the cube of the local wind speed (below rated power), the time averaged wind speed field cannot be used directly for power estimations. To account for dynamic effects on power production due to partial wake operations

caused by meandering, or the wind direction not being perpendicular to the row of turbines, a separate velocity field for power estimation is calculated using the equation

$$U_{power\ FFoR} = \sqrt[3]{\iint U^3(y - y_m, z - z_m)_{DWM\ MFoR} \cdot PDF_m(y_m, z_m)\, dy_m dz_m}, \quad (29)$$

where again y-y_m and z-z_m are the local coordinates in the MFoR and PDF_m is the probability density function for the meandering distribution. $U_{power\ FFoR}$ is the cube root of the mean value of the cube of the wind speed field in the FFoR. When this quantity is applied for power estimation, the effect that instantaneous power production is based on the local wind speed to the power of three is captured. By applying $U_{power\ FFoR}$ in eq. (25) an expression for the velocity field for power estimation as a function of radial position, $U_{power}(r)$, is found. The power production of the turbines may then be estimated using the equation,

$$P_{WTG} = \int_0^R \left[(4a(r) \cdot (1 - a(r))^2) \cdot \frac{1}{2} U_{power}^2(r) \cdot U_{power}(r)\, 2\pi r\, dr \right] \cdot f_{mek} \quad (30)$$

where $a(r)$ is the azimuthally averaged rotor induction. The first term under the integration is an estimation of the coefficient of power, C_p, followed by the kinetic energy per unit mass at the rotor, mass flow, and a factor for system losses from mechanical power to electricity (f_{mek} is estimated to be 0.9). Note that $a(r)$ refers to the average turbine induction and is not scaled by f_U and f_R, as in the DWM model boundary condition.

Results and Discussion

Validation of wake turbulence based on DWM model-predicted Reynolds stress

The method described by eqs. (19–23) for estimating the turbulence intensity in the wake of the DWM model based on the turbulent stresses is validated by comparing the mean turbulence intensity in the wake as a function of downstream distance to the Ellpisys3D AL model calculations of Keck et al. [17]. Because the DWM model deficit equation is designed to handle the wake deficit development without meandering, it is compared to AL data in the MFoR, (i.e. following the centre position of the wake deficit).

In the first analysis, the turbulence intensity found by eq. (23) was investigated without including the correction to ensure that the local turbulence intensity is always equal to or larger than the ambient turbulence intensity (i.e., using only the left term under the max operator of eq. (23)). This term represents the turbulent stresses that act on the wake deficit in the DWM model. The results in figure 8 show the mean turbulence intensity over a cross section of the wake as a function of downstream distance.

Figure 8 shows the effect of including the ABL shear contribution in the eddy viscosity calculation of the DWM wake deficit for three different ambient turbulence intensities: 6% (A), 10% (B) and 14% (C). All cases conducted for a single wind turbine with a rotor diameter of 80 m, operating in neutral stratification with a mean wind speed of 8 m/s. The figure show that the inclusion of the ABL shear contribution results in a higher mean turbulence level in the wake of the DWM model, relative to the unmodified DWM model. The effect is larger for higher turbulence intensity as the ABL shear gradient increases with turbulence intensity under neutral stratification. Compared to the unmodified DWM version, the turbulence predictions of the modified DWM model agree better with the AL reference data. The largest improvements are seen in the far-wake region (where the wake deficit shear is small) and the effect increase with increasing ambient turbulence intensity (as the ABL shear increases). The modified DWM model slightly over-predicts the turbulence intensity between 4 and 6 D behind the rotor. The over-prediction is on the order of 0.5–1.0 percentage points (pp, i.e. ΔTI). The far-wake turbulence agrees well for the 6% and 10% cases (A and B), but is underpredicted for the 14% case (C). At 10–12 D, the turbulence intensity of the 14% case is underpredicted by ~2.5pp.

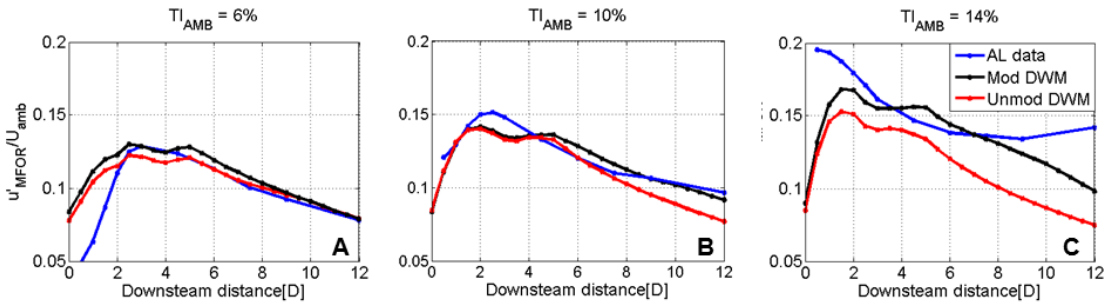

Figure 8a-c, the effect of the atmospheric shear correction on the mean turbulence intensity of wake in the meandering frame of reference as function of downstream distance from the wake-emitting turbine and ambient turbulence intensity. The wake turbulence evolution of the DWM models is compared to that of the EllipSys3D AL model for a turbine operating in ambient turbulence intensities of 6% (A), 10% (B) and 14% (C).

As mentioned earlier, before coupling the turbulence intensity estimation to calculate the average turbulence intensity at the downstream turbine, the low turbulence regions are corrected by the ambient turbulence intensity (right term of eq. (23)). These low turbulence intensity regions in the DWM model exist at a location where the velocity gradient of the deficit is close to zero. The turbulence in these regions will become low, as there is no transport equation for turbulent stresses in the DWM model, and the ABL shear correction will not have full effect due to a Wiener filter (included for numerical stability). To avoid having these effects influence the intra-turbine wake turbulence coupling, eq. (23) ensures that the minimum wake turbulence is equal to the ambient turbulence intensity level. Applying this correction yields the results presented in figure 9 for the modified DWM model. The main difference occurs in the far-wake region at high turbulence intensities, where the deviations are significantly smaller than in figure 8, and allows for a more realistic coupling of turbulence intensity to the downstream turbines.

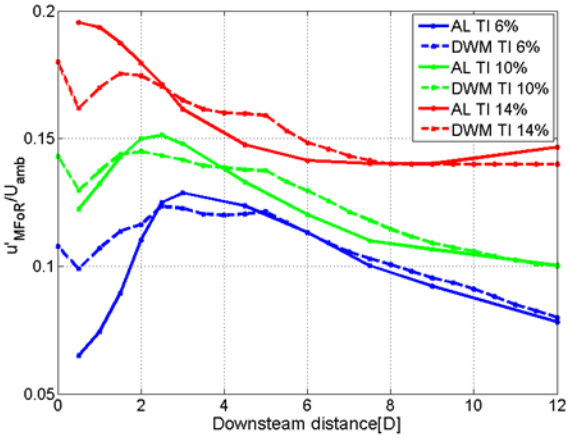

Figure 9, the DWM (dashed lines) and the Ellipsys3D AL (solid lines) model-predicted turbulence intensity in the meandering frame of reference as a function of downstream distance from the wind turbine.

The effect of the proposed DWM model improvements

The influence of the proposed atmospheric shear contribution and turbulence build-up is examined by simulating flow through a row of eight wind turbines. The wind speed is 8 m/s, the

turbulence intensity is 6% and the mean flow direction is along the row of turbines. We studied two different turbine spacings: 6D and 10 D.

Figure 10 shows the effect on power output of the individual turbines as the various effects in the DWM model are enabled and disabled. By comparing the power output for the row of turbines when all DWM effects are enabled (black solid lines) to the output if turbulence build-up is not considered (dot-dashed black lines), it is apparent that the effect of turbulence build-up is sensitive to turbine spacing. At 6 D spacing, turbulence build-up has an effect on the wake loss that is twice as large as the effect of wake meandering, but with 10 D spacing, the effect is only about 55% of that caused by wake meandering. The effect on power caused by the atmospheric shear contribution to turbulence is about 5% and 20% of the effect of wake meandering at 6 D and 10 D, respectively. Compared to the total power losses due to wake effects of the unmodified DWM model, the inclusion of wake-added turbulence and turbulence build-up over the row of turbines reduced the predicted wake losses by 9% for the 6 D case and 6% for the 10 D case. The atmospheric shear contribution to turbulence in the DWM model further reduced the power loss by about 0.8% at 6 D spacing and 1.5% for the 10 D case.

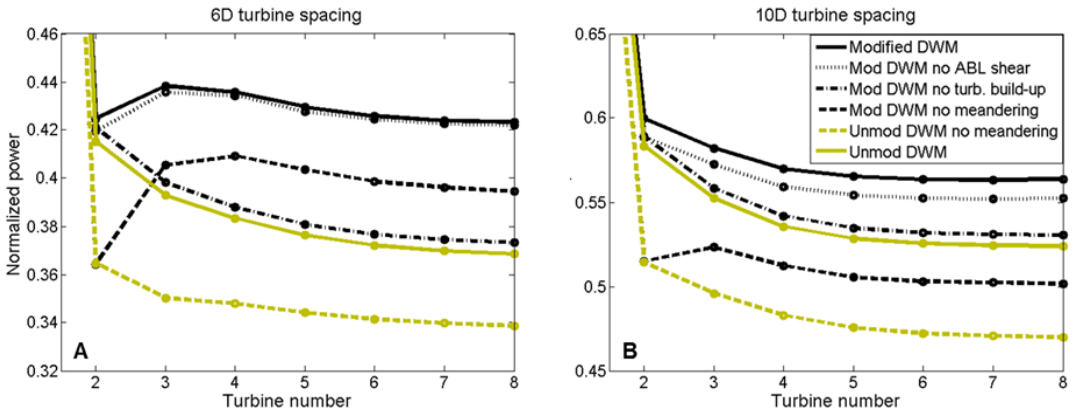

Figure 10a and b, illustrates the individual effect of the DWM model functionalities by showing the predicted power output of eight wind turbines operating in a row aligned with the mean wind direction at 6 D (A) and 10 D (B) spacings with various effects enabled.

Table 1, the development of turbulence intensity and wind speed over the row of wind turbines with the proposed atmospheric shear effect and wake turbulence build-up. The ambient conditions for both cases were 8 m/s wind speed and 6% turbulence intensity.

Mean wind speed [m/s]

	WTG 1	WTG 2	WTG 3	WTG 4	WTG 5	WTG 6	WTG 7	WTG 8
6D	8.00	5.90	6.00	6.00	5.97	5.95	5.95	5.95
10D	8.00	6.65	6.62	6.57	6.55	6.54	6.54	6.54

Turbulence intensity [%]

	WTG 1	WTG 2	WTG 3	WTG 4	WTG 5	WTG 6	WTG 7	WTG 8
6D	6.0	12.1	13.4	13.9	14.3	14.5	14.6	14.7
10D	6.0	9.7	10.1	10.3	10.4	10.5	10.6	10.6

These findings show that the proposed DWM model improvements have significant effects on the DWM deficit development. They not only influence the wake turbulence (which is the direct effect), but they also affect the mean wind speed and thereby power predictions. Table 1 shows the development of turbulence intensity and wind speed along the rows for the two presented

cases. The results suggest that an equilibrium wind speed is reached already at the second or third turbine inside the park. The turbulence requires much longer to become fully developed, and an equilibrium value is not reached before the fifth or sixth turbine. This suggests that an approach in which only the nearest upstream wake deficit affects a given turbine might be an acceptable simplification. However, for an accurate turbulence representation, the influence of more upstream wakes should be considered.

Lillgrund wind farm

The performance of the suggested DWM improvements are tested against field data and OpenFOAM AL results for the offshore Lillgrund wind farm. The power production of the Lillgrund wind farm is estimated by both the unmodified and the modified DWM models and compared to the field data presented by Dahlberg [26] and the OpenFOAM simulations of Churchfield et al. [27]. The wind speed and turbulence fields of the DWM models were compared to the OpenFOAM data, and agreement between the two models was evaluated by using eq. (16).

To simulate the Lillgrund wind farm with the DWM model, the rotor induction for the turbines is required. Since this information is not publically available, an approximate rotor description was developed based on the publically available power curve and blade profile family. This rotor description is used in the OpenFOAM AL simulation of the wind farm. The induction vector used in the DWM model for the Lillgrund turbines is based on the time-averaged velocity field at the rotors in the OpenFOAM simulation. First, the velocity field at the rotor is time-averaged and transformed from the Cartesian grid to a vector of axisymmetric values. Then, the azimuthally averaged induction vectors required by the DWM model are found by dividing the axisymmetric velocity vector at the rotor by the oncoming wind speed. For the first rotor, the ambient wind speed is used. For the wake-affected turbines, the oncoming wind speed is found by running a DWM simulation for a single rotor, and calculating the mean wind speed at the location of the downstream turbine using eqs. (21) and (22).

The layout of the Lillgrund wind farm is shown in figure 11a. The analysis presented in this article is performed for rows B (turbines 15-8) and D (turbines 30–24). Row B contains eight wind turbines that are equidistantly spaced 4.4 D apart. Row D contains seven wind turbines separated by 4.4 D; however, the turbine that would have been the fourth in this row was omitted from the actual wind farm because the water depth is too shallow to allow access by construction boats, so there is an 8.8-D gap between turbines 28 and 27.

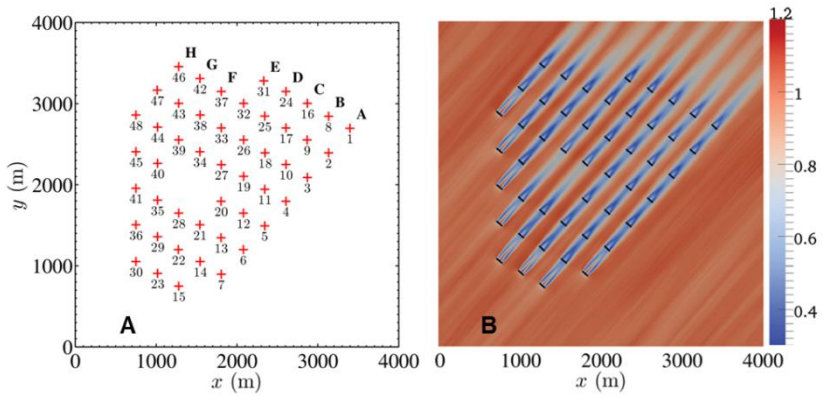

Figure 11a and b, layout of Lillgrund wind farm (A), and mean wind speed distribution from the OpenFOAM simulation at a hub height of 65 m (B).

The simulations are run in a neutral atmosphere (although there is a stable capping inversion at roughly 800 m above the surface), with a mean wind speed of 9 m/s and a turbulence intensity of 6.2%. The mean flow direction is perpendicular to the rows. The OpenFOAM data is based

on a full-scale simulation of the entire wind farm. The duration of the AL simulation is a trade-off between computational cost and uncertainty in the resulting flow field. As a "standard" AL simulation over the wind farm requires on the order of 500,000 CPU-hours to simulate the flow field for a 10 minute period, the simulations times were required to be kept around 10 minutes to maintain acceptable time consumption with the computational resources available. As shown in figure 11b, a consequence of the relatively short simulation time is that the average wind speed approaching the turbines was not entirely uniform in the whole domain. In the figure, streaks of lower (higher) mean wind speed are seen as lighter (darker) areas. An example of a low-velocity streak that could have some influence on the results is hitting turbine 15 (i.e., the first turbine of row B). This inhomogeneity of the incoming flow field should be seen as a source of uncertainty on the order of 0.165 m/s in terms of wind speed and 0.53pp in terms of turbulence intensity. This corresponds to the spatial standard deviation of the average wind speed and turbulence intensity upstream of the wind farm.

A second term of uncertainty due to the short averaging time is the misalignment of the wake deficits, relative to the mean wind direction, due to the stochastic wake meandering, see figure 12. This uncertainty component, $\sigma_{misalignment}$, is estimated using eq. (31),

$$\sigma_{misalignment} = \frac{\sigma_M \frac{d\theta}{dr}}{\sqrt{n}} \tag{31}$$

where n is the number of independent samples of wake centre position, σ_M is the wake meandering given as the standard deviation of the wake centre position, and $\frac{d\theta}{dr}$ is the radial gradient of the studied parameter (for this application axial velocity or turbulence intensity). An estimation of the uncertainty is obtained by assuming: 1) 100 independent samples of wake centre position over the 10 minute simulations, 2) a representative standard deviation of the wake centre position equal to 11.2meters (based on simulations by Keck et al. [17]), 3) a wake velocity gradient of 0.06 m/s per m and turbulence intensity gradient of 0.25 pp per meter. Applying these numbers is eq. (31) yields an uncertainty of 0.067m/s in terms of wind speed and 0.28pp in terms of turbulence intensity. However, the average wake deficit and turbulence profiles due to the turbines are still on an order of magnitude larger than the combined uncertainty caused by the low averaging time, which allowed for a high-quality comparative analysis.

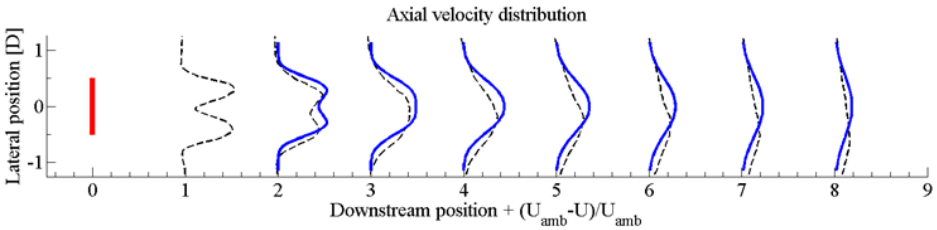

Figure 12: The misalignment of the mean wake deficit of the DWM model (solid lines) and the AL model (dashed lines) behind the first turbine due to relatively short AL simulation times. For the presented case, this misalignment is the main contributor to the resulting STE.

The uncertainty in terms of power production is based on the combined root-square sum (RSS) of the abovementioned sources of uncertainties in wind speed (which is equal to 0.178 m/s). The uncertainty in the power production is estimated as the ratio of power production based on the mean wind plus the combined uncertainty of the wind speed, to power production based on the mean wind speed alone. This yielded an uncertainty in power production of 6%.

By comparing the power production estimates presented in figure 13, we see that the unmodified DWM model (red lines) predicts lower power production under multiple wake

conditions compared to the modified DWM model (black lines). This prediction is expected, as the turbulence build-up in the modified DWM model will lead to a faster wake recovery. Compared to the OpenFOAM AL model (green lines) and the field data (blue lines), the unmodified DWM model underpredicts power production of the row of turbines.

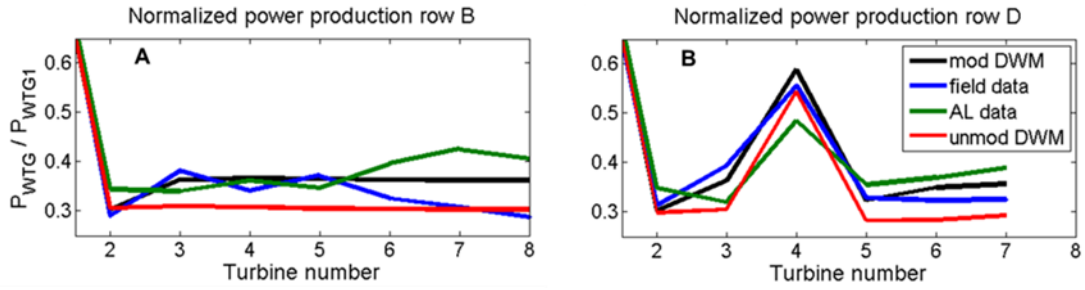

Figure 13a and b, power production of the wake-affected turbines at row B (A) and D (B) at the Lillgrund wind farm. The green lines are OpenFOAM results, blue lines are field data, and black and red lines are the DWM prediction with the modified and unmodified versions, respectively.

In general, the power prediction made by the modified DWM model agrees with the OpenFOAM AL model and the field data. The main deviation seen is the power estimation for the fourth turbine in row D, i.e., the turbine with a larger separation to the upstream turbine, where the DWM model increases slightly more than the OpenFOAM AL model and the field data. We also see that both the modified DWM model and the OpenFOAM AL model overpredict power production for the last three turbines in the rows, compared to the field data. A likely explanation for these deviations is that the field data contain some effect that is not included in the numerical simulations. The DWM model code was run with the same input as the OpenFOAM simulation, which was a neutrally stratified atmosphere with a wind speed of 9.0 m/s and a turbulence intensity of 6.2%. Although the simulations matched the observed average inflow wind speed and turbulence intensity for this wind direction, the difference in predictions for the rear of the wind farm may be caused by the fact that the field data was collected over many months. Over that time period, there was undoubtedly a range of atmospheric stability and wind speed, unlike in the fixed condition simulations. This range may affect the wake propagation and power production. The field data is only binned by wind direction at the first turbine and wind speeds outside of the turbines' region 2 (in which wake effects are maximum) are not included in the average.

Table 2 gives a quantitative analysis of the differences in mean wind speed and turbulence intensity distribution over the two rows of turbines. The table shows the STE between the OpenFOAM AL model and the DWM models calculated based on the mean flow field according to eq. (16). The values in the table are based on a single case of ambient conditions: wind speed of 9 m/s and turbulence intensity of 6.2%. For all turbines, data were collected at the cross sections located 3 and 4 D downstream of the rotor, apart from turbine 3 in row D (i.e., turbine 28 in figure 11a) where data were collected at 3, 4, 5, 6, 7, and 8 D behind the rotor. This is due to the longer undisturbed wake evolution of turbine 28. The data at used in the flow field analysis were collected from along a lateral line at hub height at each cross section. The line was 3.2 D of length, oriented perpendicular to the mean flow direction and centred on the axis of the turbine (thus extending 1.6 D in lateral direction from the mean wake centre).

Table 2, the STE in terms of mean wind speed and turbulence intensity level as a function of turbine position for the modified DWM and unmodified DWM models compared to the OpenFOAM Al model. The values are found using eq. (16) and the analysis is carried out for row B (left table) and D (right table).

	STE WS unmod DWM [m/s]	STE TI unmod DWM [%]	STE WS mod DWM [m/s]	STE TI mod DWM [%]
WTG 1	0.38	2.11	0.38	2.11
WTG 2	0.51	2.39	0.46	1.81
WTG 3	0.63	2.88	0.40	1.93
WTG 4	0.69	3.48	0.47	2.21
WTG 5	0.80	3.41	0.48	1.78
WTG 6	0.86	2.80	0.55	2.02
WTG 7	0.98	3.21	0.69	1.83
WTG 8	1.02	4.24	0.61	1.18
Mean	**0.73**	**3.07**	**0.51**	**1.86**

	STE WS unmod DWM [m/s]	STE TI unmod DWM [%]	STE WS mod DWM [m/s]	STE TI mod DWM [%]
WTG 1	0.60	2.10	0.60	2.15
WTG 2	0.46	1.70	0.43	1.28
WTG 3	0.20	1.54	0.17	1.05
WTG 4	0.55	2.67	0.40	1.50
WTG 5	0.65	3.01	0.43	1.55
WTG 6	0.71	3.62	0.44	1.70
WTG 7	0.68	3.38	0.32	1.88
Mean	**0.55**	**2.58**	**0.40**	**1.59**

The two leftmost columns in the tables are the STE between the OpenFOAM AL model and the unmodified DWM model, and the two rightmost columns represent the OpenFOAM AL results compared to the modified DWM model. The table shows that the STE, in terms of mean wind speed, is reduced from 0.73 m/s to 0.51 m/s for row B (31.1%), and 0.55 m/s to 0.40 m/s for row D (27.4%). The reduction in STE for turbulence intensity for row B is 3.07 pp to 1.86 pp (39.4%), and 2.58 pp to 1.59 pp (38.4%) for row D. Excluding the first turbine, the reduction in STE for waked turbines is found to be 31.8% for wind speed and 43.5% for turbulence intensity, by applying the proposed correction to the DWM model. The STE number should be evaluated with the uncertainty of the AL data in mind. As discussed earlier, the uncertainty of the AL simulations, which is caused by the relatively short simulation times, will increase the STE linearly. The uncertainty, 0.178 m/s and 0.60 pp for turbulence intensity, could therefore be considered to be the cause of ~39% of the discrepancies in wind speed profiles and ~35% for the turbulence intensity profiles over the rows of turbines.

Note that the STE for the modified DWM model does not increase significantly as a function of turbine position in the row. In fact, the combined STE of the first turbines is actually higher than the mean for the entire row, considering both wind speed and turbulence intensity. The unmodified DWM model has a clear trend of increasing STE numbers with turbine position. Furthermore, by comparing the STE of WTG3 in row D (i.e., the turbine with the longer undisturbed wake) to the STE of the other turbines, the DWM model agrees better with the AL model at larger downstream distances. The main reason for the increased agreement at downstream is that the gradients of the deficit are smaller, so the comparison is less sensitive to misalignment of the wake centre or difference in the wake width.

The improved agreement between the modified DWM model and the OpenFOAM AL model is also illustrated by showing the turbulence intensity, figure 14, and mean velocity, figure 15, at cross-sections located 2D, 3D and 4D downstream of turbine 1, 5 and 8 in row B of the Lillgrund wind farm. From the top row of panels (A, B and C), it can be seen that the suggested DWM modifications has little effect on the flow field in a single wake. This is due to the short distances and low turbulence intensity (6.2%), which means that the ABL shear correction has little effect, and since it is the first turbine of the row the turbulence build-up does not affect the solution.

The middle row of panels (D, E and F) shows that the DWM modification improves the agreement both in terms of wind speed and turbulence intensity when studying the wake after the fifth turbine. In terms of turbulence intensity, figure 14 shows that the unmodified DWM model (dashed red lines) under-predicts the turbulence in the wake centre and outside of the wake shear layer, but over-predicts turbulence intensity of the wake shear layer compared to the AL model. The modified DWM model (solid black lines) over-predicts the turbulence levels in the wake shear layer slightly more than the unmodified model, but overall captures the turbulence level outside of the “peaks” well. The average turbulence intensity level predicted by

the modified DWM model is therefore closer the AL model results. The middle row of figure 15, shows that the increased turbulence level of the modified DWM model results in a fast recovery, which is closer to that of the AL model. Both DWM implementations over-predict the depth of the deficit in the centre region, and under-predict the width of the wake deficit relative to the AL model results.

The bottom row of panels (G, H and I) shows the same that the same trends as previously discussed panels (D, E and F). The main differences are that both DWM implementations captures turbulence intensity of the wake shear layer better, and that both implementations over-predict the depth of the wake deficit slightly more after the eighth turbine.

It is worth noticing that the wind speed and turbulence fields of the DWM models, compared to the OpenFOAM AL flow fields, also agree fairly well at 2 D (panels A, D and G). This observation suggests that the pressure effects of the upstream rotor are small in that region, and that DWM could be valid down to 2 D. The STE at 2 D, however, is roughly four times larger than the STE at 3 D.

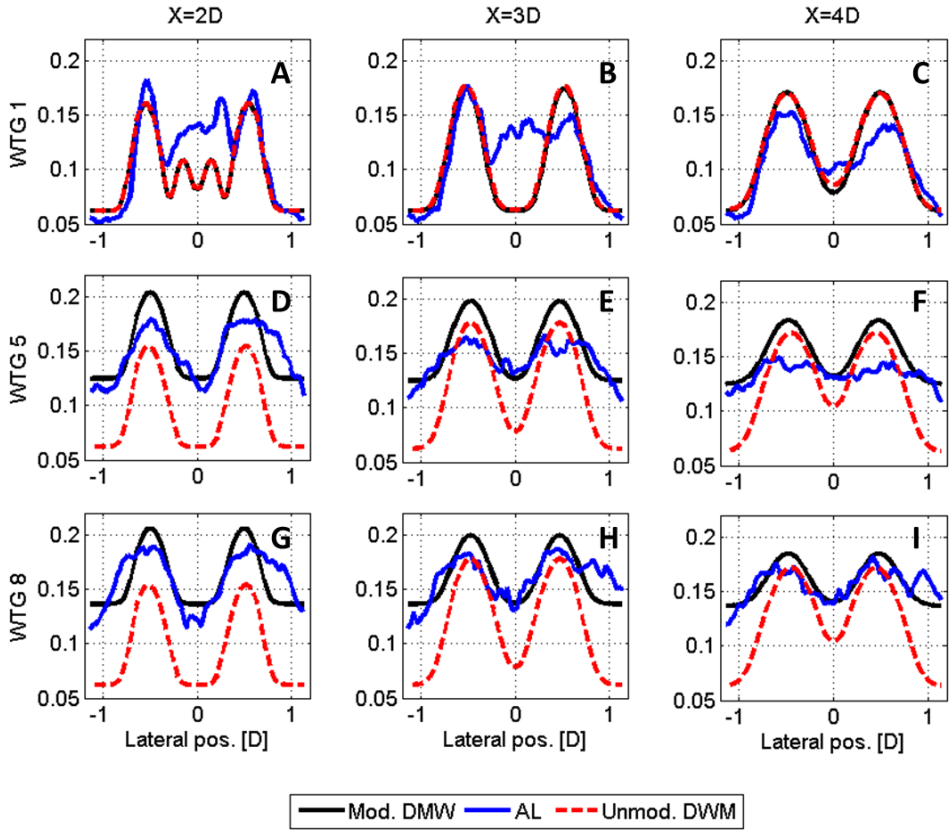

Figure 14a - i, the lateral turbulence intensity distribution at hub height of the OpenFOAM model (blue lines), the modified (black lines) and unmodified (dashed red lines) DWM models. The presented data is extracted 2D (left column), 3D (middle column) and 4D (right column) behind the 1st (top row), 5th (middle row) and 8th (bottom row)over row B of the Lillgrund wind farm.

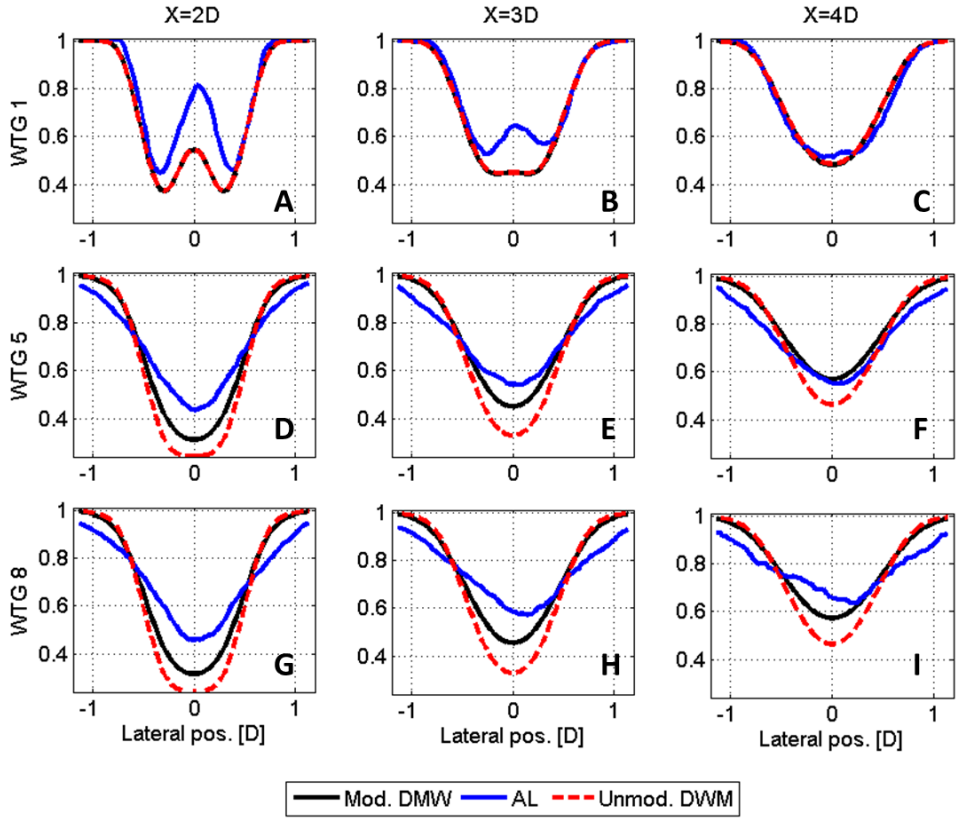

Figure 15a - i, the lateral mean velocity distribution at hub height of the OpenFOAM model (blue lines), the modified (black lines) and unmodified (dashed red lines) DWM models. The presented data is extracted 2D (left column), 3D (middle column) and 4D (right column) behind the 1st (top row), 5th (middle row) and 8th (bottom row)over row B of the Lillgrund wind farm.

Conclusion

This article presents a method to include the effect of the vertical atmospheric wind shear in the wake deficit calculation of the dynamic wake meandering (DWM) model. The main motivation behind the development is that, without the influence of the atmospheric shear, the turbulent stresses used in the DWM model wake deficit diffusion term will be too low in the far-wake region because the wake deficit gradient alone does not yield the representative strain-rate of the local velocity field. As a consequence of the improved far-wake turbulence description, the investigators have also proposed a physically consistent method for modelling the evolution of turbulence over a row of wind turbines.

After investigating the effect on the mean wind field, turbulence distribution, and power predictions by the proposed modifications, we conclude that the build-up of wake-added turbulence over the row of turbines and, to a lesser extent, the atmospheric shear contribution to wake turbulence, are significant contributors to the wake recovery process.

The modified DWM model was calibrated based on results from the Ellipsys3D AL model. The calibration was performed by varying the DWM model coefficients, based on a simplex optimization algorithm, to achieve the best agreement between the mean velocity field of the DWM model and the Elllipsy3D AL model. The azimuthally averaged velocity field in cross sections located 3 rotor diameters (D), 4.5 D, 6 D, 7.5 D, and 9 D downstream of the turbine,

from cases with ambient wind speeds of 6 m/s and 10 m/s, and turbulence intensities of 6%, 10%, and 14%, were used in the calibration. The average normalized deviation between the resulting velocity fields of the two models for all tested cases and cross sections was 0.0162.

The performance of the modified DWM model was evaluated by comparing the results of the DWM models to the results of the OpenFOAM AL model. It was shown that using the modified DWM model resulted in a reduction of the STE between the DWM model and the OpenFOAM AL model. The reduced mean difference in wind speed was on the order of 30%, and the reduced mean difference in turbulence intensity was on the order of 40% for a row of eight turbines. It was also shown that the standard error (STE) in wind speed and turbulence intensity between the OpenFOAM AL model and the modified DWM model does not increase over a row of turbines compared to the STE seen for a single turbine.

With the proposed model correction, the DWM model now contains a physically consistent method for modelling the development of the wind speed and turbulence field as the wind flows through a row of turbines in a wind farm. As the flow field is physically modelled, the DWM model can be used to extract both loads and power estimations from the same model (this is a capability that other engineering models in the wind industry are lacking). This capability, as well as the fact that the computational speed of the DWM model is maintained at sufficiently low levels to enable design calculations, allows wind farm or wind turbine designers to optimize the performance of both power production and loads simultaneously. Ultimately, this could enable the development of a comprehensive wind farm design philosophy and better wind farm control algorithms.

References

[1] Madsen, H.Aa., Larsen, G.C., Larsen, T.J., Troldborg, N. and R. Mikkelsen, Calibration and validation of the Dynamic Wake Meandering model implemented in the aeroelastic code HAWC2. Journal of Solar Energy Engineering, Volume 132, Issue 4, 041014 (14 pages), 2010.

[2] Ainslie, J.F. Calculating the flow field in the wake of wind turbines. Journal of Wind Engineering and Industrial Aerodynamics, 27, pp. 213-224, 1988.

[3] Ainslie, J.F., 1986, Wake modelling and the prediction of turbulence properties. Proceedings of the 8th British Wind energy Association Conference, Cambridge 19-21 March 1986. pp. 115-120.

[4] Larsen, G.C., Madsen, H.Aa., Thomsen, K. and Larsen, T.J., 2008, Wake meandering – a pragmatic approach, Wind Energy **11**, 377-395, 2008.

[5] Madsen, H.A., Larsen, G.C., and Thomsen, K. (2005). Wake flow characteristics in low ambient turbulence conditions. In: proceedings of Copenhagen Offshore Wind 2005.

[6] Madsen, H.Aa., Larsen, G.C., Larsen, T.J., Mikkelsen, R., and Troldborg, N. (2008). "Wake deficit-and turbulence simulated with two models compared with inflow measurements on a 2MW turbine in wake conditions," In: Scientific proceedings. 2008 European Wind Energy Conference and Exhibition, Brussels (BE), 31 Mar - 3 Apr 2008. p. 48-53.

[7] Sanderse, B. Aerodynamics of wind turbine wakes – literature review. Technical Report ECN-E-09-016, ECN, Netherlands, 2009.

[8] Keck, RE., Veldkamp, D., Madsen, H.Aa., Larsen, G.C., Implementation of a Mixing Length Turbulence Formulation Into the Dynamic Wake Meandering Model, Journal of Solar Energy Engineering, Volume 134, Issue 2, 021012 (13 pages), 2011.

[9] Sørensen, J.N. and Shen, W.Z. Numerical modelling of Wind Turbine Wakes. Journal of fluids Engineering, Volume 124, Issue 2, pp. 393-399, 2002.

[10] Sørensen, N.N. General Purpose Flow Solver Applied to Flow over Hills, Ph.D. thesis, Risø-R-827(EN), 1995.

[11] Mikkelsen, R., Actuator Disc Methods Applied to Wind Turbines, MEK-FM-PHD 2003-02, Technical University of Denmark, 2003.

[12] Troldborg, N., Actuator Line Modeling of Wind Turbine Wakes, MEK-FM-PHD 2008-06, Technical University of Denmark, 2008.
[13] OpenFOAM, Ver. 2.0.x, Silicon Graphics International Corporation (SGI), http://www.openfoam.org/git.php.
[14] Churchfield, M.J., Lee, S., Michalakes, J., and Moriarty, P.J., A Numerical Study of the Effects of Atmospheric and Wake Turbulence on Wind Turbine Dynamics, Journal of Turbulence, Vol. 13, No. 14, 2012.
[15] Mikkelsen, R., Sørensen, J.N. and Troldborg, N., Prescribed Wind Shear Modelling Combined with the Actuator Line Technique. In proceedings of the 2007 EWEC conference, Milan, 2007.
[16] Troldborg, N., Sørensen, J.N. and Mikkelsen, R., Actuator Line Simulation of Wake of Wind Turbine Operating in Turbulent Inflow. Journal of Physics: Conference Series. The Science of Making Torque from Wind. Technical University of Denmark, Lyngby, August 2007.
[17] Keck RE., Mikkelsen R., Troldborg N., de Maré M. and Hansen K.S.," Synthetic Atmospheric Turbulence and Wind Shear in Large Eddy Simulations of Wind Turbine Wake," accepted for publication April 2013, WE-1631.
[18] Mann, J. The spatial structure of neutral atmospheric surface-layer turbulence. Journal of Fluid Mechanics, 273, 141-168, 1994.
[19] Mann, J. Wind field simulation. Probabilistic Engineering Mechanics, Vol. 13, No. 4, pp. 269-282, 1998.
[20] Keck RE., de Maré M., Churchfield, M.J., Lee, S., Larsen, G.C., and Madsen, H.Aa.,"On Atmospheric Stability in the Dynamic Wake Meandering Model", re-submitted after minor revision Journal of wind energy June 2013, WE-13-0020.R1.
[21] Ratto, C.F., Section 1, in Modelling of Atmospheric Flow Fields, International Atomic Energy Agency, Vienna, Austria, 1996, pp. 16–18.
[22] Gonzalez R.C., Woods R.E., Digital image processing, Addison-Wesley Reading Mass., 1992
[23] Lagarias, J. C., J. A. Reeds, M. H. Wright, and P. E. Wright. "Convergence Properties of the Nelder-Mead Simplex Method in Low Dimensions." *SIAM Journal of Optimization*, Vol. 9, Number 1, 1998, pp. 112–147.
[24] Matlab User Guide, topic "Optimizing Nonlinear Functions."
[25] Larsen, G.C., Madsen, H.Aa., Larsen, T.J. and Troldborg, N., Wake modeling and simulation. Risø-R-1653(EN). Risø National Laboratory, Technical University of Denmark, Roskilde, Denmark, 2008
[26] Dahlberg, J.-Å., "Assessment of the Lillgrund Wind Farm: Power Performance Wake Effects," [online report] Vattenfall Vindkraft AB, 6_1 LG Pilot Report, Sept. 2009, URL:
[27] Churchfield, M.J., Lee, S., Moriarty, P.J., Martinez, L.A., Leonardi, S., Vijayakumar, G., Brasseur, J.G., A Large-Eddy Simulation of Wind-Plant Aerodynamics, AIAA paper 2012-537, 50th AIAA Aerospace Sciences Meeting, Nashville, TN, Jan. 2012.

IV: On Atmospheric Stability in the Dynamic Wake Meandering Model

On Atmospheric Stability in the Dynamic Wake Meandering Model

Rolf-Erik Keck[1,2], Martin de Maré[1,2], Matthew J. Churchfield[3], Sang Lee[3], Gunner Larsen[2] and Helge Aagaard Madsen[2]

[1] Rotor Systems, Vestas Wind Systems A/S, DK-4000 Roskilde, Denmark
[2] Wind Energy Department, Risø DTU National Laboratory for Sustainable Energy, DK-4000 Roskilde, Denmark
[3] National Renewable Energy Laboratory, 15013 Denver West Parkway, Golden, CO 80401 USA

Corresponding author:
Rolf-Erik Keck – rolf.keck@gmail.com

Abstract

The present study investigates a new approach for capturing the effects of atmospheric stability on wind turbine wake evolution and wake meandering using the dynamic wake meandering model. The most notable impact of atmospheric stability on the wind is the changes in length and velocity scales of the atmospheric turbulence. The length and velocity scales in the turbulence are largely responsible for the way in which wind turbine wakes meander as they convect downstream. The hypothesis of the present work is that appropriate turbulence scales can be extracted from the oncoming atmospheric turbulence spectra and applied to the dynamic wake meandering model to capture the correct wake meandering behaviour. The ambient turbulence in all stability classes is generated using the Mann turbulence model, where the effects of non-neutral atmospheric stability are approximated by the selection of input parameters.

In order to isolate the effect of atmospheric stability, simulations of neutral and unstable atmospheric boundary layers using large-eddy simulation are performed at the same streamwise turbulence intensity level. The turbulence intensity is kept constant by calibrating the surface roughness in the computational domain. The changes in the turbulent length scales due to the various atmospheric stability states impact the wake meandering characteristics and thus the power generation by the individual turbines.

The proposed method is compared with results from both large-eddy simulation coupled with an actuator line model and field measurements where generally good agreement is found with respect to the velocity, turbulence intensity, and power predictions.

Introduction

The dynamic wake meandering (DWM) model is a low-fidelity wind turbine wake model which was first developed at Risø DTU in 2003 (Madsen et al. [1, 2] and Larsen et al. [3]). The objective of the DWM model is to capture the large-scale meandering motion of the wake deficit as it convects downstream and predict the resulting wind turbine loads and power production, with a computational cost significantly lower than computational fluid dynamics (CFD). The wake deficit development and its meandering motions have been identified through field observations as the dominant factors in the production of wind turbine fatigue loads. An important observation is that large-scale movements of the wake deficit affect the loads of a wind turbine differently than small-scale turbulence. This implies that describing the wake turbulence with a single turbulence intensity parameter, as in the case of the Frandsen model [4], is not sufficient to accurately account for the effects of wake operations on a wind turbine.

In the DWM model, this effect is captured by assuming a split in turbulence scales in which the small-scales affecting the wake deficit evolution can be treated independently from the large turbulent scales that drive the meandering of the wake. Larsen et al. [3] provide a thorough description of the wake meandering method in the DWM, and propose a "cut-off eddy size," which distinguishes the small-scale turbulence (affecting the wake deficit evolution) from the large-scale turbulence (governing the wake meandering) of two rotor diameters. The meandering approach is validated with measurement data from the Tellus rotor (Bingöl et al. [5] and Trujillo et al. [6]). The wake meandering motion was measured using a LIDAR unit mounted on top of the nacelle.

The wake deficit model implemented in the DWM is based on the work of Ainslie [7, 8]. Ainslie applied a thin shear layer approximation of the Navier-Stokes (N-S) equations in which the turbulent closure is a simple eddy viscosity formulation. This method predicts the mean wake flow behind a wind turbine. Recently, an improved eddy viscosity model was proposed by Keck et al. [9], where a two-dimensional eddy viscosity model was included in the DWM model to better represent the radial distribution of the turbulent energy.

The DWM model also includes an expression to account for wake-added turbulence, turbulence created in the wake shear layer that is in addition to the ambient turbulence. Madsen et al. [10] implemented a wake-added turbulence formulation based on the local depth and the radial gradient of the wake deficit. While this correction well accounts for additional mechanical loads caused by the small-scale turbulence, it is not coupled to the wake deficit evolution and does not affect the development of the wakes of downstream rotors. An alternative method to capture wake-added turbulence is described by Keck et al. [11], where the turbulent stresses in the oncoming wake are used to calculate the wake turbulence intensity level at the next downstream turbine. Furthermore, the wake-added turbulence in this formulation is coupled to the wake deficit evolution at the downstream rotor, allowing for increased turbulence to build-up over a row of wind turbines.

The present work is aimed at developing a model to capture atmospheric stability effects in the DWM model. The impact of atmospheric stability on turbine wake evolution has been shown in the past. Ainslie [7] investigated the effect of atmospheric stability on meandering wakes as early as in the 1980s. However, as pointed out by Barthelmie et al. [12], few current engineering wake models incorporate the effects of atmospheric stability.

The fundamental process of atmospheric stability is well described by Obukhov [13] and Monin and Obukhov [14], in which the buoyancy-induced momentum and heat transfer affect both the turbulent length and velocity scales of the atmospheric boundary layer (ABL). A correction for the effects of stable stratification was proposed by Businger et al. [15]. The effect on ABL shear was later verified experimentally by Kirchhoff and Kaminsky [16]. In later work, a simple model for the effects of atmospheric stability on shear was also proposed by Irvin et al. [17], including a correction for stable stratification by Zoumakis [18].

The effect of atmospheric stability on wake evolution, turbine loads, and power production has become an emerging research topic. A number of studies have documented the influence of the atmospheric stability on turbine loads and power both experimentally (Barthelmie et al. [19], Wharton et al. [20], Schepers et al. [21], and Hansen et al. [22]) and numerically (Sathe et al. [23], Churchfield et al. [24], Lee et al. [25], and Lavely et al. [26]). The physical mechanism of the non-neutral ABL is to enhance (unstable) or dampen (stable) turbulent fluctuations through buoyancy forces. A modified turbulence length scale is another important feature of the non-neutral ABL. Peña et al. [27] showed that modelling atmospheric stability effects by modifying the turbulence intensity alone is not sufficient. Both the shift in length and velocity scale should be explicitly modelled to capture the full effect of the non-neutral atmosphere.

The work presented in this paper is a continuation of the research described by Keck et al. [11]. An important aspect of that article was that a strain-rate contribution from the ABL needs to be included in the wake deficit calculations to accurately model the turbulent stresses in the DWM model. The effect of the strain-rate contribution and the build-up of turbulence over a row of turbines were shown for neutral stratification. The present study will build upon the previous model augmentations to capture the effect of atmospheric stability on the wake dynamics. Since the length and velocity scales of the atmospheric turbulence change as a function of atmospheric stability, the fraction of ambient turbulent energy that affects the wake deficit evolution and the fraction that affects wake meandering, as well as the ABL shear, will change.

The objectives of this work are to:

1. Incorporate the effect of non-neutral stratification on the wake evolution in the DWM model
2. Quantify the effects on the flow field and power production of wake-affected turbines by the proposed correction
3. Validate the atmospheric stability corrected DWM model to reference data.

The article will first give a description of the DWM model as formulated prior to the atmospheric stability effect implementation to serve as baseline in the code frame-work development. This is followed by a brief description of the large-eddy simulation (LES) combined with an actuator line (AL) rotor model used to validate the proposed method. The next sections briefly describe the fundamental physics of the atmospheric stability followed by the formulation of the stability model in DWM. Finally, the result section shows 1) the effect of atmospheric stability on the ambient turbulent spectra, wake meandering, and the power production of wake-affected turbines; 2) the effect of the included atmospheric stability formulation in the DWM model; and 3) a validation of the proposed DWM model to predict the wake evolution in non-neutral atmospheric conditions by comparing the flow field and power production to the LES-AL model and field data from the North Hoyle and OWEZ offshore wind farms.

Dynamic Wake Meandering model

The baseline version of the DWM model used in this study is based on Madsen et al. [2], but employs the two-dimensional eddy viscosity model proposed by Keck et al. [9] and the wake-added turbulence with a strain-rate contribution from the ABL, also proposed by Keck et al. [11]. The wake meandering applied is based on the same principles as proposed by Larsen et al. [3]; however, a wake transport velocity equal to 80% of the free-stream velocity (as proposed by Keck at al. [28]) is employed rather than using the full free-stream velocity as proposed by Larsen et al. [3].

Wake deficit module

The wake deficit in the DWM model is governed by the steady state, axisymmetric thin shear layer approximation of the Navier-Stokes (N-S) equations in which momentum is governed by

$$u\frac{\partial u}{\partial x} + v\frac{\partial u}{\partial r} = \frac{1}{r}\frac{\partial}{\partial r}\left(v_T r \frac{\partial u}{\partial r}\right) \quad (1)$$

and continuity is maintained through

$$\frac{1}{r}\frac{\partial}{\partial r}(rv) + \frac{\partial u}{\partial x} = 0 \quad (2)$$

In these equations, the velocity components *u* and *v* are in the mean flow (x) and radial (r) directions, respectively, and ν_t is the eddy viscosity. The turbulent diffusion is accounted for with an eddy viscosity formulation based on the following mixing length model described in dimensionless from by the equation,

$$\upsilon_T = F_1 k_{amb\ DWM} TI_{amb} + \frac{F_2 k_{2\ DWM} l^{*2} \left|\frac{\partial u}{\partial r}\right|}{U_{amb} R} \quad (3)$$

where $k_{amb\ DWM}$ and $k_{2\ DWM}$ are model constants (the $k_{amb\ DWM}$ constant includes a length scale based on a hub-height equal to *2R*), TI_{amb} and U_{amb} is the ambient turbulence intensity (std(u)/ U_{amb}) and mean velocity at hub-height, and *l** is the turbulence mixing length of the wake-added turbulence. F_1 and F_2 are filter functions that govern the development of turbulent stresses in the absence of a transport equation for turbulence. The details and motivation for this turbulence formulation are provided in Keck et al. [9] and the boundary condition and filter functions applied in this work are descried in Keck et al. [11].

Before applying the eddy viscosity from eq. (3) in eq. (1), it is scaled to include a strain-rate contribution due to the ABL shear, du/dz_{ABL} by eq. (4) and (5).

$$\frac{du}{dr}_{Total} = \begin{cases} \frac{du}{dr}_{DWM} & , \left|\frac{du}{dr}_{DWM}\right| \geq \frac{du}{dz}_{ABL} \\ \frac{du}{dr}_{DWM} + \frac{1}{\pi}\int_{\alpha_1}^{\alpha_2} \left(\frac{du}{dz}_{ABL} \cdot \sin(x)\, dx\right) - (\alpha_2 - \alpha_1)\frac{du}{dr}_{DWM} & , \left|\frac{du}{dr}_{DWM}\right| < \frac{du}{dz}_{ABL} \end{cases} \quad (4)$$

$$\nu_t' = \nu_t \cdot \frac{\frac{du}{dr}_{Total}}{\left|\frac{du}{dr}_{DWM}\right|} \quad (5)$$

where du/dr_{DWM} is the azimuthally average wake velocity gradient in the wake deficit region modelled by the DWM model, du/dr_{TOTAL} is total velocity gradient with the ABL shear contribution included, and α is the angular locations where the effect of the atmospheric shear in cylindrical coordinates is larger than the wake deficit shear. α_1 and α_2, are found by $arcsin(\frac{du}{dr}_{DWM} / \frac{du}{dz}_{ABL})$ and π-α_1 respectively. The details of this correction can be found in Keck et al. [11]. The equation system described by eqs. (1) - (5) is solved using a finite-difference scheme, in which a second-order central-difference scheme in the radial direction and a first-order upwind scheme in the mean flow direction are applied. As information only moves along the mean flow direction, a solution can be obtained by "marching" downstream, solving each axial position sequentially.

Turbulence intensity in the deficit module

The wake-added turbulence in the DWM model is used to include the contribution of small-scale turbulence generated by the shear layer in the wake at the downstream turbine. This affects the loads and induction of the downstream turbine; however, the most important effect is the influence on the wake evolution of the wake-receiving turbine. The wake-added turbulence is calculated directly by the turbulent stresses in the wake deficit calculation as

$$TI_{DWM\ MFoR} = \max\left(\sqrt{\frac{1}{c_{u'w'} * (w'_{rms}/u'_{rms})} \cdot \tau_{stress\ DWM}}\ , TI_{amb}\right) \quad (6)$$

where the coefficient $C_{u'w'}$ and the ratio w'_{rms}/u'_{rms} describe the relationship between axial and radial turbulent fluctuations in the wake. These relations are different compared to atmosphere turbulence due to the significantly smaller length scale and the increased degree of anisotropy of wake turbulence. In this work, the correlation coefficient is given the value 0.3, and the ratio w'_{rms}/u'_{rms} is set to unity based on the findings of Larsen et al. [29]. The subscript *MFoR* denotes "meandering frame of reference", i.e., expressed in the reference frame following the centre of the wake deficit and the meandering movements.

The effect of wake meandering

The DWM deficit module outputs the wind speed and turbulence intensity distribution in MFoR (i.e., without any large-scale movements). The meandering can be viewed as a series of wake segments in which the wake centre has a stochastic offset in lateral and vertical direction according to some statistical distribution. If the distribution of the meandering is known, it is possible to calculate the average wind field and turbulence intensity in the FFoR as the convolution of the deficit in the MFoR (both wind speed and variance, i.e., the square of $TI_{DWM\ MFoR}$ from eq. (6)) and the distribution of the wake centre in the vertical and lateral direction due to wake meandering as follows:

$$\theta_{DWM\ FFoR}(y,z) = \iint \theta(y-y_m, z-z_m)_{DWM\ MFoR} \cdot PDF_m(y_m,z_m)\, dy_m dz_m \quad (7)$$

In this equation, θ represent the wind speed or variance, y-y_m and z-z_m are the local coordinates in the MFoR, and PDF_m is the probability density function for the meandering distribution. The subscripts *FFoR* and *MFoR* refer to fixed and meandering frame of reference (i.e., the probability of finding the wake centre at a certain location in a fixed plane perpendicular to the flow direction). The method used to find this meandering distribution is described in the "wake meandering as a function of atmospheric stability" section. The distribution of mean velocity and turbulence intensity in FFoR, given by eq. (7), is used to 1) estimate the "ambient conditions" at downstream rotors to allow for intra-turbine coupling, and 2) find the mean flow field in the simulation domain. For more information see Keck et al. [11].

Atmospheric stability

Atmospheric stability is related to the vertical distribution of virtual potential temperature, which has an important effect on the turbulence in the atmosphere due to buoyancy effects. Virtual potential temperature is the absolute temperature, with the temperature change due to expansion with altitude and moisture effects removed. In a stable atmosphere, the buoyancy forces suppress the vertical fluctuations, whereas the vertical fluctuations are enhanced in an unstable atmosphere. The neutral condition, in which buoyancy effects have negligible influence on the vertical turbulence, is only experienced a fraction of the time in the atmosphere (see Sathe et al. [23]).

The stability of the atmosphere is dictated by the direction of the heat transfer at the surface. When heat is transferred from the surface upwards this leads to an unstable ABL in which air of higher virtual potential temperature lies under air of virtual lower potential temperature. When the heat flux is directed into the surface, the air becomes cooler near the surface, and the ABL is stable. In simple terms, this can be expressed by saying that when the surface is warmer than the air, an unstable atmosphere will develop and when the surface is cooler than the air, the ABL will be stable (Stull [30]).

The most common measure to characterise atmospheric stability is the Monin-Obukhov length scale (M-O length), see Obukhov [13],

$$L = -\frac{\overline{\theta_v} u_*^3}{\kappa g \left(\overline{w'\theta_v'}\right)_s} \quad (8)$$

where θ_v is the virtual potential temperature, κ is the von Karman coefficient, g is the gravitational constant, and u_* is the friction velocity. The overbar denotes time averaging and the prime symbol ($'$) denotes fluctuation about the mean value. The physical meaning of the M-O length scale is that it is the height above the ground at which the production of turbulent energy due to buoyancy effects is equal to turbulent production due to the strain-rate of the velocity field. It is thus an estimate of the height at which buoyancy effects become important for the turbulence dynamics (Wyngaard [31]). This interpretation of the M-O length shows that numbers of large absolute value indicate near-neutral atmospheric stability, since it indicates that buoyancy-driven turbulence is negligible in a large part of the boundary layer, and numbers of small absolute value represent strong influence of buoyancy. The sign of the length scale indicates the direction of the heat flux and, thereby whether the atmosphere is

stable or unstable. The exact numbers used to characterise the stability classes as a function of M-O length varies between sources. For this investigation, the definition of Peña et al. [27], given in table 1, is used.

Table 1, the classification of atmospheric stability as a function of Monin-Obukhov length

Stability class	very stable	stable	near stable	neutral	Near unstable	unstable	very unstable
M-O Length	10 < L < 50	50 < L < 200	200 < L < 500	abs(L) > 500	-500 < L < -200	-200 < L < -100	-100 < L < -50

Mann turbulence model

The Mann turbulence model [32, 33] combines an eddy-lifetime assumption with rapid distortion theory to transform an isotropic spectral tensor to an anisotropic spectral tensor. The anisotropic spectral tensor, $\boldsymbol{\Phi}_{ij}(\boldsymbol{k})$, depends on three input parameters to characterise the turbulence: the product of the spectral Kolmogorov constant and the rate of dissipation to the power of two-thirds ($\alpha\varepsilon^{2/3}$), turbulence length scale (L_{Mann}), and degree of anisotropy (Γ). The Mann turbulence model can be used to generate a three-dimensional box containing random incompressible anisotropic turbulence. In applications it is customary to interpret the streamwise dimension as dependent on time using Taylors frozen turbulence assumption.

The spectral tensor can be used to find the power density spectra of any Reynolds stress component in any direction by spectral integration in the spectral tensor in Fourier space.

$$\boldsymbol{F}_{ij}(k_1) = \int_{-\infty}^{\infty}\int_{-\infty}^{\infty} \boldsymbol{\Phi}_{ij}(\boldsymbol{k})dk_2dk_3 \tag{9}$$

As the spectral tensor itself is the Fourier transform of the (idealised) correlation function of the turbulence, it can also be used directly to calculate statistical properties of the synthetic turbulence by inverse Fourier transform according to the relation,

$$R_{ij}(\boldsymbol{r}) = \int_{-\infty}^{\infty} \boldsymbol{\Phi}_{ij}(\boldsymbol{k})e^{-i\boldsymbol{k}\cdot\boldsymbol{r}}d\boldsymbol{k} = \overline{u_\iota(\boldsymbol{x})u_\iota(\boldsymbol{x}+\boldsymbol{r})} \tag{10}$$

From this it follows that the integral turbulent length scale in any direction can be found by eq. (11).

$$L_i = \int_0^{R_{ii}(r)>0} \frac{R_{ii}(r)}{R_{ii}(0)}dr \tag{11}$$

As indicated by the upper integration limit, the integration should only be carried out over the initial region with positive correlation. The turbulence velocity scale (or friction velocity), u^*, can also be obtained by the correlation function using eq. (12), where $R_{13}(\boldsymbol{0})$ is the equivalent to the shear stress $\langle\overline{u'w'}\rangle$.

$$u^* = \sqrt{|R_{13}(\boldsymbol{0})|} \tag{12}$$

The Mann turbulence model is derived to generate atmospheric turbulence in neutral stratification. However, Peña et al. [27] showed that with appropriate parameter selection the Mann model can be used to generate atmospheric turbulence with similar characteristics as non-neutral atmospheric turbulence. By applying the Mann parameters suggested by Peña et al. [27] and using eqs. (9)-(12) it is possible to estimate Reynolds stresses and turbulent length and velocity scales of the atmospheric turbulence in non-neutral atmospheric conditions.

Incorporating atmospheric stability effects into the DWM model

The eddy viscosity formulation used in the DWM model was not derived to include buoyancy effects due to non-neutral atmospheric stability. The hypothesis of this work is that the effects of atmospheric stability can be emulated in the DWM model by changing the length and velocity scales of the atmospheric turbulence. The characteristic length scale for an unstable atmosphere is larger than for a neutral or stable atmosphere. The effect of this shift in turbulent length scale spectra of the atmospheric turbulence is illustrated in Figure 1. The turbulence, which affects the wake meandering versus the wake deficit evolution, can be separated by applying filter based on the *jinc*-function (Goodman [34], for more details see eq. (15)). It can then be seen that the atmosphere turbulence spectra in an unstable atmosphere (top row) has a smaller portion of energy in the scales affecting the wake deficit evolution (right figures), and a larger portion in the wake meandering scales (middle figures) compared to the stable case (bottom row). The black line included in the left figures shows the *jinc*-function filter.

To illustrate the effect of atmospheric stability on wake simulations with the DWM model, consider the situation in which atmospheric stability is varied while maintaining constant turbulence intensity (where turbulence intensity only accounts for variance in the streamwise flow). The atmospheric turbulence velocity scale (u^*_{ABL}) will be approximately constant as a consequence of the constant the turbulence intensity. The turbulence length scale of the atmosphere (l^*_{ABL}), however, will vary as a function of atmospheric stability. This will have three important effects on the wake dynamics of the DWM model:

1. The ABL shear that is input to the DWM model deficit equation via eq. (4) would increase with increasing atmospheric stability. Shorter length scales means larger vertical velocity gradients.

$$\frac{du}{dz}_{ABL} \cong \frac{u^*_{ABL}}{l^*_{ABL}} \tag{13}$$

2. The turbulent energy in scales larger than 2D, affecting the wake meandering, decreases with increasing atmospheric stability.

3. For a given turbulence intensity, the amount of energy in scales smaller than 2D, which is assumed to affect the wake deficit evolution, increases with increasing atmospheric stability.

ABL length and velocity scales as a function of atmospheric stability

By applying the parameters suggested by Peña et al. [27] in the Mann model, the turbulent energy spectra in the non-neutral atmosphere can be approximated. The resulting spectral tensor can be used to estimate the atmospheric turbulent length scale as a function of atmospheric stability using eq. (11). The velocity scale of the atmospheric turbulence can be computed from eq. (12), but as the ambient turbulence intensity is an input parameter to the DWM model, it is more practical to relate the turbulence velocity scale to the turbulence intensity. This is achieved by integrating the energy content of the normal stress in flow direction ($\overline{u'u'}$) and the shear stress (-$\overline{u'w'}$) in the Mann turbulence spectra given by eq. (9). The ratio of the two Reynolds stresses is now a function of atmospheric stability and can be used to calculate the normalized turbulent velocity scale in all atmospheric stability classes from the ambient turbulence intensity using the relation,

$$u^*_{ABL} = \left[\left(TI^2_{AMB}\frac{-\overline{u'w'}}{\overline{u'u'}}\right)\right]^{1/2} \tag{14}$$

The parameters suggested by Peña et al. [27] are given as a function of height, which means that the resulting turbulence scales in the DWM model will be height dependent. In the previous version of the DWM model, the length scale of atmospheric turbulence is not explicitly given, and is invariant with respect to the height of the tower relative to the rotor radius (i.e., the length scale normalized with turbine radius has been assumed to be constant). However, as the length scale of the atmospheric

turbulence needs to be explicitly included in the wake deficit calculation of the DWM model to capture the effect of atmospheric stability, the height dependence on the turbulence length scale may also be incorporated.

Figure 2 shows the dependence of the turbulent velocity scale (left), length scales (middle), and shear (right) of the ABL on height and atmospheric stability at a fixed turbulence intensity. From the figure it can be seen that the turbulence velocity scale, which is related to turbulent shear stress, in the ABL is nearly invariant with both height and atmospheric stability. The fact that the velocity scale is nearly invariant with height is expected, as the turbulent shear stress is nearly constant in the lower part of the boundary layer. However, the fact that the velocity scale in the boundary layer is constant as atmospheric stability is varied is interesting. This requires the shear stress to be invariant with atmospheric stratification. The shear stress can be rewritten as: $-\overline{u'w'} = u'_{RMS}w'_{RMS}C_{u'w'}$, where u'_{RMS} and w'_{RMS} are the standard deviation of the fluctuation velocities in streamwise and vertical direction, and $C_{u'w'}$ is the correlation coefficient between the two fluctuating components. This means that the decrease in vertical turbulence (w'_{RMS}) in stable stratification is balanced by the stronger correlation between streamwise and vertical fluctuations ($C_{u'w'}$), which is presumably due to the increased ABL shear.

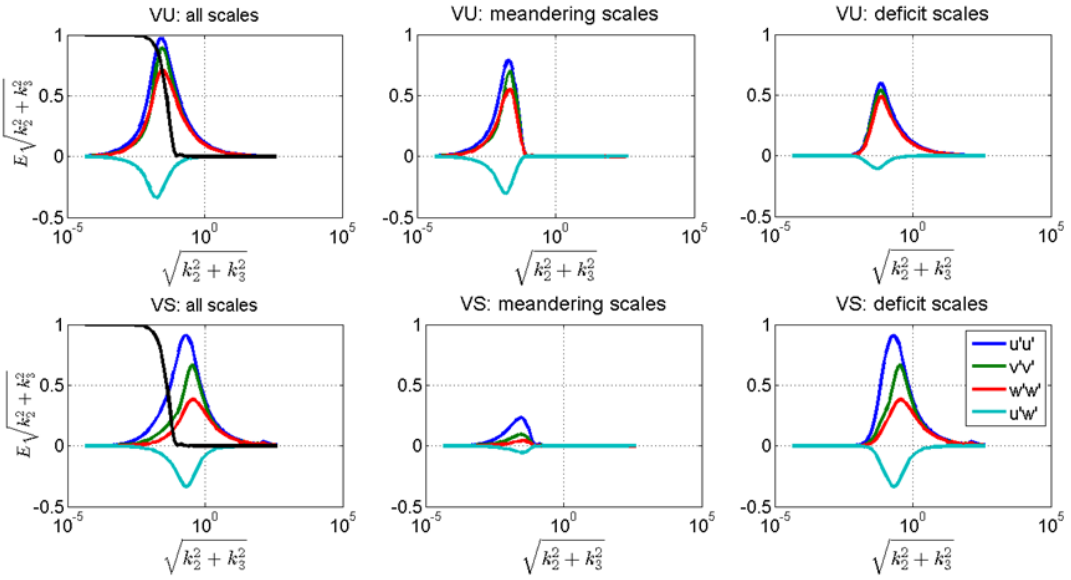

Figure 1, the turbulent energy spectra for very unstable (top row) and very stable (bottom row) atmospheric conditions derived using the Mann model with the parameters suggested by Peña et al. [27]. The left figures show the turbulent energy spectra in all scales, the middle figures show the turbulent scales which affect the wake meandering, and the right figures show the turbulence which affects the wake deficit evolution. The black line in the right figures show the filter based on the "jinc" function applied to separate the turbulence affecting the wake meandering and the wake deficit evolution.

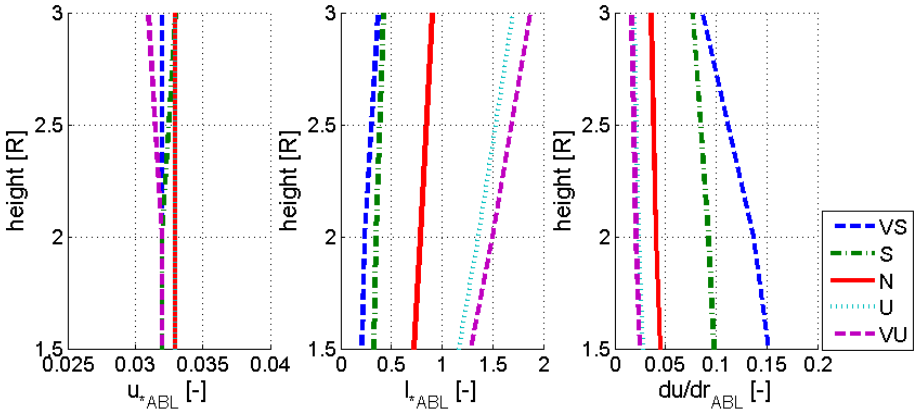

Figure 2: turbulent velocity scale, length scales, and shear in the ABL as a function of height and atmospheric stability.

Wake meandering as a function of atmospheric stability

The wake meandering in the DWM model is calculated based on the turbulent eddies experienced by a circular disc in the oncoming wind field, as described by see Larsen et al. [3]. This approach is motivated by the assumption that the wake acts as a passive tracer in the turbulence field (i.e., the movements of the wake are completely dictated by the large-scale turbulent fluctuations of the oncoming flow). Based on this assumption, the effect of atmospheric stability can be included directly by using the Mann turbulence corrected for non-neutral atmospheric turbulence, as described by Penã et al. [27], as input to the meandering algorithm.

The physical principle used to find the wake meandering is as suggested by Larsen et al. [3], but two modifications to the method are made. The wake transport velocity applied to the meandered wake deficit in the turbulence field is reduced to 80% of free-stream velocity based on the results of Keck et al. [28]. The effect of this modification is shown in Figure 3.

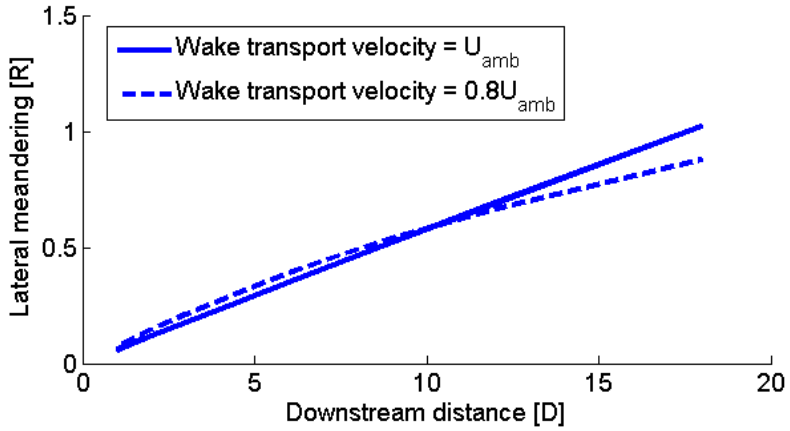

Figure 3: Wake meandering in the DWM model using a wake transport velocity of 80% (dashed lines) and 100% (solid lines) of the ambient wind speed.

Furthermore, the computational algorithm used in this work is different. Instead of averaging the wind field over the disc at every time step, as is the current method, a more computationally efficient technique is to “pre-multiply” the wind field with the circular disc to form “the wind field as seen by a circular disc”. This pre-multiplication operation is a convolution and can be carried out as a

multiplication in Fourier space, provided that the wind field and the circular disc have Fourier transforms. As the random wind field is generated in Fourier space and the transform of the circular disc is given by: $2\frac{J_1(|k|R)}{|k|R}$ (Goodman [34]), where J_1 is a Bessel function of the first kind, k is the wave number and R is the rotor radius, in this application this is a feasible approach. For wake meandering under the passive tracer assumption, the turbulent wind speed should be averaged over the disc. Assuming that the rotor disc is oriented perpendicular to the x-axis, the filter equivalent to the rotor averaging becomes eq. (15), which as mentioned above is often called the *bessinc* or *jinc* function,

$$jinc\left(\sqrt{k_2^2+k_3^2}\cdot R\right)=\frac{2\cdot J_1\left(\sqrt{k_2^2+k_3^2}\cdot R\right)}{\sqrt{k_2^2+k_3^2}\cdot R} \tag{15}$$

In order to apply eq. (15) to the spectral tensor in the Mann model, the spectral tensor is expressed in polar coordinates ($\sqrt{{k_2}^2+{k_3}^2}$, $\varphi=\arctan(k_2/k_3)$ and k_1) and the integration in eq. (9) is performed over the two latter coordinates, resulting in eq. (16).

$$\boldsymbol{F}_{ij}\left(\sqrt{k_2^2+k_3^2}\right)=\int_{-\infty}^{\infty}\int_{-\infty}^{\infty}jinc^2\left(\sqrt{k_2^2+k_3^2}\cdot R\right)\boldsymbol{\Phi}_{ij}(\boldsymbol{k})\cdot\sqrt{{k_2}^2+{k_3}^2}d\varphi\, dk_1 \tag{16}$$

In eq (16), the *jinc*-function is squared as a result of the multiplication of two wind speeds in eq. (10). Note that this squared *jinc*-filter can be applied outside of the integration, and this is the reason for using $\sqrt{k_2^2+k_3^2}$ as the dependent variable, e.g., in figure 2.

The algorithm used in this work to simulate meandering then becomes as follows:

1. Use the Mann turbulence model to generate random Fourier coefficients in three dimensions.
2. Multiply each Fourier component with eq. (15).
3. Wake-segments are released at the wake-emitting turbine at a frequency of 1Hz. The wake-segments travel downstream with a velocity of 80% of the ambient wind speed (based on the findings of Keck et al. [28]), which is referred to as the "wake transport velocity" (U_{wake}). The frozen turbulence box travels along the flow with the ambient wind speed. Consequently, the wake deficit travels at a negative speed of -20% of the ambient wind speed relative to the frozen turbulence field.
4. At every time step, the position of each emitted wake-segment is updated based on the fluctuating velocities in the streamwise, lateral and vertical direction, which are calculated based on the current position in the turbulence box. To avoid interpolation as the wake-segments move relative to the turbulence box, which otherwise causes a reduction of turbulent energy, the velocity at the location of the wake-segment is found by applying the definition of inverse Fourier transform (which is continuous and can be used to find the velocity at any location in the field, contrary to the inverse fast Fourier transform (IFFT) to generate turbulent fluctuations in a box of fixed spatial resolution as is commonly done).
5. Finally, when all the wake-segments have reached the desired downstream distance, the wake meandering is scaled by a factor determined by the square root of the ratio of the expected meandering energy to the total captured meandering energy. This ratio is a function of the dimensions of the turbulence box chosen.

Figure 4 shows the wake meandering as a function of atmospheric stability class and height. The wake meandering is quantified as the standard deviation of the wake centre position in lateral and vertical direction normalized by the rotor radius. The dependence on atmospheric stability is dominant compared to that of tower height, with the selected levels.

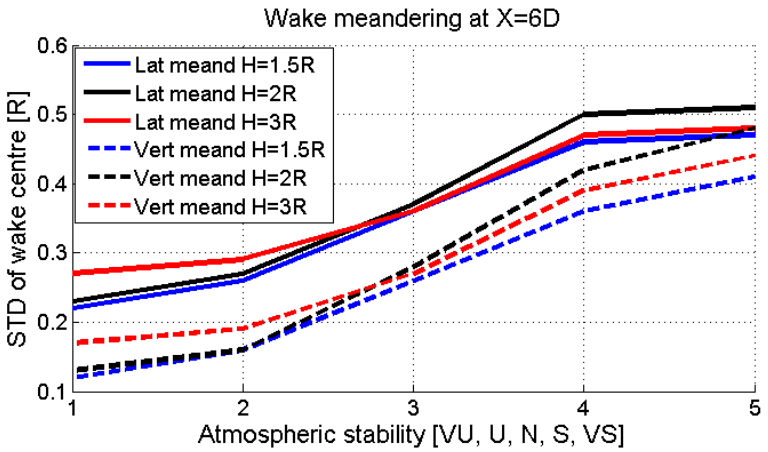

Figure 4: Wake meandering 6D downstream of the wake-emitting turbine as a function of height and atmospheric stability.

Wake deficit evolution as a function of atmospheric stability

Based on the assumption of the "split in scales" in the DWM model, the part of the ambient turbulence that affect the wake meandering is assumed not to influence wake deficit evolution in meandering frame of reference. Therefore the effect of the ambient turbulence on the wake deficit evolution can be calculated by subtracting the energy contributing to the wake meandering. As discussed in the previous section, the meandering process uses a disc-averaged turbulent wind speed. This averaging operation is equivalent to multiplication of the spectral tensor in Fourier space by the filter described by eq. (15). The remaining part of the spectral tensor thus results in the relation,

$$\boldsymbol{\Phi}_{\mathrm{ij}}(\boldsymbol{k})_{\mathrm{DEF}} = \boldsymbol{\Phi}_{\mathrm{ij}}(\boldsymbol{k})\left(1 - jinc^2\left(\sqrt{k_2^2 + k_3^2}\cdot R\right)\right) = \boldsymbol{\Phi}_{\mathrm{ij}}(\boldsymbol{k})\left(1 - \left(\frac{2\cdot J_1\left(\sqrt{k_2^2+k_3^2}\cdot R\right)}{\sqrt{k_2^2+k_3^2}\cdot R}\right)^2\right) \quad (17)$$

The length scale of the wake deficit turbulence can be found by applying the spectra tensor for the wake deficit turbulence, $\boldsymbol{\Phi}_{\mathrm{ij}}(\boldsymbol{k})_{\mathrm{DEF}}$, in eq. (11). The normalized velocity scale of the wake deficit turbulence (u^*_{DEF}) is related to the atmospheric stability and the ambient turbulence intensity by the ratio of Reynolds stresses in the "deficit scales", eq. (17).

$$u^*_{DEF} = \left[\left(TI^2_{AMB}\frac{-\overline{u'w'}_{\lambda<2D}}{\overline{u'u'}_{\lambda<2D}}\right)\right]^{1/2} \quad (18)$$

λ represents the wavelength of a turbulent eddy. Consequently, the subscript $\lambda<2D$ in eq. (18) indicates that the spectral integration is effectively only carried out over turbulent eddies smaller than 2 rotor diameters, as the rightmost term of eq. (17) removes most of the energy in scales where $\lambda = \frac{2\pi}{\sqrt{k_2^2+k_3^2}} > 2D$. Thus the rightmost term of eq. (17) works as a high pass filter.

The length and velocity scale on the ambient turbulence, including the effect of atmospheric stability, is described by eqs. (11) and (17), and eq. (18), respectively. By applying these expressions into the first term of eq. (3), it is possible to form an expression for eddy viscosity which incorporates stability effects. This is done by explicitly including the turbulent length scale of atmospheric turbulence in the equation (it was previously included in $k_{amb\,DWM}$, i. e. $k_{amb\,DWM} = k_{1\,DWM}\cdot l^*_{DEF}$), and replacing TI_{amb} by u^*_{DEF}.

$$\nu_T = F_1 k_{1\,DWM} u^*_{DEF} l^*_{DEF} + \frac{F_2 k_2 l^{*2} \left|\frac{\partial u}{\partial r}\right|}{U_{amb} R} \quad (19)$$

Note that the new model constant for eddy viscosity due to ambient turbulence ($k_{1\,DWM}$), no longer includes a length scale, and is dimensionless. Instead, the length scale is explicitly given as a function of atmospheric stratification and hub-height.

Figure 5 shows the dependence of the turbulent velocity (left) and turbulent length (middle) scales and of wake deficit turbulence on height and atmospheric stability, together with the eddy viscosity in the DWM deficit evolution that is dependent on the ambient turbulence (right). Similar to the behaviour with the wake meandering, it can be seen that atmospheric stability has a much stronger influence on the eddy viscosity in the wake than tower height, with the selected levels. Furthermore, it can be seen that the eddy viscosity of the wake deficit increases approximately linearly in stable stratification but is close to invariant with height above 1,5R in unstable stratification.

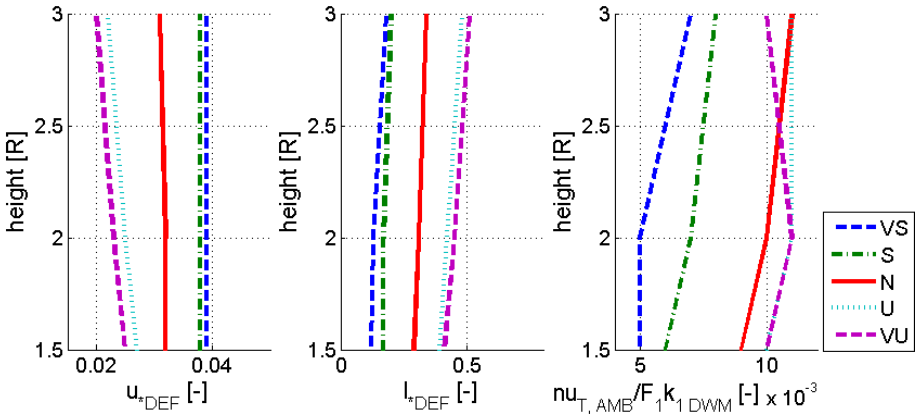

Figure 5: Turbulent velocity and length scales which affect the wake deficit evolution, together with the eddy viscosity contribution due to ambient turbulence as a function of height and atmospheric stability.

Large-Eddy Simulation and Actuator Line Model

Validation of the atmospheric stability effects in the DWM is performed by comparing the turbulence and velocity fields with results from large-eddy simulation (LES) coupled with actuator lines (AL). The LES-AL simulations are performed with tools created at the U.S. National Renewable Energy Laboratory's (NREL) as part of the Simulator for Off/Onshore Wind Farm Applications (SOWFA) [35]. The tools are based on the Open-source Field Operation and Manipulation (OpenFOAM) [36] computational fluid dynamics (CFD) toolbox, which is a collection of libraries, written in object-oriented C++, that is meant to solve complex partial differential equations using the finite-volume formulation. Parallelization is included in these libraries using the Message-Passing Interface (MPI). OpenFOAM comes with a number of standard solvers and libraries for different physical models, such as models for turbulence. The creation of custom solvers and libraries is fairly straightforward because of the highly layered object-oriented nature of the code. The solver used for these LES-AL simulations is a custom OpenFOAM-based solver designed specifically for LES of the atmospheric boundary layer. It is coupled to a custom AL wind turbine model library. A more thorough description is given by Churchfield et al. [24]

Simulation Process

Simulations were carried out over flat terrain under either neutral or stable conditions. The domain size in each case is 4 km in each horizontal direction and 1 km in the vertical direction. The driving pressure

gradient is adjusted such that the hub-height mean wind is out of the southwest, and a capping inversion is initially placed at 700 m above the surface.

First, a precursor atmospheric boundary layer LES is performed with no turbines on a mesh of uniform 12 m resolution. The lateral boundary conditions are periodic, the top is treated as a stress-free wall, and the surface stress model is applied to the lower surface. Time stepping is such that the local maximum Courant number never exceeds 0.75. Once the simulation reaches a quasi-equilibrium state, in which the mean wind begins to undergo gentle inertial oscillations and turbulence is fully developed up to the top of the boundary layer (which is capped by the capping inversion), the velocity and potential temperature field on the south and west boundaries are saved every time step for 2000 additional seconds. Also, the volume velocity and temperature field are saved once, at the start of quasi-equilibrium. For the neutral and unstable simulations, the quasi-equilibrium state is reached at 16000 s and 14000 s, respectively. The saved boundary and volume data are used as boundary and initial conditions, respectively, for the subsequent wind farm simulation. The surface temperature flux used in the neutral and unstable conditions was 0 and 0.02 K-m/s, respectively, and the surface roughnesses were 0.0003 m and 0.0002 m, respectively. These conditions yielded nearly the same hub height turbulence intensity (based on the variance of flow in the mean wind direction), but significantly different hub height turbulent kinetic energy (based on all three components of the velocity).

Once the precursor simulation is complete, the wind farm simulation is performed. It uses the same overall domain, but regions of local grid refinement down to 1.5 m resolution around the turbines and in their wakes are included to capture the smaller scales generated in the wake. The inflow lateral boundary conditions use the boundary data generated during the precursor stage, and the outflow lateral boundary conditions are set to have a zero normal gradient. The upper boundary is still treated as a stress-free wall, and the lower boundary continues to use Moeng's surface stress model (Moeng [37]). Time stepping is such that the tip of an AL rotor never traverses through more than one grid cell per time step, which is more restrictive than the normal Courant condition, but is required to properly resolve the wake formation. A few hundred seconds are required for the wakes to propagate and for the flow to come to quasi-equilibrium. Once that state is reached, the simulation continues for at least another ten minutes over during which averages and statistics are taken.

Extracting Meandering from the LES-AL simulations

In the LES-AL simulations, the vertical and horizontal meandering time series are extracted from a vertical and horizontal plane passing through the turbine position, respectively. For each time step and downstream position the best fit between the downstream wind component and a simplified wake shape is calculated. The simplified wake profile used is given by,

$$\text{wake shape}(\mathrm{x},\mathrm{z}) = e^{-\frac{(z-hubheight)^2}{(R/\sqrt{2*\log(2)})^2}} - 2^{-\frac{x}{2R}} \cdot e^{-\frac{(z-hubheight)^2}{(0.1\cdot R/\sqrt{2*\log(2)})^2}} \quad (20)$$

The wake shape depends on both the offset from the centre line, and the downstream distance from the wind turbine and is constructed by two Gaussian distributions. The first Gaussian represents the whole wake deficit and the "*full width at half maximum*" is taken to be 2R. The second term is included to represent the "aerodynamic hole" in the centre of the rotor and is taken to be 0.2R wide. In the far-wake the second term vanished, and the whole assumes a Gaussian shape.

Figure 6 shows the wake meandering found by applying the proposed algorithm. From the figures, it can be seen that the algorithm performs well for the near wake situation (left figures). However, as the wake meandering increase, the wake deficit occasionally meanders outside of the planes where data are collected. An example of this is shown in the right figures of figure 6, where the top figure shows that the wake centre is located between 2-3R off the wake enter axis for a ~50s time-period around 100s into the simulation. In this situation, the wake deficit is difficult to detect in the vertical data plane, and the vertical wake centre position is thus relatively uncertain. As a consequence, cases with more wake

meandering will have higher uncertainty in the meandering statistics by the proposed method. In the figures below, the left set of figures has a lateral standard deviation of the wake centre position of 0.45R, and the right set of figures has a lateral standard deviation of 0.86R. It appears that these kinds of effects which create meandering magnitude uncertainty, begin to occur somewhere between the levels of meandering simulated in this study.

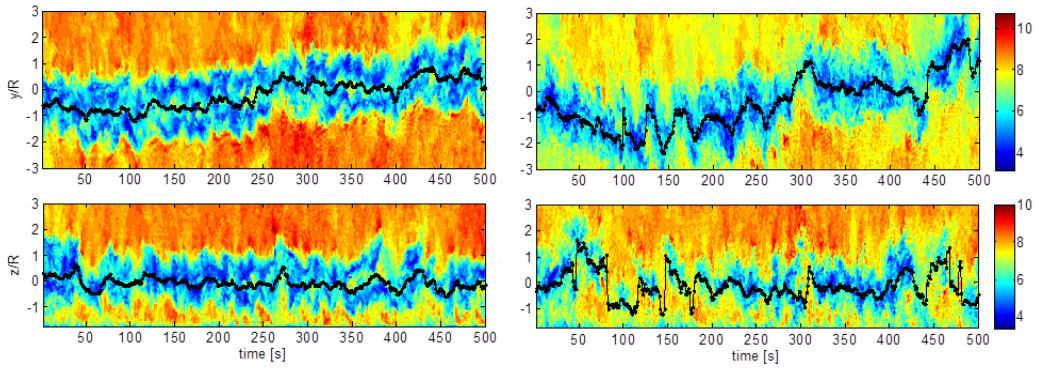

Figure 6: Horizontal (top row) and vertical (bottom row) wake meandering as a function of time extracted from an AL simulation 3D (left column) and 6D (right column) downstream of the rotor under unstable atmospheric conditions.

Description of investigation:

As mentioned above, the overall objectives of the present study are to:

1. Investigate the influence of atmospheric stability on the ambient turbulence characteristics, wake meandering, and the turbulence and wind speed distributions in a wind turbine wake.
2. Develop a method to model the most important effects of non-neutral atmospheric stability in the DWM model.

A complication that occurs when characterizing the effect of atmospheric stability on the ambient turbulence and wake evolution is that atmospheric stability is closely related to the turbulence intensity level. Furthermore, both quantities are known to be positively correlated to the turbulent mixing in the wake, and thereby increase the recovery of the turbine wake. To draw firm conclusions, and to be able to quantify the effect by atmospheric stability, it is therefore desirable to isolate the atmospheric stability from the turbulence intensity. This is difficult to achieve in field observations as the oncoming turbulence intensity is dominantly a function of wind speed, atmospheric stability, and terrain. As a consequence, most previous studies have discussed the effects of atmospheric stability and turbulence intensity together.

In this investigation, the effect of atmospheric stability is isolated by conducting a set of LES-AL simulations in unstable and neutral atmospheres at the same ambient turbulence intensity. (Unfortunately, the flow solver capability for stable atmospheric conditions is not developed yet.) This is achieved by calibrating the surface roughness in the domain for each stability class to yield turbulence intensity close to 6.2%. The simulations are conducted to mimic the conditions along rows of turbines from the offshore wind farms of OWEZ, which consist of 36 V90-3MW turbines, and North Hoyle, which consist of 30 V80-2MW turbines (See table 2).

These sets of simulations allow detailed investigations of atmospheric stability impact on the ambient turbulence spectra and the wake meandering. Unfortunately, the wake deficit evolution cannot be studied independent of the wake meandering, as are performed in Keck et al. [11], since the data required to extract the deficit in meandering frame of reference are not available (such analysis would require the data in planes perpendicular to the mean flow direction). Instead, the effect of atmospheric

stability on the wind speed and turbulence intensity evolution in fixed frame of reference (i.e., both meandering and wake deficit together) is studied.

Table 2: A list of simulation cases to study the effect of atmospheric stability on ambient turbulence and wind turbine wake evolution. The abbreviations "N" and "U" denote neutral and unstable conditions, respectively, and the abbreviation "N.H" denotes the North-Hoyle wind farm case.

Case	Turbine	WS	TI	L	Nr WTG	Spacing
N-N.H. row A	V80	8m/s	6.12%	-∞	4	11D
U-N.H. row A	V80	8m/s	6.16%	-83.6	4	11D
N-N.H. row B	V80	8m/s	6.12%	-∞	4	10D
U-N.H. row B	V80	8m/s	6.16%	-83.6	4	10D
N-N.H. row C	V80	8m/s	6.12%	-∞	5	4.4D
U-N.H. row C	V80	8m/s	6.16%	-83.6	5	4.4D
N-OWEZ row A	V90	8m/s	6.12%	-∞	3	13D
U-OWEZ row A	V90	8m/s	6.16%	-83.6	3	13D
N-OWEZ row B	V90	8m/s	6.12%	-∞	3	11D
U-OWEZ row B	V90	8m/s	6.16%	-83.6	3	11D

The second part of the investigation focuses on verifying the effect and accuracy of the proposed atmospheric stability correction for the DWM model. The atmospheric stability correction is evaluated by comparing the result of the baseline DWM model and the modified DWM model to the unsteady AL results in table 2. The accuracy of the DWM model is determined by the standard error (STE) between the mean flow field calculated by the DWM model and the AL reference data in fixed frame of reference (FFoR) using the relation,

$$STE = \sqrt{\left[\frac{1}{n_d}\sum_{d=1}^{n_d}\left(\frac{1}{n_{d,r}}\sum_{r=1}^{n_{d,r}}\left(\theta_{d,r}^{ACL} - \theta_{d,r}^{DWM}\right)^2\right)\right]} \quad (21)$$

The indexes *d*, and *r* correspond to downstream distance and radial position, and θ is the property studied. In this investigation, mean wind speed and turbulence intensity have been evaluated. The STE metric is sensitive to misalignment of the mean wake deficit of the two models as it based on the square difference between the models at each calculation node. This means that misalignment causes increased STE even though the mean level and shape are correct, as shown in figure 7.

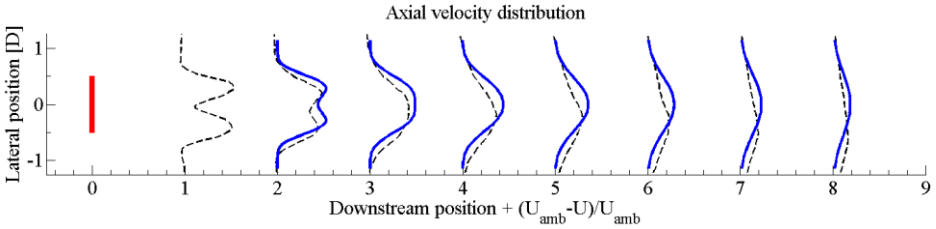

Figure 7: An illustration of the misalignment of the wake deficit of the DWM model (solid lines) and the AL model (dashed lines) behind the first turbine for the case "U-N.H. row B". This misalignment causes the STE to increase.

The misalignment mainly occurs as a consequence of the relatively short simulation time, roughly 10 minutes, of the LES-AL calculations. An estimation of the uncertainty due to wake centre misalignment for similar simulations was given in Keck et al. [11], where the uncertainty of the mean flow field based

on 10 min of simulation data in 6% ambient turbulence intensity and neutral conditions was estimated to 0.07m/s and 0.28 percentage points (i.e., *"ΔTI"*, from here on denoted pp) for wind speed and turbulence intensity respectively. As the wake meandering is roughly twice as large in very unstable atmospheric conditions the uncertainties in these cases are about 0.14m/s and 0.56pp.

Another source which contributes to the uncertainty is that the mean velocity at the hub height plane and away from the turbines and wakes in the LES-AL simulations is not uniform for the 10 min time series, as shown in figure 8. Streaks of higher and lower wind speed and turbulence intensity are present in the simulation domain. The uncertainty due to these streaks is estimated based on extracting a standard deviation of mean wind speed and turbulence intensity at hub height on the inflow boundaries. The non-uniform ambient conditions in the domain are estimated to yield an uncertainty of 0.10 m/s and 0.53pp for wind speed and turbulence intensity, respectively, in neutral conditions. The same values in the very unstable conditions are 0.11m/s and 0.71pp.

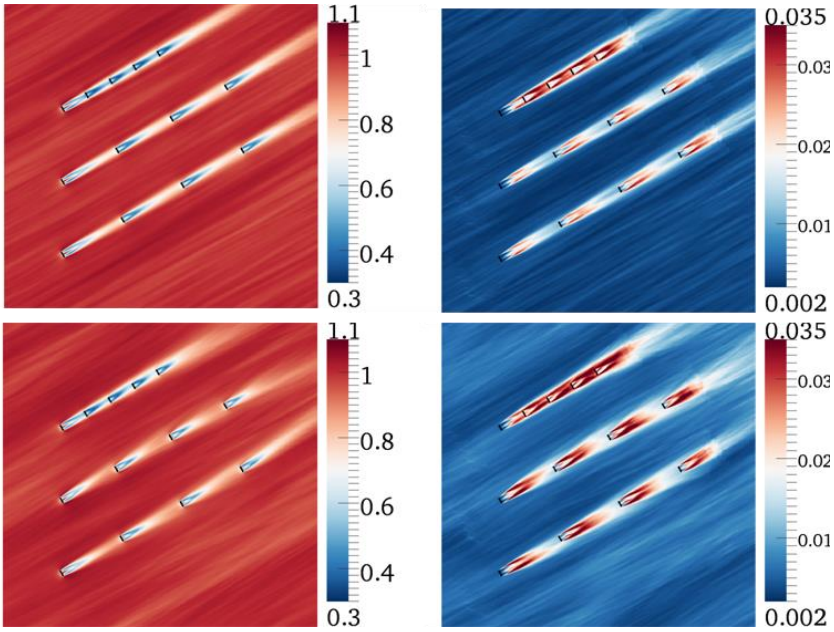

Figure 8: Contours of mean velocity normalized by hub-height free stream speed (left figures) and resolved-scale turbulent kinetic energy normalized by the square of hub-height free stream speed (right figures) in a horizontal plane at hub height in neutral (top row) and very unstable (bottom row) conditions for the North Hoyle case.

As the two sources of uncertainty can be assumed to be independent from each other, the combined uncertainty is found, as the root-square-sum, to be 0.12m/s and 0.60pp in neutral conditions and 0.18m/s and 0.92pp in very unstable conditions. When basing the comparison of the models on eq. (21), the uncertainty on the mean flow field increases the STE linearly. This means that if the true model mean profiles were identical, the STE would be equal to uncertainty of the AL simulations.

Results and discussion:

Verification of input wind field

The input turbulence fields of the two models are generated by fundamentally different methods. The ABL turbulence of the DWM is estimated using the Mann turbulence model with the input parameters

suggested by Peña et al. [27], whereas the ABL turbulence applied in the LES-AL simulations is created using a precursor LES in which the N-S equations dictate the flow. The turbulent energy spectra of the applied input velocity field are shown in figure 9. The turbulence spectra of the two models in neutral stratification are in fair agreement for all wave numbers above the cut-off frequency of the LES precursor simulation. This cut-off is grid-induced filtering in the LES precursor simulation. For the unstable case, however, the LES model contains more turbulent energy in the large scales of the lateral turbulence spectra, compared to the turbulence applied in the DWM simulation. The higher turbulence levels are seen in the range of k_1 0.002 to 0.006, corresponding to turbulent eddies of 1 to 3km in size. In this range the turbulent energy level of the LES simulations are approximately four times as high as that in the Mann turbulence of the DWM model (although it should be noted that the energy levels fluctuate largely due to the few realizations). The highest energy level in the lateral spectra of LES-AL turbulence is seen at k_1= 0.003 (2km). The corresponding number in the Mann spectra turbulence is k_1= 0.02 (250m). The findings are consistent with the findings presented by Larsen et al. [38] for using the Mann turbulence model with calibrated input parameters to simulate unstable atmospheric conditions. In the unstable cases, the LES model resolves long lines of updrafts on the scale of 1 to 3 km, which is the range in which the LES turbulence has higher lateral energy than the Mann turbulence.

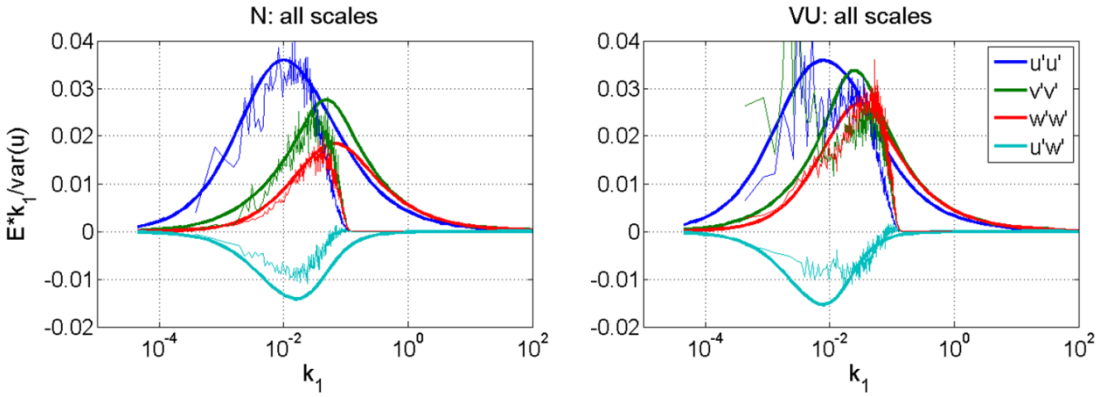

Figure 9: The turbulence energy spectra of the wind field generated by Mann model (thick lines) and that generated with by precursor LES simulations (thin lines).

As a consequence of the large length scales in the LES precursor turbulence, the most energy-containing turbulent eddies are only realized 2-3 times during the 10 min simulation time. This results in a high uncertainty in the STE comparison due to the inhomogeneous mean flow field and the alignment of the wake meandering (see figures 7 and 8). Furthermore, as seen in the subsequent analysis, the difference in the input spectra affects the lateral wake meandering for the unstable cases.

The cause of these differences in the lateral input turbulence requires further investigation. To reduce the effect of the discrepancies on the DWM validation, it would be interesting to conduct longer LES-AL simulations to obtain fully converged mean conditions for the comparison. Unfortunately, lengthening these calculations is too computationally expensive for the present study; a simulation to resolve the most energy containing structures ~30 times would require in the order of 5 million CPU-hours per case.

Validation of wake meandering with the DWM method

Figure 10 shows the lateral (left) and vertical (right) wake meandering as a function of downstream position and atmospheric stability, as calculated by the DWM method (black), the EllipSys3D LES-AL model (red) (data from Keck et al. [28]) and the OpenFOAM LES-AL model. The figure shows that the wake meandering applied in the DWM model is in fair agreement with the two LES-AL data sets for the neutral cases. For the unstable cases, however, the lateral wake meandering of the DWM model is 40%

lower compared to that of the OpenFOAM LES-AL model. This is attributed to the differences in the input spectra, as discussed above and shown in figure 9. The vertical wake meandering and the input spectrum of vertical turbulence seen in figure 9 in the unstable atmosphere of the two models correlate well, which strengthens the conclusion that the deviations in lateral wake meandering are due to the difference in lateral input turbulence.

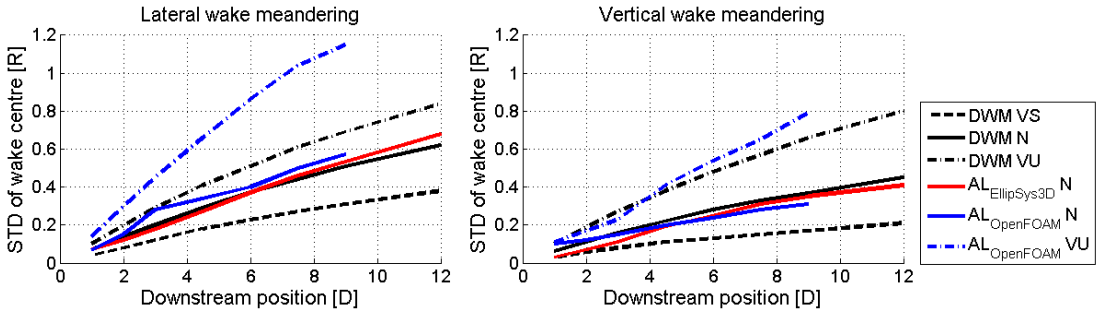

Figure 10: Wake meandering as calculated by the DWM (black), EllipSys3D LES-AL (red) and OpenFOAM LES-AL models (blue) for a rotor of 80m in diameter and 70m hub height operating in 8m/s wind speed and 6% turbulence intensity. The left figure show the lateral meandering and the right figure show the vertical meandering, both expressed as the standard deviation of the wake centre normalised by R.

Effect of the atmospheric stability correction in DWM

This section shows the effect of including the atmospheric stability correction in the DWM model. In the first analysis the STE of all unsteady cases in table 2 are calculated both with the modified (DWM B) and the unmodified (DWM A) versions of the DWM model to verify that the suggested correction increases the ability to predict the flow field under unstable atmospheric conditions, see table 3. By comparing the results it can be concluded that the atmospheric stability correction reduces the average STE by 19% in terms of wind speed and 28% in terms of turbulence intensity

Table 3: The STE (eq. (21)) of the DWM model without (A) and with (B) the atmospheric stability correction compared to the OpenFOAM LES-AL simulations for the unsteady simulations listed in table 2.

	STE WS DWM A [m/s]	STE WS DWM B [m/s]	Ratio B/A	STE TI DWM A [%]	STE TI DWM B [%]	Ratio B/A
N.H. row A	0.53	0.39	0.74	2.9	2.0	0.69
N.H. row B	0.60	0.45	0.75	3.4	2.4	0.71
N.H. row C	0.71	0.63	0.89	2.1	2.0	0.95
OWEZ row A	0.48	0.40	0.83	2.0	1.2	0.60
OWEZ row B	0.52	0.43	0.83	1.7	1.1	0.65
Mean	**0.57**	**0.46**	**0.81**	**2.4**	**1.7**	**0.72**

To illustrate the effect of the atmospheric stability correction, the velocity and turbulence intensity profiles behind the two first turbines in the *"U-N.H. row A"* case are plotted in figure 11. It can be seen that the velocity deficit of the modified DWM model is more shallow and wider with higher average turbulence intensity.

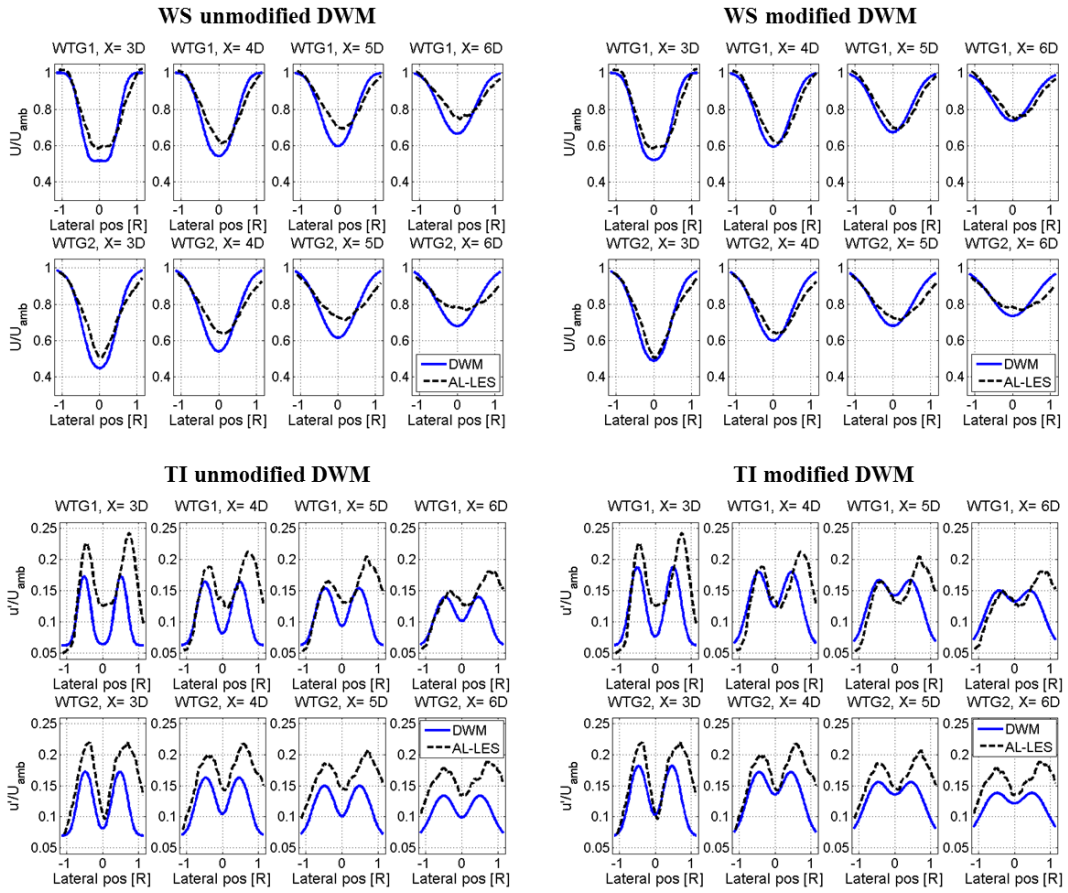

Figure 11: The velocity (top) and turbulence intensity (bottom) profiles at hub height and 3, 4, 5 and 6D (from left to right) behind the two turbines in the "U-N.H. row A" case. The top row of group depicts the result behind the first turbine and the bottom row show the result behind the second turbine in the row.

In the second analysis, the modified DWM version is used to investigate the effect on power production in single-wake operations as a function of incoming flow angle and atmospheric stability, as shown in figure 12. The ambient wind speed at hub-height is 8m/s and the turbulence intensity is 6%. The two turbines are located 7D apart. It can be seen that for this configuration the power deficit (one minus the ratio of the mean power of the second to the first turbine) is 45% larger in the very stable atmosphere (0.58) compared to a very unstable atmosphere (0.4) when the incoming flow is aligned with the axis of the two turbines. The difference decreases with increasing inflow angle to the turbines, and at a mean wind direction of 7^{o} the power deficit is independent of atmospheric stability. For inflow direction between 7^{o} and 15^{o} the power deficit is slightly increased in an unstable atmosphere. These effects are predominately governed by the wake meandering. By integrating over-all wind directions in figure 12, the loss of production due to the single wake for a site with a uniform wind distribution can be found. This yields a reduction in annual energy production (AEP) of 1.7%, 1.6%, and 1.4% for very stable, neutral, and very unstable atmosphere, respectively (under the assumption that no power loss is experienced in the 330^{o} that are not shown in the figure). The same analysis for a range of atmospheric conditions and turbine spacings is presented in figures 13 and 14.

The amount of increased turbulence intensity level experienced at the downstream turbine is also affected by the atmospheric stability. The wake-added turbulence is a combination of small-scale turbulence generated by the shear layer of the wake and "apparent" turbulence due to the wake meandering. The deeper wake deficit in stable stratification creates more shear layer generated

turbulence, whereas the apparent wake contribution is a combination of the depth of the wake deficit and the amount of wake meandering (see figure 15 to see how the ratio of the two components vary with atmospheric stability). For the case presented in figure 12, the increase in turbulence intensity at the second turbine is 5.4, 4.4, and 3.7 percentage points (pp) for very unstable, neutral and very stable atmosphere, respectively.

The same trends as in the case presented in figure 12 are seen throughout the study:

1. Stable atmospheric conditions causes larger power losses in single wake operations
2. Unstable atmospheric conditions are more turbulent at the second turbine. This is mainly due to a larger "apparent" turbulence contribution.
3. The neutral cases are, on average slightly closer to the very stable cases than the very unstable cases. The average difference for the tested cases is 0.22% in AEP from very stable to neutral and 0.33% from very unstable to neutral stratification.

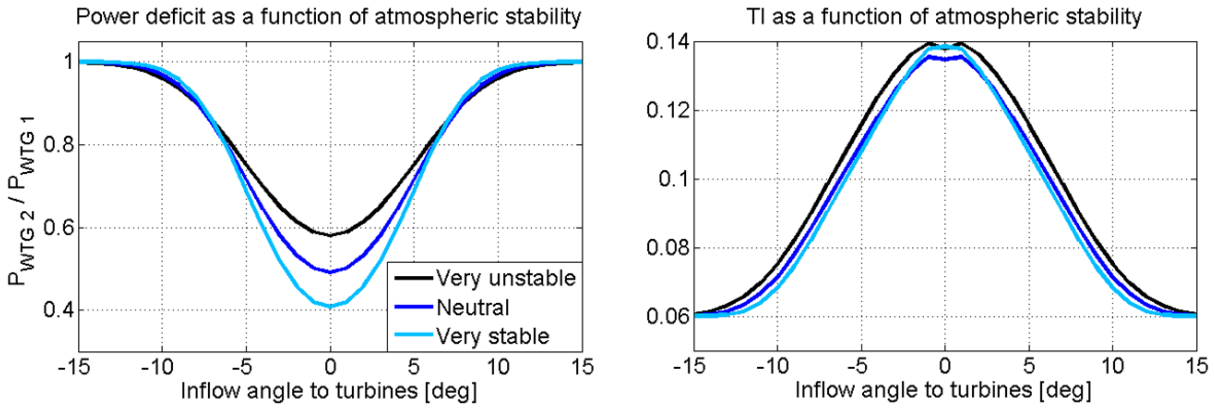

Figure 12: The power deficit (left) and turbulence intensity profiles (right) as a function of the atmospheric stability and inflow direction at a wake-affected turbine 7D downstream of the wake-emitting turbine.

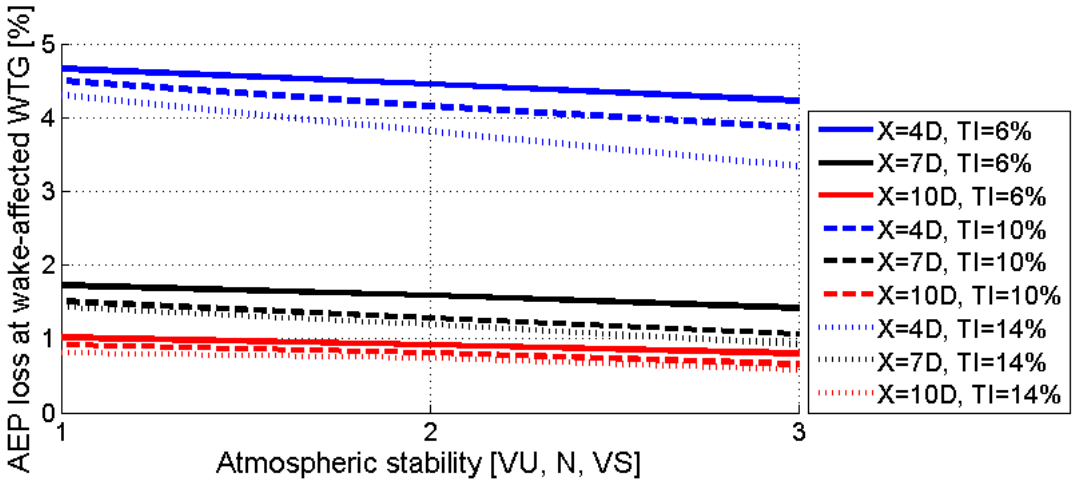

Figure 13: Loss of AEP in % at the 2nd rotor as a function of distance, turbulence intensity and atmospheric stability in single wake operation. The AEP integration of power is performed over 360°.

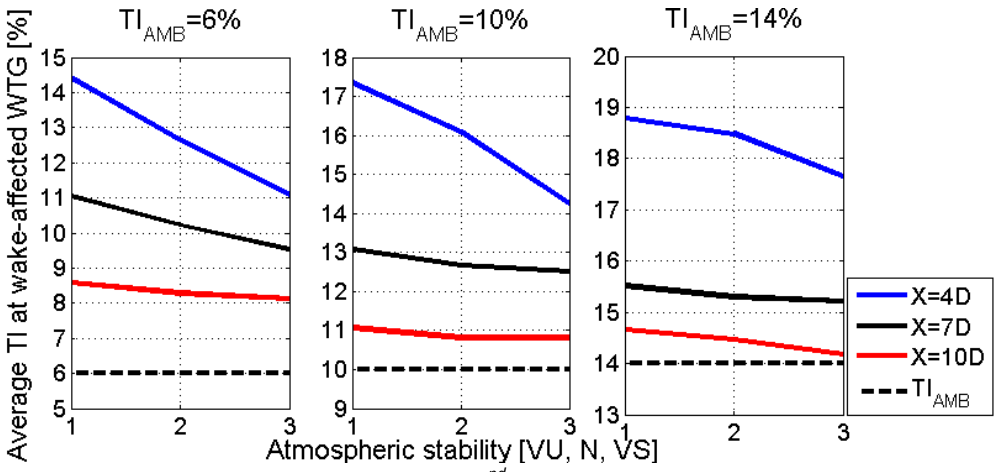

Figure 14: Average turbulence intensity level at the 2nd rotor as a function of distance, turbulence intensity and atmospheric stability in single wake operation. The turbulence intensity is averaged in a -10° to +10° sector.

Apart from an increase in the turbulence intensity (shown in figure 12), atmospheric stability also influences the composition of the wake turbulence. Figure 15 shows the composition of the wake turbulence in a cross section 6D downstream of the first turbine. The simulations are conducted in an ambient wind speed of 8 m/s and a turbulence intensity of 6%, under very stable (left), neutral (middle), and very unstable (right) atmospheric conditions. As mentioned above, the total turbulence experienced by a downstream rotor (TI_{Tot}) consists of small-scale turbulence ($TI_{Small\text{-}scale}$) and the apparent turbulence created by the meandering of the wake deficit (TI_M). From the figure it can be seen that the relative contribution to the turbulence intensity due to wake meandering is approximately twice as large in the very unstable case compared to the very stable case. The increased amount of turbulence in meandering scales will affect the fatigue loads of the wake-receiving turbine (see Madsen et al. [1], Sathe et al. [23] and Crespo et al. [39]), whereas the small-scale turbulence will mainly affect the wake deficit evolution of the wake-affected turbine.

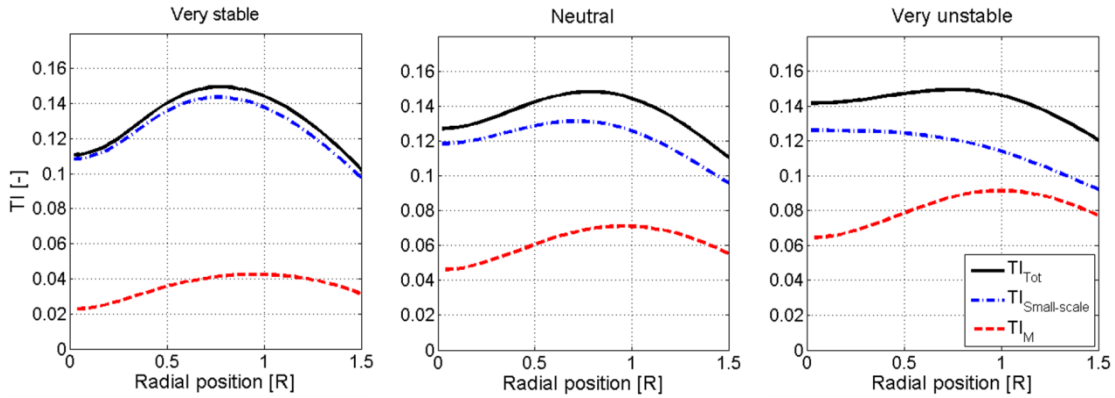

Figure 15: The composition of turbulence intensity in the wake as a function of atmospheric stability.

Wake velocity and turbulence intensity with the modified DWM model

Table 4 show the STE based on wake velocity and turbulence intensity for all the conducted cases. The average STE for the conducted cases under neutral conditions is 0.25 m/s in terms of wind speed and 1.48 pp for turbulence intensity. The average STE for the unstable cases is 0.42 m/s for wind speed and 2.78 pp for turbulence intensity. An explanation for part of this increase in STE for the unsteady cases is the higher degree of uncertainty due to wake meandering and the non-uniform inflow conditions in the

computational domain. As discussed above, the uncertainty in the AL results increase the STE linearly. According to the estimations presented above, the uncertainty of 0.12 m/s and 0.60 pp in neutral conditions and 0.18 m/s and 0.92 pp in very unstable conditions for wind speed and turbulence intensity, respectively, is responsible for 45% of the STE of wind speed and 36% of the STE of turbulence intensity.

Table 4: The STE (see eq. (21)) of the DWM model with the proposed atmospheric stability correction compared to the conducted AL simulations.

Cases:	STE WS [m/s]	STE TI [%]
N-N.H. row A	0.31	1.6
U-N.H. row A	0.39	2.0
N-N.H. row B	0.35	1.3
U-N.H. row B	0.45	2.4
N-N.H. row C	0.57	2.2
U-N.H. row C	0.63	2.0
N-OWEZ row A	0.27	1.2
U-OWEZ row A	0.40	1.2
N-OWEZ row B	0.28	1.2
U-OWEZ row B	0.43	1.1

Figures 16 and 17 show the velocity and turbulence profiles for the *"N-OWEZ row B"* and *"U-N.H. row C"* cases as computed with the DWM and LES-AL. The results show the overall agreement with the range of STE achieved by the DWM model. By observing the *"U-N.H. row C"* case, it can be seen that both the velocity and the turbulence intensity field has the correct shape and good agreement with field data even at the higher STE numbers presented in table 12.

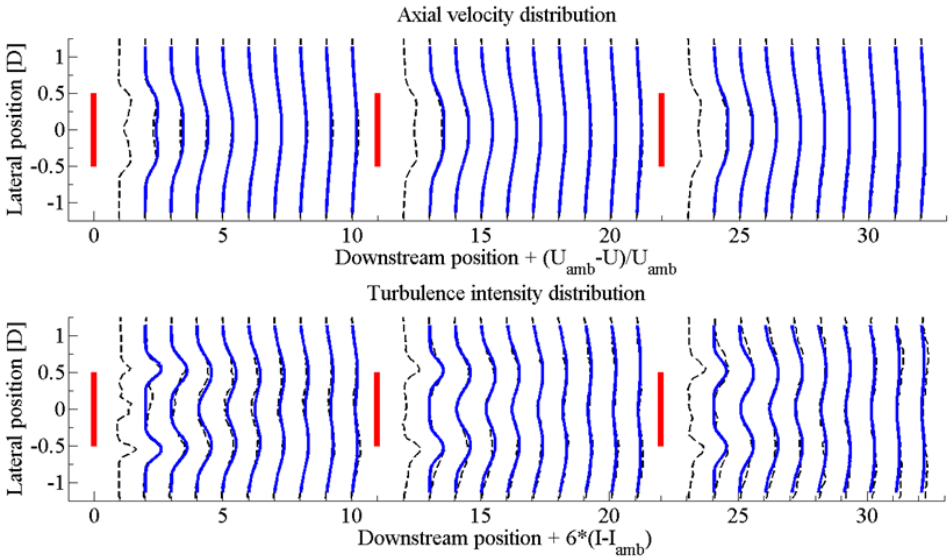

Figure 16: Comparison of the velocity (top) and turbulence intensity (bottom) profiles for the "N-OWEZ row B" case found with the LES-AL model (dashed lines) and the modified DWM model (solid lines). The thick solid lines show the rotor positions.

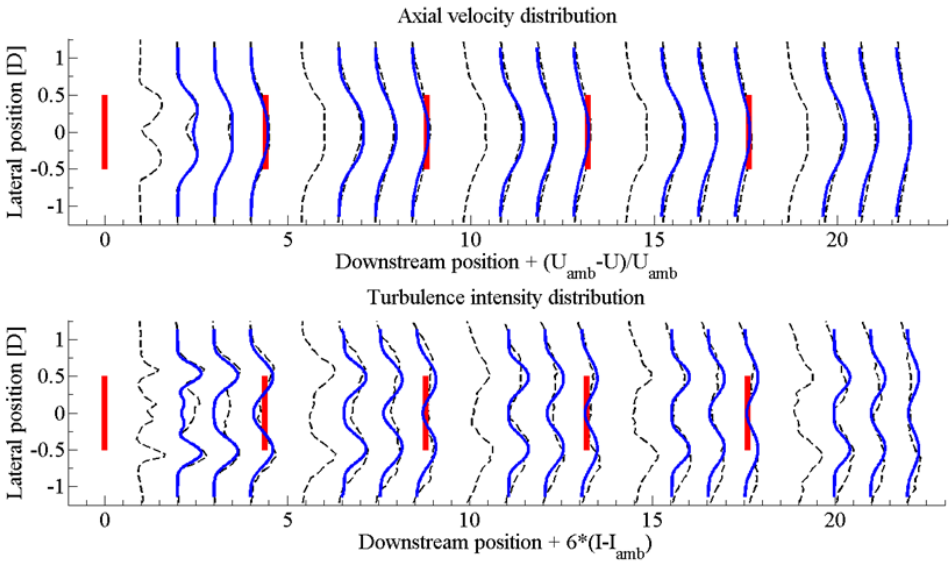

Figure 17: Comparison of the velocity (top) and turbulence intensity (bottom) profiles for the "U-N.H. row C" case found with the LES-AL model (dashed lines) and the modified DWM model (solid lines). The thick solid lines show the rotor positions.

Power production with the modified DWM model

Figure 18 shows a comparison of the power production estimates of the modified DWM model field data from the North Hoyle wind farm. All modelled cases are computed with a hub-height mean wind speed of 8 m/s and turbulence intensity of 6%, which correspond to the mean conditions of the field data. The columns represent very stable, neutral and very unstable conditions from left to right; and the rows represent 11D, 10D, and 4.4D turbine spacing from the top down (i.e., row A to C of in table 4).

The field data in Figure 17 show lower wake losses compared to the numerical results. This may be due to a larger bin size of incoming wind direction. In the DWM model, only wind aligned with the row of turbines is considered.

The main motivation for the study of power production is to verify that the DWM model can capture the average effect on power production due to non-neutral atmospheric stability by implementing the suggested modifications. The average normalized power production of the wake affected turbines for the OWEZ and the North Hoyle wind farm cases are presented together with field data in table 5.

Both the DWM model and the field data show that increasing the atmospheric stability causes larger wake effects in wind farms, even when the turbulence intensity is maintained constant. By comparing the average wake losses in the table, it is seen that the wake losses in very unstable conditions are 10% and 6% smaller compared to neutral stratification for the DWM model and the field data, respectively (however, it should be noted that the power production in neutral atmosphere for the *N.H 10D* case is an outlier and influences the field data result, as seen in table 5; excluding the *N.H 10D* case yields a 13% difference between unstable and neutral atmospheric conditions instead of the current 6%). Comparing the average wake losses in very stable conditions and neutral conditions, the DWM model predicts 12% higher losses and the field data show 13% higher losses.

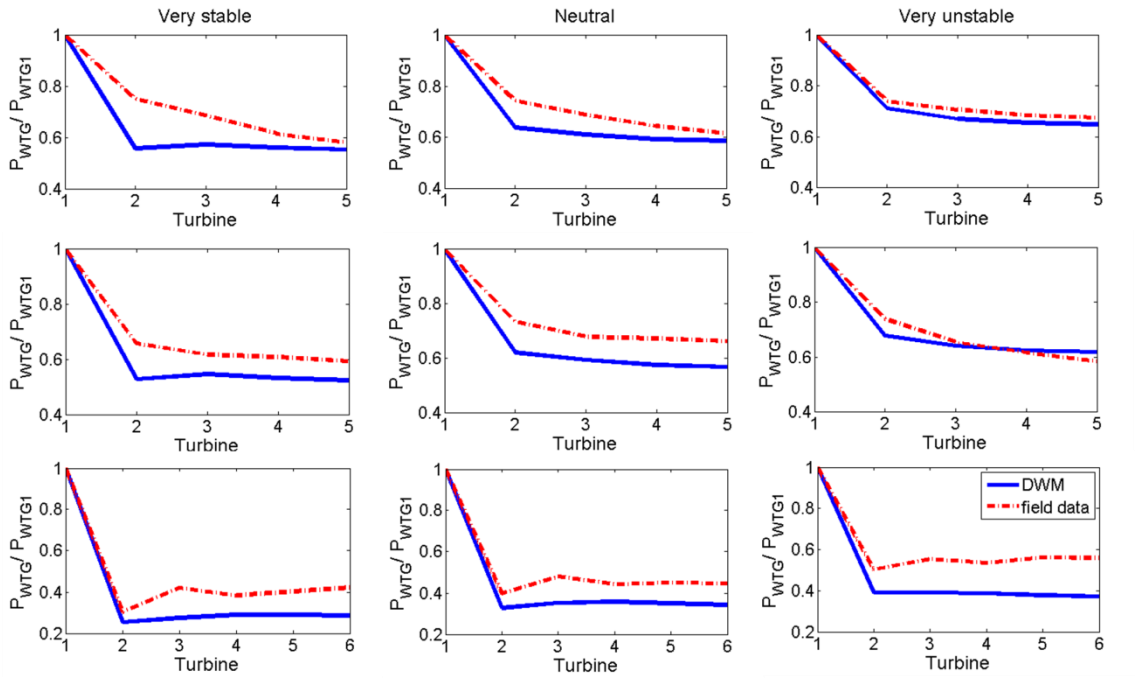

Figure 18: The power production for all turbines in the rows from the simulation cases at the North Hoyle wind farm compared to field data. The ambient hub-height conditions in all cases are wind speed of 8m/s and a turbulence intensity of 6%. The column represent atmospheric stability class (very stable, neutral and very unstable from left to right) and the rows show different turbine spacing (11, 10 and 4.4D from top to bottom).

Table 5: Average power production of all wake affected turbines, normalized against the first turbine of the row, in the North Hoyle and OWEZ simulations compared to field data. The ambient conditions in all cases are wind speed of 8m/s and a turbulence intensity of 6%.

	Field data-VS	DWM-VS	Field data-N	DWM-N	Field data-VU	DWM-VU
OWEZ 11D	0.62	0.57	0.71	0.61	0.72	0.67
OWEZ 13D	0.74	0.63	0.79	0.67	0.81	0.70
N.H 4.4D	0.39	0.28	0.44	0.35	0.54	0.38
N.H 10D	0.62	0.53	0.69	0.59	0.65	0.64
N.H 11D	0.66	0.56	0.67	0.61	0.70	0.67
Mean of COL	0.61	0.51	0.66	0.57	0.68	0.61

Conclusions

The present findings show that atmospheric stability influences the wake effects experienced in a wind farm, even when the ambient turbulence intensity (based on wind speed variance in the mean flow direction, as is typically done) is held constant. This suggests that the impact of atmospheric stability on the turbulent length scale is important for wind farm dynamics, and that the turbulence intensity alone is not sufficient to describe wake dynamics in the atmospheric boundary layer. It also suggests that turbulence intensity based on the component of flow in the mean wind direction only is insufficient and

that all three components must be considered. Specifically, the presented data show that atmospheric stability affects the length scale of the atmospheric turbulence, and that this shift in length scale influences both the wake meandering and the wake deficit evolution. Furthermore, it is shown that the effect of atmospheric stability on the AEP of a wind turbine influenced by a single wake (the turbine is only in wake in a 30° sector, but the AEP is calculated over 360°) is in the order of 0.50% comparing very unstable to very stable conditions (this is equivalent to ~25% of the AEP loss due to the wake). Although 0.5% seems small, it can translate into millions of dollars over the lifespan of a large modern wind plant, so having the capability to account for stability on AEP in the DWM model is important. The power produced by a row of wind turbines aligned with the wind direction is reduced by about 10% in very stable conditions compared to very unstable conditions, based on results from both field data and simulations of the North Hoyle and OWEZ wind farms.

The proposed increase in functionality of the DWM model to include the effects of atmospheric stability shows an improved agreement with the reference data sources compared to the baseline model. STE between the AL model and the modified DWM model are reduced by ~19% in terms of velocity field and ~28% in terms of turbulence intensity field on average.

The largest deviations are seen in the generated input turbulence in unstable atmospheric stability, where the turbulence field generated by the Mann model with the parameters suggested by Peña et al. [27] is found to contain less energy in the largest turbulence scales of the lateral component, compared to the LES precursor calculations. These findings are in agreement with the conclusions drawn by Larsen et al [38], where the calibrated Mann model was found to contain less large-scale lateral turbulence in unstable atmospheric conditions compared to field data. For the undertaken study, a consequence of the large length scale of the LES precursor turbulence (which is about 8 times larger than expected from the Mann model in unstable atmosphere) is that the eddies containing the largest amount of energy only pass through the domain a few times during the LES-AL simulations. This will yield an increased uncertainty of the local mean flow field of the LES-AL computations, affecting the STE comparison, and a larger lateral wake meandering in the LES-AL results compared to the DWM results. Suggested further work is to run the LES-AL cases longer to reduce the uncertainty, and to compare the unstable ABL turbulence fields generated by each method in detail. As mentioned above, no reference data is available for stable atmospheric conditions as this functionality is currently not available in the LES model used.

In this investigation, is has not been possible to verify the wake deficit evolution independently of the wake meandering, as is done in Keck et al. [11], as the LES-AL data required to extract the deficit in a meandering frame of reference is not available. Instead, the LES-AL and DWM flow fields in fixed frame of reference (i.e., both the velocity deficit and the wake meandering observed together) are compared. A good agreement is achieved in both magnitude and evolution of downstream profiles of mean velocity and turbulence intensity. The STE in terms of mean velocity is 0.36 m/s in neutral conditions and 0.46 m/s in very unstable conditions; and for turbulence intensity it is 1.50 pp in neutral conditions and 1.74 pp in very unstable conditions. These numbers are also influenced by the uncertainty of the LES-AL results due to the relatively short simulations times, which increase the STE linearly (as the STE is the root-square of the difference in the flow field of the DWM and the AL results). The uncertainties for the simulated cases are 0.12 m/s and 0.60 pp in neutral conditions and 0.18 m/s and 0.92 pp in very unstable conditions for wind speed and turbulence intensity, respectively. The uncertainty accounts for approximately 37% of the STE in terms of wind speed and 46% of turbulence intensity.

The effect of atmospheric stability on the power production of a row of wind turbines agrees well between the DWM model and the field data from the rows of wind turbines at the North Hoyle and OWEZ wind farms. Both show that the very stable stratification leads to about 13% higher wake losses than in neutral conditions and that very unstable conditions lead to about 10% lower wake losses compared to neutral conditions.

References:

[1] Madsen, H.Aa., Thomsen, K., and Larsen, G.C. (2003) A new method for prediction of detailed wake loads. In: S-E Thor (ed), Proceedings of *IEA Joint Action of Wind Turbines 16th Symposium*, Boulder, USA, May 2003 at NREL, pp. 171-188.

[2] Madsen, H.Aa., Larsen, G.C., Larsen, T.J., Troldborg, N., and Mikkelsen, R. (2010) *Calibration and validation of the Dynamic Wake Meandering model implemented in the aeroelastic code HAWC2*. *Journal of Solar Energy Engineering.* Volume 132, Issue 4, 041014 (14 pages).

[3] Larsen, G.C., Madsen, H.Aa., Thomsen, K., and Larsen, T.J. (2008) *Wake meandering — a pragmatic approach. Wind Energy,* **11**, 377-395.

[4] Frandsen, S.T. (2007) *Turbulence and turbulence-generated structural loading in wind turbine clusters.* Risø-R-1188(EN). Risø National Laboratory, Technical University of Denmark, Roskilde, Denmark.

[5] Bingöl, F., Mann, J., and Larsen, G.C. (2010) *Light detection and ranging measurements of wake dynamics, Part I: One-dimensional Scanning. Wind Energy.* **13,** 51-61.

[6] Trujillo, J.J., Bingöl, F., Larsen, G.C., Mann, J., and Kühn, M. (2011) *Light detection and ranging measurements of wake dynamics, Part II: two-dimensional scanning. Wind Energy.* **14,** 61-75.

[7] Ainslie, J.F. (1988) *Calculating the flow field in the wake of wind turbines. Journal of Wind Engineering and Industrial Aerodynamics*. 27, pp. 213-224.

[8] Ainslie, J.F., (1986) Wake modelling and the prediction of turbulence properties. In: *Proceedings of the 8th British Wind energy Association Conference*, Cambridge, 19-21 March 1986. pp. 115-120.

[9] Keck, RE., Veldkamp, D., Madsen, H.Aa., and Larsen, G.C. (2011) *Implementation of a mixing length turbulence formulation into the dynamic wake meandering model. Journal of Solar Energy Engineering*. Volume 134, Issue 2, 021012 (13 pages).

[10] Madsen, H.Aa., Larsen, G.C., and Thomsen, K. (2005). Wake flow characteristics in low ambient turbulence conditions. In: *Proceedings of Copenhagen Offshore Wind 2005*.

[11] Keck, R.E., de Mare, M., Churchfield, M.J., Lee, S., Larsen, G., Madsen, H.Aa. (2012) Two Improvements to the Dynamic Wake Meandering Model: Including the effects of atmospheric shear on wake turbulence and incorporating turbulence build up in a row of wind turbines. Submitted to *Journal of Wind Energy.* July

[12] Barthelmie, R.J., Hansen. K., Frandsen, S.T., Rathmann, O., Schepers, J.G., Schlez, W., Philips, J., Rados, K., Zervos, A., Politis, E.S., and Chaviaropoulos, P.K.. (2009) *Modelling and measuring flow and wind turbine wakes in large wind farms offshore. Wind Energy*. WE-08-0099.

[13] Obukhov, A.M. (1971) *Turbulence in an atmosphere with a non-uniform temperature. Boundary-Layer Meteorology 2.* 7-29.

[14] Monin, A.S., Obukhov, A.M. (1954) *Basic laws of turbulent mixing in the surface layer of the atmosphere*. Tr. Geofiz. Inst., Akad. Nauk SSSR, 151, 163–187.

[15] Businger, J., Wyngaard, J. C., Izumi, Y., & Bradley, E. F. (1971). *Flux-profile relationships in the atmospheric surface layer. Journal of the Atmospheric Sciences*. 28(2), 181-189.

[16] Kirchhoff, R.H., Kaminsky, F.C. (1983) *Wind shear measurements and synoptic weather categories for siting large wind turbines. Journal of Wind Engineering and Industrial Aerodynamics*. Volume 15, Issues 1–3, December, Pages 287-297, ISSN 0167-6105, 10.1016/0167-6105(83)90198-8.

[17] Irwin, J.S. (1967) *A theoretical variation of the wind profile power-law exponent as a function of surface roughness and stability. Atmospheric Environment.* Volume 13, Issue 1, 1979, Pages 191-194, ISSN 0004-6981, 10.1016/0004-6981(79)90260-9.

[18] Zoumakis, N. M. (1993) *The dependence of the power-law exponent on surface roughness and stability in a neutrally and stably stratified surface boundary layer. Atmosfera.* 6, 79-83.

[19] Barthelmie, R.J., Frandsen, S.T., Hansen, K., Schepers, J.G., Rados, K., Schlez, W., Neubert, A., Jensen, L.E., and Neckelmann, S. (2009) Modelling the impact of wakes on power output at Nysted and Horns Rev. In: *European Wind Energy Conference*.

[20] Wharton, S., Lundquist, J.K., Marjanovic, H. (2012) Synergistic effects of turbine wakes and atmospheric stability on power production at an offshore wind farm. LLNL-TR-524756, January

[21] Schepers, J., Obdam, T., and Prospathopoulos, J. (2011) *Analysis of wake measurements from the ECN wind turbine test site wieringermeer, EWTW. Wind Energy*. DOI:10.1002/we.488.
[22] Hansen, K., Barthelmie, R.J., Jensen, L., and Sommer, A. (2011) *The impact of turbulence intensity and atmospheric stability on power deficits due to wind turbine wakes at Horns Rev wind farm. Wind Energy*. DOI:10.1002/we.512.
[23] Sathe, A., Mann J., Barlas, T., Bierbooms, W.A.A.M., and van Bussel G.J.W. I(????) *Influence of atmospheric stability on wind turbine loads. Wind Energy*. DOI:10.1002/we.1528.
[24] Churchfield, M.J., Lee, S., Michalakes, J., and Moriarty, P.J. (2012) *A numerical study of the effects of atmospheric and wake turbulence on wind turbine dynamics. Journal of Turbulence*. Vol. 13, No. 14.
[25] Lee, S., A Clifton, and P. Moriarty. Wind turbine wakes and turbulence under various atmospheric boundary layers. Manuscript submitted to *Computer and Fluids*.
[26] Lavely, A. W., Vijayakumar, G., Kinzel, M. P., Brasseur, J. G., and Paterson, E. G. (2011) *Space-time loadings on wind turbine blades driven by atmospheric boundary layer turbulence.* AIAA. 2011-635,
[27] Peña, A., Gryning, S.-E., and Mann, J. (2010) On the length scale of the wind profile. Quarterly Journal of the Royal Meteorological Society. 136(653), 2119–2131.
[28] Keck, R.E., Mikkelsen, R., Troldborg, N., de Maré, M., and Hansen, K.. (2012) Synthetic atmospheric turbulence and wind shear in large eddy simulations of wind turbine wakes. Submitted to *Journal of Wind Energy*. August 2012
[29] Larsen, G.C., Madsen, H.Aa., Bingöl, F., Mann, J., Ott, S.,Sørensen, J.N., Okulov, V., Troldborg, N., Nielsen, M., Thomsen, K., Larsen, T.J., and Mikkelsen, R. (2007) *Dynamic wake meandering modelling. Risø-R-1607(EN).* Risø National Laboratory, Technical University of Denmark, Roskilde, Denmark,.
[30] Stull, R.B. (1988) An Introduction to Boundary Layer Meteorology, 666pp., Kluwer, Norwell, Mass..
[31] Wyngaard, J C. (2010) Turbulence in the Atmosphere. Cambridge University Press, New York. ISBN 978-0-521-88769-4.
[32] Mann, J. (1994) *The spatial structure of neutral atmospheric surface-layer turbulence. Journal of Fluid Mechanics*. 273, 141-168.
[33] Mann, J. (1998) *Wind field simulation. Probabilistic Engineering Mechanics*. Vol. 13, No. 4, pp. 269-282.
[34] Goodman, J. W. (2005) Introduction to Fourier Optics. Roberts & Company Publishers, Greenwood Village, Colo., p1.
[35] SOWFA project homepage: http://wind.nrel.gov/designcodes/simulators/sowfa/
[36] OpenFOAM, The Open Source CFD Toolbox, Version 2.1.1, [available online], URL: http://www.openfoam.com, 2012, OpenCFD Limited (ESI Group), [accessed 7 December 2012].
[37] Moeng, C.H. (1984) *A large-eddy simulation model for the study of planetary boundary layer turbulence. Journal of the Atmospheric Sciences*. Vol. 41, No. 13, July 1984, pp. 2052—2062.
[38] Larsen, G. C., Larsen, T. J., Madsen, H. A., Mann, J., Peña, A., Hansen, K. S., and Jensen, L. (2009). The dependence of wake losses on atmospheric stability characteristics. In: *Euromech Colloquium* (Vol. 508, pp. 35-37).
[39] Crespo, A., Hernandez, J., and Frandsen, S. (1999) *Survey of modelling methods for wind turbine wakes and wind farms. Wind Energy*. 2(1):1–24.

DTU Vindenergi er et institut under Danmarks Tekniske Universitet med en unik integration af forskning, uddannelse, innovation og offentlige/private konsulentopgaver inden for vindenergi. Vores aktiviteter bidrager til nye muligheder og teknologier inden for udnyttelse af vindenergi, både globalt og nationalt. Forskningen har fokus på specifikke tekniske og videnskabelige områder, der er centrale for udvikling, innovation og brug af vindenergi, og som danner grundlaget for højt kvalificerede uddannelser på universitetet.

Vi har mere end 230 ansatte og heraf er ca. 60 ph.d. studerende. Forskningen tager udgangspunkt i 9 forskningsprogrammer, der er organiseret i tre hovedgrupper: vindenergisystemer, vindmølleteknologi og grundlag for vindenergi.

Danmarks Tekniske Universitet
DTU Vindenergi
Nils Koppels Allé
Bygning 403
2800 Kgs. Lyngby
Telefon 45 25 25 25
info@vindenergi.dtu.dk
www.vindenergi.dtu.dk